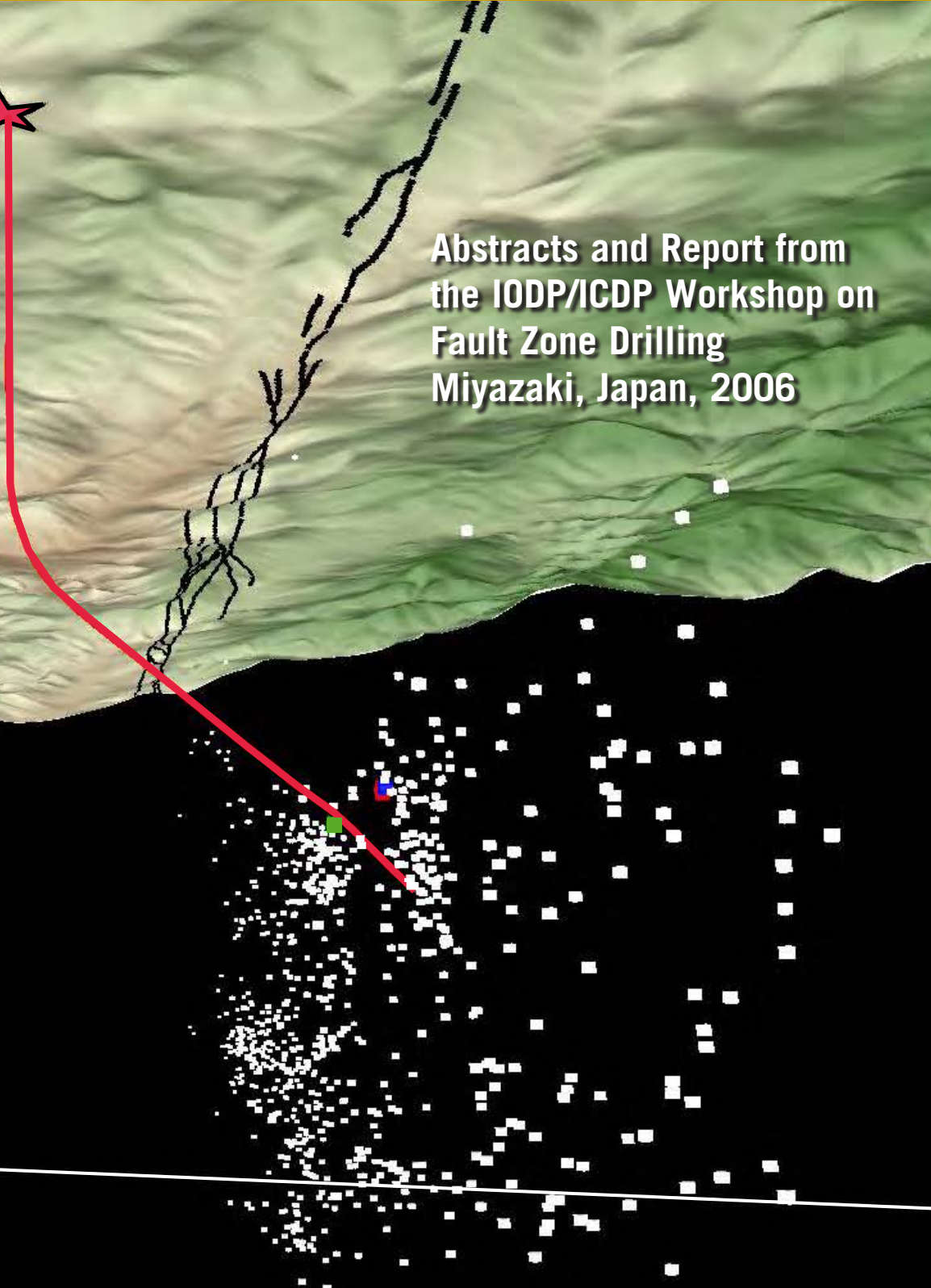
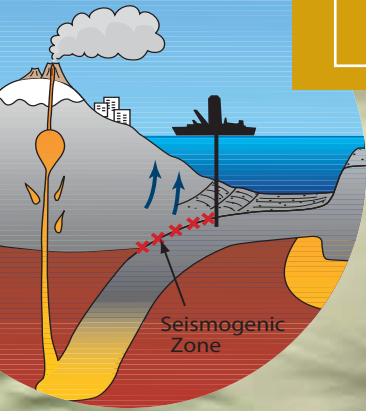


Scientific Drilling



Reports on Deep Earth Sampling and Monitoring



Abstracts and Report from
the IODP/ICDP Workshop on
Fault Zone Drilling
Miyazaki, Japan, 2006

Edited by
Hisao Ito
Jan Behrmann
Steve Hickman
Harold Tobin
and Gaku Kimura






Dear Reader:

On 23–26 May, 2006, eighty scientists and engineers from around the world met at Miyazaki, Japan, at a workshop jointly sponsored by the Integrated Ocean Drilling Program (IODP) and the International Continental Scientific Drilling Program (ICDP). The purpose of this workshop was to review the state of the art in scientific drilling into fault zones, and discuss scientific and technological issues faced by future fault zone drilling projects on land and at sea.

The workshop provided a forum for an open and detailed exchange of scientific and technical knowledge, ideas, lessons learned, and the fundamental science drivers shared by the various projects. It joined together participants from a number of active fault zone drilling projects, to address both the science and technology of drilling, sampling, testing, and long-term monitoring of active faults, especially those at plate boundaries.

Fault zone drilling projects are different from most other scientific drilling efforts. In general, fault zone targets include discontinuities and small, anomalous intervals in large rock volumes, rather than a continuous stratigraphic succession. The targets of interest are often the locations of poorest drilling conditions, such as a highly-fractured and potentially overpressured rock volume. The scientific approach shared by all fault zone drilling projects focuses on conducting extensive geophysical logging; *in situ* stress, fluid pressure and permeability measurements; core, cuttings and fluid sampling; and surface-to-borehole geophysical site characterization studies in and around active fault zones. These studies then often provide the basis for long-term downhole monitoring of seismicity, strain, fluid pressure and other parameters directly within or adjacent to an active fault zone. The technological complexity of these endeavors requires a concentrated multinational engineering effort, with step-by-step improvement of drilling, sampling, downhole measurements and long-term monitoring equipment and techniques, as fault zone drilling projects target ever-increasing depths and temperatures.

The Workshop on Fault Zone Drilling in Miyazaki was very successful in meeting these goals. It provided a forum for scientific and technological cross-fertilization between projects, and contributed to a much-needed transfer of experience and expertise from completed and ongoing fault zone drilling projects to those under development. This special issue of *Scientific Drilling* contains the workshop report, plus short and extended abstracts of many of the oral and poster presentations given at the workshop. It is hoped that this issue reflects the current trend of increased collaboration between fault zone drilling projects undertaken by IODP and ICDP, and highlights the healthy base of understanding of the mechanics of faulting and earthquake generation derived from fault zone drilling projects worldwide.


Harold Tobin Stephen Hickman Hisao Ito
 
Gaku Kimura Jan Behrman

Front cover: Seismicity of the San Andreas Fault as seen from a vantage point in the Earth looking to the northwest. Hypocenters were determined by Cliff Thurber and Haijiang Zhang (University of Wisconsin) and Steve Roecker (Rensselaer Polytechnic Institute) using data from the Parkfield Area Seismic Observatory as well as the USGS and University of California at Berkeley seismographic networks. The SAFOD main hole is shown in red, extending downward from the surface facility (star). The surface trace of the fault is shown in black draped over the topography. EarthVision plot prepared by Luke Blair (USGS). **Left Inset:** Part from "Earth system components, processes and phenomena" illustration by Asahiko Taira (CDEX) taken from the IODP initial science plan (2001).

Scientific Drilling is a semiannual journal published by the Integrated Ocean Drilling Program (IODP) with the International Continental Scientific Drilling Program (ICDP). The editors welcome contributions on any aspect of scientific drilling, including borehole instruments, observatories, and monitoring experiments. The journal is produced and distributed by the Integrated Ocean Drilling Program Management International (IODP-MI) for the IODP under the sponsorship of the U.S. National Science Foundation, the Ministry of Education, Culture, Sports, Science and Technology of Japan, and other participating countries. The journal's content is partly based upon research supported under Contract OCE-0432224 from the National Science Foundation.

Electronic versions of this publication and information for authors, can be found at <http://www.iodp.org/scientific-drilling/> and <http://www.icdp-online.org/scientific-drilling/>. Printed copies can be requested from the publication office.

IODP is an international marine research drilling program dedicated to advancing scientific understanding of the Earth by monitoring and sampling subsea-floor environments. Through multiple drilling platforms, IODP scientists explore the program's principal themes: the deep biosphere, environmental change, and solid earth cycles.

ICDP is a multi-national program designed to promote and coordinate continental drilling projects with a variety of scientific targets at drilling sites of global significance.

Publication Office

IODP-MI, CRIS Building-Room 05-101,
Hokkaido University, N21W10 Kita-ku,
Sapporo, 001-0021 Hokkaido, Japan.
Tel: +81-11-738-1075
Fax: +81-11-738-3520
e-mail: journal@iodp-mi-sapporo.org
url: www.iodp.org/scientific-drilling/

Editorial Board for Special Issue 1: Hisao Ito (Japan Agency for Marine-Earth Science and Technology), Jan Behrman (IFM-GEOMAR), Steve Hickman (U.S. Geological Survey), Harold Tobin (University of Wisconsin-Madison), Gaku Kimura (University of Tokyo).

Scientific Drilling:

Editor-in-Chief Hans Christian Larsen
Managing Editor Emanuel Soeding
Editor Ulrich Harms
Send comments to:
journal@iodp-mi-sapporo.org

Copy Editing

Glen Hill, Obihiro, Japan.

Layout, Production and Printing

Mika Saïdo (IODP-MI),
and
SOHOKKAI, Co. Ltd., Sapporo, Japan.

IODP-MI

Washington, DC, U.S.A.
Sapporo, Japan
www.iodp.org
Program Contact: Nancy Light
nlight@iodp.org

ICDP

GeoForschungsZentrum Potsdam
Potsdam, Germany
www.icdp-online.org
Program Contact: Ulrich Harms
icdp@gfz-potsdam.de

All figures and photographs courtesy of the IODP, unless otherwise specified.

Regular Number 6 of *Scientific Drilling* will be distributed in:

March 2008

Workshop Report

- 5 Joint IODP-ICDP Workshop Examines Challenges of Fault Zone Drilling

Part 1 : Scientific Motivations for Fault Zone Drilling

- 17 Fault Zone Drilling in Subduction Zones: The Accomplishments of Ocean Drilling and Associated Studies
18 Fault Characteristics, Energy Estimates, and Earthquake Recurrence: What *One* Seismologist Wants from Fault Drilling
20 Pore Pressure at Plate Boundaries: Insights from Geohydrologic Modeling
24 Dynamic Rupture Propagation Modeling
27 Fault Zone Complexity and Earthquake Ruptures

Part 2 : Overview of Recent Projects

- 29 Structure and Properties of the San Andreas Fault in Central California: Recent Results from the SAFOD Experiment
33 Drilling of the Chelungpu Fault after the 1999 Chi-Chi, Taiwan Earthquake (Mw7.6): Understanding Physics of Faulting
35 The Corinth Rift Laboratory or an *in situ* Investigation on Interactions between Fluids and Active Faults
39 The IODP Nankai Trough Seismogenic Zone Experiment
42 Drilling the North Anatolian Fault
45 Fault Zone Drilling in the Backstop to the Mediterranean Ridge Accretionary Complex off Crete, Greece

Part 3 : Fault Zone Structure, Composition, and Physical Properties

- 47 Generation Depth of the Pseudotachylite from an Out-of-Sequence Thrust in Accretionary Prism—Geothermobarometric Evidence
51 Drilling the Seismogenic Zone of an Erosional Convergent Margin: IODP Costa Rica Seismogenesis Project CRISP
55 Subsurface Structure, Fault Zone Characteristics, and Stress State in Scientific Drill Holes of Taiwan Chelungpu Fault Drilling Project
59 Drilling Investigations on the Mechanics and Structure of Faults
61 Clay Mineral Composition and Diagenesis: Effects on the Location and Behavior of Faults in the Frontal Portions of Subduction Zones
64 San Andreas Fault Zone Mineralogy, Geochemistry, and Physical Properties from SAFOD Cuttings and Core
68 Electron Microscopy of Clay Minerals in Mudrocks from the San Andreas Fault Observatory at Depth (SAFOD)
71 Real-time Mud Gas Monitoring: A Technique to Obtain Information on the Composition and Distribution of Gases at Depth While Drilling
73 Low-Velocity Damage Zone on the San Andreas Fault at Depth near SAFOD Site at Parkfield Delineated by Fault-Zone Trapped Waves
78 High-resolution Imaging of Fault Zone Structures with Seismic Fault Zone Waves
80 Modern and Ancient Out-of-Sequence Thrust in the Nankai Trough: Insight from Laboratory-Derived Properties and Seismic Data
82 Comparison between Three Out-of-Sequence Thrusts from Japan and Alaska: Implications for Nankai Drilling Targets from the Rock Record

Part 4 : The Physics of Earthquake Rupture

- 84 Seismology Inside the Fault Zone: Applications to Fault-Zone Properties and Rupture Dynamics
- 88 Monitoring of Rock Mass Behavior at the Closest Proximity to Hypocenters in South African Gold Mines
- 92 Dynamics of Earthquake Faulting in Subduction Zones: Inference from Pseudotachylytes and Ultracataclasites in an Ancient Accretionary Complex
- 94 Precise Temperature Measurements and Earthquake Heat Associated with the 1999 Chi-Chi, Taiwan Earthquake
- 97 The Coseismic Fault Weakening Processes Inferred from Frictional and Transport Properties of Fault Rocks, TCDP

Part 5 : Technological Challenges of Drilling, Testing, Sampling, and Monitoring in Fault Zones

- 98 Drilling and Completion Challenges in Fault Zones: Lessons Learned from ICDP Projects
- 100 Drilling Challenge for the NanTro Fault Zone Drilling by *Chikyu*
- 101 Coring Techniques for Scientific Investigation of Faults
- 103 Core Handling and Real-Time Non-Destructive Characterization at the Kochi Core Center: An Example of Core Analysis from the Chelungpu Fault
- 107 Third-Party Borehole Seismic Experiments during the Ocean Drilling Program
- 110 Borehole Seismic and Strain Observatories in Seafloor Settings—Experiences after ODP Legs 186, 191, 195 and Future Plans
- 113 BABHY—A New Strategy of Hydrofracturing for Deep Stress Measurements
- 117 Long-term Monitoring in Deep Boreholes in the Nankai Subduction Zone

back cover Workshop Participants

Joint IODP-ICDP Workshop Examines Challenges of Fault Zone Drilling

by Harold Tobin, Hisao Ito, Jan Behrmann,
Steve Hickman, and Gaku Kimura

doi:10.2204/iodp.sd.s01.80.2007

Introduction

This decade will likely be regarded in the geosciences as a time of an unprecedented explosion of fault zone drilling projects. The past few years have seen the initiation of projects including the Nojima Fault Drilling, San Andreas Fault Observatory at Depth (SAFOD), the Taiwan Chelungpu Fault Drilling Project (TCDP), the Gulf of Corinth Rift Laboratory (CRL) on land, and the Nankai Trough Seismogenic Zone Experiment (NanTroSEIZE) and Costa Rica Seismogenesis Project (CRISP) at sea (see Table 1 for references).

Each of these projects has unique objectives and scientific drivers, yet they share the fundamental goal of seeking direct access to zones of active faulting, particularly ones that generate earthquakes or have hosted seismic slip. This burgeoning interest in active fault drilling is taking place in the context of very rapidly growing research efforts on the mechanics and dynamics of faulting processes, integrating rock mechanics, seismology, geodesy, frictional physics, and fluid-fault interactions. There is a widespread recognition that our science lacks an integrated theory and understand-

ing of the fundamental processes governing earthquakes and fault behavior, and the factors that control their natural variability.

On 23–26 May 2006, eighty scientists and engineers from around the world gathered for the *IODP-ICDP Workshop on Fault Zone Drilling: Developing a Global Perspective* in Miyazaki City on the island of Kyushu, Japan to explore the common ground—as well as the unique aspects—of all of these projects and to develop a consensus on the state of understanding of faults in the shallow crust and challenges to target in future work. The group represented a very broad spectrum in the Earth sciences, including seismologists, rock mechanicians, structural geologists, instrumentation specialists, geochemists, and many other specialties.

We have had over a century of detailed surface seismological observations, laboratory friction studies, geological observations, and case histories of earthquakes, yet processes acting at the fault interface remain elusive—because they occur deep in the subsurface, because faults are inherently heterogeneous materials, and because the initiation and propagation of fault rupture take place through complex and commonly non-linear physical processes. The physics of

Table 1. Major Currently-Active Fault Zone Drilling Projects.

Project	Location/Earthquake	Tectonic Setting	Principal Funding Agency	Overview Reference
SAFOD: San Andreas Fault Observatory at Depth	San Andreas Fault California, U.S.A.	Continental transform	NSF-EarthScope and ICDP	Zoback et al., 2006
TCDP: Taiwan Chelungpu Fault Drilling Project	Chelungpu Fault Taiwan ROC 1999 Chi-Chi M 7.6	Arc-continent collisional thrust	Taiwan, Japan-MEXT, and ICDP	Ma et al., 2006
CRL: Gulf of Corinth Rift Laboratory	Helike Fault Zone Corinth, Greece	Continental back arc rift	EESD-European Union and ICDP	Cornet et al., 2004
NanTroSEIZE: Nankai Trough Seismogenic Zone Experiment	Nankai Trough, Southwestern Japan	Subduction zone megathrust	IODP	Tobin and Kinoshita, 2006
Nojima Fault Drilling	1995 Kobe Earthquake, Kobe, Japan	Continental transform	NIED, GSJ, Universites	Ito et al., 1999, Oshiman et al., 2001
NELSAM and SeeSA	Mining-induced seismicity in South African Mines	Intraplate, reactivated faults	ICDP, NSF, NRF South Africa, MEXT	Reches et al., 2006, Ogasawara et al., this issue
CRISP: Costa Rica Seismogenesis Project	Costa Rica	Erosional subduction zone	IODP	Ranero et al., this issue
GONAF: Geophysical Observatory on the North Anatolian Fault	North Anatolian Fault, Marmara Sea, Turkey	Continental transform	ICDP (workshop)	Dresen et al., this issue

faulting in the crust, including the entire spectrum from aseismic creep through transient slow slip to rapid seismic slip, is a fundamental Earth process but one for which no integrated theory exists. Seismology, laboratory experiments in mechanics and friction, theoretical and modeling efforts, and fault zone geology and hydrology have all led to an understanding of the complexity of faulting and to hypotheses for many of the important processes. Testing of many of these ideas requires direct access to the actual active faults in the subsurface to collect new types of data that cannot be obtained by other means (e.g., Mori, this issue). This gap is the source of the need for the present rapid expansion of fault zone drilling.

Fault zone drilling projects are quite different in many respects from most other scientific drilling efforts. While a climate history project, for example, focuses mainly on acquiring a complete stratigraphy in cores and logs, fault zone projects target very specific zones for both coring and downhole measurements. In general, fault zone targets include *discontinuities* and small anomalous intervals in large rock volumes, rather than the stratigraphic column or broader rock volume of many other projects. The targets of interest are often the exact locations of poorest drilling conditions, such as a highly-fractured damage and gouge zone with potential for excess pore pressure above hydrostatic condition, anomalous stress state, weak rock, and other drilling hazards (Higuchi and Kobayashi; and Prevedel; this issue). The scientific approach commonly focuses on obtaining very extensive downhole measurements, logs, cores, and seismic structure in and around these fault zone environments. Measurements at the time of drilling as well as long-term observations are emphasized. All of these activities are technically very demanding, and in some cases they diverge from “standard” industrial borehole practice, so that creative new uses of existing technology or development of new technology is required.

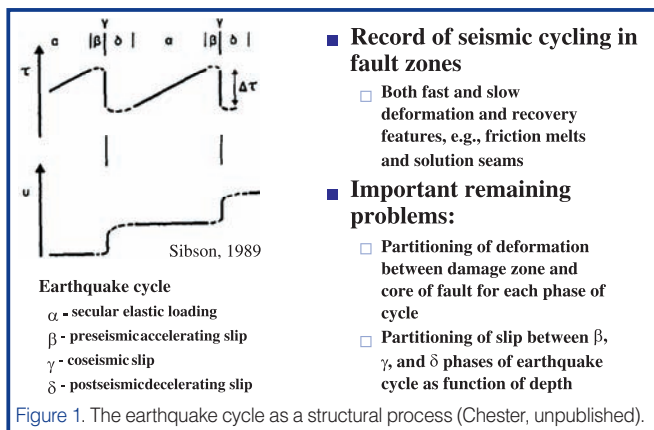
Science Drivers for Fault Zone Drilling

Understanding the complex physics of tectonic faulting, earthquakes, and the generation of tsunami in the Earth's crust is among the grand remaining challenges of the geosciences. Because earthquakes take place deep below the Earth's surface, direct observation of processes acting in the faults themselves has generally not been possible; what we know about earthquake processes is derived from seismologic observations, geodetic deformation, and studies of exhumed rocks containing products of slip at depth long ago. Researchers have learned and inferred a great deal from these studies, but they are inherently limited. Much of fault zone drilling is aimed at understanding earthquake slip, but in fact fault physics encompasses a spectrum of slip and slip rates ranging from purely aseismic behavior, such as steady creep, through events such as slow earthquakes and creep, to true seismicity (Fig. 1).

Workshop Organization

The Miyazaki workshop provided an overview of past, active, and planned drilling projects in diverse tectonic settings. The range of plate boundary fault systems was very well represented, including convergent (both subduction and collision) thrust-fault systems, divergent (rift) normal-fault systems, and transform strike-slip fault systems. Intraplate, relatively small-scale but active (and in some cases very destructive), faults are also under intensive study in projects reported on and discussed at the workshop. The workshop comprised three meeting days, all in plenary session, and a full-day field trip between the second and third meeting day to visit spectacular seaside exposures of the Nobeoka thrust fault near the town of Nobeoka. This thrust fault is interpreted as an exhumed formerly active plate boundary thrust fault at seismogenic depths in a subduction-related accretionary complex (Kondo et al., 2005). The field trip vividly illustrated the challenges of fault zone drilling, as scientists and engineers examined a zone of chaotically folded, fractured, and damaged rock tens of meters thick surrounding a fault core only tens of centimeters thick with even thinner slip surfaces embedded within it (see cover illustration; Tsuji et al.; and Ujiie; this issue). These narrow zones and wider unstable rock areas would present a challenge as targets of drilling, core recovery, and downhole measurement.

Participants (see back cover) contributed to an agenda organized around a series of themes. The first day of the workshop was devoted to several presentations discussing the motivations for fault zone drilling, including how to get seismologists, fault geologists, and those of other interested disciplines working together using common terminology and ideas. It also featured overviews of the main recent and active drilling projects, summarized below, and of key topics such as fault zone structure, seismology, hydrology, and modeling of fault physics. The second day began with a session devoted to seismology, strain measurements of several forms, and remote geophysical detection of physical properties in and around faults. This was followed by a session focused on the structure and composition of fault zones from outcrops and borehole samples and logging. Each session was accompanied by plenary discussion, which ultimately led to the consensus recommendations described below. The third day was devoted to the field trip to the Nobeoka thrust, where fault structures were observed in outcrop. Finally, on the fourth day of the meeting, several presentations described newly proposed or emerging future projects, and then the rest of the day was devoted to technological challenges for sampling, sample handling, drilling and completion, and downhole measurements and monitoring. The workshop was closed out with an extended period of plenary discussion, highlighting many of the areas of future opportunity as well as challenges. Posters on many specific projects and topics related to all of these sessions were displayed for the duration of the meeting, and the contents of many are reflected in the extended abstracts of this volume.



Significant recent progress in understanding the mechanics of earthquakes and fault slip has been achieved through new seismological and geodetic observations, fault geology, laboratory experiments, and theory (Fig. 2). However, the factors controlling stable vs. unstable slip on faults remain poorly understood, impairing our ability to evaluate associated hazards. At present, there is no unified theory of fault slip to account for earthquake nucleation and propagation, nor to explain the mechanisms of strain across the spectrum of different deformation rates now being observed with durations ranging from seconds to years. Our understanding of the mechanics and dynamics of plate boundary faulting is severely limited by a lack of information on ambient conditions and mechanical properties of active faults at depth. A major present goal in earthquake mechanics research is thus direct *in situ* sampling and instrumentation by drilling into the seismogenic zone of active faults, including both inter- and intra-plate fault systems in many tectonic settings.

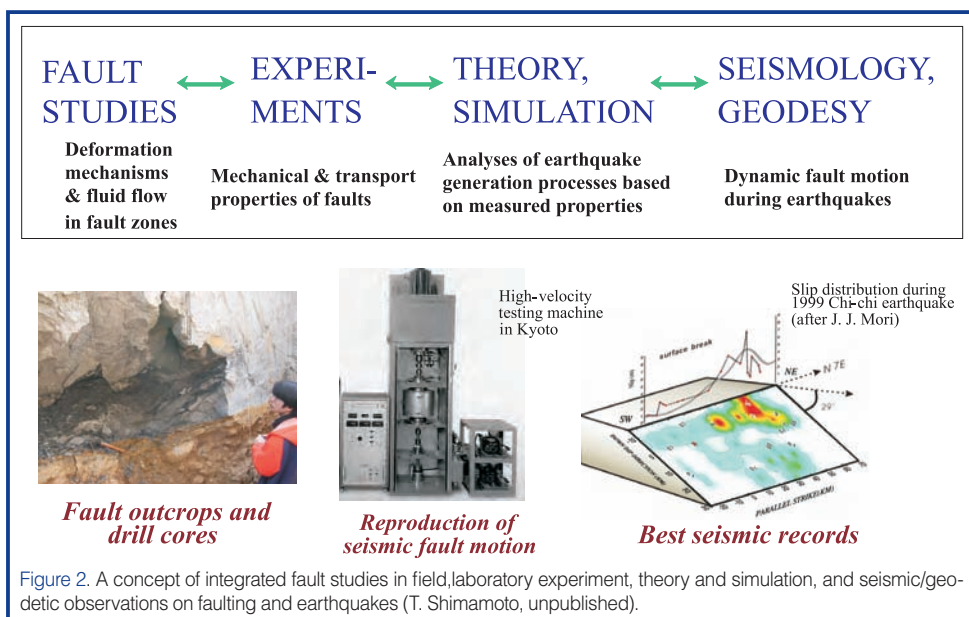
Here, we briefly summarize some of the key scientific motivations for engaging in fault zone drilling that were especially highlighted at the workshop. Two recently published reviews of fault zone drilling activity by Reches and Ito (2007) and Zoback et al. (2007) both discuss the principal specific scientific goals of recent, active, and planned projects in detail, and it would be redundant to duplicate them here.

Zoback et al. (2007) summarized the fundamental motivation well, writing: "It is currently impossible to differentiate between—or even adequately constrain—the numerous conceptual models of active faults proposed over the years (Fig. 3). For this reason, the Earth science community is left in the untenable position of having no generally accepted paradigm for the mechanical behavior of faults at depth." This fundamental igno-

rance drives the research objectives of many of the projects touched on at this workshop. Some of the key questions include the following. What are the deformation mechanisms of fault slip in both aseismic and seismic conditions? Why is slip sometimes seismic, sometimes aseismic, and sometimes in an intermediate state, and what governs the transitions among these processes? How do earthquakes nucleate, and how does rupture grow and stop? Are there precursory phenomena in the fault or near field that indicate a preparatory phase to earthquake or slip nucleation? If so, can a prediction or early warning strategy based on borehole observation be developed? What are the processes governing tsunamigenic slip? What is the role of fluid content and fluid pressure in modulating faulting processes, especially during rapid seismic slip? How does permeability of the fault zone evolve interseismically and coseismically? What is the stress tensor in and around a fault zone throughout the earthquake cycle or other slip? What controls localization of slip vs. distributed strain in faulting? Fault zone drilling is justified by the need to shed light on these and related questions if we are to develop that paradigm for faults at depth.

Most, but not all, of the fault zone drilling efforts highlighted during the workshop focus on elucidating earthquake processes, though some have focused on aseismic faulting, particularly in accretionary prisms (Moore, this issue). The objectives and activities of the various fault zone drilling projects can be summarized as falling into three basic categories:

1. *Direct sampling of fault zone and surrounding rocks and fluids:* Acquiring samples (core, cuttings, and fluids) from the subsurface in a relatively pristine state for further study is a universal high priority (see Part 3 section this issue on Fault Zone Structure, Composition, and Physical Properties). The mineralogy, microstructure and fabric, mechanical properties, and fluid content and composition are all relevant to discovery of the physical processes involved in aseismic



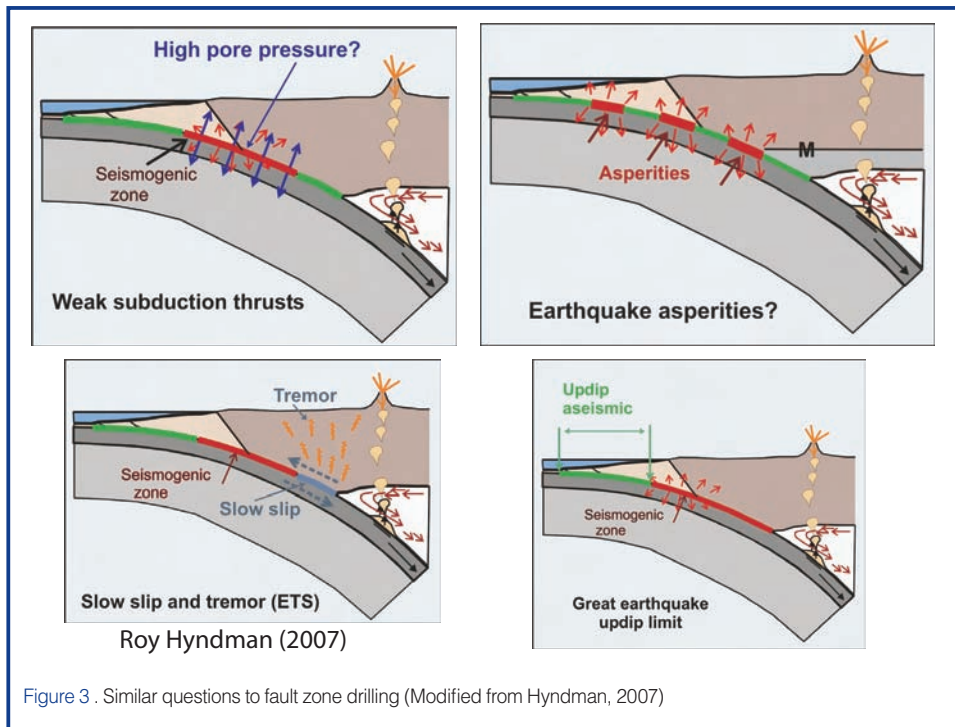


Figure 3. Similar questions to fault zone drilling (Modified from Hyndman, 2007)

seismic preparation phase—before nucleation of a major event—that might be detectable through near-field observations in the subsurface. Transient slip events, fault creep, and bursts of microseismicity may take place during the interseismic period on large faults and provide important information on mechanical process and constitutive properties. In other cases, such as deep mine fault drilling and seismicity studies, the monitoring is tied to active manipulation of the pore pressure and stress field, for a more explicit form of *in situ* experimentation (Ogasawara et al., this issue).

Current and Completed Projects

and seismic faulting. Only samples obtained from *in situ* positions can unequivocally be associated with fault processes uncontaminated by later alteration. Samples provide material for geological, geochemical, and petrophysical analyses to deduce the record of fault processes in the rocks (including ephemeral properties derived from very recent slip in some cases, such as TCDP or Nojima drilling). They also provide ground-truth to calibrate remote-sensed geophysical measurements based on seismic velocity and reflectivity, resistivity, gravity, and other observations over much larger volumes of the crust surrounding the borehole.

2. Conducting active tests or observations *in situ* in faults through borehole access: Besides the samples obtained through drilling, the borehole itself is a window into the fault zone and the faulting process. Borehole logging for detection of physical properties and imaging of stratigraphy, fractures, breakouts, and other features; downhole experimentation such as hydrologic testing through the use of borehole seals (packers); and collection of fluid samples are all emphasized to varying degrees in these projects (e.g., Hickman et al.; and Ito, this issue).

3. Monitoring the fault zone over time in borehole observatories: Long-term access to and use of the boreholes are key elements of most of these projects, though they are limited in many cases by technical challenges or budget. Monitoring of seismic activity, temperature, the strain field, pore fluid pressure, and seismic velocity structure of the fault zone and surroundings are consensus objectives across most of these programs. Borehole-based observations can be complemented by surface instruments such as land-surface or ocean-bottom broadband seismometers. A key question in fault zone studies is whether there is any evidence for a pre-

The workshop included presentations and exploration of virtually all of the major fault drilling projects worldwide in the past two decades. Most of these projects are represented by one or more papers in the accompanying extended abstract section. One interesting theme that emerges from this review is the following specific strengths associated with land-based and ocean-based drilling. ODP fault zone drilling at sea has been tightly integrated with high quality geophysical imaging (usually 3-D seismic reflection datasets that allow precise targeting), has made very productive use of logging-while-drilling (LWD) technology and cores by drilling multiple holes at the same location, and has deployed multiple sealed boreholes for hydrologic and other observations (Moore; Ranero; and Tobin and Kinoshita; this issue). The results include a great deal of quantitative information about the physical and hydrological properties of faults in relatively shallow (and aseismic) positions beneath the ocean floor in subduction zones. On land, by contrast, a major emphasis has been on sophisticated downhole experimentation and imaging, including seismology, hydraulic fracturing tests, breakout analysis, and more (Cornet; and Ellsworth et al., this issue). Land based boreholes have also obtained very high quality core in many cases, permitting detailed structural and petrological analyses of fault zone properties (Hung et al.; Lin et al.; Nielson; and Omura; this issue). It is therefore clear from the brief review below that oceanic and continental drilling studies of faults have been complementary operations to date, each advancing our understanding on different topics.

The section below is meant merely as a brief introduction to each area; an exhaustive review of the literature for each is beyond the scope of this paper. In roughly chronological order, the major projects discussed at the workshop were as follows.

KTB Project, Germany: The Kontinentales Tiefbohrprogramm der Bundesrepublik Deutschland (KTB), or German Continental Deep Drilling Program, was drilled from 1990 to 1994 in southeastern Germany. It is one of the deepest drilled holes on Earth, having reached 9101 m below the surface (Emmermann and Lauterjung, 1997). While not primarily intended as a fault zone project, KTB drilling did cross a tectonically inactive thrust fault system in metamorphic crystalline rock. Drilling activity, including fluid circulation and hydraulic fracturing tests and other perturbations of the borehole environment, caused microseismic activity in the near-field to the borehole, permitting analysis of the *in situ* state of stress (Zoback et al., 1993), presence of fluids and hydrologic properties, and thermal properties of the continental crust in this region. Many techniques used in continental drilling were pioneered or refined during KTB drilling.

Barbados Accretionary Wedge, Atlantic Ocean (ODP 110, 156, 171A): The Barbados wedge was the focus of substantial effort during DSDP and ODP, aimed at understanding the faulting conditions, ambient pore fluid pressure (Fig. 4), and mechanics in a very low angle (~2 degree dip) décollement thrust fault at the base of an accretionary wedge (see Moore, this issue). A high quality 3-D seismic survey (Shipley et al., 1994) imaged the décollement plane reflector in unprecedented detail, and served as the basis for targeting drilling into the ~30–40-m thick décollement zone in areas of contrasting reflection amplitude and character, all in the relatively shallow and presumed aseismic portion of the plate interface at the base of the accretionary wedge. Drilling and logging measurements made while drilling (LWD) demonstrated that the fault zone was a mechanically very weak interval with high excess pore fluid pressure and patchily distributed areas of anomalously high porosity (Moore et al., 1998). Installation of a borehole seal (CORK), downhole testing, and other studies at Sites 948 and 949 have shown that the fault zone has effective permeability that is strongly pressure dependent and varies over ~4 orders of magnitude with fluid pressure (Fisher, 2005; see also Saffer, this issue).

Nankai Trough Accretionary Wedge, Muroto Region, Western Pacific Ocean (ODP 131, 190, 196): Drilling by ODP of the central Nankai Trough region off Shikoku island also focused on the décollement zone at the outer toe of the accretionary deformation, and provided a detailed understanding of the mechanics of the fault zone (Moore et al., 2001). The 20–30-m-thick fault zone encountered at Sites 808 and 1174 is a zone of strong brittle fracture deformation that separates hydrologically distinct regimes above and below the fault; the footwall is at least partially sealed and pressurized with superhydrostatic pore fluid, limiting the effective normal stress that can act at the fault plane (Screaton et al., 2002). Microstructural and fabric analysis established that the décollement zone represents a virtually total strain decoupling of the footwall beneath the detachment, with basinal stress and strain state, and the accretionary wedge in the hanging wall, with hetero-

geneous and tectonically-enhanced strain (Byrne et al., 1993). These observations imply the décollement acts as a plane of very low shear strength during deformation. LWD measurements, especially resistivity and density data, suggest that the décollement fault has a core of compacted but fractured rock that is dilated in the high pore fluid pressure environment (Bourlange et al., 2003).

Nojima Fault Projects, Japan: Soon after the Kobe earthquake in 1995 (M6.9), several research teams drilled multiple boreholes into and across the shallow portion of the Nojima fault (the locus of that event) from ~750 m to ~1800 m depth (Ito et al., 1999; Omura, this issue,). Detailed compositional and structural analyses identified a narrow fault core of gouge and surrounding damage zone, with asymmetric structure in the footwall and hanging wall (Boullier et al., 2001; Fujimoto et al., 2001; Ito et al., 1996; Ohtani et al., 2001; Tanaka et al., 2001). Shear wave splitting studies of aftershocks showed a rapid evolution of fast direction after the earthquake, interpreted as evidence of fracture healing during a 12 month post-seismic period (Tadokoro and Ando, 2002). The preliminary results were collected in the special 2001 volume of *The Island Arc*. From repeated injection tests, permeability change with time was observed (Tadokoro et al., 2000). The structural properties (fault-zone width, shear wave velocity, and Qs) of the Nojima Fault were studied using the Love-wave-type fault-zone trapped waves (LTWs) recorded at two borehole seismic stations, which were con-

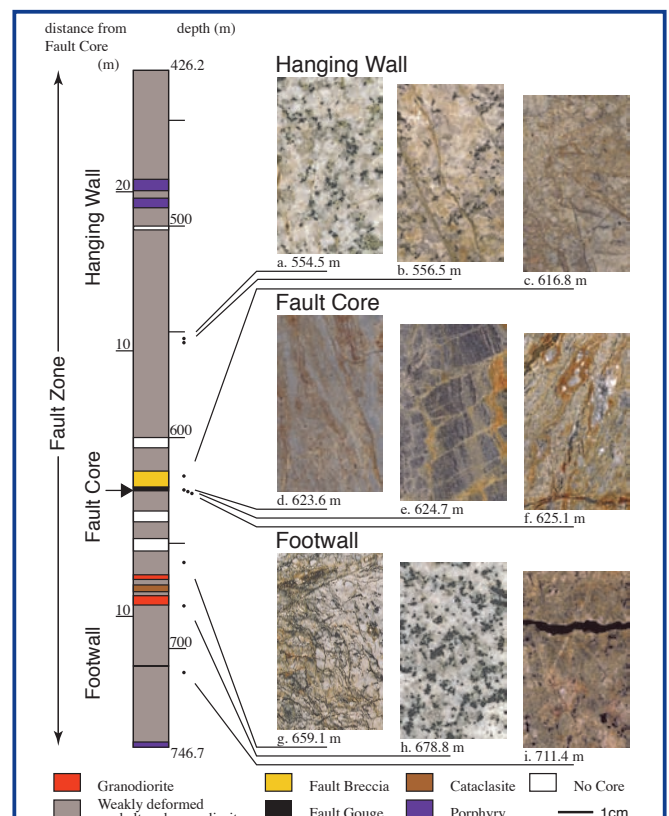


Figure 4. Fault zone structure of the Nojima fault. **Hanging wall:** Intensity of minor shear zones and the content of brown feldspar increase, and the mafic mineral content decreases toward the fault core. **Fault core:** Note three types of fault gouge. **Footwall:** These rocks are much less intensely deformed and altered than in hanging wall (Modified from Ohtani et al., 2000).

structed after the 1995 Kobe earthquake (Mizuno et al., 2007).

Costa Rica Convergent Margin, Nicoya Region, Eastern Pacific Ocean (ODP 170, 205): The Costa Rica margin off the Nicoya Peninsula in northwestern Costa Rica has been the site of two ODP expeditions that penetrated the décollement and other faults in two principal locations at depths of a few hundred meters below sea floor. Drilling demonstrated that the décollement fault overrides the subducting plate and all of the sedimentary section lying on top of it, such that the fault develops in a layer of extreme mechanical weakness made up of unconsolidated sediments (Silver et al., 2000). Structural studies and geochemical tracers of hydrological flow paths suggest that two strongly decoupled systems exist above and below the ~20-m-thick main fault zone, which acts simultaneously as a low-permeability barrier to cross fault flow and a high-permeability channel for along-fault flow (Tobin et al., 2001). Installation of a sealed borehole CORK during Leg 205 documented an apparently weakly overpressured décollement zone that exhibits temporal pressure excursions tied to apparent aseismic transients recorded geodetically on land (Davis and Villinger, 2006).

Corinth Rift Laboratory, Greece: The Gulf of Corinth is a location of back-arc extension within the Hellenic Arc system and is among the most seismically active areas of Europe (Cornet, this issue). The Corinth Rift Laboratory (CRL) Project drilled into the Aigion fault at 760 m depth and continued to 1000 m, encountering cataclastic fault rocks in a karstic carbonate host-rock environment. The fault zone forms a strong hydrologic barrier with an associated pressure differential across it. Transients in pore pressure have been detected associated with remote earthquakes (Cornet et al., 2004). Plans for upcoming activities at CRL include near-term deployment of a string of high-frequency three-component geophones, packers, pressure transducers, tiltmeters, and thermistance meters across the fault penetration, and also a proposed 4.5-km-deep borehole to monitor pore pressure and other features of the seismogenic zone (Cornet, this issue).

Taiwan Chelungpu Drilling Project, Taiwan: The devastating 1999 M7.6 Chi-Chi earthquake in Taiwan was a thrust event in a collisional tectonic setting that exhibited very large slip (>10 m), including large surface displacements, on the Chelungpu fault. The principal objective of drilling was to sample the main slip surface or zone, if one could be identified, in the relatively short post-seismic period. The fault zone was drilled in 2004 and 2005 in an area of high-velocity large slip during the main shock, and crossed the fault zone and several hundred meters of the footwall in two adjacent holes (Ma et al., 2006). The main slip zone and several subsidiary (or older) fault cores were identified in the borehole at ~1100 m depth (Hung et al., this issue). Studies of the fault gouge particle size, thickness, and composition have yielded quantitative estimates for the work done in forming gouge

and damage (fracture energy), contributing to the understanding of energy budgets during earthquakes (Ma et al., 2006; Ma and Tanaka, this issue). Borehole hydrologic tests, temperature logging, and sample-based frictional experiments have all contributed to a tight integration of borehole derived information with seismological observations.

San Andreas Fault Observatory at Depth, California, U.S.A.: SAFOD targeted the San Andreas fault in a location at the transition from the locked zone that has ruptured repeatedly in M~6 earthquakes and the creeping segment to the north, where no large earthquakes have been observed. The location was chosen in part for the wealth of geophysical and other data generated during the decades-long Parkfield Experiment, where microseismic activity is very well located. The primary objectives included drilling into and across the San Andreas in a highly deviated (~55°) hole to sample and log the fault zone environment and materials, and to place instruments into the nucleation zone of one or more repeating earthquakes of magnitude 1–2. Fault rock properties, stress, pore pressure, and temperature *in situ*, and near-field observations of the earthquake process are key objectives of the research program (Ellsworth et al., this issue). A pilot hole was drilled in 2002 (Hickman et al., 2004), then the main hole crossed and logged the SAF in 2005. A zone ~230 m wide of low seismic velocity and density was detected at ~3100 m below the surface, in host rock of siltstones, shales, and sandstones, interpreted as a broad damage zone (Schleicher et al.; Solum et al.; and Wiersberg and Erzinger; this issue). Within this zone, several narrower bands of apparently more concentrated deformation, and velocity reduction were detected, including locations where the casing installed in the borehole has deformed since installation, interpreted as due to active fault creep. Temperature measurements to date and deduced stress orientation (Boness and Zoback, 2006) are consistent with the paradigm of a weak fault in a strong crust. Phase 3 drilling in 2007 targets continuous coring of three holes across the active fault traces as sidetracks from the main hole, and will finish with installation of a monitoring system to be placed within the rupture patch of M2 earthquakes (Ellsworth et al.; Hickman et al.; this issue).

Fault Drilling in South African Mines (NELSAM and SeeSA): Deep gold mines in South Africa, among the deepest in the world, contain Precambrian age faults that have been reactivated and accessed by recent mining operations. These faults have been extensively used as natural laboratories for research programs by several groups from Japan, the U.S.A., Europe, and South Africa. Ogasawara et al. (2002; this issue) describe installation of strainmeters and arrays of accelerometers in faults in several different mines as part of the project Semi-controlled Earthquake-generation Experiments in South African deep gold mines (SeeSA). Large strains were recorded co-seismically during events of magnitude ranging from -1 to 3.0. Even the smallest events showed source processes as complex as those of larger earthquakes, and

hypothesized accelerating strain phenomena preceding seismic events were generally not observed. The Natural Earthquake Laboratory in South African Mines project (NELSAM) has taken the strategy of densely instrumenting a network of faults in the TauTona mine (Reches, this issue) with accelerometers, seismometers, strainmeters, temperature sensors, creep-meters, an electromagnetic radiation system, and acoustic emissions detection, in anticipation of magnitude ~2 events expected to be induced by mining operations.

Recent Progress in Technology

In response to scientific objectives, recent progresses in drilling (Higuchi and Kobayashi, this issue), logging, coring and observatory (Ito, this issue) were reported at the workshop. It was emphasized that operational issues (such as penetration rate, hole stability, direction control, over/under pressure) and quality control on core and borehole conditions should be carefully considered according to the scientific objectives.

For the logging, the following new technologies are discussed:

- LWD is crucial to make measurements in unstable formations, and provides extremely fast a full set of data allowing full characterization before coring.
- Wireline logging has higher resolution and, in particular sonic tools, offers measurements not available in LWD (anisotropy, full waveforms, permeability).
- Care must be taken when using LWD, wireline logging, and coring in different holes.
- Future IODP vessels will allow measurements that were not available in ODP.

Designing the wells for life is a paradigm change in scientific drilling and involves permanent monitoring and well completion technologies. One of the advantages of borehole observatory is noise reduction (Fig. 5; Ito, this issue), and new technologies on deep borehole observatory have been developed.

Planned Future Projects

In this section, we summarize a few additional projects that have been funded or for which planning and/or pilot drilling activity is underway and advanced. Additional projects that are currently at the proposal stage are highlighted in the accompanying abstracts (Kopf and Bohnoff, this issue).

Nankai Trough Seismogenic Zone Project (NanTroSEIZE): As the December 2004 Sumatra earthquake and Indian Ocean tsunami so tragically demonstrated, large subduction earthquakes represent one of the greatest natural hazards on the planet. Accordingly, drilling into and instrumenting

an active interplate seismogenic zone are very high priorities in the IODP Initial Science Plan (2001). Through a decade-long series of national and international workshops, a consensus emerged that the Nankai Trough is an ideal place to attempt drilling and monitoring of the seismogenic plate interface. Factors in this selection include the relatively shallow extent of large slip and moment release in the 1944 M8.1 Tonankai earthquake, the good quality imaging of targets for drilling through multichannel seismic reflection surveys (including 3-D), and the vast amount of geophysical study that has gone into characterizing this subduction zone (Tobin and Kinoshita, 2006). NanTroSEIZE targets a series of thrust fault crossings at depths below the sea floor from <1000 m to >5000 m, to span the hypothesized up-dip transition from seismic to aseismic faulting processes. Coring, logging, downhole measurements, and the establishment of multiple instrumented boreholes spanning this zone are key objectives to address the questions of what controls the onset of seismogenic behavior with depth and how the faults behave spatially and temporally during interseismic and coseismic periods. The first phase of NanTroSEIZE drilling operations has now been scheduled for the fall of 2007 (Tobin and Kinoshita, this issue).

Costa Rica Seismogenesis Project (CRISP): CRISP is focused on access to the plate interface of a subduction zone where there is apparent “tectonic erosion” (the physical transfer of mass from the overriding plate to the downgoing plate at a subduction zone through thrust faulting). Erosional margins likely feature fault systems formed of protolith and fluid/heat conditions very different from accretionary margins such as Nankai (von Huene et al., 2004), because they may juxtapose crystalline crust of the upper plate with the downgoing basaltic slab and/or quantities of subducted sediment in the seismogenic zone. The CRISP-proposed project to IODP aims to drill first into the shallow portion of the plate

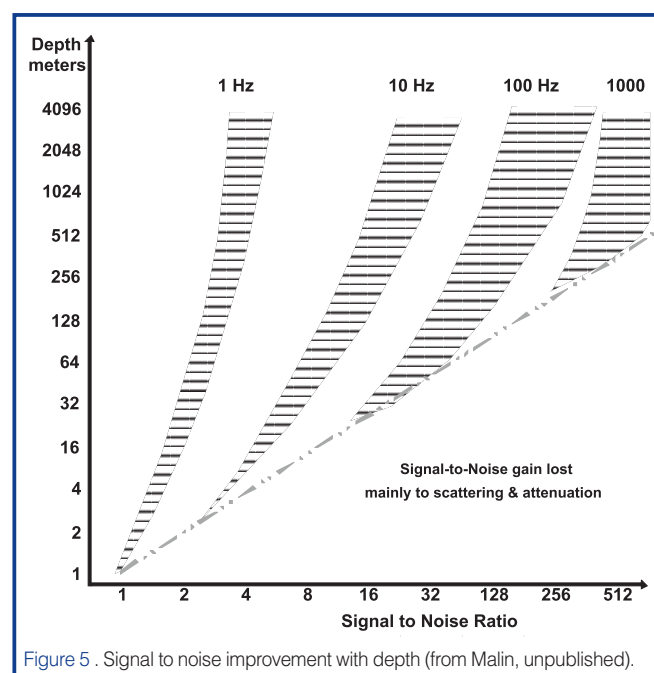


Figure 5. Signal to noise improvement with depth (from Malin, unpublished).

interface at 1–3 km below the sea floor, to sample the rock and fluid inputs and outputs to and from the seismogenic plate boundary, then in a later phase to drill to depths of ~7 km below the sea floor, into the slip region of a 2002 magnitude 6.4 earthquake (Ranero et al., this issue).

Proposed North Anatolian Fault (NAF) Drilling: The North Anatolian fault is a strike-slip plate bounding continental fault that represents the greatest known seismic hazard to life and property in Europe (Dresen et al., this issue). This fault separates the Anatolian block from Eurasia, and has produced a devastating series of M~7 earthquakes in the past century, most recently the Izmit and Düzce quakes of 1999. The fault zone extends through the bed of the Marmara Sea near Istanbul, a location of identified seismic gap on the NAF. Coulomb stress analysis suggests that the 1999 earthquakes transferred positive stress change to this offshore segment, and an estimated probability of a major M~7 earthquake is 35%–70% in the next 30 years (Parsons, 2004). Dresen et al (this issue) propose an ICDP project involving a 2000-m-deep borehole to be drilled from an island in the near vicinity of the NAF to monitor seismicity, stress and stress changes, heat, and fluid flow. The goal is a monitoring system to better understand the temporal evolution and interseismic behavior of the NAF, with an eye also toward elucidating seismic hazards to the millions of inhabitants of the city of Istanbul and surrounding regions.

Outcomes of the Workshop— Recommendations for Future Efforts

Exploration at this workshop identified a host of topics and issues related to the science and technology of fault zone drilling. A common theme of these projects is that they seek to acquire three basic types of data: (1) studies of samples, including cores, cuttings, and fluids; (2) “spot” downhole measurements, including wireline and LWD/MWD logging, packer systems and other downhole testers, and borehole/casing surveys; and (3) long-term monitoring data, including seismicity, strain and tilt, temperature, and continuous fluid sampling.

All of these areas were the subject of extensive discussion during the workshop. The most essential conclusion was that the Fault Zone Drilling Workshop was in a sense an introductory meeting—individuals working on the many IODP, ICDP, national, and other projects came together to identify common themes and challenges. The dialogue has started and has already led to enhanced interaction among the various scientific constituencies in the time since the workshop was held. The most useful way forward would be for IODP and ICDP to take the sponsorship role to make sure that dialogues continue on a number of key, specific areas in the future. Before and after the 2006 workshop, the economic environment for mounting ambitious drilling efforts has steadily worsened, from the standpoint of business and funding of high-cost, high-risk science in several countries.

Nevertheless, we suggest that IODP and ICDP can realize greater efficiency and success in future operations by leading efforts to combine force and expertise in new approaches to fault zone drilling.

Specific Recommendations: A number of recommendations for future efforts emerged during the numerous plenary discussions held throughout the workshop, as well as through the more informal interactions during poster sessions, evenings, and the field trip. These recommendations in some cases were for new driving questions and new strategies for subsurface access to faults; others were of a more technical or organizational nature.

The following overarching recommendations emerged:

- IODP and ICDP are urged to engage in joint efforts to develop optimal drilling techniques and drilling/casing/completion technologies specific to the fault zone environment.
- Through focused workshops, IODP and ICDP and the community should develop or document “best practices” statements for coring systems, core handling, and core orientation and for cuttings and fluids.
- Information exchange between IODP/ICDP/other drilling communities should be strengthened.
- The community should prioritize the development of plan(s) for a rapid drilling response to a suitable earthquake, on national and/or international levels.
- Sensor and deployment systems for monitoring should be identified/developed that are robust at temperatures of 120°C–160°C or greater (and have low power consumption for oceanic settings).
- New fault zone drilling proposals should be fostered through workshops networking with existing teams.

Grouping together several of these recommendations into themes, the motivation behind each and the specific recommendations as workshop outcomes are as follows.

1. Follow up with smaller working-group workshops on specific technical topics: The workshop identified many specific areas where new approaches and new technologies are either needed or have been developed for some projects but not yet widely adopted. We recommend that future joint efforts of IODP and ICDP include focused, small-team meetings to develop detailed “best-practices” for each area. Example topics for such working groups might be as broad as “Site Characterization” and as specific as “Core Orientation Methods”. Other suggested areas for focus include: (1) improvements to core and fluid handling, such as developing more sophisticated approaches to capturing ephemeral properties in core, dealing with broken or fragile fault core, performing more scientific measurements using cuttings and drill mud, developing best practices for drilling fluid composition for scientific drilling, as deep land drilling and riser drilling at sea become more prevalent; (2) develop-

ing improved site characterization methods including optimal arrays and methods for earthquake location; (3) careful attention to downhole measurements such as hydrologic and stress testing, weighing value of data vs. risks to the borehole; (4) developing best practices for a host of drilling techniques/technologies for the fault zone environment, including casing strategies, mud weight balancing to optimize borehole stability, and directional control (vertical and deviated); and (5) development of completion and long-term monitoring best practices (see below in this section).

One challenge to developing these workshops is that many of the principal scientists and drilling/measurement experts are involved in one or more of the major current projects and are simply spread too thin to lead such efforts. This leads to an overwhelming recommendation—expand the scientific and technical interest group for fault zone drilling and foster new teams and new team members. As activity has increased, such a growth in the pool of scientists has been occurring in Japan, the U.S.A., Europe, and Taiwan. This must continue to be encouraged through high-profile meetings, publications, and other venues.

2. Enhance cross-communication among active and emerging projects: Because fault drilling projects are necessarily regional and often nationally supported, they require an explicit effort to keep lines of communication open. In particular, there are two principal organizations that support large-scale and international efforts at drilling into faults: IODP and ICDP. These two organizations are separated by sea level, an essentially meaningless boundary in terms of the scientific motivation for drilling faults, yet drilling on land vs. at sea requires different platforms and drilling technologies. Workshop participants perceived a continued division at times between the activities of these two organizations, in part because of different organizational structures and systems. Clearly, however, overcoming the considerable technical challenges of carrying out ambitious drilling and casing, logging, or especially long-term monitoring (for examples, see Prevedel, this issue) would greatly benefit from a much tighter cooperation between IODP and ICDP, as well as national organizations (such as DOSECC). One widely endorsed recommendation was to develop industry/academia fault zone drilling advisory panels for technical issues such as drilling and completion strategies, and development of long-term monitoring instrumentation. Further recommendations include standardization of the engineering process for development of new coring methods, logging instruments, and monitoring systems. For example, the benefits of standard borehole seismometer strings were highlighted by two presentations (e.g., Stephen, this issue), so that each team spends less time “reinventing the wheel.”

We endorse the recommendation for IODP and ICDP to intensify the exchange of information on technology, and to establish a common advisory or support panel for fault zone drilling.

3. Develop long-term monitoring systems and strategies capable of performing in the fault zone subsurface environment:

The discussion of strategies for long-term monitoring system deployment was among the liveliest of the workshop. Participants generally agreed that monitoring over time is an absolutely essential aspect of studies in fault physics, since so many key processes are transitory or time-dependent in some way. Key parameters to monitor include seismicity, seismic velocity structure, strain and/or tilt, pore fluid pressure, temperature, and pore fluid chemistry. The fault zone environment at depth—where both temperature and pressure are greatly elevated, fluids may be corrosive, and return access is likely to be difficult or impossible—necessitates careful attention to monitoring schemes. Several key general practices emerged from this discussion. The principal one is to design for a long-term robust lifespan of the borehole as an observatory. Deep fault zone boreholes are large investments of capital and labor and must produce data for many years to realize their full potential. Thus, simple sensors are best; passive, non-powered instruments (e.g., geophones) should be preferred when possible. Some advocated maximizing use of passive instruments on the outside of installed casings, based on the logic that some form of measurement is better than none at all, and even if they fail, outside-casing instruments do not obstruct access to the interior of the borehole for other measurements. Redundancy was highlighted as an important objective, since individual sensors are prone to failure. The question of cementing in certain instruments, such as broadband seismometers and strainmeters, brought out a strong debate. On one hand, these instruments require very stable installations to work for years, favoring cementing in open holes. On the other hand, cementing them in blocks access to the hole for other instruments and may make it difficult or impossible to replace instruments that have failed. The choice depends on the balance of objectives unique to each project.

Workshop participants identified an urgent need for instruments and sensors robust for long periods of time at elevated temperatures and pressures. Lifespan is traded against stability at high temperatures in particular, such that a particular instrument might have a five-year life at 80°C, but only a six-month life at 120°C, for example. Broadband seismometers for installations above ~100°C do not exist, and accelerometers, fiber optic sensors, and other alternatives do not have acceptable resolution or absolute precision. These roadblocks are common to all projects, land or sea, so one recommendation from this workshop is that IODP and ICDP develop joint efforts in long-term monitoring system development. A joint working group or panel would be ideal.

4. Explore the potential for a rapid-response drilling plan:

This is the most specific recommendation, but it is necessary because such a plan would require a new approach to planning for drilling. A number of workshop participants emphasized the scientific merit of drilling into a fault soon after slip during a large earthquake in order to measure the transient

signal of frictional heating and other properties before they decay (Kano et al.; Mori; this issue). A goal of drilling in weeks to months (rather than years) post-event was recommended. Participants agreed that a candidate earthquake would have magnitude of roughly 6 to 7 or greater, would be well recorded locally, would have significant fault slip in the upper few thousand meters subsurface, and would be located in a region easily accessible for drilling. The most significant challenge is that a rapid-response drilling program would require (a) a well developed plan that is focused and has clear objectives, yet is generic enough to apply to any earthquake and (b) funding in place in advance, with an agreed-upon set of criteria for initiating the plan when a suitable earthquake occurs. In addition, there has to be a carefully thought out technical plan to mobilize a rig on relatively short notice. These requirements contrast sharply with the typical process of developing a specific drilling program over many years. One additional challenge to overcome is that such a plan would work best if candidate events in many, or at least more than one, country could be considered, so as to shorten the likely wait for a suitable event, but funding agencies' national interest and issues with permits might make it difficult to make this a strongly international effort. Despite these potentially formidable obstacles, the sense of the workshop was that this initiative should be explored. Since the Miyazaki workshop, an ICDP workshop proposal has been submitted to further explore the rapid response concept.

Extended Abstracts in This Volume

The collection of volunteered extended abstracts that follows this section represents a snapshot of many of the themes highlighted in both presentations and posters during the workshop. It is not intended to comprehensively capture the range of subjects discussed during the workshop, nor the full extent of current endeavor in this field. Nevertheless, the thirty-six abstracts here represent examples of current efforts in many areas. We have chosen to group them roughly into sections with the themes of (1) *Scientific Motivations for Fault Zone Drilling*, containing abstracts dealing with the broader issues that can be best or only addressed through drilling, and including (2) *overviews of many of the major projects*; (3) *Fault Zone Structure, Composition, and Physical Properties*, with papers principally on lithology, mineralogy, structural fabrics, and seismic and hydrologic properties; (4) *The Physics of Earthquake Rupture*, concerned with near-field seismology and fault physics as addressed through modeling and laboratory experimentation; and (5) *Technological Challenges of Drilling, Testing, Sampling, and Monitoring in Fault Zones*, which deals with new techniques for core handling and sampling, borehole instrumentation, downhole active testing of formation properties, logging, and drilling and completion operations in the fault zone environment. These reflect the key themes and challenges discussed in the section above. It is our intention that publication of this volume will stimulate new collaborations and links among developing research efforts on land and at sea, and also will

encourage ambitious new programs to tackle these challenges. The improved understanding of fault processes will depend on a multi-pronged, multi-disciplinary approach using new tools and collecting novel types of data.

Concluding Remarks

A principal objective of the Miyazaki joint workshop was to bring together the land-based and ocean-based fault zone communities for an exchange of information and ideas, and an exploration of the commonalities and differences in working in these very different environments. On this aspect the workshop can only be judged a resounding success. New collaborations began during the four days of the meeting, and tighter integration of projects has begun. For example, an ICDP workshop has now been scheduled for summer 2007 to explore an on-land extension of the NanTroSEIZE offshore transect (see http://www.icdp-online.org/contenido/icdp/front_content.php?client=29&idcat=309&lang=28&idart=1931). The Mediterranean Ridge proposal (Kopf and Bohnoff, this issue) is another example of integrated land-sea drilling plans. All the projects, past or future, reviewed at this workshop have unique motivations, strategies for success, advantages and challenges, and it is likely that only by advancing on many of these simultaneously will the fault zone research community make substantial progress in coming years.

This workshop established a single global community of researchers on drilling-based fault studies. With two well established, highly visible and successful organizations in place (ICDP and IODP) to support scientists' efforts, it is our hope and expectation that the legacy of the workshop will be a dynamic, multi-disciplinary, and integrated research program in coming years.

Acknowledgements

We are very grateful for the support of both the Integrated Ocean Drilling Program (IODP) and the International Continental Drilling Project (ICDP) for their generous co-sponsorship of the costs of holding this workshop. In particular, we thank Dr. Manik Talwani of IODP for sparking the idea to hold a joint workshop, and Dr. Ulrich Harms of ICDP for unstinting support. The staff at the Phoenix SunGaia Hotel in Miyazaki provided excellent support in all respects. The most essential person for the success of the Fault Zone Drilling workshop was certainly Dr. Kelly Kryc of IODP-MI, who carried out the workshop organization with great professionalism, patience, and good humor. Production of this workshop report white paper and special volume of *Scientific Drilling* would not have taken place without the hard work and supreme patience of Emanuel Soeding, Mika Saido, and Hans-Christian Larsen of the journal, and we are indebted to them for their efforts.

References

- Boness, N. and Zoback, M.D., 2006. A multi-scale study of the mechanisms controlling shear velocity anisotropy in the San Andreas Fault Observatory at Depth. *Geophysics*, 7(5):F131–F146, doi:10.1190/1.2231107.
- Boullier, A.-M., Ohtani, T., Fujimoto, K., Ito, H., and Dubois, M., 2001. Fluid inclusions in pseudotachylytes from the Nojima fault, Japan. *J. Geophys. Res.*, 106:21965–21977.
- Bourlange, S., Henry, P., Moore, J.C., Mikada, H., and Klaus, A., 2003. Fracture porosity in the décollement zone of Nankai accretionary wedge using Logging While Drilling resistivity data. *Earth Planet. Sci. Lett.*, 209:103–112, doi:10.1016/S0012-821X(03)00082-7.
- Byrne, T., Maltman, A., Stephenson, E., Soh, W., and Knipe, R., 1993. Deformation structures and fluid flow in the toe region of the Nankai accretionary prism. In Hill, I.A., Taira, A., Firth, J.V., et al., *Proc. ODP, Sci. Results, 131*: College Station, Texas (Ocean Drilling Program), 83–101.
- Cornet, F.H., Bernard, P., and Moretti, I., 2004. The Corinth Rift Laboratory. *Comp. Rend. Geosci.*, 336:235–241, doi:10.1016/j.crte.2004.02.001.
- Davis, E.E. and Villinger, H.W., 2006. Transient formation fluid pressures and temperatures in the Costa Rica forearc prism and subducting oceanic basement: CORK monitoring at ODP Sites 1253 and 1255. *Earth Planet. Sci. Lett.*, 245(1-2):232–244. doi:10.1016/j.epsl.2006.02.042.
- Earth Oceans and Life: Integrated Ocean Drilling Program Initial Science Plan, 2003-2013, 2001. International Working Group Support Office, Washington, D.C., 110 p., Available from: <http://www.iodp.org/isp>
- Emmermann, R. and Lauterjung, J., 1997. The German Continental Deep Drilling Program KTB: Overview and major results. *J. Geophys. Res.*, 102:18179–18201, doi:10.1029/96JB03945.
- Fisher, A., 2005. Marine hydrogeology: recent accomplishments and future opportunities. *Hydrogeol. J.*, 13:69–97, doi:10.1007/s10040-004-0400-y.
- Fujimoto, K., Tanaka, H., Higuchi, T., Tomida, N., Ohtani, T., and Ito, H., 2001. Alteration and mass transfer inferred from the Hirabayashi GSJ drill penetrating the Nojima fault, Japan. *The Island Arc*, 10:401–410.
- Hickman, S., Zoback, M.D., and Ellsworth, W.E., 2004. Introduction to special section: Preparing for the San Andreas Fault Observatory at Depth. *Geophys. Res. Lett.*, 31:L12S01, doi:10.1029/20040GL20688.
- Hyndman, R.D., 2007. The seismogenic zone of subduction thrust faults: what we know and don't know. In *The Seismogenic Zone of Subduction Thrust Faults*, Eds.: Dixon, T.H. and Moore, C., Columbia University Press, 15–40.
- Ito, H., Kuwahara, Y., Miyazaki, T., Nishizawa, O., Kiguchi, T., Fujimoto, K., Ohtani, T., Tanaka, H., Higuchi, T., Agar, S., Brie, A., and Yamamoto, H., 1996. Structure and physical properties of the Nojima fault by the active fault drilling, *Butsuri-Tansa*, 49, 522–535.
- Ito, H., Fujimoto, K., Tanaka, H., and Lockner, D., 1999. Proceedings of the international workshop on the Nojima fault core and borehole data analysis. *Geological Survey of Japan Interim Report No. EQ/00/1*, USGS Open-File 895 Report 000-129.
- Kondo, H., Kimura, G., Masago, H., Ohmori-Ikehara, K., Kitamura, Y., Ikesawa, E., Sakaguchi, A., Yamaguchi, A., and Okamoto, S., 2005. Deformation and fluid flow of a major out-of-sequence thrust located at seismogenic depth in an accretionary complex: Nobeoka Thrust in the Shimanto Belt, Kyushu, Japan. *Tectonics*, 24:TC6008, doi:10.1029/2004TC001655.
- Ma, K.-F., Tanaka, H., Song, S.-R., Wang, C.-Y., Hung, J.-H., Tsai, Y.-B., Mori, J., Song, Y.-F., Yeh, E.-C., Soh, W., Sone, H., Kuo, L.-W., and Wu, H.-Y., 2006. Slip zone and energetics of a large earthquake from the Taiwan Chelungpu-fault Drilling Project. *Nature*, 444:473–476, doi:10.1038/nature05253.
- Mizuno, T., Kuwahara, Y., Ito, H., and Nishigami, K., 2007. Spatial variations in fault-zone structure along the Nojima fault, central Japan, as inferred from borehole observations of fault-zone trapped waves. *Bull. Seism. Soc. Amer.*, in press.
- Moore, G.F., Taira, A., Klaus, A., Becker, L., Boeckel, B., Cragg, A., Dean, A., Fergusson, C.L., Henry, P., Hirano, S., Hisamitsu, T., Hunze, S., Kastner, M., Maltman, A.J., Morgan, J.K., Murakami, Y., Saffer, D.M., Sánchez-Gómez, M., Screaton, E.J., Smith, D.C., Spivack, A.J., Steurer, J., Tobin, H.J., Ujiie, K., Underwood, M.B., and Wilson, M., 2001. New insights into deformation and fluid flow processes in the Nankai Trough Accretionary Prism: results of Ocean Drilling Program Leg 190. *Geochem. Geophys. Geosyst.*, 2, doi:10.129/2001GC000166.
- Moore, J.C., Klaus, A., Bangs, N.L., Bekins, B., Buecker, C.J., Brueckmann, W., Erickson, S.N., Hansen, O., Horton, T., Ireland, P., Major, C.O., Moore, G.F., Peacock, S., Saito, S., Screaton, E.J., Shimeld, J.W., Stauffer, P.H., Taymaz, T., Teas, P.A., and Tokunaga, T., 1998. Consolidation patterns during initiation and evolution of a plate-boundary décollement zone: Northern Barbados accretionary prism. *Geology*, 26:811–814, doi:10.1130/0091-7613(1998)026<0811:CPDIAE>2.3.CO;2.
- Ogasawara, H., Yanagidani, T., and Ando, M., 2002. Seismogenic process monitoring. *Proceedings of a Joint Japan-Poland Symposium on Mining and Experimental Seismology*, Kyoto, Japan (A.A. Balkema), 414 pp.
- Ohtani, T., Fujimoto, K., Ito, H., Tanaka, H., Higuchi, T., Tomida, N., 2000. Fault rocks and past to recent fluid characteristics from the borehole survey of the Nojima fault ruptured in the 1995 Kobe earthquake, southwest Japan. *J. Geophys. Res.*, 105, 16161–16171.
- Ohtani, T., Tanaka, H., Fujimoto, K., Higuchi, T., Tomida, N., and Ito, H., 2001. Internal structure of the Nojima fault zone from the Hirabayashi GSJ drill core. *The Island Arc*, 10:392–400.
- Oshiman, N., Shimamoto, T., Takemura, K., and Wibberley, C.A.J., 2001. Nojima Fault Zone Probe. *The Island Arc*, 10:195–505.
- Parsons, T., 2004. Recalculated probability of $M \geq 7$ earthquakes beneath the Sea of Marmara, Turkey. *J. Geophys. Res.*, 109: B05304, doi:10.1029/2003JB002667.
- Reches, Z. and Ito, H., 2007. Scientific drilling of active faults: Past and future. In Harms, U., Koeberl, C., and Zoback, M.D. (Eds.), *Continental Scientific Drilling: A Decade of Progress and Challenges for the Future*, Heidelberg, Germany

(Springer), doi:10.1007/978-3-540-68778-8_6.

- Screaton, E., Saffer, D., Henry, P., Hunze, S., and the Leg 190 Scientific Party, 2002. Porosity loss within the underthrust sediments of the Nankai accretionary complex: Implications for overpressures. *Geology*, 30(1):19–22, doi:10.1130/0091-7613(2002)030<0019:PLWTUS>2.0.CO;2.
- Shipley, T.H., Moore, G.F., Bangs, N.L., Moore, J.C., and Stoffa, P.L., 1994. Seismically inferred dilatancy distribution, northern Barbados Ridge décollement: Implications for fluid migration and fault strength. *Geology*, 22:411–414, doi:10.1130/0091-7613(1994)022<0411:SIDDNB>2.3.CO;2.
- Silver, E.A., Kastner, M., Fisher, A.T., Morris, J., McIntosh, K.D., and Saffer, D.M., 2000. Fluid flow paths in the Middle America Trench and Costa Rica margin. *Geology*, 28:679–682, doi:10.1130/0091-7613(2000)28<679:FFPITM>2.0.CO;2.
- Tadokoro, K. and Ando, M., 2002. Evidence for rapid fault healing derived from temporal changes in S wave splitting. *Geophys. Res. Lett.*, 29(4), 1047, doi:10.1029/2001GL013644.
- Tadokoro, K., Ando, M., and Nishigami, K., 2000. Induced earthquakes accompanying the water injection experiment at the Nojima fault zone, Japan: Seismicity and its migration. *J. Geophys. Res.*, 105:6089–6104, doi:10.1029/1999JB900416.
- Tanaka, H., Fujimoto, K., Ohtani, T., and Ito, H., 2001. Structural and chemical characterization of shear zones in the freshly activated Nojima fault, Awaji Island, southwest Japan. *J. Geophys. Res.*, 106:8789–8810.
- Tobin, H. and Kinoshita, M., 2006. NanTroSEIZE: the IODP Nankai Trough seismogenic zone experiment. *Sci. Drill.*, 2:23–27, doi:10.2204/iodp.sd.2.06.2006.
- Tobin, H., Vannuchi, P., and Meschede, M., 2001. Structure, inferred mechanical properties, and implications for fluid transport in the décollement zone, Costa Rica convergent margin. *Geology*, 29:907–910, doi:10.1130/0091-7613(2001)029<0907:SIMPAT>2.0.CO;2.
- von Huene, R., Ranero, C.R., and Vannucchi, P., 2004. A model for subduction erosion. *Geology*, 32:913–916, doi:10.1130/G20563.1.
- Zoback, M., Hickman, H., and Ellsworth, W., 2006. Structure and properties of the San Andreas fault in central California: Preliminary results from the SAFOD experiment. *Geophys. Res. Abstr.*, 8:02474.
- Zoback, M.D., Apel, R., Baumgartner, J., Brudy, M., Emmermann, R., Engeser, B., Kessels, W., Fuchs, K., Rischmuller, H., Rummel, F., and Vernik, L., 1993. Upper-crustal strength inferred from stress measurements to 6 km depth in the KTB borehole. *Nature*, 365:633–634, doi:10.1038/365633a0.
- Zoback, M.D., Hickman, S., and Ellsworth, W., 2007. The role of fault zone drilling, 2007, In Kanamori, H., and Schubert, G. (Eds.), *Earthquake Seismology - Treatise on Geophysics*. Amsterdam, The Netherlands (Elsevier), in press.

Authors

Harold Tobin, Associate Professor, Department of Geology and Geophysics, University of Wisconsin-Madison, 1215 West Dayton Street, Madison, Wis. 53706, U.S.A., e-mail: htobin@wisc.edu.

Hisao Ito, Center for Deep Earth Exploration (CDEX) – Japan Agency for Marine-Earth Science and Technology (JAMSTEC), 3173-25 Showa-machi, Kanazawa-ku, Yokohama, Kanagawa, 236-0001, Japan.

Jan Behrmann, Marine Geodynamics, IFM-GEOMAR, Wischhofstr. 1-3, 24148, Kiel, Germany.

Steve Hickman, U.S. Geological Survey, MS977, 345 Middlefield Road, Menlo Park, Calif., 94025, U.S.A.

Gaku Kimura, Department of Earth and Planetary Sciences, Graduate School of Science, The University of Tokyo, 7-3-1 Hongo, Bunkyo-ku, Tokyo, 113-0033, Japan.

Fault Zone Drilling in Subduction Zones: The Accomplishments of Ocean Drilling and Associated Studies

by J. Casey Moore

doi:10.2204/iodp.sd.s01.12.2007

Subduction zones produce the world's largest earthquakes and cumulatively account for 90% of the global seismic moment release. The production of such large earthquakes is probably due to the shallow inclination (typically $<20^\circ$) of the major plate-boundary subduction thrust. Thus, in comparison to vertically-oriented transform faults, subduction thrusts have a large area in the seismogenic zone, or the depth interval mechanically capable of producing earthquakes.

Beginning with the later stages of the Deep Sea Drilling Program (DSDP) and continuing through the Ocean Drilling Program (ODP), Earth scientists have concentrated on drilling through the subduction thrust. Restrictions of the riserless drilling process required that the drilling focus on relatively shallow portions of the subduction thrust with burial depths limited to about 1 km below the seafloor.

Subduction thrusts convey the oceanic crust and overlying sedimentary deposits to the seismogenic zone and beyond. Hence, we can know the material that is entering the subduction thrust and trace its evolution with depth, both by direct sampling and experimental studies of its changing mechanical properties and mineral phases. Where drilled, subduction thrusts consist of zones of scaly mudstone 20–40 m thick. They are characterized by consolidative deformation where intergranular porosity is declining; these fault rocks include a fracture porosity and permeability that may be intermittently dilated by high fluid pressure. Hydrologic tests show that permeability varies with fluid pressure. Geochemical evidence suggests that separate fluid systems may exist around the subduction thrust, in the underthrust sediments, **and in the subjacent oceanic crust**. Geochemical evidence further suggests fluids associated with the subduction thrusts are typically far-traveled along this shallowly inclined fault.

Logging while drilling (LWD) has been an effective tool for determining *in situ* physical properties, establishing borehole structure, and inferring stress orientations in ODP boreholes in subduction zones. Physical property results indicate impedance values (velocity \times density) that are consistent with the seismic reflection images. Structural features from analysis of LWD resistivity images are similar in orientation and type to those measured from reoriented cores. Borehole breakouts indicate stress orientations mirroring those determined from structural features of the

borehole and also consistent with plate convergence vectors.

Because subduction thrusts dip shallowly, they may be well imaged with seismic reflection techniques. Seismic reflection images, coupled with drilling results, indicate that the fluids being expelled from the consolidating, dehydrating subduction zone deposits may be channelized during transport along the subduction thrust. Seismic data also suggest progressive underplating of the underthrust sediments with depth; the quantity of water in the underthrust sediments also diminishes with depth. Models, also well linked to drilling results, suggest the fluid pressure initially rises tens of kilometers landward of the deformation front and then diminishes towards the upper aseismic-seismic transition along the subduction thrust.

A combination of seismological information and thermal models suggests that the upper aseismic to seismic transition begins at temperatures of about 125°C . Here, the combined effects of consolidation and a series of diagenetic-metamorphic reactions apparently foster the onset of stick-slip behavior. At some localities incoming sediment may have been underplated by the depth of the seismogenic zone, leaving the basaltic oceanic crust as the lower plate of the subduction thrust. The fluid system of the oceanic crust, documented by ocean drilling, may be important here in controlling the mechanics of faulting.

Subduction thrusts probably transition from thick consolidating zones at shallow depths to more localized fault surfaces in the seismogenic zone. Candidates for such seismogenic faults in exhumed subduction complexes include layers of frictional melts (pseudotachylytes), zones of fluidized but unmelted fault rock, and intervals of conspicuous veining. A major challenge in drilling into the seismogenic zone will be recognition of the active fault surface, especially when it is included in a large volume of previously deformed rocks. Careful inspection of borehole images and cores, as well as monitoring of the borehole, will be essential in unequivocal specification of the active subduction thrust at depth.

Author

J. Casey Moore, Earth and Planetary Sciences, University of California Santa Cruz, Santa Cruz, Calif., 95064, U.S.A., e-mail: cmoore@es.ucsc.edu.

Fault Characteristics, Energy Estimates, and Earthquake Recurrence: What *One* Seismologist Wants from Fault Drilling

by Jim Mori

doi:10.2204/iodp.sd.s01.42.2007

There are some significant differences between the way seismologists and geologists typically look at faulting from large earthquakes. Seismologists tend to analyze waveform data which can usually resolve structures on the order of tens of kilometers; possibly down to one kilometers there is very good near-field data. Also, the derived physical properties are averaged over this scale length. Although it is difficult to resolve small scale features, seismologic studies have the advantage of seeing all depths of the fault. In contrast fault zone geologists can make direct observations of the fault zone structures and properties, which are quite different from the remote sensing techniques of seismologists. Geologists tend to look at structures on the scale of microns to meters when examining the cores obtained from drilling into faults. These observations are spot measurements and it is often difficult to assess how representative they are of the entire fault. Also, fault zone sample studies are usually limited to a few kilometers depth, which may barely be in the range of the seismogenic zone that produces the seismic waves. These differences mean that seismologists and geologists are often looking at quite different aspects of the earthquake process. The approaches are different, but can also be complementary.

Drilling Depth

The depth of drilling is an important point for fault zone investigations. To compare physical properties obtained in cores with seismological results obtained from waveform analyses, it is necessary to reach depths of the seismogenic zone, that is the regions of fault slip that have significant stress change to produce seismic waves. The shallow regions of faults, where materials have low rigidity, likely slip sympathetically with the seismogenic zone but do not produce seismic waves. The depth of the beginning seismogenic zone depends on local geology and probably is a transition zone. Waveform inversion studies suggest that the seismogenic zone may be as shallow as 1 km for the Chi-Chi, Taiwan earthquakes (Ji et al., 2001). It would be interesting if geologic studies could distinguish between seismic and non-seismic slip of the fault.

Temperature Measurements

One of the fundamental issues in understanding the physical mechanisms of earthquakes is clarifying the level of friction on the fault. One way to estimate the frictional levels

during the faulting is to measure the heat produced. Measurements of the heat flow associated with the San Andreas fault have long been discussed over the past decades (e.g., summarized in Scholz, 2002, section 3.4.4). A more direct estimate would be to measure the fault zone temperatures immediately after a large earthquake. There were informal discussions to measure fault-zone temperatures following the large 1992 Landers and 2001 Denali earthquakes, although measurements were not done. Currently, the only available data of fault-zone temperatures following an earthquake are for the 1999 Chi-Chi, Taiwan earthquake (Kano et al., 2006). This result infers a very low level of dynamic friction during the earthquake; however, the measurement was made 5 years after the earthquake, when the temperature signal was quite small, and it is difficult to make clear interpretations. To obtain better estimates of the fault-zone heat, measurements more quickly (a few months) after a large earthquake are necessary (Fig.1).

Asperities

Fault slip during large earthquakes is usually heterogeneous with regions of large and small slip. The areas of large slip are often termed 'asperities'. These areas of large slip dominate the energy radiation and may control the rupture process. There are also suggestions that the stress accumulation during the interseismic period is different on the asperities, compared to the rest of the fault. The actual physical process that controls the stress accumulation and large slip of the asperities is currently an active topic of discussion in seismology. Yamanaka and Kikuchi (2004)

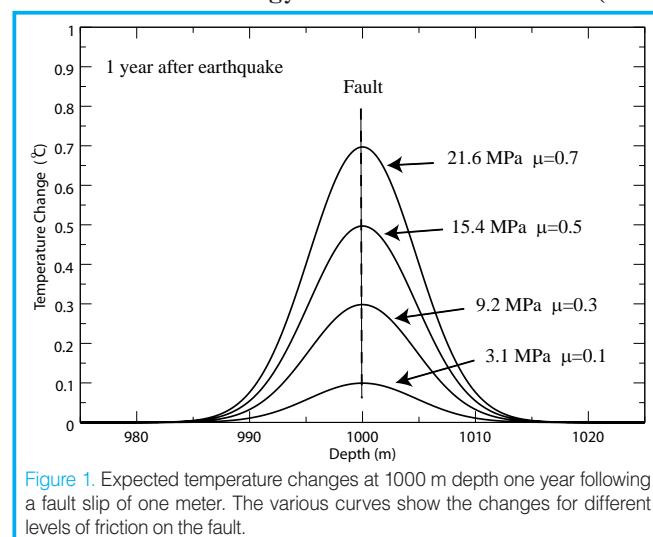


Table 1. Complementary differences between typical seismology studies and fault zone investigations.

Seismological Observations—Macroscopic	Fault Zone Investigations—Microscopic
Scales of km to tens of km, average properties of the fault zone	Scales of nanometers to meters for spot measurements
Remote sensing of entire depth range of fault zone	Direct samples from shallow depths of the fault
Estimates of total seismic radiated energy	Estimates of heat generated by temp. measurements after earthquakes
Estimates of non-radiated (fracture?) energy	Determination grain size, crack distributions for energy estimates
Seismic determination of slip weakening distance	Estimates of fault frictional properties from core samples

suggest that asperities are persistent features that are characteristic of a fault zone. However, results from the two recent Parkfield earthquakes and also large subduction earthquakes along the New Britain trench (Park and Mori, 2007) indicate that asperity distributions can be different for repeated ruptures of the same zone. Some related seismological issues that might be answered by detailed analyses of fault zone structures from drilling include the following:

- Are repeating earthquakes on a fault occurring on the same exact fault plane?
- Are the locations of asperities (areas of large slip) the same in repeating earthquakes?
- What is the physical cause of asperities?
- How does each earthquake contribute to making the fault zone?
- What is the fracture/healing process on the fault?

Macro- and Microscopic Observations

Kanamori and Heaton (2002) emphasize the importance for understanding and integrating small and large scale results for fault zone studies. The physical processes that occur on microscopic scales of the fault zone are reflected in the macroscopic observations made by seismologists.

Table 1 lists some of the different and complementary aspects of seismological and borehole studies of earthquakes and fault zones. For example, detailed analyses of near-field seismograms for large earthquakes can give estimates of both the radiated and non-radiated energy. The non-radiated energy is thought to be dissipated by processes such as fracture formation and heat production. These dissipated processes can be studied with direct measurements of temperature, crack distributions, and grain sizes obtained from borehole observations.

Onshore and Offshore Drilling

The logistics of drilling crustal faults on land and drilling faults offshore, such as large megathrust subduction zones, are quite different and are addressed by the differences in the programs of the International Continental Scientific Drilling Program (ICDP) and the Integrated Ocean Drilling Program (IODP). Crustal onshore faults tend to be shallower and more accessible to drilling investigations. For large offshore subduction zones, identifying and reaching the fault surfaces with drilling is a difficult endeavor. Drilling both faulting environments is important for understanding the

physical structures of the fault zones. There are also opportunities for cooperative onshore/offshore drilling projects that can combine observations of the same fault zone.

Wish List

Finally, to address the issues mentioned above, I would recommend that a fault zone drilling program would include the following (roughly in order of difficulty).

- Design projects to combine microscopic and macroscopic observations
- Drill to sufficient depth to reach the seismogenic zone (region that produces seismic waves)
- Drill soon after a large earthquake to measure temperature changes caused by faulting
- Use deep boreholes for measurements of earthquakes and strain (borehole observatories)
- Sample a fault in the same place before and after an earthquake

References

- Ji, C., Helmberger, D.V., Song, T.R., Ma, K.-F., and Wald, D.J., 2001. Slip distribution and tectonic implication of the 1999 Chi-Chi, Taiwan, earthquake. *Geophys. Res. Lett.* 28:4379–4382, doi:10.1029/2001GL013225.
- Kanamori, H. and Heaton, T.H., 2002. Microscopic and macroscopic physics of earthquakes. In Rundle, J., Turcotte, D.L., and Klein, W. (Eds.), *Geocomplexity and the Physics of Earthquakes*, *Geophysical Monograph no. 120*, Washington, DC (American Geophysical Union), 147p.
- Kano, Y., Mori, J., Fujio, R., Ito, H., Yanagidani, T., Nakao, S., and Ma, K.F., 2006. Heat signature on the Chelungpu fault associated with the 1999 Chi-Chi, Taiwan earthquake. *Geophys. Res. Lett.*, doi:10.1029/2006GL026733.
- Park, S. and Mori, J., 2007. Are asperity patterns persistent? Implication from large earthquakes in Papua, New Guinea. *J. Geophys. Res.*, doi:10.1029/2006JB004481.
- Scholz, C.H., 2002. *The Mechanics of Earthquakes and Faulting*. Cambridge (Cambridge University Press), 471 p.
- Yamanaka, Y. and Kikuchi, M., 2004. Asperity map along the subduction zone in northeastern Japan inferred from regional seismic data. *J. Geophys. Res.*, 109, B07307, doi:10.1029/2003JB002683.

Author

Jim Mori, Disaster Prevention Research Institute, Kyoto University, Gokasho, Uji, Kyoto, 611-0011, Japan, e-mail: mori@eqh.dpri.kyoto-u.ac.jp.

Pore Pressure at Plate Boundaries: Insights from Modeling

by Demian Saffer

doi:10.2204/iodp.sd.s01.32.2007

Introduction

Fluids play a key role in a wide range of mechanical and transport processes in the Earth's crust. Fluid flow can efficiently redistribute heat and solutes; as a result, fluid assisted transport and fluid rock interaction are important controls over the rate and extent of metamorphism, precipitation, and sealing of fractures. Fluid-rock reaction and precipitation impact permeability and fault strength (Chester et al., 1993). In addition to its chemical effects, pore fluid mediates the strength of brittle rocks because pore pressure controls effective stress (Hubbert and Rubey, 1959). In particular, elevated pore fluid pressure has been invoked as a cause of mechanical weakness along plate boundary faults and within the surrounding crust, at subduction zones (Davis et al., 1983) and along continental transforms (Irwin and Barnes, 1975). Because fluid pressure is central to a host of hypotheses explaining apparent fault weakness, direct measurements and indirect constraints on fluid pressure and flow are high priorities for fault zone drilling.

Numerical models provide key tools to link observations at shallow depths or the surface with borehole observations, and to test hypotheses generated on the basis of such data. These efforts can complement deep drilling by helping to direct measurement strategies, and by estimating pressures and flow patterns at depths and over a larger spatial extent than reached by drilling. In the context of understanding fluid pressure at plate boundaries, modeling efforts have provided insights into many fundamental questions, including: What are the magnitudes and spatial patterns of suprahydrostatic pore pressure? What controls pore pressure, and how should it vary—systematically between margins or with depth? Are hypothesized fluid sources sufficient to generate fault-weakening overpressures? What role do permeable zones (faults, sands) play in drainage, and in localizing pressure or flow?

Here I summarize three studies in which hydrologic models are combined with available data to better understand pore pressure and its mechanical effects at plate boundaries (Table 1). In the first example, field and laboratory data constrain a simple analytic model, which elucidates fluid flow patterns and controls on pore pressure buildup during initial loading at subduction zones. In the second example, regional scale numerical models are used to quantify the influence of fundamental geologic factors on pore pressure,

and consequently on rock strength, in subduction zones. In the third example, models are used to evaluate hypotheses for pore pressure generation and compartmentalization invoked to explain mechanical weakness along the San Andreas fault system in central California.

Example 1: Simple Model for Dewatering at the Toe of Subduction Margins

At subduction zones, as incoming sediments are off-scraped or underthrust at the trench, elevated pore pressures result from rapid loading of low-permeability sediment (Table 1). Pore pressure within the sediment underthrust at the trench is especially important for the mechanical strength of the plate boundary fault system, because the main décollement localizes immediately above this sediment, and at many margins downsteps into the section within a few to tens of kilometers from the trench. Along transects where Ocean Drilling Program (ODP) drilling has penetrated the underthrust section at the Nankai, northern Barbados, and Costa Rican subduction zones, it maintains anomalously high porosity for its burial depth, suggesting under-consolidation and associated high fluid pressure. Quantitative estimates of *in situ* pore pressure have been obtained from laboratory consolidation tests on core samples, and from observed compaction trends both in boreholes and inferred from seismic data (Screaton et al., 2002; Tobin and Saffer, 2003). At all three margins, the different methods yield consistent results and indicate development of overpressures that increase systematically with distance from the trench. Estimated pore pressures suggest nearly undrained conditions at the base of the section (excess pressures equal to the load emplaced by subduction burial) and partially drained conditions at the top.

To first order, the data can be explained by a simple model describing a layer subjected to a continuously increasing load, in which fluid escapes upward to a free surface (Wissa et al., 1971; Fig. 1). In the model, pore pressure varies systematically with distance from the trench and depends upon the thickness of the consolidating sediment layer (H), the permeability and compressibility of the sediment layer (described by a single variable, C_v), and the plate convergence rate (v_p). For each margin, laboratory measurements constrain sediment permeability and compressibility. Notably, v_p , H , and C_v are different for each of the three locations, yet all of the data are consistent with a generic model in which degree

Table 1. Parameters of 2-D numerical models of subduction zones.

Example	Model Source Terms	Scale	Permeability
Subduction zones (toe)	Loading by underthrusting (virtual)	100's of m	Sediment permeability measured in laboratory, function of porosity
Subduction zones (regional)	Prescribed porosity loss based on drilling and seismic data	10's of km	Sediment permeability measured in laboratory, function of porosity; range of fault permeabilities explored
San Andreas Fault System	Fluid release by prograde metamorphism	~10km	Function of depth; range of fault permeabilities explored

of under-consolidation depends on the relative magnitudes of loading rate, drainage path length, and sediment hydraulic properties (Fig. 1). The agreement between observation and model implies that upward drainage to a highly permeable décollement dominates dewatering to distances of at least ~5–10 km landward of the trench. The model results also suggest that severe under-consolidation should persist for tens of kilometers from the trench (Saffer, 2007).

Example 2: Regional Scale Hydrologic Models of Subduction Complexes

In several studies, 2-D numerical models of subduction zones have been used to estimate pore pressures and test hypotheses about the nature of fluid flow at the regional scale (tens of kilometers; Bekins et al., 1995; Screamon et al., 1990). In these models, pore pressure and flow are driven by sediment compaction (Table 1). Fluid sources from compactive dewatering are incorporated at each node within the model domain, and are constrained by porosity data from boreholes and inferred from seismic velocity data (these models are described in detail by Bekins and Dreiss, 1992; see also Screamon et al., 1990). Sediment bulk permeability in the models is constrained by laboratory data, and a range of fault zone permeability has been investigated. Fault permeability is typically assumed to be higher than that of the sediment matrix, based on observations of (1) fluid expulsion at the seafloor and (2) chemical and thermal anomalies centered on faults. For several well studied margins, modeled pore pressure is in excellent agreement with that measured in borehole observatories (Barbados; Bekins and Screamon, 2007) and estimated by methods described in the previous example (Nankai and Costa Rica; Spinelli et al., 2006; Tobin and Saffer, 2003).

Regional scale models have also been used to evaluate the relative importance of factors that control pore pressure and ultimately the taper angle of subduction accretion complexes. The factors include sediment and fault permeability, incoming sediment thickness, convergence rate, and partitioning of sediment between accretion and underthrusting. By isolating and quantifying the influence of each of these factors on pore pressure, a comprehensive sensitivity analysis provides a basic framework for considering observations from active subduction complexes. As in the case of burial at the toe of subduction systems described above, the results show that pore pressure in accretionary wedges can be viewed as a balance between factors which drive pore pressure (source terms) and those that limit flow (permeability and drainage path length). Sediment permeability and incoming sediment thickness are most important, whereas fault permeability and the partitioning of sediment have small effects (Fig. 2).

By combining the hydrologic model with critical taper theory, systematic relationships emerge between the fundamental factors that govern fluid pressure and stable taper angle (Saffer and Bekins, 2006). For example, as sediment permeability is increased, modeled pore pressure decreases and allows taper angles to steepen. With increased sediment thickness, increased pore pressure drives a decrease in taper angle (Fig. 2). In general, low permeability and thick incoming sediment sustain high pore pressures consistent with shallowly tapered geometry, whereas high permeability and thin incoming sediment should result in steep geometry. The model results compare favorably with available data from active accretionary complexes—active margins characterized by a significant proportion of fine-grained sediment within the incoming section (such as the northern Barbados Trench and the eastern Nankai Trough) exhibit thin taper

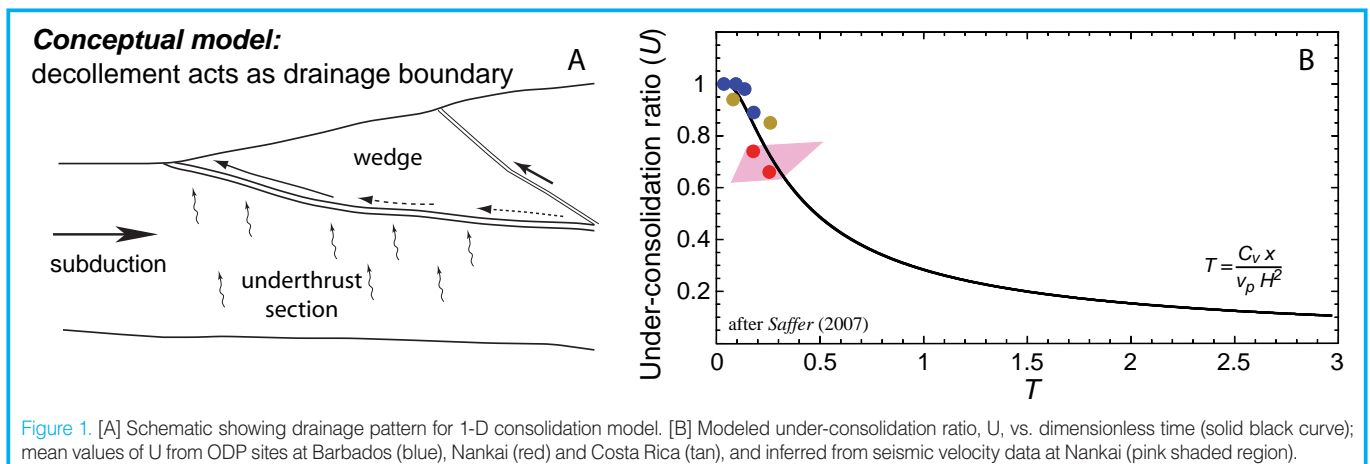


Figure 1. [A] Schematic showing drainage pattern for 1-D consolidation model. [B] Modeled under-consolidation ratio, U, vs. dimensionless time (solid black curve); mean values of U from ODP sites at Barbados (blue), Nankai (red) and Costa Rica (tan), and inferred from seismic velocity data at Nankai (pink shaded region).

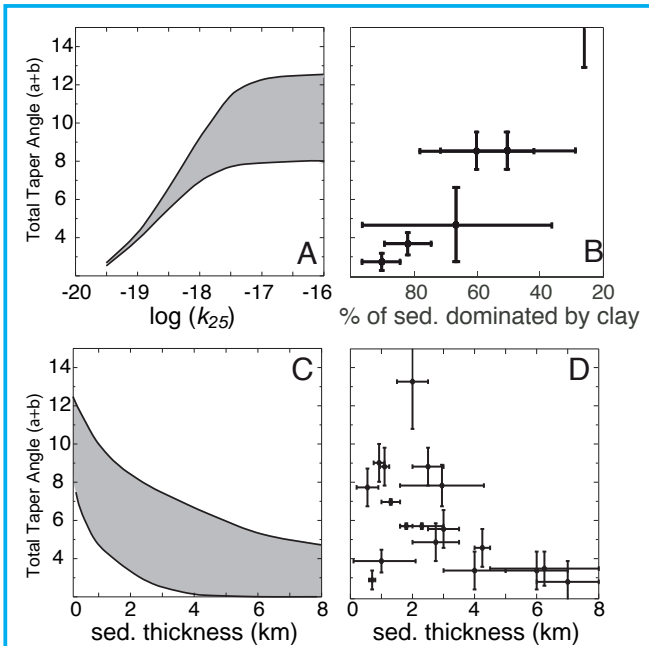


Figure 2. [A] Model results showing influence of permeability (plotted as log permeability at 25% porosity) on taper angle of accretionary wedges. [B] Data from active accretionary complexes where drilling has documented lithologies of incoming sediment, showing relationship between proportion of clay in sediment and taper angle. [C] Model results. [D] Data from active accretionary complexes, showing influence of sediment thickness on taper angle. After Saffer and Bekins (2006).

angles, whereas those characterized by a higher proportion of sandy turbidites (such as Cascadia, Chile, and Mexico) have steep taper angles. Observations from active margins also indicate a strong trend of decreasing taper angle with increased sediment thickness. One key implication is that hydrologic properties should strongly influence the strength of the crust in a wide range of geologic settings.

Example 3: A Test of Hypotheses Along the San Andreas Fault System

Along the San Andreas fault in California, heat flow observations and inferred stress orientations have been interpreted to indicate that the fault moves under considerably smaller shear stresses than predicted by laboratory-derived values for rock friction (Zoback et al., 1987). Elevated fluid pressures are one likely candidate to explain the apparent fault weakness—such overpressures may be either regionally extensive resulting in a weak fault embedded within a weak crust (Hardebeck and Hauksson, 2000), or localized along the fault resulting in a weak fault embedded within a strong crust (Zoback et al., 1987). Several hypotheses have been proposed to explain the generation of fluid pressure in the vicinity of the fault. In the study summarized here, Fulton et al. (2005) used numerical models to investigate (1) whether fluid produced by prograde metamorphism of the Franciscan assemblage is a likely candidate for generating significant and lasting overpressures along the fault system, and (2) if so, whether overpressures can be localized along the fault.

The apparent correlation between CO₂ discharge, ¹⁸O enrichment, geologic structure, and observed seismicity

patterns originally led Irwin and Barnes (1975) to suggest that fluids of metamorphic origin sourced from dehydration of Franciscan rocks are trapped and forced into the fault zone, causing fluid overpressures in areas where overlying low permeability Great Valley sediments and serpentinite act as a barrier to upward fluid expulsion. Fulton et al. (2005) quantitatively tested this hypothesis using a two-step approach. First, the spatial and temporal distribution of fluid sources from prograde dehydration was estimated from theoretical values of whole-rock H₂O content and P-T histories for the Franciscan crust in the wake of northward migration of the Mendocino Triple Junction (MTJ) (Table 1). Second, the fluid sources were incorporated into transient 2-D models of fluid flow within cross sections perpendicular to the fault. In the models, permeability of the Salinian and Franciscan crust was constrained by the work of Ingebritsen and Manning (1999) and assumed to decrease logarithmically with depth. In addition to a 500-m-thick low-permeability serpentinite body (k=10⁻²⁰ m⁻²) extending across the eastern half the model domain at a depth of 2 km, model simulations also explore a range of fault permeability architectures including a fault barrier, a fault conduit, and a combined conduit-barrier.

For models that incorporate both a serpentinite cap and fault barrier, overpressures as large as 62% of lithostatic pressure develop within 4 Myr of MTJ passage (a region extending ~200 km south of the present day location of the MTJ), where sources are abundant. However, simulated pressures dissipate within several thousand years because fluid sources die out due to stabilization in temperature and the low remaining H₂O content in lower crustal rocks. Overall, the presence of a low permeability cap can enhance regional overpressure development; however, none of the structures investigated allowed overpressures to localize along the fault (Fig. 3). The results suggest that metamorphic dehydration within the Franciscan crust has the potential to cause regional overpressure and weakening of the crust for

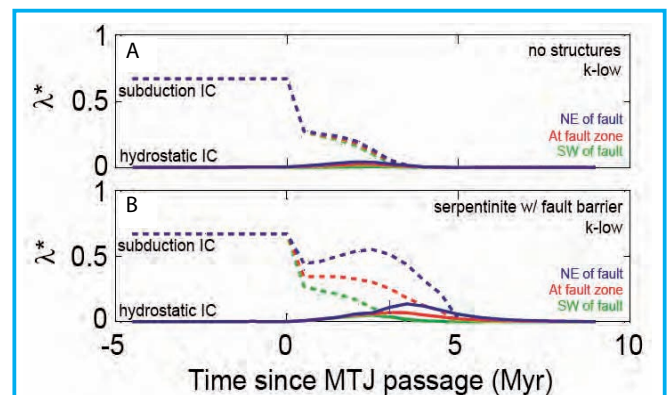


Figure 3. Model results showing the development of overpressures in the crust to the NE (blue), to the SW (green), and within (red) the San Andreas fault, for [A] a simple model with no geologic structures and [B] models incorporating a serpentinite “cap” and a fault barrier. Overpressures are plotted using the normalized pore pressure ratio $\lambda^* = (P_{\text{fluid}} - P_{\text{hydrostat}}) / (P_{\text{lithostat}} - P_{\text{hydrostat}})$. In both panels, solid curves show hydrostatic initial condition, and dashed curves show an elevated pore pressure initial condition associated with subduction north of the MTJ.

~4 Ma after MTJ passage, currently encompassing a region ~200 km south of the MTJ, but is limited as a sole mechanism for long-term weakening of the San Andreas fault along much of its length because overpressures cannot be sustained or localized along the fault.

Summary

In the examples summarized above, the integration of hydrologic modeling with datasets enabled by drilling—including laboratory studies on core samples and down-hole measurements—has provided insight into first-order questions about the magnitude, distribution, and mechanisms of elevated pore pressure in tectonically active environments. However, the utility of such models is closely tied to the availability of key datasets. Although data from the land surface (or seafloor) are important, drilling provides the most powerful and direct constraints on pore pressure and fluid flow in the subsurface. In particular, the hydraulic properties of faults and wall rock at relevant scales are key unknowns in most models; down-hole and long-term perturbation tests are one effective way to constrain these quantities. Likewise, rock sampling and geochemical data are critical toward better defining the fluid source terms that drive flow in these dynamic environments. Down-hole pressure and temperature measurements provide key data to test flow models. In this context, fault zone drilling in conjunction with surface measurements will provide vital data to clarify the role of fluids in faulting and to more definitively test hypotheses for fluid pressure development and its mechanical and chemical effects.

References

- Bekins, B. and Screaton, E., 2007. Pore pressure and fluid flow in the northern Barbados accretionary complex. *In* Dixon, T., Moore, C. J., Eds. *The Seismogenic Zone of Subduction Thrusts*, New York (Columbia University Press), 148–170.
- Bekins, B.A. and Dreiss, S.J., 1992. A simplified analysis of parameters controlling dewatering in accretionary prisms. *Earth Planet. Sci. Lett.*, 109:275–287, doi:10.1016/0012-821X(92)90092-A.
- Bekins, B.A., McCaffrey, A., and Dreiss, S.J., 1995. Episodic and constant flow models for the origin of low chloride waters in a modern accretionary complex. *Water Resour. Res.*, 31:3205–3215, doi:10.1029/95WR02569.
- Chester, F.M., Evans, J.P., and Biegel, R.L., 1993. Internal structure and weakening mechanisms of the San Andreas fault. *J. Geophys. Res.*, 98:771–786.
- Davis, D., Suppe, J., and Dahlen, F.A., 1983. Mechanics of fold-and-thrust belts and accretionary wedges. *J. Geophys. Res.*, 88:1153–1172.
- Fulton, P.M., Saffer, D.M., and Bekins, B.A., 2005. Crustal dehydration and overpressure development on the San Andreas fault. *Eos Trans. AGU*, 86(52), Fall Meet. Suppl., Abstract T43C-02.
- Hardebeck, J.L. and Hauksson, E., 2000. The San Andreas fault in southern California: A weak fault in a weak crust. *In* Kovach, R. (Ed.), *Proceedings of the 3rd Conference on Tectonic Problems of the San Andreas Fault System*, September 6–8, 2000, Stanford University.
- Hubbert, M.K. and Rubey, W.W., 1959. Role of fluid pressure in mechanics of overthrust faulting. *Geol. Soc. Am. Bull.*, 70:115–166, doi:10.1130/0016-7606(1959)70[115:ROFPIM]2.0.CO;2.
- Ingebritsen, S.E. and Manning, C.E., 1999. Geological implications of a permeability-depth curve for the continental crust. *Geology*, 27:1107–1110, doi:10.1130/0091-7613(1999)027<1107:GIOAPD>2.3.CO;2.
- Irwin, W.P. and Barnes, I., 1975. Effect of geologic structure and metamorphic fluids on seismic behavior of the San Andreas Fault system in central and northern California. *Geology*, 3:713–716, doi:10.1130/0091-7613(1975)3<713:EOGSAM>2.0.CO;2.
- Saffer, D.M., 2007. Pore pressure within under thrust sediments in subduction zones. *In* Dixon, T., Moore, C. J., Eds., *The Seismogenic Zone of Subduction Thrusts*, New York (Columbia University Press), 692 p.
- Saffer, D.M. and Bekins, B.A., 2006. An evaluation of factors influencing pore pressure in accretionary complexes: Implications for taper angle and wedge mechanics. *J. Geophys. Res.*, 111:B04101, doi:10.1029/2005JB003990.
- Screaton, E.J., Wuthrich, D.R., and Dreiss, S.J., 1990. Permeabilities, fluid pressures, and flow rates in the Barbados ridge complex. *J. Geophys. Res.*, 95:8997–9007.
- Screaton, E.J., Saffer, D.M., Henry, P., Hunze, S., and the Leg 190 Shipboard Scientific Party, 2002. Porosity loss within under-thrust sediment of the Nankai accretionary complex: Implications for overpressures. *Geology*, 30:19–22, doi:10.1130/0091-7613(2002)030<0019:PLWTUS>2.0.CO;2.
- Spinelli, G., Saffer, D.M., and Underwood, M.B., 2006. Hydrogeologic responses to three-dimensional temperature variability, Costa Rica subduction margin. *J. Geophys. Res.*, 111:B04403, doi:10.1029/2004JB003436.
- Tobin, H.J. and Saffer, D.M., 2003. Fluid pressure in the shallow plate interface at the Nankai Trough subduction zone. *Eos Trans. AGU*, 84(46), Fall Meet. Suppl., Abstract T41A-04.
- Wissa, A.E.Z., Christian, J.T., Davis, E.H., and Heiberg, S., 1971. Consolidation at constant rate of strain. *J. Soil Mech. Found. Div., ASCE*, 97(SM10):1393–1413.
- Zoback, M.D., Zoback, M.L., Mount, V.S., Suppe, J., Eaton, J.P., Healy, J.H., Oppenheimer, D., Reasenber, P., Jones, L., Raleigh, C.B., Wong, I.G., Scotti, O., and Wentworth, C., 1987. New evidence on the state of stress of the San Andreas Fault, *Science*, 238:1105–1111, doi:10.1126/science.238.4830.1105.

Author

Demian Saffer, Department of Geosciences, The Pennsylvania State University, 310 Deike Building, University Park, Pa. 16802, U.S.A., e-mail: dsaffer@geosc.psu.edu.

Dynamic Rupture Propagation Modeling

by Satoshi Ide

doi:10.2204/iodp.sd.s01.05.2007

Resolving earthquake dynamic rupture is essential to understand the physics behind earthquake rupture. This paper first reviews the current status of the slip inversion, and then discusses the scaling of earthquake dynamic rupture.

Slip inversion methods have been developed since the 1980s to study the heterogeneity of spatio-temporal slip distribution of earthquakes. Several methods have been applied to many earthquakes using various data, such as near-field strong-motion records, far-field broadband records, and geodetic observations including GPS and InSAR. Some attempts have been made to compile a catalog of slip models to study their general features. Increasing the amount of data and communication speed allows even quasi-real time analysis of slip inversion, which gives an impression that these analyses are easy and straightforward. However, each slip model is based on some assumptions that are not always described well in research papers and can be a reason for apparent large discrepancies between models. For example, the models presented for the 1999 Izmit, Turkey earthquake (M_w 7.6) were quite different (Fig. 1) as shown in Ide et al. (2005). Basic characteristics, such as the locations of large slip and even the starting point of the rupture, were quite different. The data seem not to be insufficient; some strong motion stations are located close to the surface trace of the source fault, and some geodetic measurements are available. However, mainly due to uneven distribution of stations and inaccurate timings of seismometers, the data cannot resolve the growth process of earthquake rupture and the assumptions made by each research group to determine the characteristics of their slip model.

We have to use many model-dependent assumptions to obtain slip models. These include data selection and preprocessing, model settings such as fault plane geometry and parameterization, and inversion method including the assumption of probability function of error. Among them, the most uncertain factor is how to calculate synthetic data that we compare with observed data. Usually we assume layered structures to calculate seismic waveforms. It has been demonstrated that a reliable 3-D structure can increase the resolution of slip inversion, but such structure information is practically unavailable in many cases. The method of Empirical Green's functions, which uses the records of small earthquakes as theoretical waves, provides a good approximation of waves in complex structures, but to find a set of

good small events is not easy. Computation of seismic waveform is the bottleneck of current slip inversion.

Even now, the number of well resolved earthquakes is limited to about ten. Nevertheless, we find some general features of slip models. Earthquakes generally consist of successive ruptures of subevents, which are sometimes referred to as asperities with vague definition. The pulse-like rupture propagation is now widely accepted. As reported for some earthquakes, such as the 1906 San Francisco and the 2002 Denali, rupture pulses can propagate faster than the S-wave speed, but the average propagation velocity does not exceed it. Well resolved slip models can be used to discuss dynamic properties of earthquake rupture. Fault constitutive relationships and their characteristic parameters, slip weakening distance D_c and fracture energy G_c , have been estimated for some well resolved earthquakes, such as the 1992 Landers, the 1995 Kobe, and the 2000 Tottori. While D_c tends to be overestimated, G_c is a relatively stable parameter controlled mainly by rupture propagation velocity.

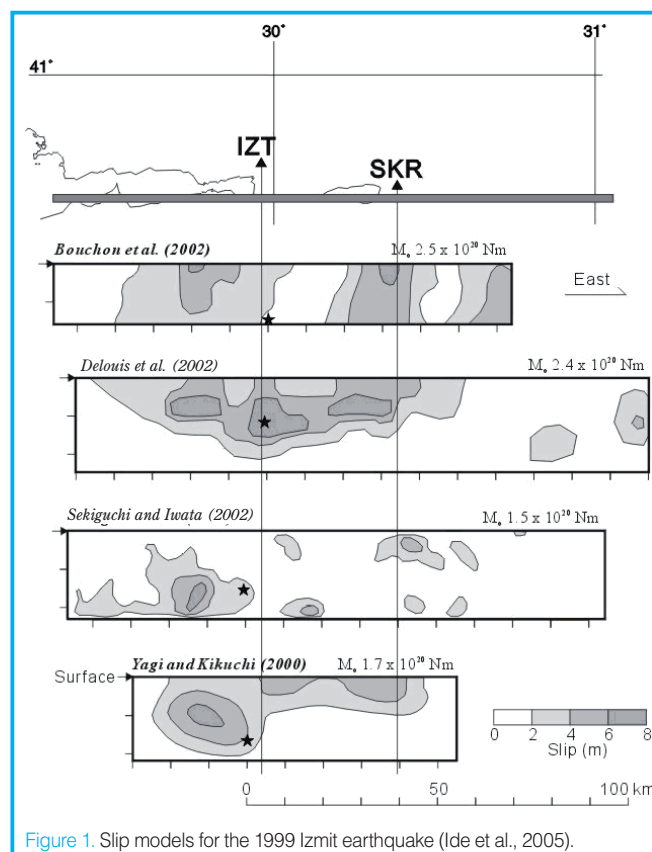


Figure 1. Slip models for the 1999 Izmit earthquake (Ide et al., 2005).

Earthquake faults and slip generally satisfy geometrical similarity; in other words, earthquakes have similar stress drop. If earthquakes are also temporally similar having similar rupture velocities, we expect to observe an almost constant ratio between seismic energy and seismic moment. Although there is still room for discussion whether the ratio is strictly constant, its change is small compared to the wide difference in seismic moment (about 15-fold).

While the scaling for these macroscopic parameters is well documented, the study for the scaling of earthquake complexity has started only recently. For example, Somerville et al. (1999) pointed out that the size of asperity (large slipped areas) scales as the square of the cubic root of seismic moment, suggesting geometrical similarity. Using a large catalog of slip models, Mai and Beroza (2000) also found similar scaling for seismic moment and fault length and width. However, they also showed that the scaling is different for the width of strike slip events, which is an evidence of a break of self-similarity. Sometimes, small earthquakes are assumed to be simple compared to large ones; however, this concept is not so obvious. Moreover, recently estimated slip models for microearthquakes ($\sim M_w 1$) in a South Africa gold mine (Yamada et al., 2005) do have a subevent sequence, and characteristic time, length, and slip amount are all smaller by a factor of 1000 compared to those of the Kobe earthquakes. The information about scaling laws and their limitation are quite useful to construct hypothetical earthquake models for strong motion prediction.

Slip models can be used to scale dynamic parameters, too. Fracture energy G_c is a relatively reliable parameter calculated for many slip models. The average fracture energy estimated for earthquakes of M_w 5 to 7 is almost proportional to seismic moment, although the examples are limited.

All the previously mentioned studies for earthquake scaling compare small and large earthquakes using different measures that are comparable to the final size of events, but there are other ways to compare. One is the scaling of complexity during rupture growth of one earthquake—namely, comparison between the initial and final stages of one event. Once we recognize this scaling law, we can recognize whether one small rupture is the initial part of a large event or just a small event. Unfortunately, traditional slip inversion cannot solve this problem. Recently, we developed a new method suitable to this problem, which we refer to as the multiscale slip inversion method (Uchide and Ide, 2006). The initial stage of an earthquake can be investigated using high-frequency seismic waves near the onset of signal, while traditional inversion details overall rupture propagation. We can prepare a set of observation equations on these two scales, or with some additional intermediate scales. These observation equations are unified into a multiscale observation equation using a renormalized multiscale slip model. By solving this equation in the same way as traditional slip inversion problem, we obtain a multiscale slip model with changing resolution as the rupture grows.

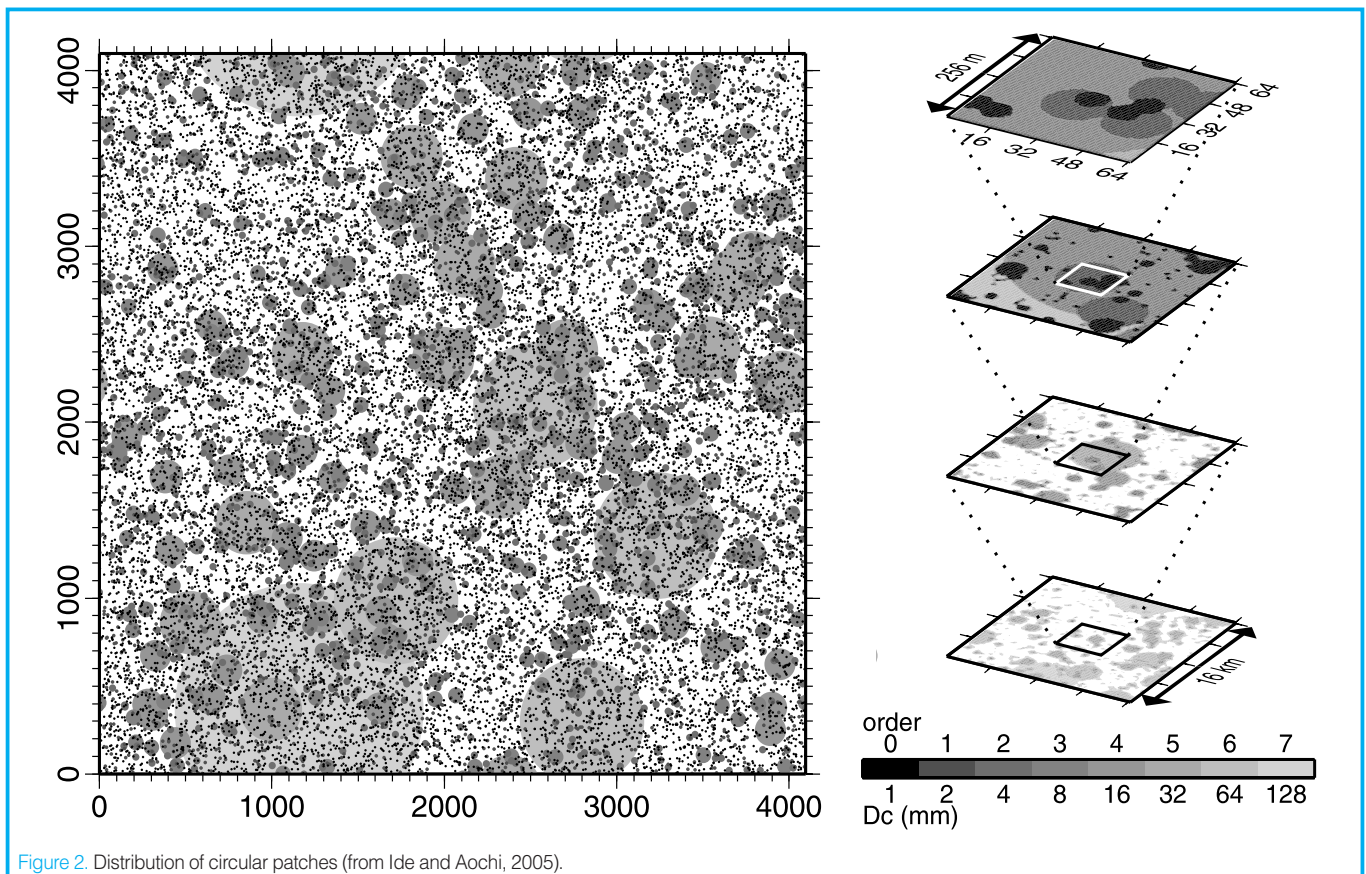


Figure 2. Distribution of circular patches (from Ide and Aochi, 2005).

We first applied this method to the mid-Niigata prefecture earthquake in 2004 in Japan. The spatio-temporal slip distribution is obtained as a nested spatio-temporal slip distribution on an assumed fault plane. Unlike ordinary slip models, this model contains a detailed rupture process in the first 1 s. The resolution in the next 1 s is worse, but the model area increases. Finally, we obtain the full scale rupture process with low resolution, which is similar to the result of traditional slip inversion. We observe several slip pulses in different directions even in the first 1 s. In every scale, slip rate is about 1 m s^{-1} , suggesting similarity.

When the earthquake is a self-similar process, how does a rupture propagate? Ide and Aochi (2005) have modeled self-similar dynamic ruptures assuming a heterogeneous distribution of circular patches on a planar crack (Fig. 2). Two points of the model are that 1) slip weakening distance D_c scales with the size of patch, and 2) the size-number distribution of patches satisfies a power law. Assuming that a rupture starts from one of the smallest patches, we solve the elastodynamic equation using the boundary integral equation method with the renormalization technique. Some ruptures grow into very large events, while most ruptures remain small. The moment rate function of a large event begins with a so-called initial phase which may also contain an initial phase in a smaller scale. Therefore, the rupture process is statistically self-similar. The rupture speed is subshear in average, but it can locally exceed S-wave speed, which is consistent with recent observations and slip models.

Whether a self-similar dynamic rupture growth is a good approximation of an earthquake remains to be proven. The answer to this question is important, not only because it is fundamental for the physics behind earthquakes, but also because it can be the basis of various practical usages of small earthquakes, such as assessment of earthquake predictability and predication of strong motion. Slip inversion is a useful tool to assist in resolving this question, and we have to overcome many problems to obtain sufficient numbers of reliable slip models, which are required for a statistical discussion.

References

- Bouchon, M., Toksöz, N.M., Karabulut, H., Bouin, M.-P., Dietrich, M., Aktar, M., and Edie, M., 2002. Space and time evolution of rupture and faulting during the 1999 Izmit (Turkey) earthquake. *Bull. Seismol. Soc. Am.*, 92:256–266, doi:10.1785/0120000845.
- Delouis, B., Giardini, D., Lundgren, P., and Salichon, J., 2002. Joint inversion of InSAR, GPS, teleseismic, and strong motion data for the spatial and temporal distribution of earthquake slip: Application to the 1999 Izmit mainshock. *Bull. Seismol. Soc. Am.*, 92:278–299, doi:10.1785/0120000806.
- Ide, S. and Aochi, H., 2005. Earthquakes as multiscale dynamic ruptures with heterogeneous fracture surface energy. *J. Geophys. Res.*, 110:B11303, doi:10.1029/2004JB003591.
- Ide, S., Beroza, G.C., and McGuire, J.J., 2005. Imaging earthquake source complexity. *Seismic Earth: Array Analysis of Broadband Seismograms. Geophys. Monogr. Ser.* 157:117–135.
- Mai, P.M. and Beroza, G.C., 2000. Source scaling properties from finite-fault-rupture models. *Bull. Seismol. Soc. Am.*, 90:604–614, doi:10.1785/0119990126.
- Sekiguchi, H. and Iwata, T., 2002. Rupture process of the 1999 Kocaeli, Turkey, earthquake estimated from strong-motion waveforms. *Bull. Seismol. Soc. Am.*, 92:300–311, doi:10.1785/0120000811.
- Somerville, P., Irikura, K., Graves, R., Sawada, S., Wald, D., Abrahamson, N., Iwasaki, Y., Kagawa, T., Smith, N., and Kowada, A., 1999. Characterizing crustal earthquake slip models for the prediction of strong ground motion. *Seismol. Res. Lett.*, 70:59–80.
- Uchide, T. and Ide, S., 2006. Development of multiscale slip inversion method and its application to the 2004 mid-Niigata prefecture earthquake. *Eos Trans. AGU*, 87(52), Fall Meet. Suppl., Abstract S42C-01.
- Yagi, Y. and Kikuchi, M., 2000. Source rupture process of the Kocaeli, Turkey, earthquake of August 17, 1999, obtained by joint inversion of near-field data and teleseismic data. *Geophys. Res. Lett.*, 27:13–1969.
- Yamada, T., Mori, J.J., Ide, S., Kawakata, H., Iio, Y., and Ogasawara, H., 2005. Radiation efficiency and apparent stress of small earthquakes in a South African gold mine. *J. Geophys. Res.*, 110:B01305, doi:10.1029/2004JB003221.

Author

Satoshi Ide, Department of Earth and Planetary Science, University of Tokyo, 7-3-1, Hongo, Bunkyo, Tokyo, 113-0033, Japan, e-mail: ide@eps.s.u-tokyo.ac.jp

Fault Zone Complexity and Earthquake Ruptures

by Ryosuke Ando and Teruo Yamashita

doi:10.2204/iodp.sd.s01.18.2007

Earthquake ruptures are propagated inside fault zones that consist of structures spanning a wide spectrum of lengths. A natural fault is known to consist of hierarchy structure ranging from the scale of fine grains forming a gouge or ultracataclasite zone along the principal slip plane (Fig. 1, top) up to that of fault system consisting of discrete fault segments (Fig. 1, bottom) and/or branched fault segments (Fig. 1, middle and bottom). Although the physics of earthquakes has been well studied on microscopic and macroscopic scales (Fig. 1, top and bottom, respectively) based on laboratory experiments and seismic inversion analysis, respectively, the effects on a mesoscopic scale (Fig. 1, middle) are poorly understood. Since these structures interact with earthquake ruptures, one of the seismologically fundamental problems is to understand how they are formed and evolved associated with the earthquakes that are the most intensive activities on fault zones.

In this study we focus on the investigation of the formation of branches in mesoscopic and macroscopic scales, and their effects on dynamic ruptures. In our model, branch fault segments are assumed to be nucleated at some discrete points on the main fault, which implies that the main fault is weak locally at these points. Each branch is assumed to be nucleated at each prescribed point on the main fault once the main fault tip passes, and the following fracture criterion is satisfied there. We also assume branches are extending in the direction of the maximum shear traction at each branch. Our studies rely on a simple slip-weakening law as the fracture criterion and the friction law:

$$\tau(S) = \frac{\tau_p - \tau_r}{D_c} (D_c - S) H(D_c - S) + \tau_r \quad (1)$$

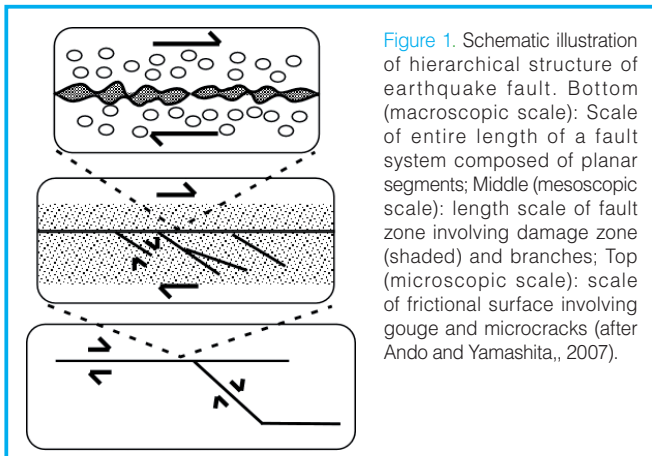


Figure 1. Schematic illustration of hierarchical structure of earthquake fault. Bottom (macroscopic scale): Scale of entire length of a fault system composed of planar segments; Middle (mesoscopic scale): length scale of fault zone involving damage zone (shaded) and branches; Top (microscopic scale): scale of frictional surface involving gouge and microcracks (after Ando and Yamashita, 2007).

where τ_p , τ_r , S , D_c , and H (s) denote the peak shear strength, residual shear stress, slip, critical slip displacement, and a unit step function, respectively. The boundary integral equation method (BIEM) is employed to numerically solve the elastodynamic response of the medium. This method has advantages (in the treatment of non-planar fault geometry) and problems (where rupture paths are not specified but dynamically determined as the ruptures are extended).

Figure 2 shows snapshots of a typical example of fault growth. First, the main fault starts its extension and begins to nucleate branches. However, the nucleated branches do not begin their growths when the extension of the main fault is not long enough because of insufficient enhancement of stress (Fig. 2A). As the size of the main fault increases, the shear stress is magnified near its extending tip. If such stress enhancement becomes sufficiently large, branches can begin their growths while their extensions are arrested after attaining certain lengths (Fig. 2B and C). The spatial distribution of these arrested branches forms a roughly triangular zone on one side of the main fault. The lengths of these branches increase with main fault size. As the main fault extends further and its size exceeds a certain critical length L_m , a limited number of branches continue to grow together

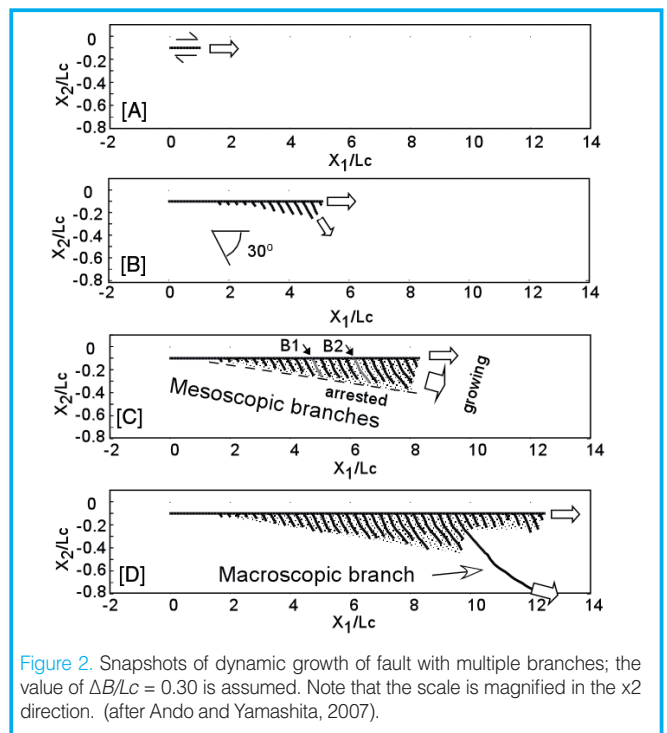


Figure 2. Snapshots of dynamic growth of fault with multiple branches; the value of $\Delta B/L_c = 0.30$ is assumed. Note that the scale is magnified in the x2 direction. (after Ando and Yamashita, 2007).

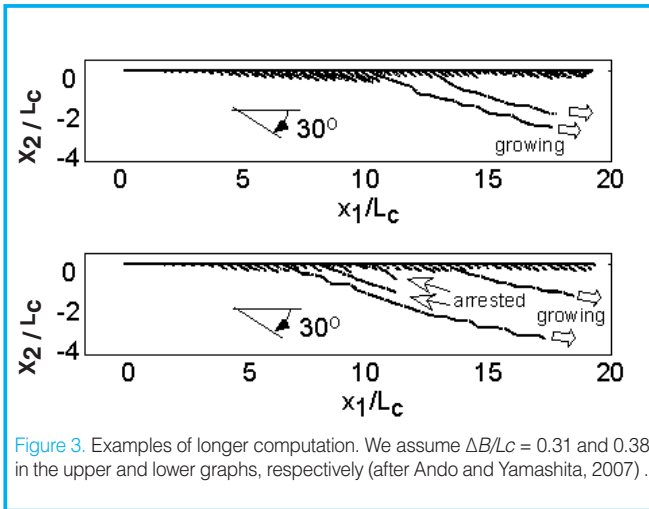


Figure 3. Examples of longer computation. We assume $\Delta B/L_c = 0.31$ and 0.38 in the upper and lower graphs, respectively (after Ando and Yamashita, 2007).

with the main fault without arresting. This suggests that complicated fault geometry can be generated dynamically. It is also shown in the figure that the emergence of such a large-scale branch tends to suppress the growth of the next nucleated branches in its neighborhood, which is due to the stress shadow effect as will be discussed below. Such phenomena are also observed in Figure 3, which shows an example of longer simulation time.

Figure 4 shows the extending velocity of the tip of main fault soon attains a constant value with the extension. Comparing the velocity at each position between this multiple branch model and the case of a planar fault, we can clearly see that the dynamic branching reduces the rupture velocity of the main fault; the assumed physical parameters are identical between them (except the geometry). This data will contribute to the formation of approximately self-similar shapes for the spatial distribution of meso-branches.

We further investigate the effect of mesoscopic branches as the stress-slip relationship on a macroscopic scale, neglecting the thickness of the fault zone. Figure 5 shows this relationship obtained at each point along the main fault by calculating shear stress and displacement immediately outside the fault zone. The critical slip weakening distance D_c and the fracture energy G_c become proportional to the

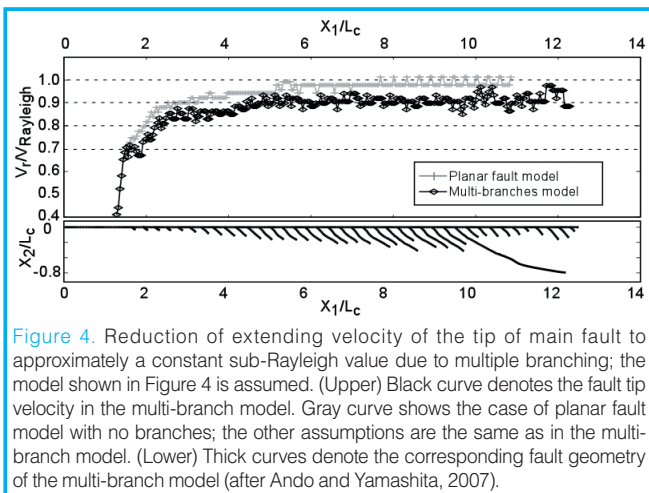


Figure 4. Reduction of extending velocity of the tip of main fault to approximately a constant sub-Rayleigh value due to multiple branching; the model shown in Figure 4 is assumed. (Upper) Black curve denotes the fault tip velocity in the multi-branch model. Gray curve shows the case of planar fault model with no branches; the other assumptions are the same as in the multi-branch model. (Lower) Thick curves denote the corresponding fault geometry of the multi-branch model (after Ando and Yamashita, 2007).

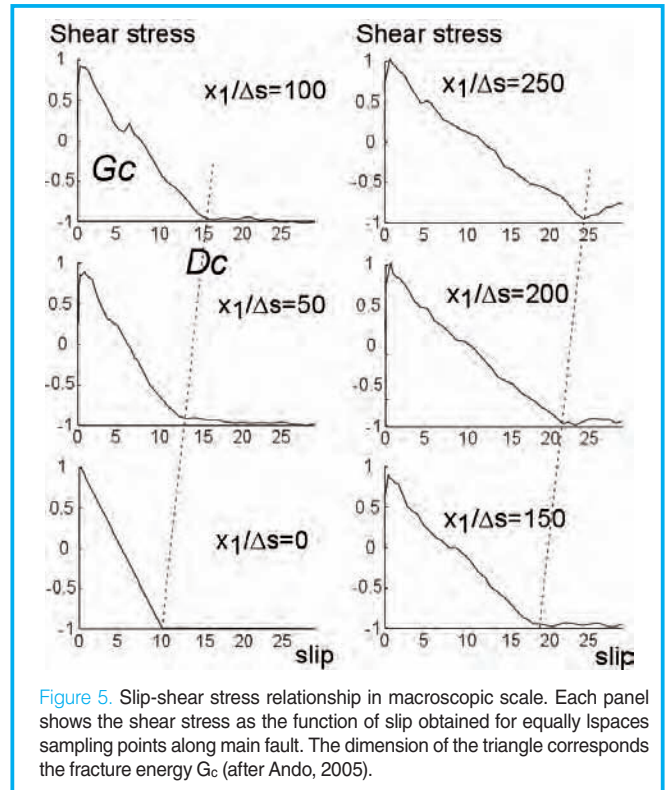


Figure 5. Slip-shear stress relationship in macroscopic scale. Each panel shows the shear stress as the function of slip obtained for equally spaced sampling points along main fault. The dimension of the triangle corresponds the fracture energy G_c (after Ando, 2005).

distance of rupture propagation. This explains why the observed constant rupture velocity (Fig.4) decreased under a sub-Rayleigh speed. Note that this simple scaling is satisfied as long as the rupture propagation distance is smaller than a critical length L_m .

References

Ando, R. and Yamashita, T., 2007. Effects of mesoscopic-scale fault structure on dynamic earthquake ruptures: Dynamic formation of geometrical complexity of earthquake faults, *J. Geophys. Res.*, 112, B09303, doi:10.1029/20062006JB004612.

Ando, R., 2005. Development of efficient spatio-temporal boundary integral equation method and theoretical study on dynamics of fault zone formation and earthquake ruptures (in Japanese), Univ. of Tokyo, Tokyo.

Authors

Ryosuke Ando, National Research Institute for Earth Science and Disaster Prevention, 3-1 Tennodai, Tsukuba, Ibaraki, 305-0006, Japan, e-mail:ando@bosai.go.jp.

Teruo Yamashita, Earthquake Research Institute, The University of Tokyo, 1-1-1 Yayoi, Bunkyo-ku, Tokyo, Japan.

Structure and Properties of the San Andreas Fault in Central California: Recent Results from the SAFOD Experiment

by Stephen Hickman, Mark Zoback, William Ellsworth, Naomi Boness, Peter Malin, Steven Roecker, and Clifford Thurber

doi:10.2204/iodp.sd.s01.39.2007

The San Andreas Fault Observatory at Depth (SAFOD) is a 3.2-km-deep borehole observatory drilled into the San Andreas fault zone at seismogenic depths to study directly the physical and chemical processes controlling faulting and earthquake generation. SAFOD forms one component of EarthScope, a major Earth Science facility program of the U.S. National Science Foundation; the other two funded components are U.S. Array, a continental-scale seismic network, and the Plate Boundary Observatory, an extensive network of GPS receivers and strainmeters deployed across the western U.S. SAFOD is being conducted in collaboration with the U.S. Geological Survey and the International Continental Scientific Drilling Program (ICDP). A detailed scientific rationale for drilling into active faults (including an overview of past and ongoing fault zone drilling projects) is presented in Zoback et al. (2007).

SAFOD is located in central California within the transition between the creeping and locked sections of the San Andreas Fault, 9 km NW of Parkfield, Calif. and just NW of the rupture zone of the 2004 M6.0 Parkfield earthquake. The fault displays a range of behaviors at this site. At the surface, it is creeping at a rate of 1.8 cm yr⁻¹, with most of the fault displacement localized to a zone no more than 10 m wide (Burford and Harsh, 1980; Schulz, 1989). Numerous earthquakes occur directly on the San Andreas fault at this location, and they define the fault to be a narrow, near-vertical seismically active zone with a top at about 3-km depth (Fig. 1).

An important feature of microearthquakes along the San Andreas fault at SAFOD is that they occur in families of repeating events. The University of California - Berkeley High Resolution Seismic Network has observed individual earthquakes to recur every few years at precisely the same location and with the same magnitude (Nadeau and McEvilly, 1997; Nadeau et al., 2004). Repeating sources of up to M2 are located at depths as shallow as 3 km at the SAFOD site, and they play a key role in guiding SAFOD drilling.

In preparation for drilling of the main SAFOD borehole, a 2.2-km-deep vertical pilot hole was funded by the ICDP and rotary drilled in 2002 at the SAFOD site, located 1.8 km to the southwest of the surface trace of the San Andreas fault (Fig. 2). Results from the pilot hole were instrumental in defining the background geological and geophysical setting of the fault at this location, and in providing information on

geologic structure and earthquake locations needed for planning of the main SAFOD experiment. Results from the SAFOD Pilot Hole and related site characterization studies were presented by Hickman et al. (2004) and in associated papers published in two special issues of Geophysical Research Letters.

During Phases 1 and 2 in the summers of 2004 and 2005, the SAFOD main hole was rotary drilled vertically and then deviated across the entire San Andreas fault zone through the zone of repeating microearthquakes, passing beneath the surface trace of the San Andreas fault at a depth of 3.1 km (Fig. 2C). From its inception, a major goal of SAFOD has been to drill into, sample, and monitor one or more of the repeating M2 earthquake sources (green, red, and blue earthquakes in Figs. 1 and 2) to follow the buildup and release of strain through multiple earthquake cycles.

Extensive drill cuttings were obtained during Phases 1 and 2, and a real-time analysis of gases in the drilling mud was carried out (Wiersberg and Erzinger, 2007 a, b). In addition, about sixty meters of spot core was acquired from the SAFOD main borehole at vertical depths of 1.5 km, 2.5 km, and 3.2 km, and sidewall cores were collected in the lower section of the hole. An extensive suite of open-hole

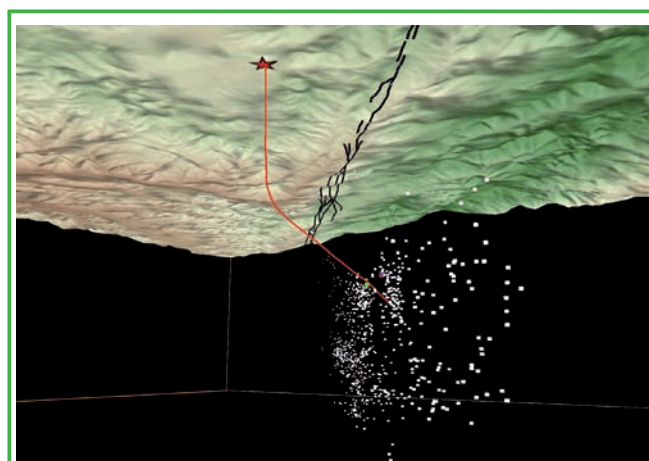


Figure 1. Seismicity of the San Andreas fault as seen from a vantage point in the earth looking to the northwest. Hypocenters were determined using tomoDD by Haijiang Zhang (University of Wisconsin - Madison) utilizing data from the Parkfield Area Seismic Observatory, supplemented by data from local USGS and University of California - Berkeley network stations. The San Andreas fault is made visible by more than 1000 microearthquakes. The SAFOD main hole is shown in red, extending downward from the surface facility (star). The surface trace of the fault is shown in black draped over the topography (3-D EarthVision plot by Luke Blair, USGS).

geophysical logs was obtained along almost the entire length of the well. For a complete description of drill cuttings, core samples and geophysical logs acquired during SAFOD Phases 1 and 2 see the ICDP Web site on SAFOD, link to Public Data (safod.icdp-online.org). Preliminary results from SAFOD Phases 1 and 2 were presented in two special sessions of the December 2005 American Geophysical Union meeting, and numerous publications are in print or under review detailing early results from SAFOD. Results from analyses of drill cuttings and cores from SAFOD are discussed in Solum et al. (2007), Schleicher et al. (2007), and references cited therein.

Four major geologic units were encountered along the trajectory of the SAFOD main hole. In the vertical section of the wellbore, the near-surface Quaternary and Tertiary sediments were found to be underlain by Salinian granite at a depth of ~700 m. After the borehole was deviated toward the fault, arkosic sediments (most likely locally-derived from Salinian granite) were encountered about 300 m NE of the drill site, perhaps after crossing the Buzzard Canyon fault, a NW-trending strike-slip fault exposed at the surface that trends sub-parallel to the San Andreas (M. Rymer, personal comm.). Approximately 1200 m NE of the drill site, a possibly ancestral trace of the San Andreas was crossed as the lithology changed abruptly to claystones and siltstones of the Great Valley Formation, found throughout central California on the east side of the San Andreas.

Geophysical logs and cuttings analysis indicate that the San Andreas fault is a zone of anomalously low P- and S-wave velocity and resistivity that defines a relatively broad (~200-m-wide) damage zone (Fig. 3). The location of a currently active trace of the San Andreas fault is revealed by casing deformation (indicated by the red line in Fig. 3) detected through repeated multifinger caliper logs. This active fault is associated with a narrower (~30-m-wide), more highly localized zone of low P- and S-wave velocity and resistivity embedded within the broader damage zone. Serpentinites and talc were also found in cuttings immediately adjacent to this deforming zone (Moore and Rymer, 2007; Solum et al., 2006, 2007), which might be responsible for the predominantly creeping behavior of the San Andreas fault at this location as well as its low long-term strength. Work is now underway to determine if this actively deforming fault trace is associated with repeating microearthquakes in the SAFOD target region.

Stress measurements in the SAFOD pilot hole and main hole provide strong evidence in support of the hypothesis that the San Andreas is a weak fault imbedded in an otherwise strong crust. Horizontal differential stress magnitudes in the pilot hole were found to be high adjacent to the fault, while the orientation of maximum horizontal stress at depth in the hole indicates low levels of shear stress resolved onto the fault itself (Hickman and Zoback, 2004). Shear-wave anisotropy measurements in the SAFOD main hole further indicate that the direction of maximum horizontal compression remains nearly perpendicular to the fault to within a few hundred meters of the active fault trace at depth (Boness and Zoback, 2006). In addition, heat flow measurements in the SAFOD pilot hole and main hole (to 3.1 km depth) are consistent with shallower data in the region which show no evidence of frictionally-generated heat (Williams et al., 2004; 2006).

Beginning in February 2006, we conducted a series of instrumental investigations in the SAFOD main hole in close proximity to where fault movement is actively deforming the borehole casing. A digitally telemetered pair of 3-component 15-Hz geophones was mechanically clamped inside the casing to record very local earthquakes at a sample rate of 4000 sps. The tool also contains a biaxial tiltmeter. We succeeded in

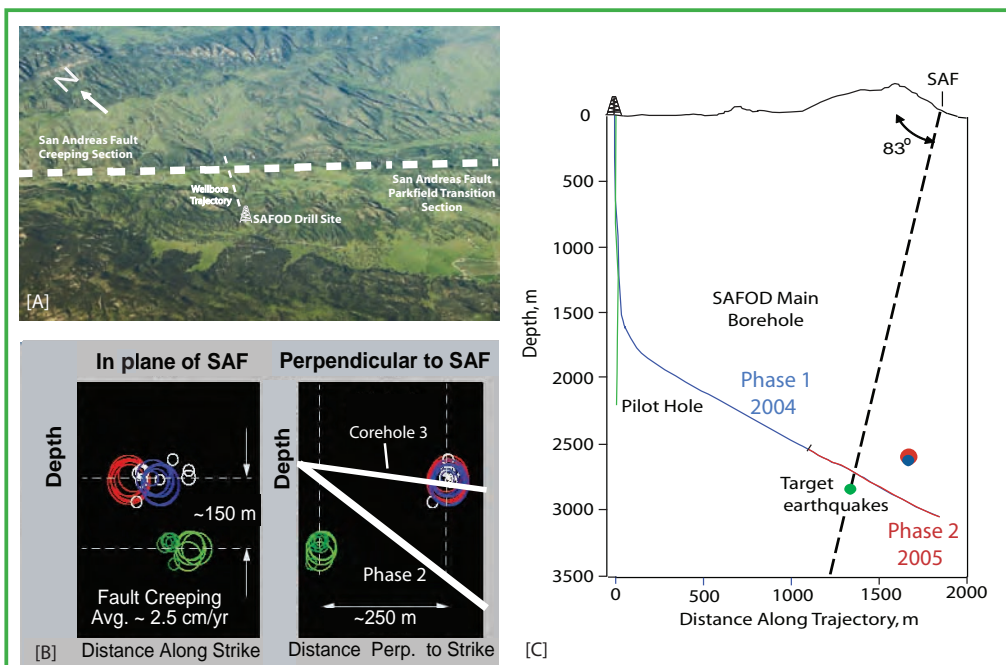


Figure 2. [A] The SAFOD drill site is located at the southeastern end of the creeping section of the fault, where the surface creep rate begins to gradually decrease in the Parkfield section. [B] There are three groups of repeating earthquakes in the target area. As shown in the cross-section in a plane parallel to the fault, the groups of repeaters shown in red, blue, and green correspond to M~2 earthquakes that recur every ~2.5 years. As shown in the cross-section perpendicular to the fault, the red and blue repeaters occur on a different strand of the fault than the green repeaters. Hence, there are multiple active fault traces at depth. The white lines schematically illustrate the location of the SAFOD main borehole—drilled in the summers of 2004 and 2005—and a core hole targeting the microearthquakes to be drilled in 2007. [C] Trajectories of the SAFOD pilot hole and main hole. The microearthquake locations are to the southwest of the surface trace of the fault.

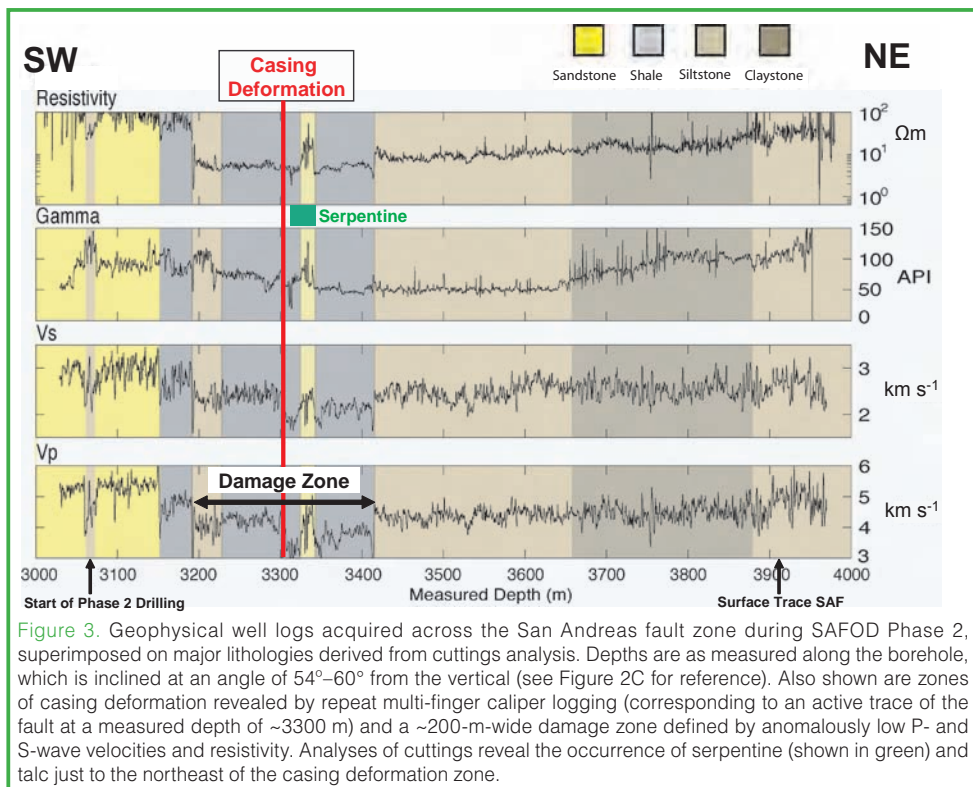


Figure 3. Geophysical well logs acquired across the San Andreas fault zone during SAFOD Phase 2, superimposed on major lithologies derived from cuttings analysis. Depths are as measured along the borehole, which is inclined at an angle of 54°–60° from the vertical (see Figure 2C for reference). Also shown are zones of casing deformation revealed by repeat multi-finger caliper logging (corresponding to an active trace of the fault at a measured depth of ~3300 m) and a ~200-m-wide damage zone defined by anomalously low P- and S-wave velocities and resistivity. Analyses of cuttings reveal the occurrence of serpentine (shown in green) and talc just to the northeast of the casing deformation zone.

recording a wide variety of seismic phenomena with this instrumentation, which are discussed in more detail by Ellsworth et al (2007). Notably, several of the M2 target earthquakes were recorded in the very near-field, at distances down to ~400 m. SAFOD downhole seismometers also recorded a new type of seismic wave that arrives between the P- and S-waves and appears to be a “leaky mode” PSV fault guided wave; the well known SH-type fault guided waves were also seen. If borne out by more complete modeling, these observations provide strong support for the hypothesis that continuous narrow, low-velocity fault zones extend deep into the seismogenic crust. We also successfully conducted several “virtual earthquake” experiments in which small explosive charges were detonated next to surface seismograph stations to measure the travel time from the station to the borehole seismometer. Using travel time reciprocity, these data are being used to determine with greater accuracy the absolute locations of the SAFOD target earthquakes in preparation for Phase 3.

During Phase 3 of SAFOD, planned for the summer of 2007, continuous cores will be acquired from three multi-lateral holes branching off the main SAFOD borehole to directly sample the damage zone (Fig. 3) and both the creeping and seismically active faults at depth (Fig. 2B). These core samples will be extensively studied in the laboratory to compare and contrast the composition, deformation mechanisms, physical properties, and rheological behavior of creeping and seismogenic fault rocks at realistic *in situ* conditions. At the conclusion of SAFOD Phase 3, an array of instruments will be deployed in the cased borehole in the immediate vicinity of the repeating M2 target earth-

quakes for long-term monitoring of near-field radiated seismic energy, deformation, fluid pressure, and seismicity through multiple earthquake cycles (Fig. 4). This will allow scientists to test—for the very first time—a variety of hypotheses related to earthquake rupture nucleation, propagation, and arrest, as well as the possible role of fluid pressure in controlling fault strength and earthquake periodicity.

References

- Boness, N. and Zoback, M.D., 2006. A multi-scale study of the mechanisms controlling shear velocity anisotropy in the San Andreas Fault Observatory at Depth. *Geophysics*, 7(5):F131–F146, doi:10.1190/1.2231107.
- Burford, R.O., and Harsh, P.W., 1980. Slip on the San Andreas fault in central California from alignment array surveys. *Bull. Seismol. Soc. Am.*, 70:1233–1261.
- Ellsworth, W., Malin, P.E., Imanishi, K., Roecker, S.W., Nadeau, R., Oye, V., Thurber, C.H., Waldhauser, F., Boness, N.N., Hickman, S.H., and Zoback, M.D., 2007. Seismology inside the fault zone: applications to fault-zone properties and rupture dynamics. *Scientific Drilling Special Issue*, 1:85–88.
- Hickman, S. and Zoback, M.D., 2004. Stress measurements in the SAFOD pilot hole: implications for the frictional strength of the San Andreas Fault. *Geophys. Res. Lett.*, 31:L15S12.
- Hickman, S., Zoback, M.D., and Ellsworth, W.E., 2004. Introduction to special section: Preparing for the San Andreas Fault Observatory at Depth. *Geophys. Res. Letters*, 31, L12S01, doi:10.1029/2004GL20688.
- Moore, D.E. and Rymer, M.J., 2007. Talc-bearing serpentinite and the creeping section of the San Andreas fault. *Nature* 448, 795–797, doi:10.1038/nature06064
- Nadeau, R.M. and McEvilly, T.V., 1997. Seismological studies at Parkfield V: Characteristic microearthquake sequences as fault-zone drilling targets. *Bull. Seismol. Soc. Am.*, 87:1463–1472.
- Nadeau, R.M., Micheline, A., Uhrhammer, R.A., Dolenc, D., and McEvilly, T.V., 2004. Detailed kinematics, structure and recurrence of micro-seismicity in the SAFOD target region. *Geophys. Res. Lett.*, 31:L12S08, doi:10.1029/2003GL019409.
- Schleicher, A.M., van der Pluijm, B.A., Warr, L.N., and Solum, J.G., 2007. Electron Microscopy of Clay Minerals in Mudrocks from the San Andreas Fault Observatory at Depth (SAFOD). *Scientific Drilling Special Issue* 1:68–70.
- Schulz, S.S., 1989. Catalog of creepmeter measurements in California from 1966 through 1988. *U.S. Geological Survey Open-File Report* 89-650.
- Solum, J.G., Hickman, S.H., Lockner, D.A., Moore, D.E., van der

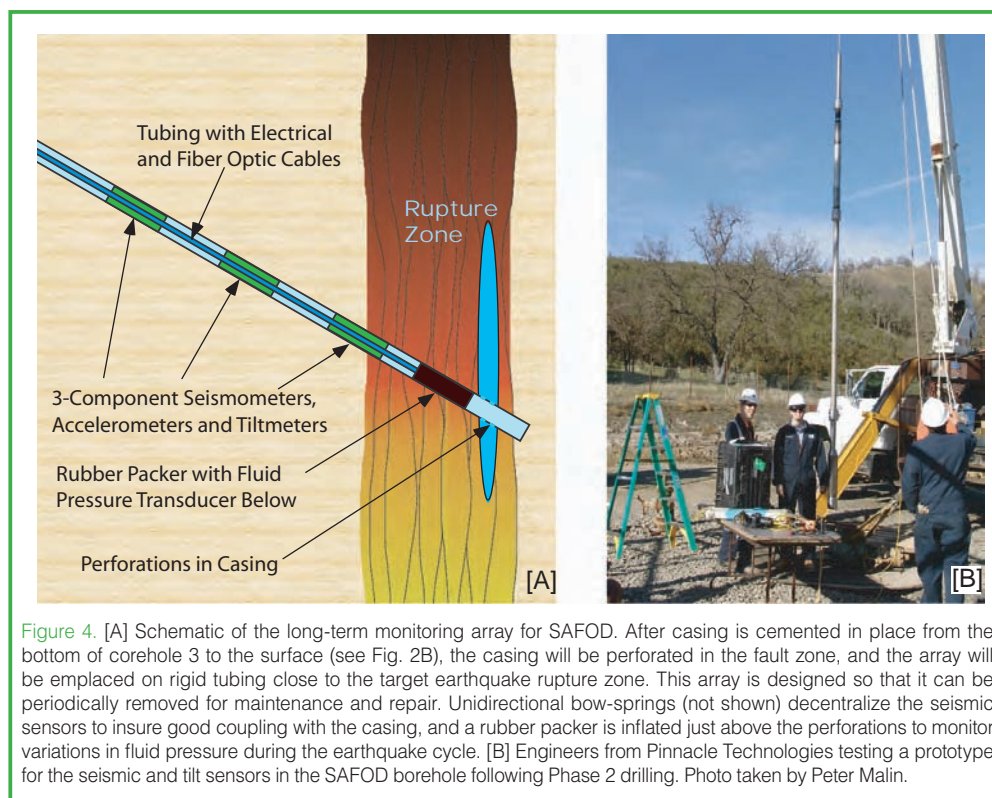


Figure 4. [A] Schematic of the long-term monitoring array for SAFOD. After casing is cemented in place from the bottom of corehole 3 to the surface (see Fig. 2B), the casing will be perforated in the fault zone, and the array will be emplaced on rigid tubing close to the target earthquake rupture zone. This array is designed so that it can be periodically removed for maintenance and repair. Unidirectional bow-springs (not shown) decentralize the seismic sensors to insure good coupling with the casing, and a rubber packer is inflated just above the perforations to monitor variations in fluid pressure during the earthquake cycle. [B] Engineers from Pinnacle Technologies testing a prototype for the seismic and tilt sensors in the SAFOD borehole following Phase 2 drilling. Photo taken by Peter Malin.

Related Web Link

safod.icdp-online.org

Authors

Stephen Hickman, U.S. Geological Survey, 345 Middlefield Road, Mail Stop 977, Menlo Park, Calif., 94025, U.S.A., e-mail:hickman@usgs.gov.

Mark Zoback, Stanford University, Mitchell Building, Room 359, Stanford, Calif., 94305-2215, U.S.A.

William Ellsworth, U.S. Geological Survey, 345 Middlefield Road, Mail Stop 977, Menlo Park, Calif., 94025, U.S.A.

Naomi Boness, Chevron Energy Technology Company, 6001 Bollinger Canyon Road, San Ramon, Calif., 94583,

U.S.A.

Peter Malin, Duke University, 109A Old Chem, Box 90227, Durham, N.C., 27708, U.S.A.

Steven Roecker, Department of Earth and Environmental Sciences, Rensselaer Polytechnic Institute, Troy, N.Y., 12180, U.S.A.

Clifford Thurber, Department of Geology and Geophysics, University of Wisconsin, 1215 West Dayton Street, Madison, Wis., 53706, U.S.A.

Pluijm, B.A., Schleicher, A.M., and Evans, J.P., 2006. Mineralogical characterization of protolith and fault rocks from the SAFOD main hole. *Geophys. Res. Lett.*, 33:L21314, doi: 10.1029/2006GL027285.

Solum, J.G., Hickman, S., Lockner, D.A., Tembe, S., Evans, J.P., Draper, S.D., Barton, D.C., Kirschner, D.L., Chester, J.S., Chester, F.M., van der Pluijm, B.A., Schleicher, A.M., Moore, D.E., Morrow, C., Bradbury, K., Calvin, W.M., and Wong, T.-F., 2007. San Andreas fault zone mineralogy, geochemistry and physical properties from SAFOD cuttings and core. *Scientific Drilling Special Issue 1*:64–67.

Wiersberg, T. and Erzinger, J., 2007a. A helium isotope cross-section study through the San Andreas Fault at seismogenic depths. *Geochem. Geophys. Geosyst.*, 8(1):Q01002, doi:10.1029/2006GC001388.

Wiersberg, T. and Erzinger, J., 2007b. Real-time mud gas monitoring: A technique to obtain information on the composition and distribution of gases at depth while drilling. *Scientific Drilling Special Issue 1*:71–72.

Williams, C.F., Grubb, F.V., and Galanis, S.P., 2004. Heat flow in the SAFOD pilot hole and implications for the strength of the San Andreas Fault. *Geophys. Res. Lett.*, 31:L15S14, doi:10.1029/2003GL019352

Williams, C.F., Grubb, F.V., and Galanis, Jr, S.P., 2006. Heat flow measurements across the San Andreas Fault near Parkfield, California - preliminary results from SAFOD. *Eos Trans. AGU*, 87(52), Fall Meet. Suppl., Abstract S33B-0241.

Zoback, M.D., Hickman, S., and Ellsworth, W., 2007. The role of fault zone drilling. In Kanamori, H., and Schubert, G. (Eds.), *Earthquake Seismology - Treatise on Geophysics*. Amsterdam (Elsevier), in press.

Drilling of the Chelungpu Fault after the 1999 Chi-Chi, Taiwan Earthquake (Mw7.6): Understanding Physics of Faulting

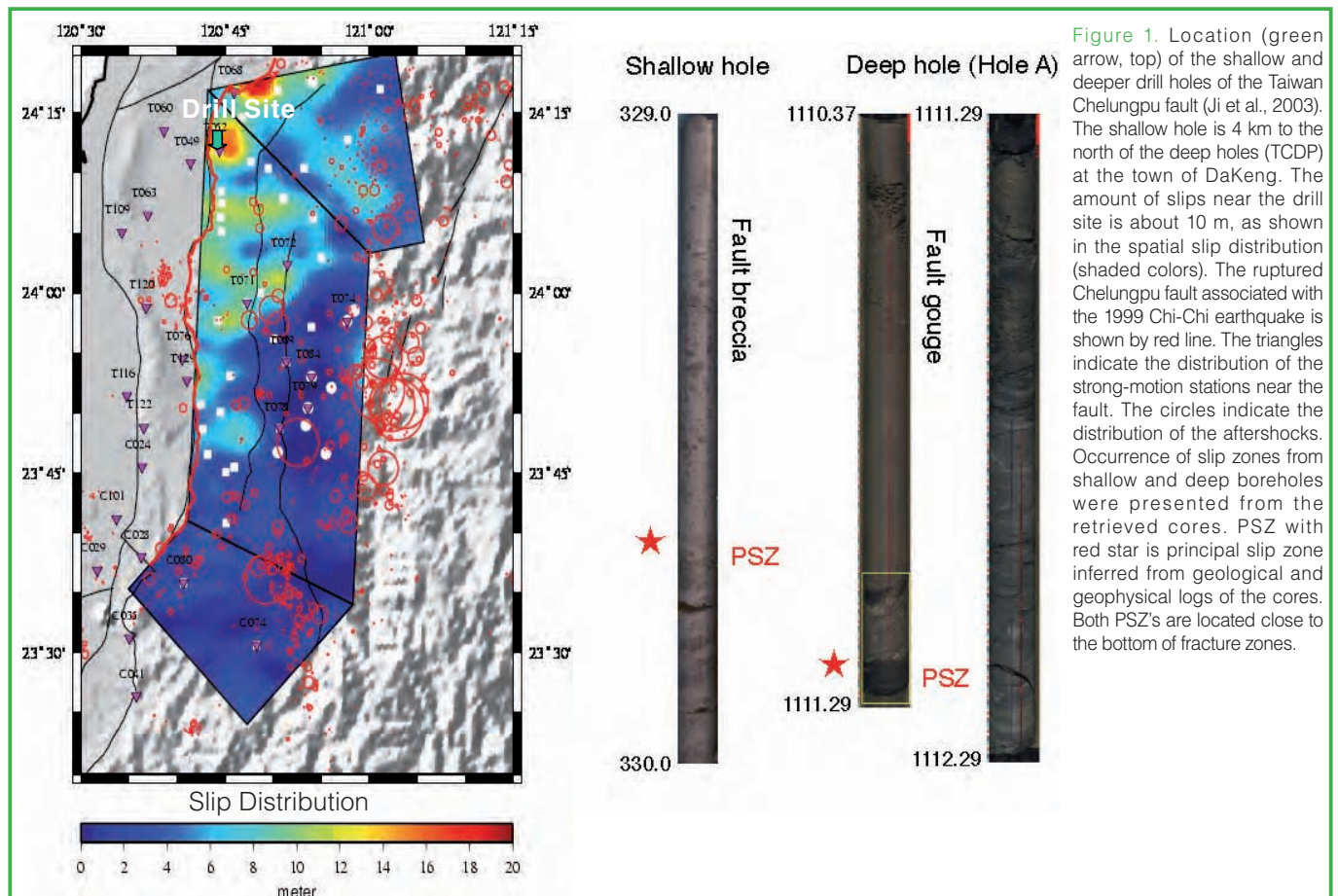
by Kuo-Fong Ma and Hidemi Tanaka

doi:10.2204/iodp.sd.s01.10.2007

The 21 September 1999 Chi-Chi, Taiwan earthquake (Mw 7.6) ruptured the N-S trending Chelungpu fault with a major 90-km structure that dips shallowly (30°) to the east, and principally slips within and parallel to bedding of the Pliocene Chinshui shale. A shallow borehole was drilled into the northern portion of the fault in the year 2000 (Fig. 1) in order to sample the slip zones that had large slip (>10 m) during the earthquake. The borehole was drilled at an angle of about 50° to the west, penetrating the fault at a drilling depth of around 300 m in January, 2001 (Tanaka et al., 2002). The success of the shallow hole drilling led to the deeper holes drilling named TCDP (Taiwan Chelungpu-fault Drilling Project; Ma et al., 2006), which drilled two vertical holes 40 m apart (Hole A to a depth of 2 km, and Hole B to a depth of 1.3 km) and a side-track from Hole B (Hole C, depth 0.95–1.2 km) about 2 km east of the surface rupture and 3 km to the south of the shallow hole, near the town of DaKeng (Fig. 1). TCDP carried out continuous coring for depths of 500 m to 2000 m, 950 m to 1300 m, and 950 m to 1200 m for

Hole A, Hole B, and Hole C, respectively. Geophysical well logs were carried out in Hole A to collect seismic velocities, densities, and digital images.

For the shallow hole, the distributed fracture zone ranges from 285 m to 330 m depth, which contained nine slip zones. The neutron geophysical logs show that the porosity abruptly increases in the drilling interval between 285 m and 330 m, suggesting that this zone would be the newest, being fractured during co-seismic slip by the Chi-Chi earthquake. Slip zones are basically composed of fault gouge and fault breccia. The fault gouge is brighter gray than host rocks. The boundary between fault gouge and host rock is gradual and is associated with a thin transition zone (<2 mm) from host rock to fault gouge. The mineral grains are more disaggregated nearer to the slip zone. Grains in fault gouge are of extremely fine cryptocrystalline materials (<2 μm diameter), and the maximum size is about 25 μm in diameter. Microscopic textures were not indicative of frictional melting, such as



spherulitic or dendritic crystal morphology, microlites or grassy matrix in the slip zones. In the deep holes, the Chelungpu fault zone from the Hole A core is observed within the Chinsui shale at depths from 1105 m to 1115 m, and consists of fractured rocks, fault breccia, and thin fault gouge layers. The degree of fracturing increases from the top to the bottom of the zone. Near the bottom of the broad zone of deformation, a 12-cm-thick primary slip zone (PSZ) can be identified based on the presence of ultra-fine grained fault gouge and increased fracture density at depths of 1111.23 m to 1111.35 m. A corresponding feature was also found in Hole B core at the depths of 1136.50 m to 1136.62 m, confirming the fault dip of 30°E. The geophysical logging measurements of low seismic velocities and low electrical resistivity around 1111 m depth also confirm that this is the main fault zone (Wu et al., 2007). The PSZ observed in the core from Hole C after splitting and polishing shows several layers of slip zones associated with several repeating earthquakes. The individual slip zone has a thickness of about 2–3 cm with a 5-mm ultra-fine grain zone at the bottom. Among the slip zones, the bottom zone in the PSZ, 2-cm in thickness, suffered the least disturbance from later events, suggesting that this narrow band might be the major slip zone (MSZ) that corresponds to the Chi-Chi earthquake. Other estimates of the thickness for the slip zone from nearby sites are 50–300 µm observed at the surface near the DaKeng drill site, and 1 cm from a fault core at a depth of 330 m in shallow drilling. These determinations of slip zone thicknesses are all from layers located near the bottom of the fracture zone. The variation of thickness of the slip zone at different depths might correspond to differences in normal stress as observed in Nojima fault core and other exhumed faults (Gratier et al., 2003; Tanaka et al., 2007).

The grain size distribution of the major slip zone was observed to estimate the surface fracture energy to compare with the seismic fracture energy to understand the energy partition of the earthquake. Direct measurements of the heat generated by this large earthquake were made for the shallow and deep holes. The local increases in the temperature profile across the fault observed both in shallow and deep holes were interpreted to be the residual heat generated during the earthquake. The frictional heat was calculated from temperature anomaly data observed at the depth associated with the identified slip zones of the Chi-Chi earthquake. Using the thermal parameters measured on-site with non-destructive methods as constraints, the analyses of the temperature anomalies lead to low estimates of the dynamic shear stress and to small values of the frictional coefficient. These results suggest the involvement of dynamic weakening mechanisms of faulting, such as thermal pressurization, during the large earthquake.

References

Gratier, J.-P., Favreau, P., and Renard, F., 2003. Modeling fluid transfer along California faults when integrating pressure solution

crack sealing and compaction process. *J. Geophys. Res.*, 108(No. B2):2104, doi:10.1029/2001JB000380.

- Ji, C., Helmberger, D.V., Wald, D.J., and Ma, K.-F., 2003. Slip history and dynamic implications of the 1999 Chi-Chi, Taiwan, earthquake. *J. Geophys. Res.*, 108(B9), 2412, doi:10.1029/2002JB001764.
- Ma, K.-F., Tanaka, H., Song, S.-R., Wang, C.-Y., Hung, J.-H., Tsai, Y.-B., Mori, J., Song, Y.-F., Yeh, E.-C., Soh, W., Sone, H., Kuo, L.-W., and Wu, H.-Y., 2006. Slip zone and energetics of a large earthquake from the Taiwan Chelungpu-fault drilling project. *Nature*, 444:473–476, doi:10.1038/nature05253.
- Tanaka, H., Wang, C.-Y., Chen, W.-M., Sakaguchi, A., Ujiie, K., Ito, H., and Ando, M., 2002. Initial science report of shallow drilling penetrating into the Chelungpu fault zone, Taiwan. *Terr. Atm. Oceanic Sci.*, 13(3):227–251.
- Tanaka, H., Omura, K., Matsuda, T., Ikeda, R., Kobayashi, K., Murakami, M., and Shimada, K., 2007. Architectural evolution of the Nojima fault and identification of the activated slip layer by Kobe earthquake. *J. Geophys. Res.*, 112 (B7), B07304, doi:10.1029/2005JB003977.
- Wu, H.-Y., Ma, K.-F., Zoback, M., Boness, N., Ito, H., Hung, J.-H., and Hickman, S., 2007. Stress orientations of Taiwan Chelungpu-Fault Project (TCDFP) hole-A as observed from geophysical logs. *Geophys. Res. Lett.*, 34:L01303, doi:10.1029/2006GL028050.

Authors

Kuo-Fong Ma, Department of Earth Science and Institute of Geophysics, National Central University, No.300, Johngda Rd., Johngli City, Taoyuan County 32001, Taiwan (R.O.C.), e-mail: fong@earth.ncu.edu.tw.

Hidemi Tanaka, Solid Earth Science Group, Department of Earth and Planetary Sciences, The University of Tokyo, Faculty of Science Building #1, Hongou 7-3-1, Bunkyo-ku, Tokyo, 113-0033, Japan.

The Corinth Rift Laboratory or an *in situ* Investigation on Interactions between Fluids and Active Faults

by François Henri Cornet

doi:10.2204/iodp.sd.s01.20.2007

Objectives

Earthquakes result from the sudden acceleration of a preliminary long-term slow deformation process. The objective of the Corinth Rift Laboratory (CRL) is to investigate *in situ* this quasistatic deformation process and mechanisms leading to a sudden catastrophic acceleration. Of particular interest is the characterization of the structure of the deforming zones and of the progressive localization of deformation. Special attention is given to the role of fluids but also on the influence of faults on regional fluid flow.

Corinth Rift Laboratory

The Gulf of Corinth, in western Greece, is one of the most seismically active regions in Europe. It is possibly the fastest continental rift in the world and provides an ideal site for an *in situ* investigation of the physics of earthquake sources and for developing efficient seismic hazard reduction procedures. It was selected several years ago, after an International Continental Scientific Drilling Program (ICDP) supported workshop (Cornet et al., 1997), as a site for developing an *in situ* laboratory, the CRL.

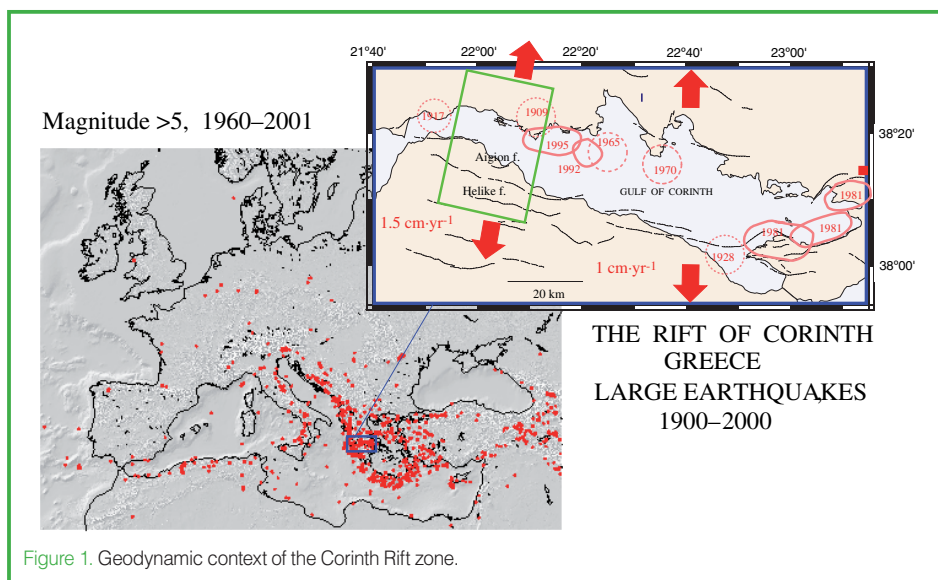
The Corinth Rift (Fig. 1), which separates the Peloponnese from continental Greece, is a 110-km-long, N 110° E-oriented graben, bound by systems of very recent steeply dipping normal faults less than 2 Myr old (Armijo et al., 1996; Jolivet et al., 2004; Le Pichon et al., 1995). This structure is the site of continental break-up, with up to 1.5 cm yr⁻¹ of north-south extension and a few millimeters per year uplift of the southern shore (Avalone et al., 2004; Briole et al., 2000; Pantosti et al., 2004). This rapid opening is associated with a shallowly north-dipping seismic zone located at depths ranging from 6 km to 12 km (Bernard et al., 2006; Gautier et al., 2006; Rigo et al., 1996). Five events with magnitude larger than 5.8 have been recorded in this region within the last forty years. The rifting is associated with the subduction to the southwest of Peloponnese but

also possibly to the propagation of the North Anatolian Fault.

CRL (www.corinth-rift-lab.org; Comptes Rendus Geosciences, 2004) is located in the vicinity of the city of Aigion, some 40 km east of Patras. It covers an area about 30 km × 30 km, extending across the gulf between Aigion on the southern shore and Eratini on the northern shore. This area was chosen for several reasons:

- The local strain rate and the microseismicity are highest (1.5 × 10⁻⁶ per year);
- The faults in this area have not been the site of any earthquake of magnitude larger than 5.5 for more than a century (three centuries for the western part). Further, from GPS data analysis, these faults are considered to be in the final stage of their seismic cycle (a few decades) and in a state of accelerated strain (Bernard et al. 2006);
- These faults were recently loaded by the 1995, magnitude 6.2, so-called Aigion earthquake, at the north eastern edge of the area (Bernard et al., 1997);
- The gulf is less than 8 km wide there, allowing on-land access to instrumented sites.

The CRL involves the monitoring of seismic activity with a network of twelve three-component (2-Hz) seismic stations and three broadband stations; the monitoring of surface deformation by continuous GPS, high resolution surface



tiltmeters, and downhole strainmeters; and the monitoring of water level or flow rate variations of natural springs and their changes in chemical composition, including rare gas content. In addition, it involves deep boreholes (presently two) for better characterization of the geological structure and for *in situ* monitoring of fluid-fault interactions.

One of the goals of the CRL is to understand the geometric connections between the outcropping steeply dipping fault planes and the deeper shallowly dipping seismogenic zone. Another goal is to explore the relationship between seismic and non-seismic deformation, with particular attention to the role of circulating fluids, for only about 40% of observed deformations (last five years) can be accounted for by the cumulated seismic activity.

More than five years of observation are presently available (Fig. 2). Of particular interest is the microseismic crisis (maximum magnitude 3.5) along the Aigion fault, that started about one month after the 1000-m-deep AIG10 borehole (Cornet et al., 2004) modified the hydraulic conditions in the upper part of the fault (October 2004). The destabilization of the fault in its upper portion is evidenced by minute (40–80 Pa) pressure drops (Fig. 3) dynamically triggered by large distant earthquakes (magnitude ≥ 8 with epicenters located more than 10,000 km away). The crisis, which lasted about five months, migrated westward and downward and generated more than 2000 events, many of which are multiplets. Preliminary results outline the

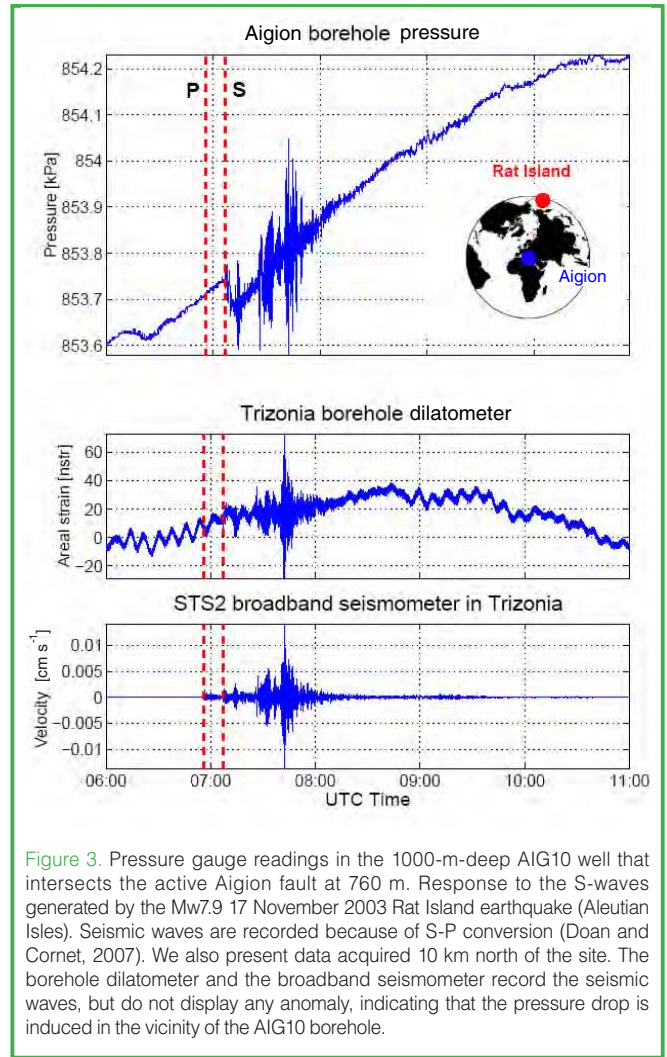


Figure 3. Pressure gauge readings in the 1000-m-deep AIG10 well that intersects the active Aigion fault at 760 m. Response to the S-waves generated by the Mw7.9 17 November 2003 Rat Island earthquake (Aleutian Isles). Seismic waves are recorded because of S-P conversion (Doan and Cornet, 2007). We also present data acquired 10 km north of the site. The borehole dilatometer and the broadband seismometer record the seismic waves, but do not display any anomaly, indicating that the pressure drop is induced in the vicinity of the AIG10 borehole.

existence of subvertical slip planes, some of which are strike slip (Bourouis et al., 2005; Cornet et al., 2005) as well as low dip fault planes. This is in contrast with the other most significant seismic crisis (2001) observed during the five-year life span of CRL existence that occurred in a zone that was thought to be inactive. The 2001 crisis is much more localized and is thought to have been associated with upward fluid motion (Lyon-Caen et al., 2004).

The 1000-m-deep AIG10 well intersects around 760 m the 10-km-long Aigion normal fault that was reactivated during the 1995 magnitude 6.2 Aigion earthquake. Below the Aigion fault, the AIG10 well entered a karstic limestone with a 0.9 MPa overpressure, while the aquifer just above the fault was found also to be artesian with a 0.45 MPa overpressure. The fault is about 10 m thick and involves an argileous 60-cm-thick core. Within this clay zone, observed slip direction is consistent with the maximum principal stress component being normal to the main fault plane (Sulem, 2007).

Also significant is the observation of a transient creeping process (Fig. 4), preceding by about half an hour a local magnitude 3.5 earthquake in December 2002, which involved the shallow part of the Psathopyrgos Fault, at about 2 km in

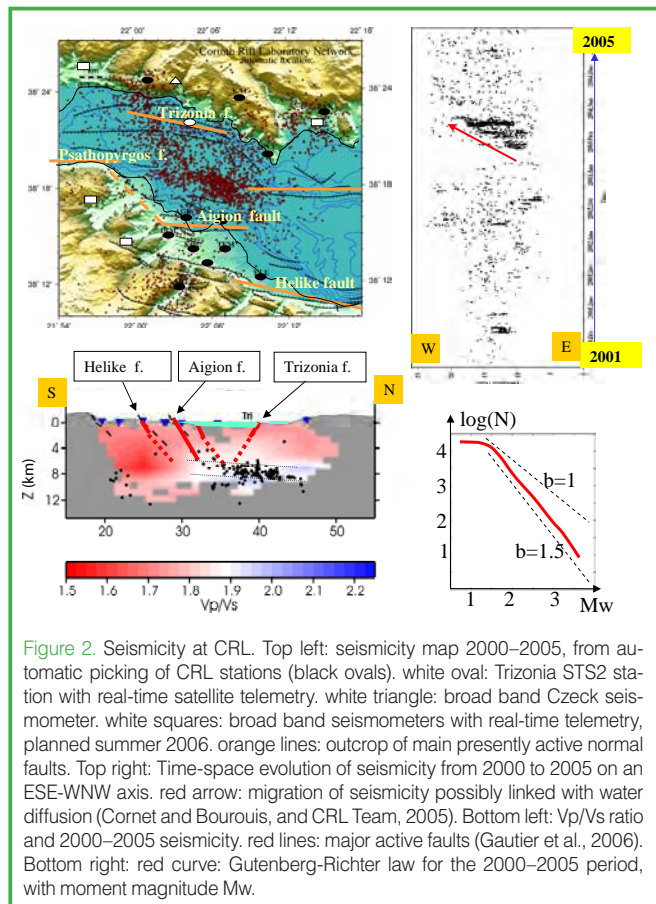


Figure 2. Seismicity at CRL. Top left: seismicity map 2000–2005, from automatic picking of CRL stations (black ovals). white oval: Trizonia STS2 station with real-time satellite telemetry. white triangle: broad band Czech seismometer. white squares: broad band seismometers with real-time telemetry, planned summer 2006. orange lines: outcrop of main presently active normal faults. Top right: Time-space evolution of seismicity from 2000 to 2005 on an ESE-WNW axis. red arrow: migration of seismicity possibly linked with water diffusion (Cornet and Bourouis, and CRL Team, 2005). Bottom left: Vp/Vs ratio and 2000–2005 seismicity. Red lines: major active faults (Gautier et al., 2006). Bottom right: red curve: Gutenberg-Richter law for the 2000–2005 period, with moment magnitude Mw.

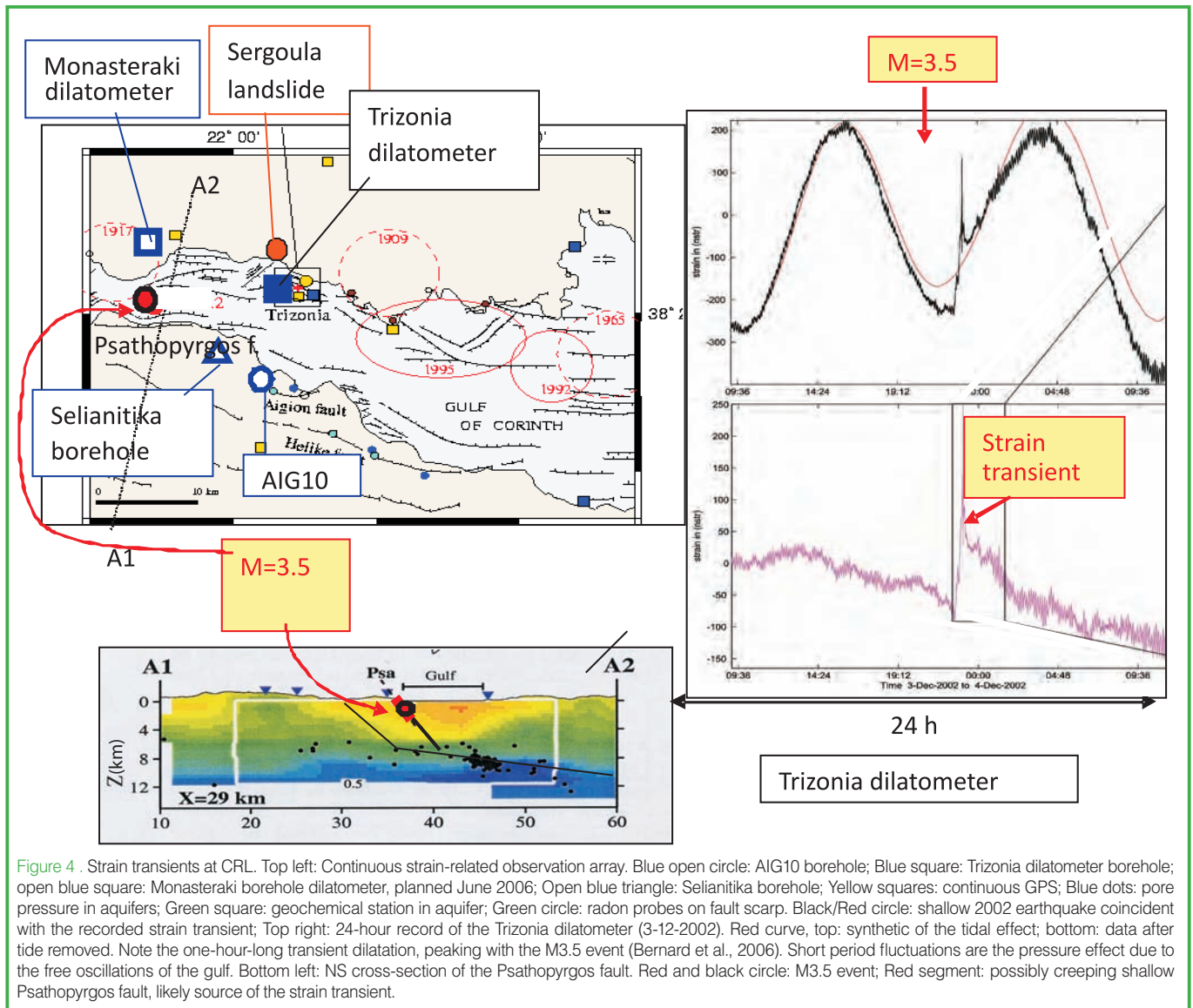


Figure 4 . Strain transients at CRL. Top left: Continuous strain-related observation array. Blue open circle: AIG10 borehole; Blue square: Trizonia dilatometer borehole; open blue square: Monasteraki borehole dilatometer, planned June 2006; Open blue triangle: Selianitika borehole; Yellow squares: continuous GPS; Blue dots: pore pressure in aquifers; Green square: geochemical station in aquifer; Green circle: radon probes on fault scarp. Black/Red circle: shallow 2002 earthquake coincident with the recorded strain transient; Top right: 24-hour record of the Trizonia dilatometer (3-12-2002). Red curve, top: synthetic of the tidal effect; bottom: data after tide removed. Note the one-hour-long transient dilatation, peaking with the M3.5 event (Bernard et al., 2006). Short period fluctuations are the pressure effect due to the free oscillations of the gulf. Bottom left: NS cross-section of the Psathopyrgos fault. Red and black circle: M3.5 event; Red segment: possibly creeping shallow Psathopyrgos fault, likely source of the strain transient.

depth (equivalent magnitude 5), i.e., well above the seismogenic zone of the area (Bernard et al., 2006). This earthquake was also the largest of a seismic swarm located about 15 km west of the CRL seismic network that lasted six weeks and involved deeper parts of the same fault.

The present plan is to deploy a complete suite of packers, high frequency (2.5 KHz sampling rate) 3C geophones, hydrophones (2.5 KHz sampling rate), high precision pressure transducers, thermistors, and tilt meters on both sides of the Aigion fault (February 2007). These data will be part of a feasibility study for drilling down to 5 km for sampling circulating fluids and monitoring high frequency signals within the seismogenic zone.

Acknowledgements

CRL was developed from 1999 to 2003 mostly through European funding and with the support of the International Continental Drilling Program for the drilling of AIG10. It has benefited greatly also from continuous support from the

French National Centre for Scientific Research (CNRS) since 1999.

References

- Armijo, R., Meyer, B., King, G.C.P., Rigo, A., and Papanastassiou, D., 1996. Quaternary evolution of the Corinth Rift and its implications for the late Cenozoic evolution of the Aegean. *Geophys. J. Int.*, 126:11–53.
- Avallone, A., Briole, P., Agatza-Balodimou, A.M., Billiris, H., Charade, O., Mitsakaki, C., Nercessian, A., Papazissi, K., Paradissis, D., and Veis, G., 2004. Analysis of eleven years of deformation measured by GPS in the Corinth Rift Laboratory area. *C. R. Geoscience*, 336(4–5):301–312.
- Bernard, P., Briole, P., Meyer, B., Lyon-Caen, H., Gomez, J.M., Tiberi, C., Berge, C., Cattin, R., Hatzfeld, D., et al., 1997. The Ms=6.2, June 15, 1995 Aigion earthquake (Greece): evidence for low angle normal faulting in the Corinth rift. *Journal of Seismology*, 1:131–150.
- Bernard, P., Lyon-Caen, H., Briole, P., Deschamps, A., Boudin, F., Macropoulos, K., Papadimitriou, P., Lemeille, F., Patau, G.,

- Billiris, H., Paradissis, D., Papazissi, K., Castarède, H., Charade, O., Necessian, A., Avallone, A., Pacchian, F., Zaradnick, J., Sacks, S., and Linde, A., 2006. Seismicity, deformation and seismic hazard in the western rift of Corinth: new insights from the Corinth rift laboratory (CRL). *Tectonophysics*, 426:7–30.
- Bourouis, S., Bouin, M.P., Patau, G., Bernard, P., Lyon-Caen, H., and Deschamps, A., 2005. The Corinth Rift laboratory – Multiplet analysis of the January 2004 microseismic crisis. European Geosciences Union Annual Meeting, Vienna.
- Briole, P., Rigo, A., Lyon-Caen, H., Ruegg, J.C., Papazissi, K., Mitsakaki, C., Balodimou, A., Veis, G., Hatzfeld, D., and Deschamps, A., 2000. Active deformation of the Corinth Rift, Greece : results from repeated Global Positioning Systems surveys between 1990 and 1995. *J. Geophys. Res.*, 105:25605–25625.
- Comptes Rendus Geoscience, 2004. 336(4/5); (special issue on Corinth Rift, with 25 papers).
- Cornet, F.H., Bourouis, S., and the CRL Team, 2005. Estimate of hydraulic diffusivity at 8 km depth in the Corinth Rift (Greece) from seismic activity migration. AGU Fall Meeting, San Francisco.
- Cornet, F.H., Borm, G., McEvelly, T., and Vardoulakis, I., (Orgs.), 1997. Development of a multi-borehole observatory at the Gulf of Corinth, Athens. In Proceedings of the 1st workshop on the development of a multiborehole observatory at the Gulf of Corinth. 26–28 October 1997, Athens. 1997 ICDP 1996–1997 report available at <http://www.corinth-rift-lab.org>.
- Cornet, F.H., Doan, M.L., Moretti, I., and Borm, G., 2004. Drilling through the active Aigion Fault: The AIG10 well observatory. *C. R. Geoscience*, 336:395–406.
- Doan, M.L. and Cornet, F.H., 2007. Small pressure drop triggered near a fault by small teleseismic waves. *Earth Planet. Sci. Lett.*, in press.
- Gautier, S., Latorre, D., Virieux, J., Deschamps, A., Skarpeles, S., Sotiriou, A., Serpetsidaki, A., and Tselentis, A., 2006. A new passive tomography of the Aigion Area (Gulf of Corinth, Greece) from the 2002 data set. *Pageoph.*, 163(2–3):431–453, doi:10.1007/s00024-005-0033-7.
- Jolivet, L., Famin, V., Mehl, C., Parra, T., Avigad, D., and Aubourg, C., 2004. Progressive strain localisation, crustal scale boudinage and extensional metamorphic domes in the Aegean sea. *American Geological Society, Special paper 380*, 185–210.
- Le Pichon, X., Chamot-Rooke, N., Lallement, S., Noomen, R., and Veis, G., 1995. Geodetic determination of the kinematics of central Greece with respect to Europe: implications for Eastern Mediterranean tectonics. *J. Geophys. Res.*, 100(B7):12675–12690.
- Lyon-Caen, H., Papadimitriou, P., Deschamps, A., Bernard, P., Makropoulos, K., Pacchiani, F., and Patau, G., 2004. First results of the CRL seismic network in the western Corinth Rift: evidence for old fault reactivation. *C. R. Geoscience*, 336:343–352.
- Pantosti, D., De Martini, P.M., Koukouvelas, I., Stamatopoulos, L., Palyvos, N., Pucci, S., Lemeille, F., and Pavlides, S., 2004. Palaeoseismological investigations of the Aigion Fault (Gulf of Corinth, Greece). *C. R. Geoscience*, 336:335–342.
- Rigo, A., Lyon-Caen, H., Armijo, R., Deschamps, A., Hatzfeld, D., Makropoulos, K., Papadimitriou, P., Kassaras, P., and Kassaras, L., 1996. A microseismic study of the western part of the Gulf of Corinth (Greece): implications for the large-scale normal faulting mechanisms. *Geophys. J. Int.*, 126:663–688.
- Sulem, J., 2007. Stress orientation evaluated from strain localisation analysis in Aigion fault. *Tectonophysics*, 442(1):3–13.

Related Web Link

<http://www.corinth-rift-lab.org>

Author

François Henri Cornet, Institut de Physique du Globe de Strasbourg, 5 rue René Descartes, 67000 Strasbourg, France, e-mail: francois.cornet@eost.u-strasbg.fr.

The IODP Nankai Trough Seismogenic Zone Experiment

by Harold Tobin and Masataka Kinoshita

doi:10.2204/iodp.sd.s01.30.2007

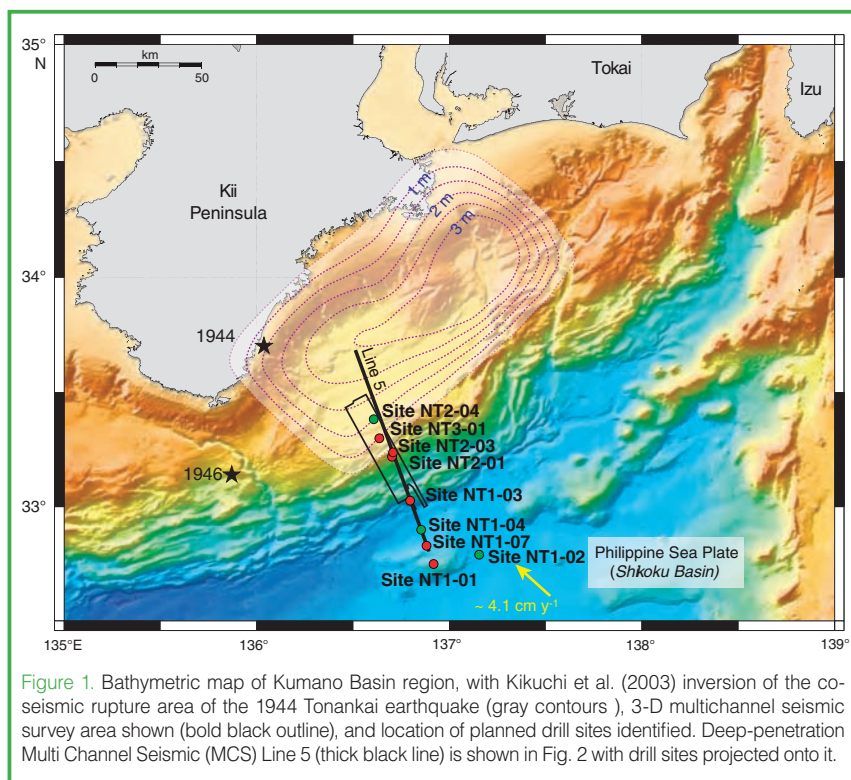
Introduction

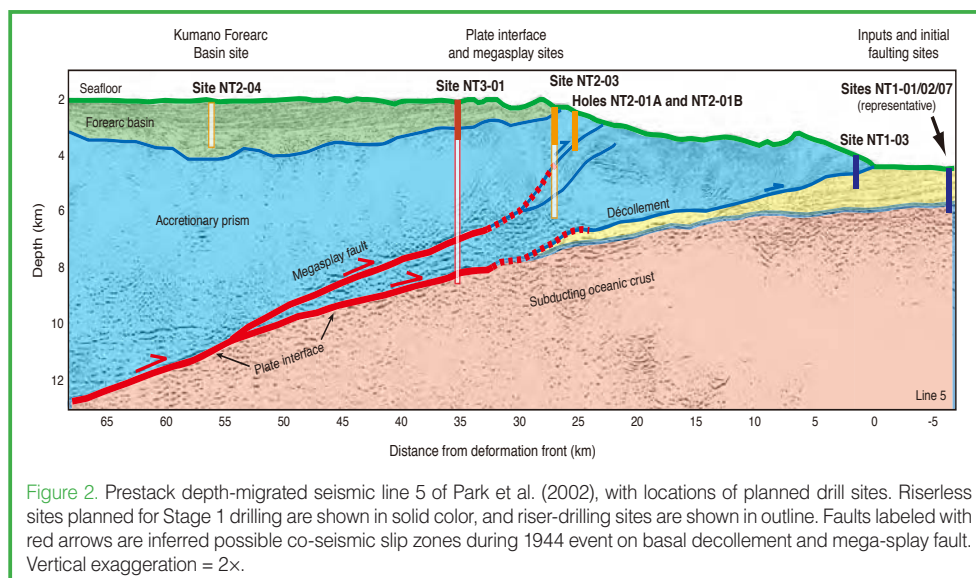
The Integrated Ocean Drilling Program's (IODP) Nankai Trough Seismogenic Zone Experiment (NanTroSEIZE) attempts to drill into, sample, and instrument the updip portion of the Nankai subduction megathrust asperity. Access to the interior of active faults in which *in situ* processes can be monitored and fresh fault zone materials can be sampled is of fundamental importance to the understanding of earthquake mechanics. Great subduction earthquakes (with their accompanying tsunamis) represent one of the greatest natural hazards on the planet. Accordingly, drilling into and instrumenting an active interplate seismogenic zone was identified as a very high priority in the IODP Initial Science Plan, 2001. Through a decade-long series of international workshops, a consensus was made that the Nankai Trough subduction zone was an ideal place to attempt drilling the seismogenic plate interface. The first stage of NanTroSEIZE drilling operations is now scheduled for the late summer of 2007. It involves parallel deployment of the new U.S. Scientific Ocean Drilling Vessel (SODV) and the riser vessel *Chikyu*.

The fundamental goal of the NanTroSEIZE science plan (Tobin and Kinoshita, 2006; Kinoshita et al., 2006) is the creation of a distributed observatory spanning the updip limit of seismogenic and tsunamigenic behaviors at a location where great subduction earthquakes occur, allowing us to observe the hydrogeologic behavior of subduction megathrusts and the aseismic-to-seismic transition of the megathrust system. This will involve drilling of key elements of the active plate boundary system at several locations off the Kii Peninsula of Japan from the shallow onset of the plate interface to depths where earthquakes occur (Figs. 1 and 2). At this location, the plate interface and active megasplay faults implicated in causing tsunami are accessible to drilling in the region of coseismic rupture in the 1944 Tonankai magnitude 8.0 earthquake. The most ambitious objective is to access and instrument the Nankai plate interface within the seismogenic zone. The

science plan entails sampling and long-term instrumentation of (a) the inputs to the subduction conveyor belt, (b) faults that splay from the plate interface to the surface that may accommodate a major portion of coseismic and tsunamigenic slip, and (c) the main plate interface at depths of ~4–6 km.

In addition to NanTroSEIZE, there is a burgeoning interest in active fault drilling, represented by the San Andreas Fault Observatory at Depth (SAFOD), Taiwan Chelungpu Fault Drilling Project (TCDP), Corinth Rift Laboratory (CRL), Nojima Fault Drilling Project, and other active projects on land and at sea (Reches and Ito, 2007). This is taking place in the context of rapidly growing research efforts on the mechanics and dynamics of faulting processes that integrate rock mechanics, seismology, geodesy, frictional physics, and fluid-fault interactions. Despite recent advances, there is at present no unified theory of fault slip to account for earthquake nucleation and propagation, nor to explain the mechanisms of strain across the spectrum of observed deformation rates ranging from seconds to years. Consequently, the question of whether precursor signals exist for major earthquakes, even in theory, remains under discussion. Progress on these topics is severely limited by a lack of information on





studies suggest that only here did past coseismic ruptures clearly extend shallow enough for drilling (Baba and Commins, 2005; Ichinose et al., 2003), and, consequently, an updip zone of large slip (asperity) has been identified and targeted. Coseismic slip during events like the 1944 Tonankai earthquake likely occurred on the megasplay fault rather than on the décollement beneath it, though slip on either plane is permissible given the available data. Therefore, the megasplay fault is a primary drilling target equal in importance to the basal décollement zone.

ambient conditions and mechanical properties of active faults at depth. Extant rheological models for how faults behave depend on specific physical properties at the fault interface and in the surrounding rock volume. Coefficients of friction, permeability, pore-fluid pressure, state of stress, and elastic stiffness are examples of such parameters that can best (or only) be measured through drilling and through geophysical sensing of the surrounding volume.

Geological and Geophysical Background

Subduction zones like the Nankai Trough, on which great earthquakes ($M > 8.0$) occur, are especially favorable for study because the entire width (dip extent) of the seismogenic zone ruptures in each great event. Thus, the future rupture area is perhaps more predictable than for smaller earthquakes. The Nankai Trough region is among the best-studied subduction zones in the world. It has a 1300-year historical record of recurring and typically tsunamigenic great earthquakes, including the 1944 Tonankai ($M 8.1$) and 1946 Nankaido ($M 8.3$) earthquakes (Ando, 1975; Hori et al., 2004). The rupture area and zone of tsunami generation for the 1944 event are now reasonably well understood (Baba and Cummins, 2005; Ichinose et al., 2003). Land-based geodetic studies suggest that the plate boundary thrust here is strongly locked (Miyazaki and Heki, 2001). Similarly, the relatively low level of microseismicity near the updip limits of the earthquakes in the 1940s (Obana et al., 2004) implies significant interseismic strain accumulation on the megathrust; however, recent observations of very low frequency (VLF) earthquake event swarms apparently taking place within the accretionary prism in the drilling area (Obara and Ito, 2005) demonstrate that interseismic strain is not confined to slow elastic strain accumulation, but also is released as slow events.

In the Kumano Basin, the seismogenic zone lies ~6000 m beneath the seafloor (Nakanishi et al., 2002). Slip inversion

Overall Project Scientific Objectives

Conditions for stable versus unstable sliding—which define seismic versus aseismic behavior—have long been the subject of research and debate, as has the frictional strength of likely fault zone material. Fault zone composition, consolidation state, normal stress magnitude, pore-fluid pressure, and strain rate may affect the transition from aseismic to seismic slip (Saffer and Marone, 2003). NanTroSEIZE will sample fault rocks over a range of pressure and temperature (P-T) conditions across the aseismic-seismogenic transition; the composition of faults and fluids and associated pore pressure and state of stress and will address partitioning of strain spatially between the décollement and splay faults. NanTroSEIZE will also install borehole observatories to provide *in situ* monitoring of these critical parameters (by monitoring of seismicity, strain, tilt, pressure, and temperature) over time, and test whether interseismic variations or detectable precursory phenomena exist prior to great subduction earthquakes.

The overarching hypotheses to be addressed are as follows:

- Systematic, progressive material and state changes control the onset of seismogenic behavior on subduction thrusts.
- Subduction zone megathrusts are weak faults.
- Within the seismogenic zone, relative plate motion is primarily accommodated by coseismic frictional slip in a concentrated zone.
- Physical properties, chemistry, and state of the fault zone change systematically with time throughout the earthquake cycle.
- The mega splay (out-of-sequence thrust; OOST) thrust fault system slips in discrete events, which may include tsunamigenic slip during great earthquakes.

Wiring the Seismogenic Fault

There are several borehole observatories installed on land and at sea. Over 700 on-land borehole observatory stations were installed at NIED (National Institute for Earth Science and Disaster Prevention) around Japanese islands. Basically, stations consist of **broadband seismometers and tiltmeters**. Comparable seismometer arrays have been deployed at the SAFOD, Nojima, and TCDP sites. Araki et al. (2004) installed a tiltmeter-strainmeter-broadband seismometer system in a seafloor borehole at the forearc of the **Japan Trench**.

The NanTroSEIZE observatory will be constructed based on all the experience obtained through the above mentioned installations. Since the temperature at 6 km below sea floor will exceed 150°C, we anticipate serious difficulties with any instrumentation of the seismogenic megathrust zone. Since good coupling of the instruments to the formation is essential, we need to develop a good clamping method and a good cementing method between the open hole and casing. Significantly tilted holes will prevent instruments from residing within measurable ranges. Wellhead seals are required for safety and environmental reasons, and this reduces the number of feedthroughs of electric and hydraulic conductors across the wellhead. We plan to develop a sub-seafloor A/D conversion and telemetry system. Finally, borehole data will be connected to a currently developed seafloor cable network off the **Kumano area**.

The Nankai Trough area poses a big challenge for ultra-deep drilling, but it is hoped that the outcome will be much larger than the investment for this project.

References

- Ando, M., 1975. Source mechanisms and tectonic significance of historical earthquakes along the Nankai Trough, Japan. *Tectonophysics*, 27(2):119–140, doi:10.1016/0040-1951(75)90102-X.
- Araki, E., Shinohara, M., Sacks, S., Linde, A., Kanazawa, T., Shiobara, H., Mikada, H., and Suyehiro, K., 2004. Improvement of seismic observation in the ocean by use of seafloor boreholes. *Bull. Seismol. Soc. Am.*, 94:678–690, doi:10.1785/0120020088.
- Baba, T. and Cummins, P.R., 2005. Contiguous rupture areas of two Nankai Trough earthquakes revealed by high resolution tsunami waveform inversion. *Geophys. Res. Lett.*, 32(8): L08305, doi:10.1029/2004GL022320.
- Hori, T., Kato, N., Hirahara, K., Baba, T., and Kaneda, Y., 2004. A numerical simulation of earthquake cycles along the Nankai Trough in southwest Japan: lateral variation in frictional property due to the slab geometry controls the nucleation position. *Earth Planet. Sci. Lett.*, 228(3–4):215–226. doi:10.1016/j.epsl.2004.09.033.
- Ichinose, G.A., Thio, H.K., Somerville, P.G., Sato, T., and Ishii, T., 2003. Rupture process of the 1944 Tonankai earthquake (Ms 8.1) from the inversion of teleseismic and regional seismograms. *J. Geophys. Res.*, 108(B10):2497, doi:10.1029/2003JB002393.
- Kinoshita, M., Moore, G., von Huene, R., Tobin, H., and Ranero, C.R., 2006. The seismogenic zone experiment. *Oceanogr.*, 19:28–38, 2006.
- Miyazaki, S. and Heki, K., 2001. Crustal velocity field of southwest Japan: subduction and arc-arc collision. *J. Geophys. Res.*, 106(B3):4305–4326, doi:10.1029/2000JB90031.
- Nakanishi, A., Takahashi, N., Park, J.-O., Miura, S., Kodaira, S., Kaneda, Y., Hirata, N., Iwasaki, T., and Nakamura, M., 2002. Crustal structure across the coseismic rupture zone of the 1944 Tonankai earthquake, the central Nankai Trough seismogenic zone. *J. Geophys. Res.*, 107(B1):2007, doi:10.1029/2001JB000424.
- Obana, K., Kodaira, S., and Kaneda, Y., 2004. Microseismicity around rupture area of the 1944 Tonankai earthquake from ocean bottom seismograph observations. *Earth Planet. Sci. Lett.*, 222(2):561–572. doi:10.1016/j.epsl.2004.02.032.
- Obara, K. and Ito, Y., 2005. Very low frequency earthquake excited by the 2004 off the Kii Peninsula earthquake: a dynamic deformation process in the large accretionary prism. *Earth Planets Space*, 57:321–326.
- Park, J.-O., Tsuru, T., Kodaira, S., Cummins, P.R., and Kaneda, Y., 2002. Splay fault branching along the Nankai subduction zone. *Science*, 297(5584):1157–1160. doi:10.1126/science.1074111.
- Reches, Z. and Ito, H., 2007. Scientific drilling of active faults: Past and future., In Harms, U., Koeberl, C., and Zoback, M.D. (Eds.), *Continental Scientific Drilling*, Heidelberg (Springer), 235–258, doi:10.1007/978-3-540-68778-8_6.
- Saffer, D.M. and Marone, C., 2003. Comparison of smectite- and illite-rich gouge frictional properties: application to the up-dip limit of the seismogenic zone along subduction megathrusts. *Earth Planet. Sci. Lett.*, 215(1–2):219–235. doi:10.1016/S0012-821X(03)00424-2.
- Tobin, H. and Kinoshita, M., 2006. NanTroSEIZE: the IODP Nankai Trough seismogenic zone experiment. *Sci. Drill.*, 2:23–27, doi:10.2204/iodp.sd.2.06.2006.

Authors

Harold Tobin, Department of Geology and Geophysics, University of Wisconsin, 1215 West Dayton Street, Madison, Wis., 53706 U.S.A., e-mail: htobin@wisc.edu.

Masataka Kinoshita, IFREE (Institute for Frontier Research on Earth Environment), JAMSTEC (Japan Agency for Marine-Earth Science and Technology), 2-15 Natsushima-cho, Yokosuka-city, Kanagawa 237-0061, Japan.

Drilling the North Anatolian Fault

by Georg Dresen, Mustafa Aktar, Marco Bohnhoff, and Haluk Eyidogan

doi:10.2204/iodp.sd.s01.17.2007

The North Anatolian Fault Zone (NAFZ) represents a ~1400-km-long plate boundary that slips at an average rate of 20–30 mm yr⁻¹. It separates the westward moving Anatolian block in the south from Eurasia in the north (McClusky et al., 2000). Comparison of long-term slip rates (6.5 mm yr⁻¹ for the last 13 Ma, 17 mm yr⁻¹ for the last 5 Ma,) with Holocene and GPS-derived slip rates (20–25 mm yr⁻¹) indicate an accelerated movement in the recent geological past. During the twentieth century, the NAFZ has ruptured over 900 km of its length. A series of large earthquakes starting in 1939 near Erzincan in eastern Anatolia propagated westward towards the Istanbul-Marmara region in northwestern Turkey. A large part of the Sea of Marmara today represents a seismic gap along a ≥100-km-long segment which did not rupture since 1766 and may have accumulated a slip deficit of 4–5 m. It is believed to be capable of generating two M_{7.1} earthquakes within the next decades or could even rupture in a large single event.

The most recent devastating earthquakes in the region occurred in 1999 near Izmit and Düzce with magnitudes greater than 7. Their western termination of rupture is located offshore below the eastern Sea of Marmara possibly extending to just south of the Princes Islands within ~20 km of Istanbul (Fig.1).

Below the Sea of Marmara, the NAFZ branches in two prominent offshore fault segments (Fig. 1) that bound a pull-apart depocenter (Cinarcik Basin) in the NE and SE containing 16–20 mm yr⁻¹ GPS-derived surface displacement at present. The NAFZ is again exposed on the western

Dardanelles Peninsula merging with the Ganos Fault. Here, the last M_{>7} earthquake occurred in 1912 rupturing approximately 60 km into the Sea of Marmara.

In the eastern Sea of Marmara, five seismic events with M_{>6} have occurred since 1509. The events in 1509, 1754, 1766, and 1894 generated tsunamis with waves exceeding 6 m in height in some cases. Also, the 1999 Izmit earthquake, reflecting pure strike-slip faulting, generated a minor tsunami with local wave heights >2 m.

Current seismic activity in the eastern Marmara Sea indicates the seismic gap south of Istanbul and a complex fault network active at the transition between the western end of the Izmit earthquake rupture (Fig. 2; Aktar et al., 2004; Karabulut et al., 2002). The majority of focal mechanism solutions indicate dominant strike-slip motion with minor normal faulting activity; however, existing seismicity images of the region lack the spatial and temporal resolution required for an accurate definition of seismic versus aseismic zones. This is due to the magnitude threshold of the existing seismic networks that is currently limited to about magnitude 2.

Our knowledge of the stress state at the NAFZ is rudimentary (Heidbach et al., 2004). Stress orientation with respect to the fault zone as given in the World Stress Map is mainly based on a small number of focal mechanisms of larger seismic events. Maximum compressive stress is generally oriented at 35°–45° with respect to the fault trend, so the NAFZ does not appear to be a weak fault in contrast to other major plate bounding faults. No data exist on stress magnitudes and on heat flow close to the NAFZ for the entire Marmara Sea area.

Positive Coulomb stress changes in the Marmara region suggest that the Izmit earthquake significantly increased the seismic hazard for the Istanbul-Marmara region. The Izmit event has increased the 2004–2034 probability for an earthquake M₇ by 2–6 times. Estimated thirty-year probability for an event M₇ is 35%–70% (Parsons., 2004; Parsons et al., 2000; Wright et al., 2001).

We currently investigate aftershock focal mechanisms of the Mw=7.4 Izmit earthquake of 17 August 1999, on the western North Anatolian Fault Zone (Bohnhoff et al., 2006). Spatial clustering and orientation of 446 fault plane solutions were analyzed. Aftershock clusters define four individual

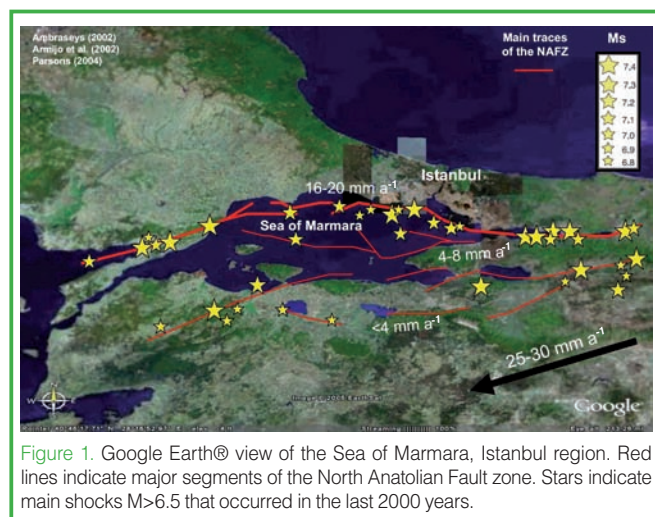


Figure 1. Google Earth® view of the Sea of Marmara, Istanbul region. Red lines indicate major segments of the North Anatolian Fault zone. Stars indicate main shocks M_{>6.5} that occurred in the last 2000 years.

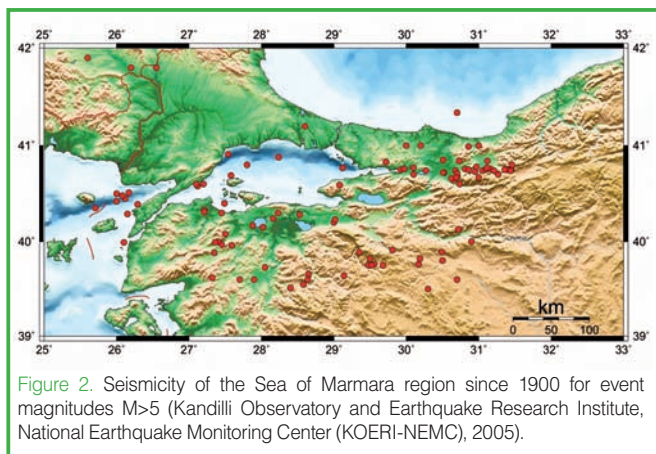


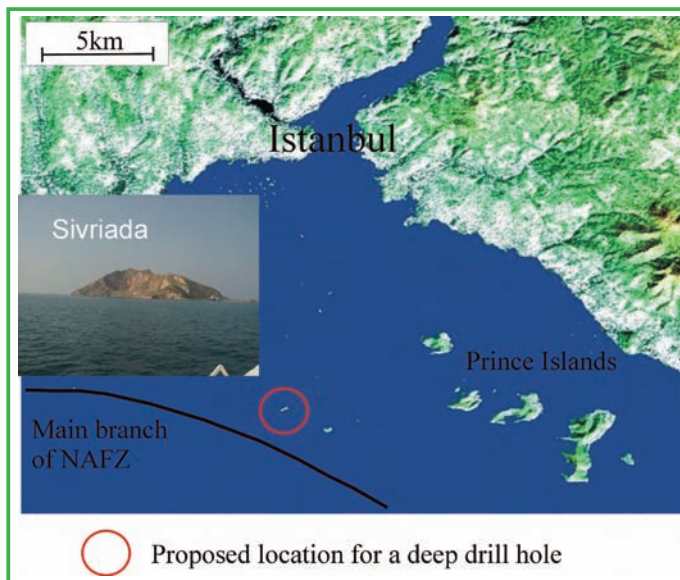
Figure 2. Seismicity of the Sea of Marmara region since 1900 for event magnitudes $M > 5$ (Kandilli Observatory and Earthquake Research Institute, National Earthquake Monitoring Center (KOERI-NEMC), 2005).

fault segments. The distribution of aftershock focal mechanisms corresponds to fault segmentation of the NAFZ in the Izmit-Düzce region produced by coseismic slip. Areas with high coseismic slip show aftershocks that are dominantly strike-slip, but low-slip barriers show mostly normal faulting aftershocks.

Focal mechanisms surrounding epicenters of the Izmit and subsequent Düzce main shock ($M_w=7.1$, 12 November 1999) indicate dominantly strike-slip but also normal faulting. Below the easternmost portion of the Sea of Marmara, alignments of aftershocks suggest branching of the NAFZ into three or more active segments that differ significantly in orientation of focal mechanisms.

Stress tensor inversions of the aftershock focal mechanisms show systematic rotations of the local stresses following the Izmit main shock. We conclude that the Izmit earthquake caused significant stress partitioning along the rupture. The direction of stress rotation is related to the orientation of the individual fault segments along the NAFZ.

We propose to drill a deep borehole close to the main branch of the NAFZ on the outermost Princes Islands close to the Istanbul metropolitan region and to install a multipa-



rameter deep borehole observatory (Fig. 3). Regarding recent seismic activity, the Princes Islands are located on a transition between the western end of the Izmit rupture and a fault segment showing very low activity, suggesting that this part of the fault is currently locked.

The deep-borehole observatory will allow an enhanced monitoring of microseismic activity, stress, heat and fluid flow near the NAFZ. The location of the observatory represents the only possible long-term monitoring site of seismic activity in the vicinity of Istanbul, and it is located at a NAFZ segment that is considered a seismic gap. Owing to post-seismic stress redistribution after the Izmit earthquake, the area is likely subjected to enhanced stresses.

The observatory will be installed at the bottom of a 2000-m-deep vertical borehole. The vertical seismometer array will be combined with an array of seismometers in shallow boreholes. A deep borehole observatory will permit observing earthquake activity close to the seismically active region of the fault zone at a depth between 4 km and 15 km. A chain of borehole seismometers will enhance the accuracy of hypocenter determinations and significantly decrease the magnitude-detection threshold. This would allow studying the rupture process of small-magnitude earthquakes close to their source region in unprecedented detail.

The orientation and magnitude of local stresses and strains at the fault and their change with depth can be determined. This will assist estimating the *in situ* strength of a major plate boundary fault. Fluid pressures in close proximity to active fault strands of the NAFZ will be monitored. The proposed borehole observatory will allow us to address the following fundamental problems, partly in combination of with a shallow borehole array and offshore campaign measurements:

- Is the North Anatolian Fault Zone in northwestern Turkey a weak or a strong plate boundary?

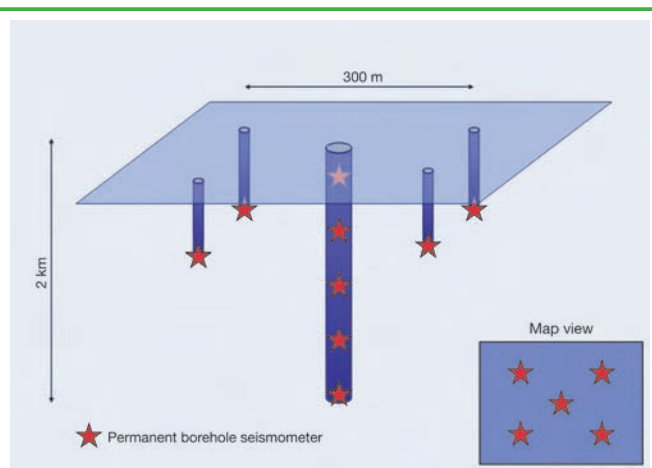


Figure 3. [Left] Proposed location for a deep drill hole on the Princes Islands near (~2–3 km from) the main fault of the NAFZ. View of Princes Islands (insert: Sivriada). [Right] Schematic view of the seismometer array proposed for a deep drill hole on the Princes Islands.

- What is the orientation of the principal stresses at the fault zone? Do stresses at the fault zone vary with depth and time?
- How does the structural heterogeneity of the fault affect the earthquake nucleation process?
- How is the dynamic propagation of a shear rupture affected by the fault structure?
- How is deformation partitioned between aseismic creep and seismic slip at the termination of a major earthquake rupture?
- What is the continuation of the faults at depth? Is there a deep-seated master fault in the Sea of Marmara south of Istanbul?

Currently, discussion of fault kinematics in the Marmara segment of the NAFZ has been controversial (Armijo et al., 2002, 2005; Le Pichon et al., 2001, 2003). Fault kinematics have important consequences for the seismic hazard assessment pertinent to the Istanbul area. For example, Armijo et al. (2005) suggested a maximum seismic risk for a well defined 70–100-km-long fault segment between the 1912 and 1999 ruptures where a slip deficit of 4–5 m might have accumulated (this is capable of generating a $M=7$ event). This is in agreement with recurrence intervals of 270 years for this region with regard to the 1766 event. Other studies suggest that the fault is less segmented and might rupture through its entire length of up to 150 km. The proposed deep-borehole geophysical observatory close to the NAFZ will permit us to examine some of the key questions pertinent to faulting activity and earthquake mechanics in general and seismic hazard assessment for the Istanbul area in particular.

References

- Aktar, M., Özalaybey, S., Ergin, M., Karabulut, H., Bouin, M.P., Tapýrdamaz, C., Biçmen, F., Yörük, A., and Bouchon, M., 2004. Fault zone heterogeneity and variations of seismicity parameters across 1999 İzmit-Düzce earthquake sequence. *Tectonophysics*, 391:325–334, doi:10.1016/j.tecto.2004.07.020.
- Ambraseys, N., 2002. The seismic activity of the marmara sea region over the last 2000 years. *Bull. Seismol. Soc. Am.*, 92:1:1–18, doi:10.1785/0120000843.
- Armijo, R., Meyer, B., Navarro, S., King, G., and Barka, A., 2002. Asymmetric slip partitioning in the Sea of Marmara pull-apart: A clue to propagation processes of the North Anatolian fault? *Terra Nova*, 14(2):80–86, doi:10.1046/j.1365-3121.2002.00397.x.
- Armijo, R., Pondard, N., Meyer, B., Uçarkus, G., Mercier de Lépinay, B., Malavieille, J., Dominguez, S., Gustcher, M.-A., Schmidt, S., Beck, C., Çagatay, N., Çakir, Z., Imren, C., Eris, K., Natalin, B., Özalaybey, S., Tolun, L., Lèfevre, I., Seeber, L., Gasperini, L., Rangin, C., Emre, O., and Sarikavak, K., 2005. Submarine fault scarps in the Sea of Marmara pull-apart (North Anatolian fault): Implications for seismic hazard in Istanbul. *Geochem. Geophys. Geosyst.*, 6(6):Q06009, doi:10.1029/2004GC000896.
- Bohnhoff, M., Grosser, H., and Dresen, G., 2006. Strain partitioning and stress rotation at the North Anatolian fault zone from aftershock focal mechanisms of the 1999 İzmit $M_w=7.4$ earthquake. *Geophys. J. Int.*, in press.
- Heidbach, O., Barth, A., Connolly, P., Fuchs, F., Müller, B., Reinecker, J., Sperner, B., Tingay, M., and Wenzel, F., 2004. Stress maps in a minute: The 2004 world stress map release. *Eos Trans.*, 85(49):521–529.
- Karabulut, H., Bouin, M.-P., Bouchon, M., Dietrich, M., Cornou, C., and Aktar, M., 2002. The seismicity in the Eastern Marmara Sea after the 17 August 1999 İzmit Earthquake. *Bull. Seismol. Soc. Am.*, 92(1):387–393, doi:10.1785/0120000820.
- LePichon, X., Pengör, A.M.C., Demirbağ, E., Rangin, C., Ýmren, C., Armijo, R., Görür, N., Çađatay, N., Mercier de Lépinay, B., Meyer, B., Saatçýlar, R., and Tok, B., 2001. The active Main Marmara Fault. *Earth Planet. Sci. Lett.*, 192:595–616, doi:10.1029/2002JB001862.
- LePichon, X., Chamot-Rooke, N., Rangin, C. and Sengör, A.M.C., 2003. The North Anatolian fault in the Sea of Marmara. *J. Geophys. Res.*, 108(B4):2179, doi: 10.1029/2002JB001862.
- McClusky, S., Balassanian, S., Barka, A., Demir, C., Ergintav, S., Georgiev, I., Gurkan, O., Hamburger, M., Hurst, K., Kahle, H., Kastens, K., Kekelidze, G., King, R., Kotzev, V., Lenk, O., Mahmoud, S., Mishin, A., Nadariya, M., Ouzounis, A., Paradissis, D., Peter, Y., Prilepin, M., Reilinger, R., Sanli, I., Seeger, H., Tealeb, A., Toksöz, M.N., and Veis, G., 2000. Global positioning system constraints on plate kinematics and dynamics in the eastern Mediterranean and Caucasus. *J. Geophys. Res.*, 105:5695–5719, doi:10.1029/1999JB900351.
- Parsons, T., 2004. Recalculated probability of $M \geq 7$ earthquakes beneath the Sea of Marmara, Turkey. *J. Geophys. Res.*, 109: B05304, doi:10.1029/2003JB002667.
- Parsons, T., Toda, S., Stein, R.S., Barka, A., and Dieterich, J.H., 2000. Heightened odds of large earthquakes near Istanbul: An interaction-based probability calculation. *Science*, 288:661–664, doi:10.1126/science.288.5466.661.
- Wright, T., Fielding, E., and Parsons, B., 2001. Triggered slip: observations of the 17 August 1999 İzmit (Turkey) earthquake using radar interferometry. *Geophys. Res. Lett.*, 28(6):1079–1082, doi:10.1029/2000GL011776.

Authors

- Georg Dresen**, GeoForschungsZentrum Potsdam, Sektion 3.2 Deformaton und Rheologie, Telegrafenberg, D-14473, Potsdam, Germany, e-mail: dre@gfz-potsdam.de.
- Mustafa Aktar**, Bogazici University, Kandilli Observatory and Earthquake Research Institute (KOERI), Cangelkoy, Istanbul, 81220, Turkey.
- Marco Bohnhoff**, GeoForschungsZentrum Potsdam, Haus D, Projectbereich 3.2, Telegrafenberg, D-14473, Potsdam, Germany.
- Haluk Eyidogan**, Istanbul Technical University, Mining Faculty, Department of Geophysics, 34469, Maslak, Istanbul, Turkey.

Fault Zone Drilling in the Backstop to the Mediterranean Ridge Accretionary Complex off Crete, Greece

by Achim Kopf and Marco Bohnhoff

doi:10.2204/iodp.sd.s01.14.2007

Regional Geological Setting

Scientific drilling and the installation of downhole seismic instrumentation to observe seismicity at a low-magnitude detection threshold are powerful tools to monitor densely populated areas in Southern Europe, such as the Athens metropolitan region, to minimize societal and environmental dangers, which millennia ago destroyed entire cultures, two of the seven wonders of the world (Colossus of Rhodes 224 BC, Lighthouse on Pharos 365 AD) and several historical sites in the circum-Mediterranean. The Eastern Mediterranean hosts one of the most prominent retreating convergent margins worldwide that was capable of generating $M > 8$ earthquakes (365 AD, western Crete) and exhaustive volcanic eruptions (1650 BC, Santorini) in historic times.

The Hellenic Subduction Zone (HSZ) in the Eastern Mediterranean Sea represents a mature subduction zone where African crust is thrust (i.e., subducted) beneath Eurasia and where a wide backstop area of partly old accreted strata (marine), partly HP/LT rocks (the exhumed island of Crete as forearc high), an extensional submerged landward forearc (Cretan Sea), and a volcanic arc and backarc basin (Aegean Sea) evolved. The HSZ is an ideal natural laboratory

to study collisional processes which are well recorded over the past ca. 35 million years, including an intermittent stage of micro-continent collisions between about 30 Ma and 20 Ma, followed by breakoff of the subducting slab, and incipient collision with the passive African margin today (Thomson et al., 1998). The island of Crete represents a horst structure developed within the last 5 million years in the central forearc, and it provides excellent onshore access to the internal structure of the forearc at various levels (for overall geodynamic situation in map view, see Fig. 1).

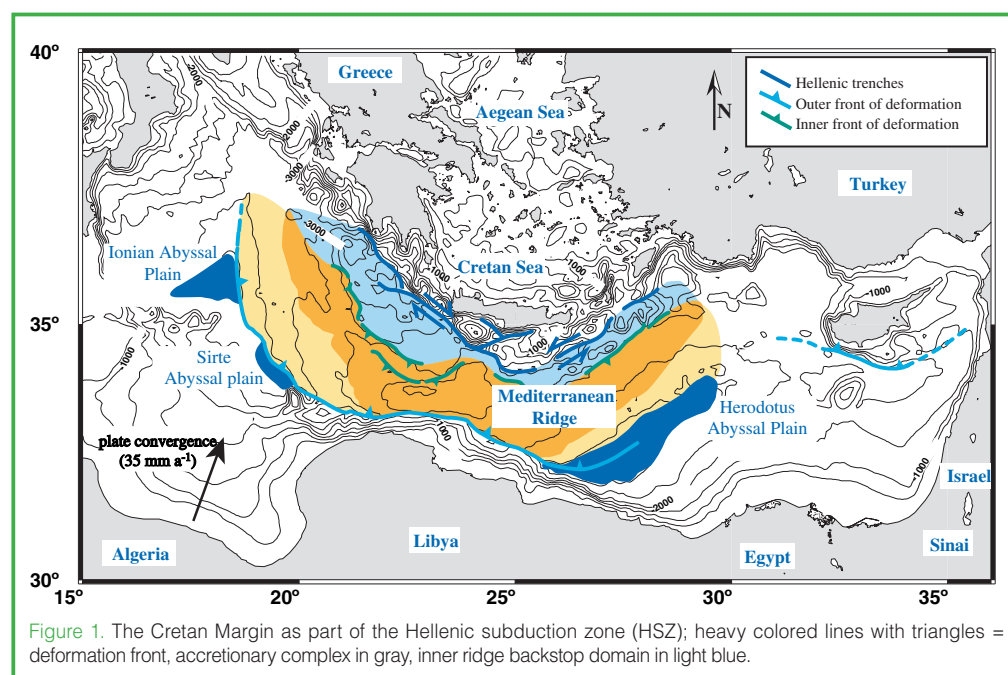
Scientific Drilling

An “amphibic” scientific drilling approach is planned for the HSZ, comprising a northern (International Continental Scientific Drilling Project (ICDP)-driven) and a southern (Integrated Ocean Drilling Program (IODP)-driven) domain. Having been kicked off at an ICDP workshop on Crete in 1998, proposals for backstop drilling in the Cretan Sea (ICDP), on Crete (ICDP), and in the Mediterranean Sea (IODP) were developed and later combined to an onshore-offshore deep drilling transect along the HSZ (Fig. 2). With moderately deep marine drill sites (ca. 1 km depth) in the backstop region south of Crete, one continental 3–4-km-deep drill hole onshore Crete, and further ICDP (Glad800) offshore holes within the Cretan Sea (i.e., the forearc-backarc transi-

tional zone) and the volcanic arc (i.e., the submerged Kolumbo volcano as part of the Santorini volcanic complex), we anticipate a substantial contribution to the understanding of earthquake hazard and mitigation, tectonic evolution, and rheology of active collision zones. In this paper, we focus on the marine drilling project where three drill sites are anticipated to penetrate active fault zones.

Fault Zone Drilling in the Backstop

Within ODP (Ocean Drilling Program) and its



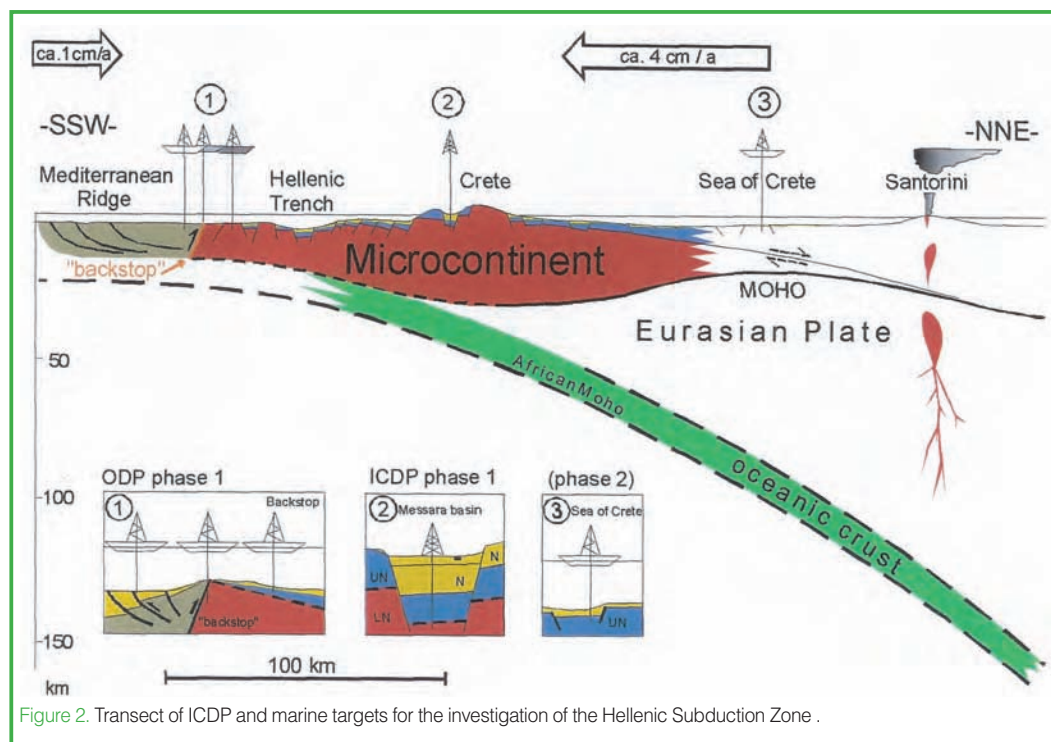


Figure 2. Transect of ICDP and marine targets for the investigation of the Hellenic Subduction Zone .

predecessor DSDP (Deep Sea Drilling Project), several convergent margins have been investigated; however, all these regions have in common that drilling focused entirely on the frontal portion of the forearc prism. Due to this shortcoming, Kopf et al. (1999) proposed to drill a transect of three sites south of the island of Crete (E Mediterranean) from the distal part of the Mediterranean Ridge accretionary prism (MedRidge) across its backstop. Following geophysical surveys and analog modeling, drilling a backstop (or buttress) setting is essential to elucidate fundamental deep fluid flow processes and deformation mechanisms within an accretionary prism and its buttress. Variability in fluid flux across the wedge to its buttress must influence fluid budgets of the accretionary complex, and earlier work attested that flux rates in the backstop domain exceed those near the toe of the accretionary complex (Kopf et al., 2001). The marine transect aims to illuminate (1) mass and fluid transfer at an accreting convergent margin, (2) the significance of spatial variability of fluids from mineral dehydration and diagenetic alteration at depth, and their interaction with the rock, and (3) their possible effect on seismicity. Each of the three 1-km-deep drill holes in the backstop domain will penetrate deep-seated thrusts and backthrust faults whose fluids act as windows down to several kilometers depth. Fluids will be indicative of enhanced dewatering reactions and possibly cause earthquake swarms in the area. Monitoring of fluid-flow and pressure variations would have profound effects on the understanding of fluid budgets and global mass balances, and seismogenesis.

The three fault zones to be penetrated by ocean drilling are:

- (i) An active backthrust fault within the distal part of the accretionary complex, which is juxtaposed by a small (1 km across) mud volcano;
- (ii) The backthrust contact between the Inner Ridge backstop and the accretionary complex; and
- (iii) A reverse fault in the higher Cretan submarine forearc, which separates the exhumed HP/LT units from the overlying thrust nappes forming the bulk part of the island of Crete.

Seismic reflection data suggest fluid migration and activity of each of these fault zones, the

latter being the most exciting one since the former detachment fault plane will provide us a window to the depth of slab break off.

References

- Kopf, A., Klaeschen, D., and Mascle, J., 2001. Extreme efficiency of mud volcanism in dewatering accretionary prisms. *Earth Planet. Sci. Lett.*, 189(3-4):295-313, doi:10.1016/S0012/821X(01)00278-3.
- Kopf, A., Robertson, A.H.F., Sreaton, E.J., Mascle, J., Parkes, R.J., Foucher, J.P., DeLange, G.J., Stöckhert, B., and Sakellariou, D., 1999. Backstop hydrogeology of a wide accretionary complex south of Crete, Eastern Mediterranean Sea. *Full drilling proposal (#555) for the Ocean Drilling Program*, 25p.
- Thomson, S.N., Stöckhert, B., and Brix, M.R., 1998. Thermochronology of the high-pressure metamorphic rocks of Crete, Greece: Implications for the speed of tectonic processes. *Geology*, 26:259-262, doi:10.1130/0091-7613(1998)026<0259:TOTH PM>2.3.CO;2.

Authors

Achim Kopf, Research Center Ocean Margins (RCOM), University of Bremen, Leobener Strasse, 28359 Bremen, Germany, e-mail: akopf@uni-bremen.de.

Marco Bohnhoff, GeoForschungsZentrum Potsdam, Telegrafenberg D424, 14473 Potsdam, Germany.

Generation Depth of the Pseudotachylyte from an Out-of-Sequence Thrust in Accretionary Prism—Geothermobarometric Evidence

by Shin'ya Okamoto, Gaku Kimura, Asuka Yamaguchi, Haruka Yamaguchi, and Yoko Kusuba

doi:10.2204/iodp.sd.s01.41.2007

Introduction

Major out-of-sequence thrusts (OOSTs) in accretionary prisms are faults which generate great earthquakes in subduction zones, such as the 1944 Tonankai and 1946 Nankai earthquakes in the Nankai Trough (Cummins and Kaneda, 2000; Park et al., 2002), the 1964 Alaska earthquake in the Aleutian Trench (Plafker, 1972), and the 2005 Sumatra earthquake in the Sunda Trench (Ammon, 2006). The 1999 Chi-Chi Earthquake in Taiwan along the Chelungpu Fault (Chen et al., 2001) also occurred in the same setting as other OOSTs, even though the fault is exposed on land.

Because great earthquakes of $M_w > 8.0$ dominantly take place in accretive margins (Ruff and Kanamori, 1983), understanding the faulting mechanisms of a major OOST is one of the keys in determining the earthquake generation process as such.

An on-land, fossilized, major OOST thrust exhumed from seismogenic depth can be observed in the early Tertiary Shimanto Belt, Kyushu, Japan (Kondo et al., 2005). The shear zone associated with the thrust is thicker than 100 m and is characterized by the development of crack-fillings and crack-seal veins, which suggest that the shear zone was filled by geothermal fluids at depth. Velocity analysis of the rocks in the shear zone shows high and low velocities in the hanging wall and footwall, respectively. This is consistent with the impedance contrast expected from negative polarities of the modern out-of-sequence thrust deeper than 10 km in the Nankai Trough (Tsuji et al., 2006).

A pseudotachylyte-bearing subsidiary fault was recently discovered from the shear zone in the hanging wall (Okamoto et al., 2006). The pseudotachylyte is characterized by ubiquitous association of fluid implosion breccias and mineral veins of quartz and carbonates. This occurrence is very different from that of continental pseu-

dotachylytes developed under dry conditions and suggests abundant fluid association, thermal pressurization, and hydrofracturing preceding frictional melting (Okamoto et al., 2006).

It is important to constrain the exact pressure-temperature conditions of the setting for the pseudotachylyte, because its occurrence is a key to understanding the faulting mechanism if the slip took place in depth. From this point of view, we estimated the pressure-temperature conditions on the basis of fluid inclusion analysis from the mineral veins.

Geological Setting of the Nobeoka Thrust

The Nobeoka thrust is a major OOST bounding the northern and southern Shimanto belts of the Cretaceous-Tertiary accretionary complex in Kyushu, southwest Japan (Fig. 1A). The thrust is traceable for more than 300 km parallel to the modern Nankai Trough.

Hanging wall rocks of the thrust are composed of the Eocene Kitagawa group mainly consisting of plastically deformed phyllites and sandstones. Footwall strata of the Eocene Hyuga group are composed of a shale matrix mélange with sandstone and basaltic blocks deformed mainly by brittle mechanisms. Deformation fabrics of both of these rocks are consistent with the sense of shear along the Nobeoka thrust (Kondo et al., 2005). Geothermometry using vitrinite reflectance and $\text{CH}_4\text{-H}_2\text{O}$ fluid inclusion data indicates that the Kitagawa and the Hyuga groups experi-

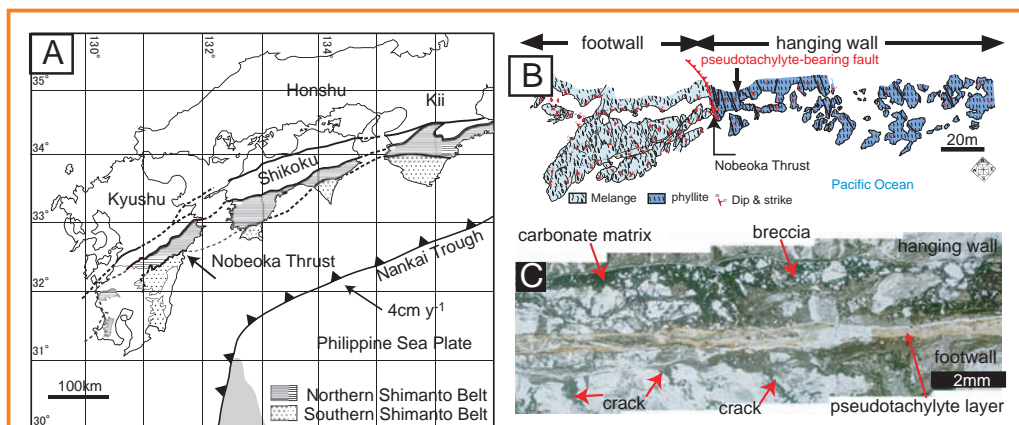


Figure 1. [A] Geological setting of the Nobeoka thrust and distribution of the Shimanto belt in southwest Japan. [B] Sketch map of horizontal exposure of the Nobeoka thrust and shear zone on the tidal flat (addition to Kondo et al., 2005). [C] Photomicrograph of the slipped part of the pseudotachylyte-bearing subsidiary fault. Translucent fault core (pseudotachylyte) is bounded by breccia in the dark carbonate matrix (modified from Okamoto et al., 2006).

enced heating up to maximum temperatures of ~320°C and ~250°C, respectively (Kondo et al, 2005).

The Nobeoka thrust is characterized by a cataclastic fault core about 20 cm thick and by a plastic and brittle damage zone whose thickness is several tens of meters in the hanging wall and about 100 meters in the footwall. Ubiquitous subsidiary shear fractures, with orientations parallel to that of the fault core of the Nobeoka thrust, are present in the damaged zones.

Kondo et al. (2005) pointed out from the viewpoint of thermal models (Hyndman and Wang, 1993; Hyndman et al., 1997) that the Nobeoka thrust was formed at seismogenic depths, in comparison with the OOST in the modern Nankai Trough (Park et al., 2002).

Experimental velocity measurements of fault rocks from the damaged zone of the Nobeoka thrust show 4–5 km s⁻¹ for the hanging wall and 3–4 km s⁻¹ for the footwall, presenting a clear impedance contrast, and thus a good analog of the deep seismogenic part of a negative polarity of the major OOST in the modern Nankai Trough (Tsuji et al., 2006).

Occurrence of Pseudotachylyte and Veins

A pseudotachylyte-bearing fault was found in one of the subsidiary faults in the hanging wall, about 10 m above the fault core of the Nobeoka thrust (Fig. 1B; Okamoto et al., 2006). The fault is composed of two different parts along the fault surface: narrow, planar slip sections and wider zones along dilation jogs. The planar slip section shows two types of fault rock. One is a carbonate matrix-supported breccia, and the other is the pseudotachylyte (Fig. 1C). Lines of evidence for frictional melting are discussed by Okamoto et al. (2006). The dilation jogs are filled with carbonate matrix-supported breccia (Okamoto et al., 2006), and the breccias are composed of fragmented host rocks of phyllites several tens of microns to millimeters in size. The carbonate matrix constitutes micron-scale calcite

and ankerite, filling the inter-calcite grain boundaries (Fig. 1C).

Crosscutting relationships of veins are as follows (Fig. 2A, B). The oldest veins (V1) occur in the phyllites. Most of them are composed of quartz and are involved in the plastic deformation accommodated by pressure solution (Kondo et al., 2005). Younger quartz veins (V2) are not deformed by such mechanisms, but keep precipitation-related idiomorphic crystal textures. Carbonate veins (V3) fill tension cracks cutting V1 and V2 quartz veins (Fig. 2A, B). The carbonates are connected to the matrix carbonates of the breccias

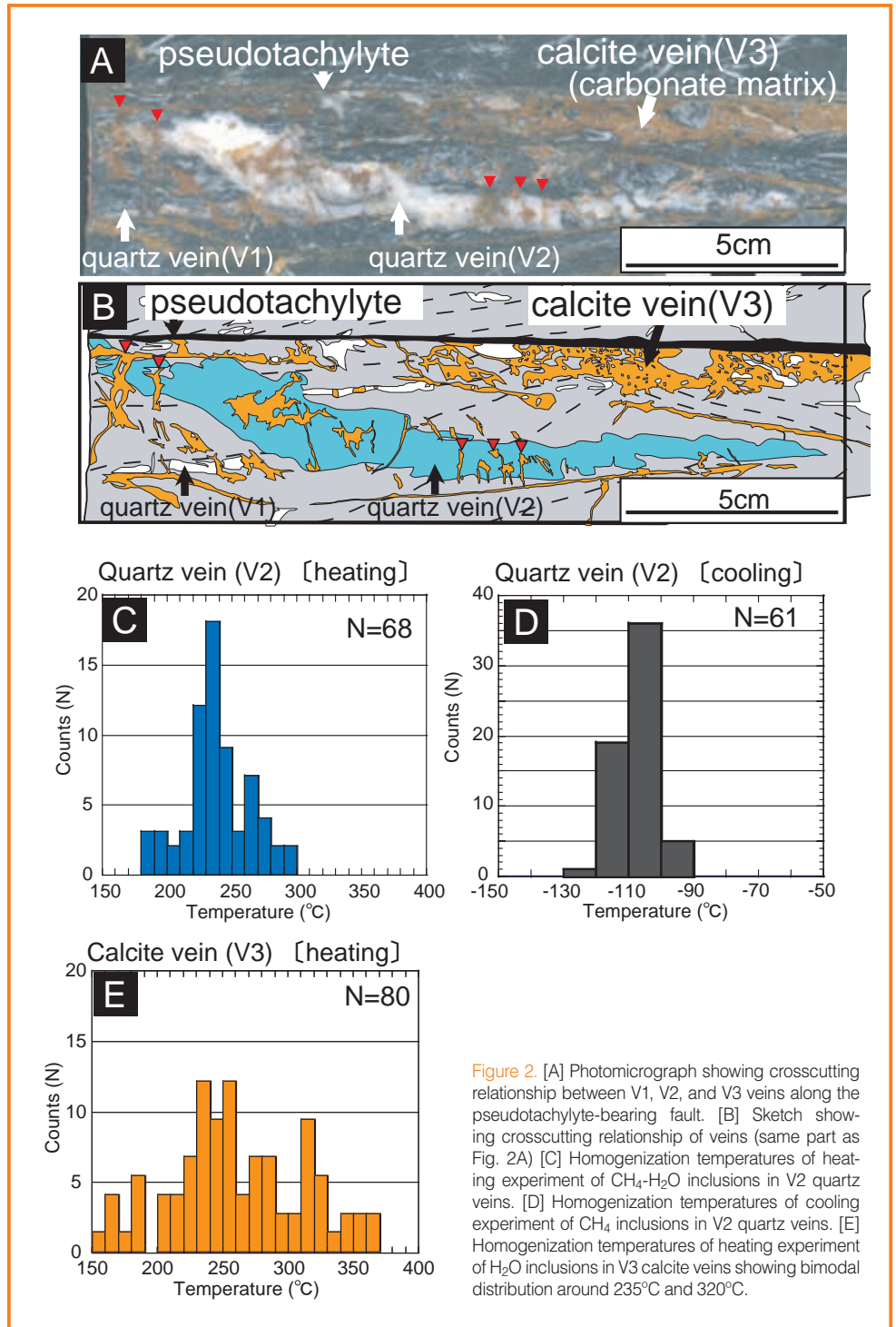


Figure 2. [A] Photomicrograph showing crosscutting relationship between V1, V2, and V3 veins along the pseudotachylyte-bearing fault. [B] Sketch showing crosscutting relationship of veins (same part as Fig. 2A) [C] Homogenization temperatures of heating experiment of CH₄-H₂O inclusions in V2 quartz veins. [D] Homogenization temperatures of cooling experiment of CH₄ inclusions in V2 quartz veins. [E] Homogenization temperatures of heating experiment of H₂O inclusions in V3 calcite veins showing bimodal distribution around 235°C and 320°C.

(Fig. 2A, B). All vein generations are cut by pseudotachylyte (Fig. 2A, B) in slipped parts of the fault. As described in Okamoto et al. (2006), the pseudotachylyte pinches out at dilation jogs filled by carbonate matrix-supported breccia. These occurrences suggest that the breccia formation and carbonate matrix precipitation were preceded by the frictional melting and maintained during the slip.

Occurrences and Compositions of Fluid Inclusions

V2 quartz and V3 calcite veins contain abundant fluid inclusions. V2 quartz veins include single-phase and two-phase inclusions. The single-phase inclusions are composed only of methane, which is shown by a remarkable peak of 2919.2 cm^{-1} using Raman micro-spectroscopy. Two-phase inclusions consist of vapor and liquid phases. A broad peak from 3100 cm^{-1} to 3500 cm^{-1} indicates water, and a peak of 2917.2 cm^{-1} coincides with the methane peak. The results suggest that water is saturated with methane, and water and methane co-exist as immiscible fluids (Vrolijk et al., 1988). No solid carbon dioxide was observed during the cooling experiments (see next section), suggesting that carbon dioxide content is less than 10% (Burruss, 1981).

V3 calcite veins contain only two-phase inclusions. They consist of vapor and liquid phases. Only the water peak from 3100 cm^{-1} to 3600 cm^{-1} is detected by Raman micro-spectroscopy. Therefore, the vapor and liquid phases are both composed of water.

Results of Fluid Inclusion Analysis

Sixty-eight and sixty-one inclusions, respectively, were analyzed by heating and cooling experiments for V2 quartz veins, while eighty inclusions were analyzed by heating experiments for the V3 calcite veins. Results are shown in Fig. 2C, D, E.

Homogenization temperatures of fluid in V2 quartz veins range from 180°C to 296°C (Fig. 2C) with a modal peak at 230°C – 240°C . Cooling experiments represent a range from -130°C to -90°C (Fig. 2D). Pressure estimation on the basis of the methane saturation curve (Mullis, 1979) and the results of heating and cooling experiments shows a range of 102–272 MPa. The homogenization temperatures of fluids in the V3 calcite veins were 154°C – 362°C and present bimodal peaks. The primary peak is at 230°C – 260°C , and the secondary one is at 310°C – 320°C (Fig. 2E). The primary peak coincides with that of the V2 quartz veins, and the secondary peak is higher.

Deformation History and its Thermal Conditions

The crosscutting relationships suggest that the deformation history of the hanging wall was as follows:

1. Ductile deformation related to phyllitic cleavage formation. V1 quartz veins are involved in this deformation. Vitrinite reflectance suggests that the temperature was about 320°C (Kondo et al., 2005)
2. Tension cracking and V2 quartz vein precipitation. No more phyllitic cleavages overprint this vein generation, and fluid inclusion analysis suggest that the hanging wall rock was uplifted at about 235°C .
3. Slip initiation, breccia formation, and carbonate precipitation. These events may have started at about 235°C , reaching about 320°C by frictional heating, and ending with finally cooling to about 235°C .
4. Continuing slip resulting in frictional melting. Temperatures along the fault may have been more than 1700°C locally, as quartz grains show signs of plastic deformation and melting (Okamoto et al., 2006).

Background Geothermal Gradient and Depth at the Initial Stage of Slip

The paleo-geothermal gradient in the northern Shimanto belt is estimated at 20 – $30^{\circ}\text{C km}^{-1}$ based on metamorphic parageneses (Toriumi and Teruya, 1988), while the paleo-geothermal gradient in the footwall of the Nobeoka thrust is estimated at 28 – $47^{\circ}\text{C km}^{-1}$ based on fluid inclusion analysis (Kondo et al., 2005). However, no studies of the thermal conditions of the hanging wall of the Nobeoka thrust have been reported so far. Here, the geothermal gradient is estimated as follows based on the fluid inclusion analyses described above.

It is assumed that the densest methane fluid inclusions were trapped under nearly lithostatic conditions, because the veins are interpreted to be deposited soon after fracturing under the near-lithostatic fluid pressures (Hashimoto et al., 2003; Matsumura et al., 2003; Vrolijk, 1987). Densities are assumed to be 2700 kg m^{-3} and 1000 kg m^{-3} , respectively for solid and fluid.

Thus, fluid pressure (P) is expressed as a function of depth (h) and porosity (θ) as

$$P = \int [2700(1 - \theta) + 1000\theta] g dh$$

where g is the gravity acceleration, θ is a porosity at depth h expressed by the empirical equation $\theta = Ae^{-bh}$ of Bray and Karig (1985). The equation can be rewritten as

$$P = \int [2700(1 - Ae^{-bh}) + 1000Ae^{-bh}] g dh$$

where A and b are constants, 0.65 and 1.54, respectively. The maximum P value of V2 quartz veins is estimated to be about 240 MPa when a temperature of 235°C is assumed.

Then, solving the equation for h , the depth is calculated as 8.6 km. This yields $27^{\circ}\text{C km}^{-1}$ of geothermal gradient, which is consistent with previous results from the northern Shimanto belt. Geologic occurrences of the Nobeoka thrust, therefore, present excellent information for faulting mechanisms of seismogenic OOST in depth.

Acknowledgements

This study was supported by the Research Program for Plate Dynamics of the Japan Agency for Marine-Earth Science & Technology, and the 21st Century Center of Excellence Program of the University of Tokyo. Our field work was supported by T. Kanda, University of Miyazaki. We are grateful to all the participants of the IODP-ICDP Workshop on Fault Zone Drilling held in Miyazaki for fruitful discussions and comments.

References

- Ammon, C.J., 2006. Megathrust investigations. *Nature*, 440:31–32, doi:10.1038/440031a.
- Bray, C.J. and Karig, D.E., 1985. Porosity of sediments in accretionary prisms and some implications for dewatering processes. *J. Geophys. Res.*, 90:768–778.
- Burruss, R.C., 1981. Analysis of fluid inclusions - Phase-equilibria at constant volume. *Am. J. Sci.*, 281:1104–1126.
- Chen, Y.-G., Chen, W.-S., Lee, J.-C., Lee, Y.-H., Lee, C.-T., Chang, H.-C., and Lo, C.-H., 2001. Surface rupture of 1999 Chi-Chi earthquake yields insights on active tectonics of central Taiwan. *Bull. Seismol. Soc. Am.*, 91:977–985.
- Cummins, P.R. and Kaneda, Y., 2000. Possible splay fault slip during the 1946 Nankai earthquake. *Geophys. Res. Lett.*, 27:2725–2728.
- Hashimoto, Y., Enjohji, M., Sakaguchi, A. and Kimura, G., 2003. *In situ* pressure-temperature conditions of a tectonic melange: Constraints from fluid inclusion analysis of syn-melange veins. *Island Arc*, 12:357–365, doi:10.1046/j.1440-1738.2003.00405.x.
- Hyndman, R.D. and Wang, K., 1993. Thermal constraints on the zone of major thrust earthquake failure – the Cascadia Subduction Zone. *J. Geophys. Res.*, 98:2039–2060.
- Hyndman, R.D., Yamano, M., and Oleskevich, D.A., 1997. The seismogenic zone of subduction thrust faults. *Island Arc*, 6:244–260, doi:10.1111/j.1440-1738.1997.tb00175.x.
- Kondo, H., Kimura, G., Masago, H., Ohmori-Ikehara, K., Kitamura, Y., Ikesawa, E., Sakaguchi, A., Yamaguchi, A., and Okamoto, S., 2005. Deformation and fluid flow of a major out-of-sequence thrust located at seismogenic depth in an accretionary complex: Nobeoka Thrust in the Shimanto Belt, Kyushu, Japan. *Tectonics*, 24:TC6008, doi:10.1029/2004TC001655.
- Matsumura, M., Hashimoto, Y., Kimura, G., Ohmori-Ikehara, K., Enjohji, M., and Ikesawa, E., 2003. Depth of oceanic-crust underplating in a subduction zone: Inferences from fluid-inclusion analyses of crack-seal veins. *Geology*, 31:1005–1008, doi:10.1130/G19885.1.
- Mullis, J., 1979. The system methane-water as a geologic thermometer and barometer from the external part of the central Alps. *Bull. Mineral.*, 102:526–536.
- Okamoto, S., Kimura, G., Takizawa, S., and Yamaguchi, H., 2006. Earthquake fault rock indicating a coupled lubrication mechanism. *e-Earth*, 1:23–28.
- Park, J.O., Tsuru, T., Kodaira, S., Cummins, R., and Kaneda, Y., 2002. Splay fault branching along the Nankai subduction zone. *Science*, 297:1157–1160, doi:10.1126/science.1074111.
- Plafker, G., 1972. Alaskan earthquake of 1964 and Chilean earthquake of 1960 — implications for arc tectonics. *J. Geophys. Res.*, 77:901–925.
- Ruff, L. and Kanamori, H., 1983. Seismic coupling and uncoupling at subduction zones. *Tectonophysics*, 99(2–4):99–117, doi:10.1016/0040-1951(83)90097-5.
- Toriumi, M. and Teruya, J., 1988. Tectono-metamorphism of the Shimanto Belt. *Mod. Geol.*, 12:303–324.
- Tsuji, T., Kimura, G., Okamoto, S., Kono, F., Mochinaga, H., Saeki, T., and Tokuyama, H., 2006. Modern and ancient seismogenic out-of-sequence thrusts in the Nankai accretionary prism: Comparison of laboratory-derived physical properties and seismic reflection data. *Geophys. Res. Lett.*, 33:L18309, doi:10.1029/2006GL027025.
- Vrolijk, P., 1987. Tectonically driven fluid-flow in the Kodiak accretionary complex, Alaska. *Geology*, 15:466–469.
- Vrolijk, P., Myers, G., and Moore, J.C., 1988. Warm fluid migration along tectonic mélanges in the Kodiak accretionary complex, Alaska. *J. Geophys. Res.*, 93:10313–10324.

Authors

- Shin'ya Okamoto**, Department of Earth and Planetary Sciences, Graduate School of Science, The University of Tokyo, 7-3-1 Hongo, Bunkyo-ku, Tokyo, 113-0033, Japan.
- Gaku Kimura**, Department of Earth and Planetary Sciences, Graduate School of Science, The University of Tokyo, 7-3-1 Hongo, Bunkyo-ku, Tokyo, 113-0033, Japan; and Institute for Research on Earth Evolution (IFREE), Japan Agency for Marine-Earth Science and Technology, 2-15 Natsushima-cho, Yokosuka, Kanagawa, 237-0061, Japan, e-mail: gaku@eps.s.u-tokyo.ac.jp.
- Asuka Yamaguchi**, Department of Earth and Planetary Sciences, Graduate School of Science, The University of Tokyo, 7-3-1 Hongo, Bunkyo-ku, Tokyo, 113-0033, Japan.
- Haruka Yamaguchi**, Department of Earth and Planetary Sciences, Graduate School of Science, The University of Tokyo, 7-3-1 Hongo, Bunkyo-ku, Tokyo, 113-0033, Japan; and Institute for Research on Earth Evolution (IFREE), Japan Agency for Marine-Earth Science and Technology, 2-15 Natsushima-cho, Yokosuka, Kanagawa, 237-0061, Japan.
- Yoko Kusuba**, Department of Earth and Planetary Sciences, Graduate School of Science, The University of Tokyo, 7-3-1 Hongo, Bunkyo-ku, Tokyo, 113-0033, Japan.

Drilling the Seismogenic Zone of an Erosional Convergent Margin: IODP Costa Rica Seismogenesis Project CRISP

by César R. Ranero, Paola Vannucchi, Roland von Huene
and the CRISP proponents

doi:10.2204/iodp.sd.s01.29.2007

Introduction

Interplate subduction zone earthquakes occur in the seismogenic zone, down dip of the transition from stable slip to unstable slip along the plate boundary megathrust. Currently, mineral transformations and fluid migration are thought to govern the stable to unstable slip transition. In the seismogenic zone, subducting clastic material in the subduction channel changes structure and physical properties and releases fluid as it migrates toward the mantle. Where sediment accretion dominates a convergent margin, the subducted clastic input is trench sediment, and the subducted plate is likened to a conveyor belt traveling from the trench into conditions of elevated temperature and pressure. Trench sediment has been sampled, and the diagenetic and metamorphic changes can be inferred. Moore and Saffer (2001) describe the decrease in porosity and increase in temperature with depth, which results in a transition from opal to quartz, the transformation of clay minerals, cementation by carbonate, zeolites, and quartz, all accompanied by pressure solution. However, where subduction erosion dominates a convergent margin, material input to the seismogenic zone is unknown because it is derived from the base of the upper plate, beyond the sampling capabilities of past

scientific ocean drilling (von Huene et al., 2004). Mineral transformations involved in seismogenesis at erosional margins may be very different from those at accretionary margins. Zones of upper plate subduction erosion have never been drilled, nor does geophysics resolve their structure, lithology, and physical properties (Fig. 1). The Japanese riser drill ship *Chikyu* in the Integrated Ocean Drilling Program (IODP) provides the opportunity to drill the seismogenic zone of an erosional margin and this is the objective of CRISP (Costa Rica Seismogenesis Project).

Subduction erosion along the plate boundary of the Middle America convergent margin: During CRISP the seismogenic zone of the Middle America erosional convergent margin will be sampled and instrumented. A key feature is the unconformable surface across the top of crystalline basement of the upper plate, a regional unconformity imaged in seismic records. Drilling on DSDP Legs 67 (1979) and 84 (1981) revealed that the inferred accretionary prism of Guatemala is instead an extension of the upper plate igneous basement covered unconformably by Eocene to Miocene shallow water sediment. Drill samples from the lower slope contain microfossils that are now more than 3 km deeper than the water depth in which they lived. Microfossil depth indicators in the

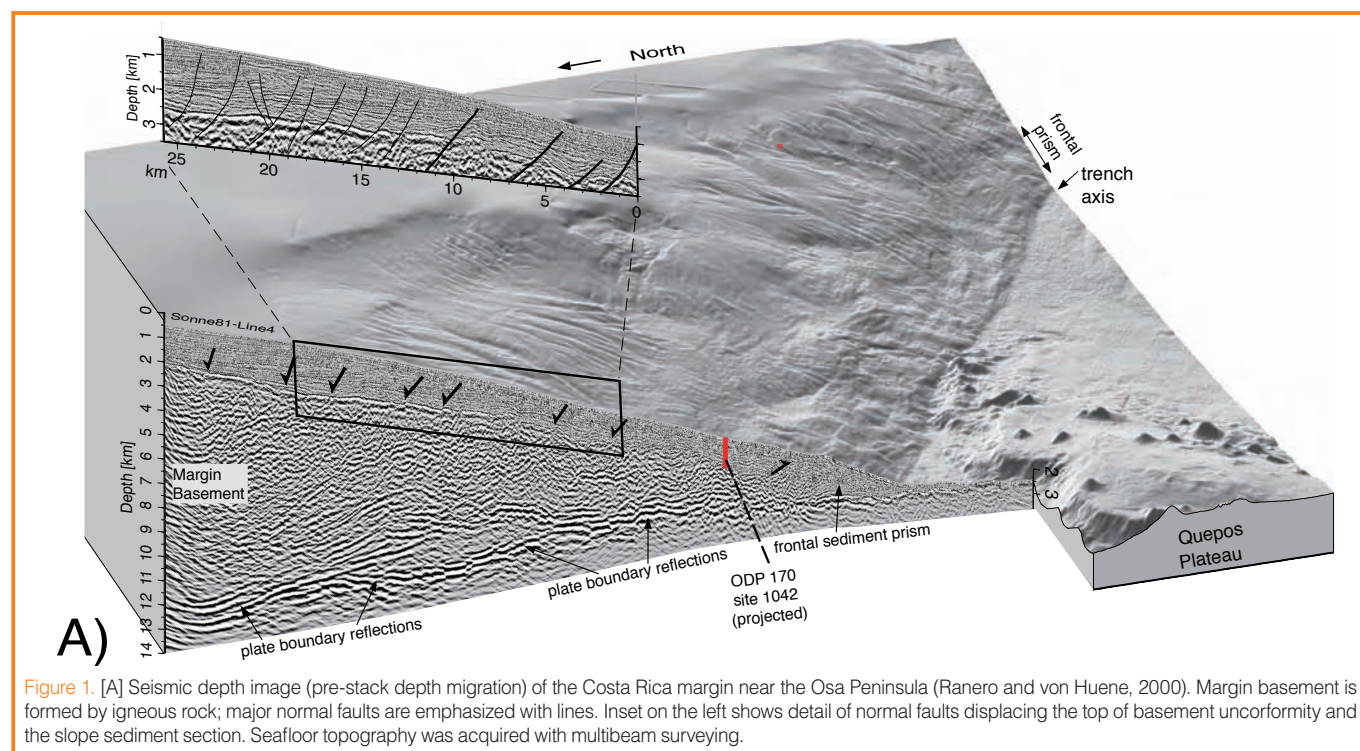


Figure 1. [A] Seismic depth image (pre-stack depth migration) of the Costa Rica margin near the Osa Peninsula (Ranero and von Huene, 2000). Margin basement is formed by igneous rock; major normal faults are emphasized with lines. Inset on the left shows detail of normal faults displacing the top of basement unconformity and the slope sediment section. Seafloor topography was acquired with multibeam surveying.

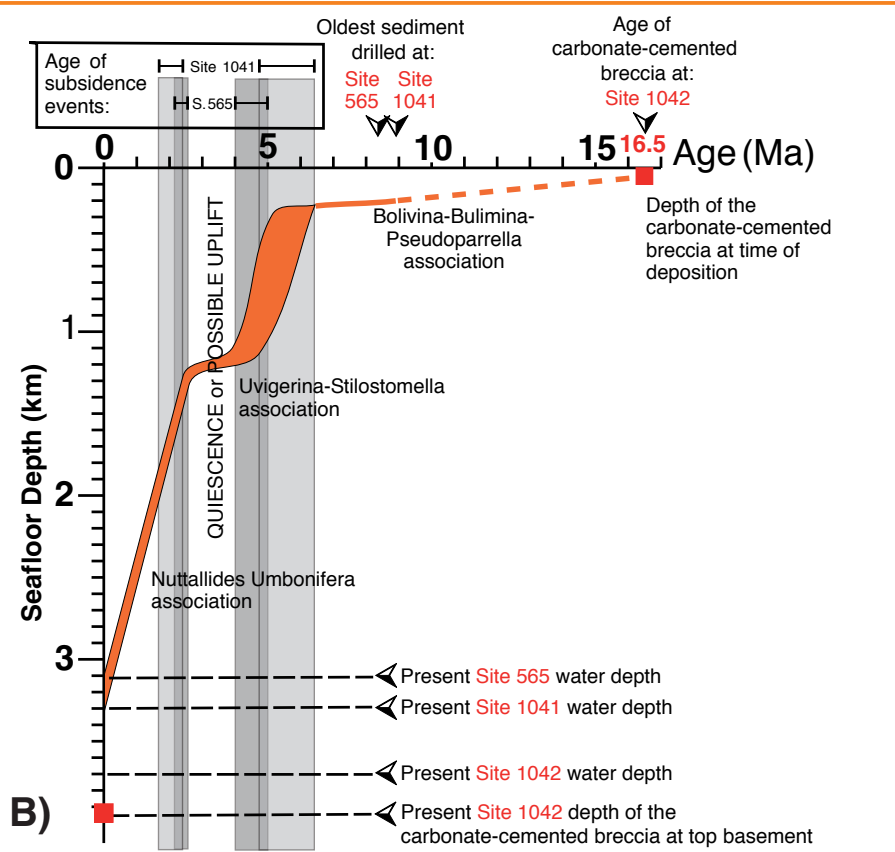


Figure 1. [B] Long-term subsidence history of the Costa Rica margin composed with data from several drill sites offshore the Nicoya Peninsula. Paleodepth information was obtained from studies of benthic foraminifera in the slope sediment, indicating a non-linear subsidence (two main pulses) of about 4 km for the middle continental slope (Vannucchi et al., 2003).

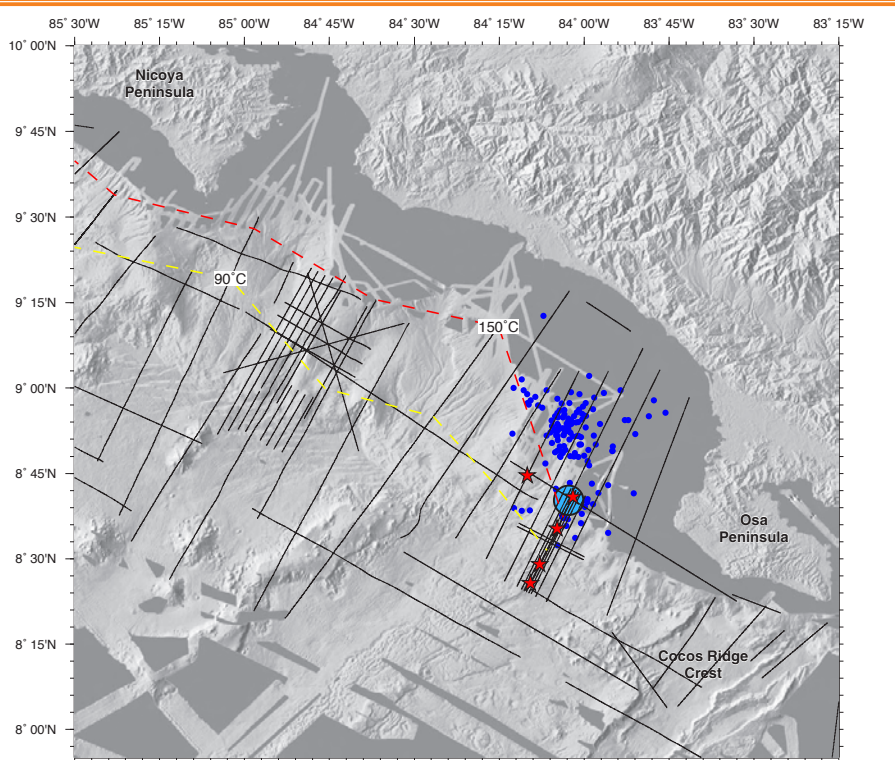


Figure 2. Multibeam bathymetry and topography of the Costa Rica margin between Nicoya and Osa Peninsula. Dashed lines delineate the 90°C and 150°C temperature isotherms along the plate boundary. Large blue circle marks nucleation area of the 2002 Mw6.4 earthquake, and small blue circles are aftershocks occurring during 6 days after the main shock (I. Arroyo, unpublished). Drill site in the upper slope is located on the nucleation area of the 2002 Mw6.4 earthquake (see Fig. 4). Black lines indicate tracks of multichannel seismic reflections profiles collected during SONNE 81 and BGR99 cruises.

overlying sediment record the progressive margin subsidence since Miocene times (Vannucchi et al., 2004). Subsidence from the surf zone to trench depths requires crustal thinning by erosion of material along the underside of the upper plate.

Drilling on ODP Leg 170 (1996) off Nicoya confirmed that, like Guatemala, the Costa Rican unconformity surface has subsided from shallow water in the past few Myr (Vannucchi et al., 2003) similarly to the neighbor segment off Nicaragua (Ranero et al., 2000). Additionally, the igneous basement subsequently dredged from the lower continental slope of Nicaragua indicated an extension of the continental framework to the trench there. In seismic records the regional unconformity can be followed continuously from the ODP Leg 170 drill transect off Nicoya to the proposed Osa Peninsula drill transect.

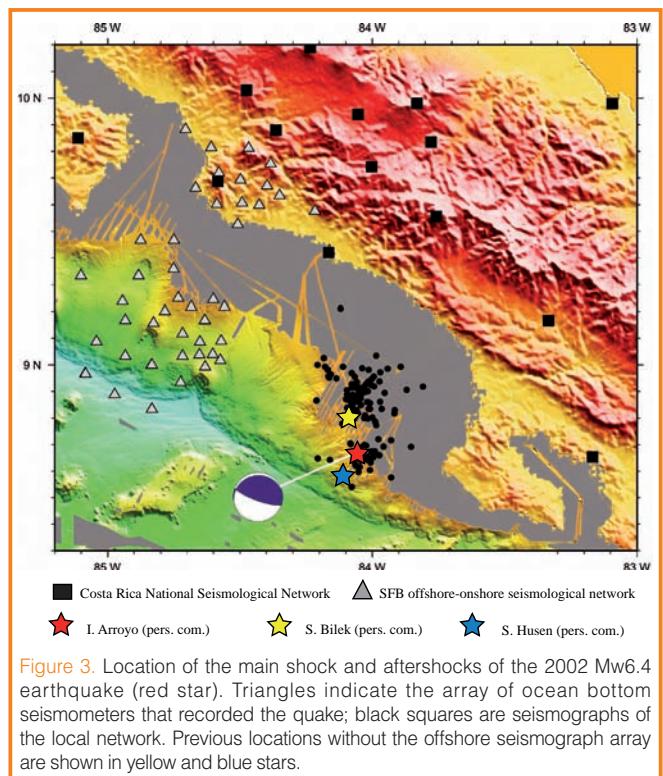
Ongoing erosion is indicated by morphology of the slope (Fig. 2). Osa bathymetric high forms the southern flank of a major embayment where erosion and slope retreat are accelerated by subduction of Cocos Ridge and its associated seafloor ridges and seamounts. The regional erosion surface was ground truth during Leg 170, and the current retreat of the continental slope provides evidence of vigorous tectonic erosion where CRISP drilling is proposed.

Results from recent work: Researchers in the German SFB 574 (Kiel University) have used high-resolution geophysical tools to map the mounds at a series of mid-slope vent sites. In all, about 125 vent sites were located along ~600 km of the margin off Costa Rica and Nicaragua, and they seem to be common from Panama to Mexico. Material and fluids were sampled from several mounds, and probe heat flux measurements were collected across a number of sites. Cameras just above the seafloor displayed abundant chemo-synthetic carbonates and fauna at the vent sites.

The mounds are a few hundreds to one thousand meters across with a very hummocky topography. They occur in the area of normal faulting and locally appear at fault scarps. Heat flux over and around the mounds is high compared to the regional background values, **indicating venting of deeply-sourced fluid** (Grevemeyer et al., 2004). Pore fluid chemistry documents low **chlorinity fluids, and chemical modeling** indicates that they come from dehydration of clays (Hensen et al., 2004). **First-order estimates of fluid flow budget across the forearc** indicate that most fluid released during dehydration of sediment in the subduction channel traverses the upper plate and is released across the **mid-slope vent sites** (Ranero et al., 2007). Dehydration of the sediment subducting with the lower plate is proposed as one of the significant causes for the transition to stick-slip behavior and seismogenesis. The massive fluid release across the upper plate of **erosional margins is one of the unique processes** investigated during CRISP.

Also unique to CRISP is the possibility to drill the nucleation area of the 20 November 2002, Mw6.4 interplate thrust earthquake. The earthquake was recorded on an array of ocean bottom seismometers as well as on the Costa Rican National Seismological Network on land (Fig. 3). The full array provides a **database for accurate relocation of the earthquake and its aftershocks** (I. Arroyo, in preparation). The main shock is essentially located in the position of the proposed **5-km-deep riser drill hole to the seismogenic zone**. Downhole instrumentation, including seismometers, will provide a 3-D seismic image around the drill hole with a radius of several kilometers **including the area of the Mw6.4 nucleation**. Attribute analysis of the seismic data will permit an estimation of the **general physical properties of the upper plate and plate boundary**.

CRISP: The shallow dip of the subduction zone off southern Costa Rica and the **relatively high** temperature of the subducting ocean crust bring materials and processes involved in seismogenesis to depths reachable by drilling with the riser ship *Chikyu*. CRISP is structured in non-riser (Program A) and riser (Program B) stages that systematically lead from shallow non-riser to deep riser drilling (Fig. 4). Program A provides background information for Program B, **which reaches the unstable slip of the seismogenic zone**. Program A drilling allows the characterization of lower plate oceanic igneous rock and hydrology before subduction, **as well as under the front of the margin**. With standard ODP



drilling technology it also provides the samples to characterize upper plate basement rock. Logging and instrumentation will provide accurate information on the upper plate thermal structure, interplate earthquake nucleation, and rupture propagation, which are key for a successful planning of deeper riser drilling. In Program B, the riser sites locations are constrained with the results from downhole instruments and conventional geophysical experiments, rock mechanics laboratory experiments, and forward modeling. Program B drilling reaches 3 km below seafloor to sample for the first

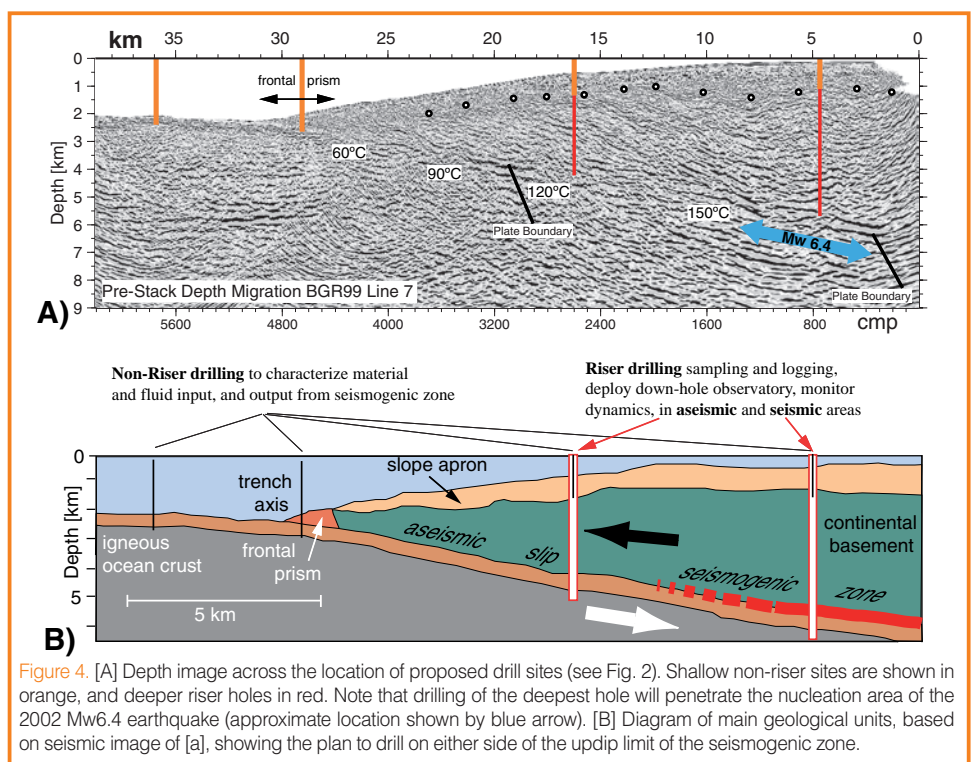


Figure 4. [A] Depth image across the location of proposed drill sites (see Fig. 2). Shallow non-riser sites are shown in orange, and deeper riser holes in red. Note that drilling of the deepest hole will penetrate the nucleation area of the 2002 Mw6.4 earthquake (approximate location shown by blue arrow). [B] Diagram of main geological units, based on seismic image of [a], showing the plan to drill on either side of the updip limit of the seismogenic zone.

Subsurface Structure, Fault Zone Characteristics, and Stress State in Scientific Drill Holes of Taiwan Chelungpu Fault Drilling Project

by Jih-Hao Hung, Kuo-Fong Ma, Chien-Yin Wang, Shen-Rong Song, Hisao Ito, Weiren Lin, and En-Chao Yeh

doi:10.2204/iodp.sd.s01.27.2007

Introduction

The 1999 Chi-Chi earthquake (M_w 7.6) produced a >90-km-long surface rupture zone along the north-south trending, west-vergent Chelungpu fault. The most striking feature of the coseismic displacement field is that areas of large surface displacement lie above the footwall ramp of the thrust and at the northern termination (up to 12 m). An important question that needs to be addressed is what physical properties or dynamic processes within the fault zone cause large coseismic displacements in the northern segment. Hypotheses that have been proposed include 1) change of the fault-plane geometry (Yue et al., 2005); 2) static (long-term) physical properties such as intrinsic low coefficient of friction, high pore-pressure, and solution-transport chemical processes; and 3) dynamic change of physical properties during slip. To address the above questions two holes (A and B) were drilled for the Taiwan Chelungpu Fault Drilling Project (TCDP) during 2004–2005 at Dakeng, west-central Taiwan, where large surface slip (~10 m) was observed. Continuous coring and geophysical downhole logging in two holes 40 meters apart were completed from a depth of 500–2003 m (Hole A) and 950–1350 m (Hole B). Data from the drilled holes provide a unique opportunity to understand deformation mechanisms and physical properties of the Chelungpu fault where large slip occurred in the Chi-Chi earthquake.

Subsurface Structure and Fault-Zone Characteristics

Subsurface structure, stratigraphy, and corresponding log depth encountered in Hole A are shown in Fig. 1. Regional bed attitude above FZA1712, identified from cores and FMI/FMS images in Hole A and from correlation of fault zones between Hole A and Hole B, is trending N15°-E21°, dipping 20°–40° (30° on average) toward SE. Nonetheless, intervals of increasing (from 30° to 75°) or decreasing (from 70° to 20°) dip, as well as changes of dip azimuth, appear across fault zones. A gradual increase of bedding dip with depth starts from FZA1712, and a drastic change of dip from 20°–40° to 60°–80° occurs across FZA1855 where steep to overturned beds extend to the bottom hole.

A total of twelve fault zones identified in Hole A are located in the Plio-Pleistocene Cholan Formation, Pliocene Chinshui Shale, and Miocene Kueichulin Formation. Common fault rocks in the cores include intensely deformed fault core (clayey gouge) and adjacent highly fractured damage zones (fault breccia). The fault gouge is composed of ultra-fine-grained clay minerals and massive to foliated fabrics; occasionally, thin layers of indurate black material appear within the gouge zone. A typical example is the Chelungpu fault zone, FZA1111 (Fig. 2). The fault is bedding-parallel consisting of fault breccia and fault gouge 1109 m to 1112 m.

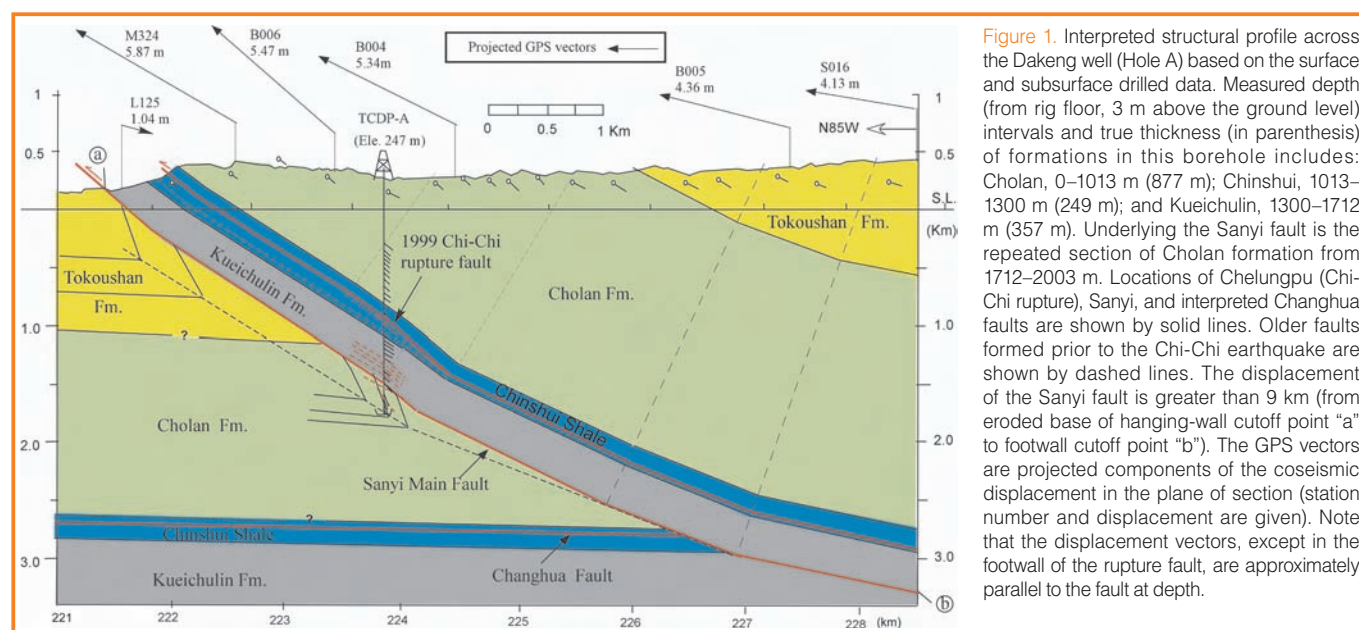


Figure 1. Interpreted structural profile across the Dakeng well (Hole A) based on the surface and subsurface drilled data. Measured depth (from rig floor, 3 m above the ground level) intervals and true thickness (in parenthesis) of formations in this borehole includes: Cholan, 0–1013 m (877 m); Chinshui, 1013–1300 m (249 m); and Kueichulin, 1300–1712 m (357 m). Underlying the Sanyi fault is the repeated section of Cholan formation from 1712–2003 m. Locations of Chelungpu (Chi-Chi rupture), Sanyi, and interpreted Changhua faults are shown by solid lines. Older faults formed prior to the Chi-Chi earthquake are shown by dashed lines. The displacement of the Sanyi fault is greater than 9 km (from eroded base of hanging-wall cutoff point “a” to footwall cutoff point “b”). The GPS vectors are projected components of the coseismic displacement in the plane of section (station number and displacement are given). Note that the displacement vectors, except in the footwall of the rupture fault, are approximately parallel to the fault at depth.

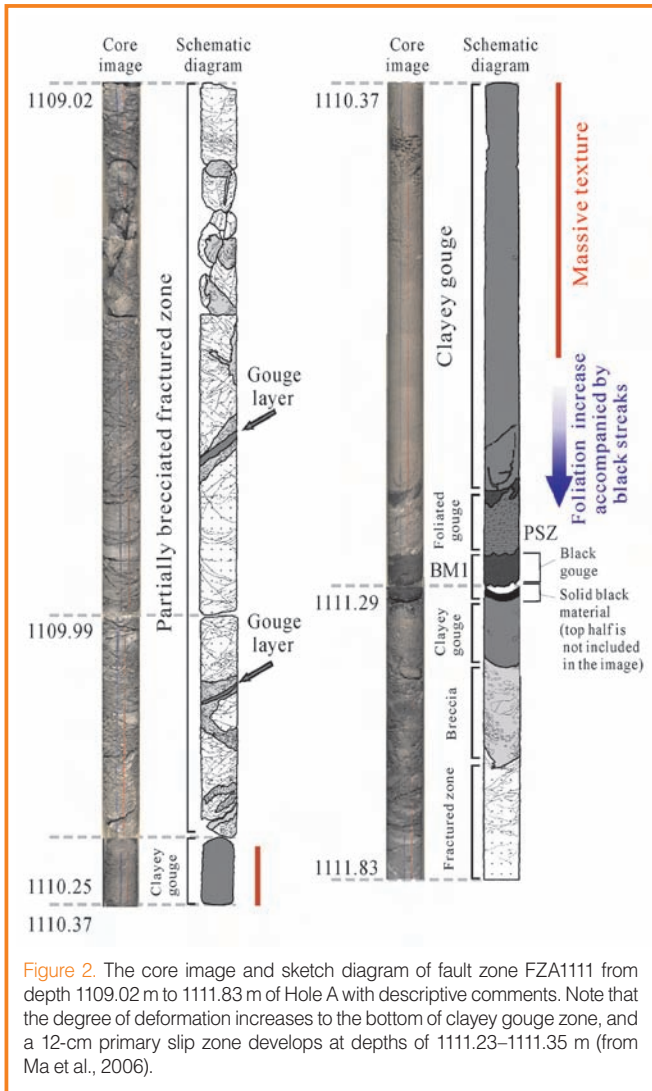


Figure 2. The core image and sketch diagram of fault zone FZA1111 from depth 1109.02 m to 1111.83 m of Hole A with descriptive comments. Note that the degree of deformation increases to the bottom of clayey gouge zone, and a 12-cm primary slip zone develops at depths of 1111.23–1111.35 m (from Ma et al., 2006).

The degree of fracturing increases from the top of the damage zone towards the gouge zone in which the fabrics changed from massive to foliate between 1110.25 m and 1111.35 m. The Chi-Chi major slip zone (MSZ, about 2 cm thick) is contained within the 12-cm-thick primary slip zone (PSZ), which is located near the bottom of this broad gouge zone (Ma et al., 2006).

In spite of large surface displacements, no temperature anomaly was observed near FZA1111 due to circulation of mud immediately after the drilling. Nevertheless, Kano et al. (2006) reported a heat anomaly of 0.06°C during repeated temperature measurements 6 months after the completion of drilling.

In situ Stress Measurements

Leak-off test: A standard commercial procedure of open-hole, extended leak-off tests was conducted in Hole B at depths between 940 m and 1350 m to determine *in situ* magnitudes of maximum (S_{Hmax}) and minimum (S_{Hmin}) horizontal stresses. Successful leak-off tests have been done at four locations in Hole B—1279.6, 1179.0, 1085.0, and

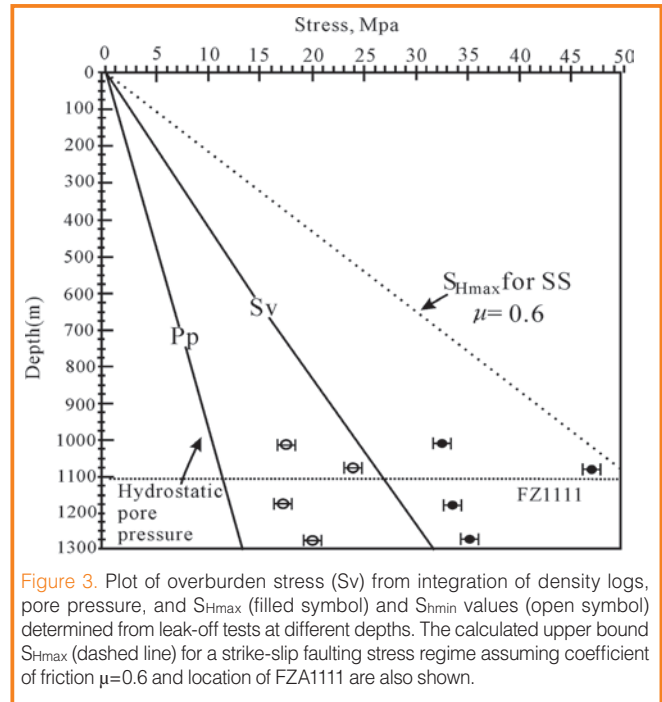


Figure 3. Plot of overburden stress (S_v) from integration of density logs, pore pressure, and S_{Hmax} (filled symbol) and S_{Hmin} values (open symbol) determined from leak-off tests at different depths. The calculated upper bound S_{Hmax} (dashed line) for a strike-slip faulting stress regime assuming coefficient of friction $\mu=0.6$ and location of FZA1111 are also shown.

1019.5 m—with two above and two below the FZB1137 (equivalent to FZA1111). Given the depth of overburden, we can calculate the vertical stress from integration of density logs and compile with pore pressure and hydrofracturing data from various depths (Fig. 3). The measurements clearly indicate a strike-slip fault regime after the Chi-Chi earthquake in this area.

Wellbore failure: *In situ* stresses S_{Hmax} determined from borehole breakouts and drilling-induced tensile fractures from Hole A and Hole B (Fig. 4) show that a significant change of S_{Hmax} azimuth occurs across the depth of 1300 m (also a stratigraphic boundary between the Chihshui shale and the Kueichulin Formation). The S_{Hmax} was oriented at 103°–138° with an average of 123° in the section of 700–1300 m, as opposed to 137°–164° (154° on average) from 1300 m to 1700 m. Borehole breakouts are relatively better developed in the Kueichulin Formation than in other places. This observation agrees with stronger anisotropy (stress magnitude) in the Kueichulin Formation, as shown by the shear wave anisotropy.

Shear Seismic Wave Anisotropy

Data from Dipole-Shear Sonic Imager (DSI™, Schlumberger) logs acquired over the interval of 508–1870 m in Hole A were used to assess shear wave velocity anisotropy. Analyses at these depths are shown by scatter plots and rose diagrams for nine discrete intervals of similar orientations of fast shear wave polarization (Fig. 5). A prominent NW-SE fast shear polarizing direction was generally observed except in a few depth zones, such as 738–770 m, 785–815 m, and 1517–1547 m. In particular, a very consistent mean direction with small dispersion of 115°±1°–2° (95% confidence interval) appears in the strongly aniso-

tropic Kueichulin Formation at 1300–1650 m. Relatively consistent fast shear polarization directions appear across FZA1111 (average 165° between 1105 m and 1115 m) compared to the interval of 1078–1190 m with trending in a much broader range of 130°–170°. Thus, there is no observable systematic change of trend on fast shear polarization across the Chi-Chi slip zone. On the other hand, from the change of fast shear azimuth at depth 1000 m and contrasting degree of anisotropy across the depth of 1300 m, the perturbation of regional stresses may have occurred within the upper and lower boundaries of the Chinshui Shale as suggested from detailed study of borehole breakouts (Wu et al., 2007).

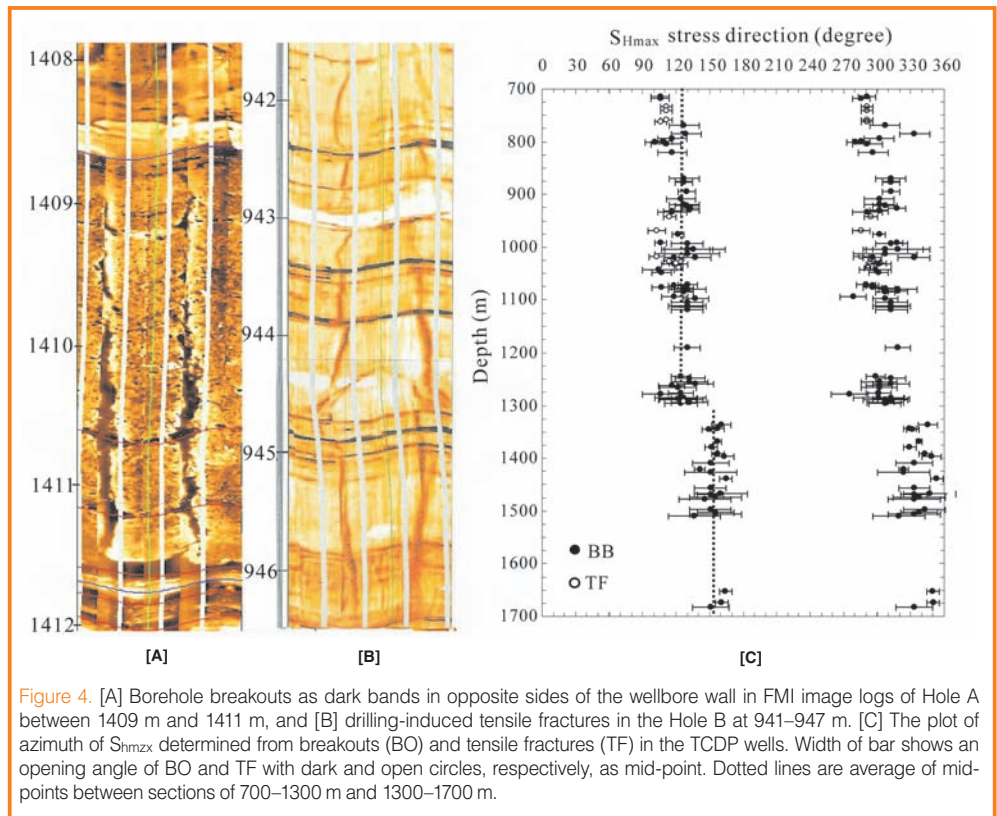


Figure 4. [A] Borehole breakouts as dark bands in opposite sides of the wellbore wall in FMI image logs of Hole A between 1409 m and 1411 m, and [B] drilling-induced tensile fractures in the Hole B at 941–947 m. [C] The plot of azimuth of S_{Hmax} determined from breakouts (BO) and tensile fractures (TF) in the TCDP wells. Width of bar shows an opening angle of BO and TF with dark and open circles, respectively, as mid-point. Dotted lines are average of mid-points between sections of 700–1300 m and 1300–1700 m.

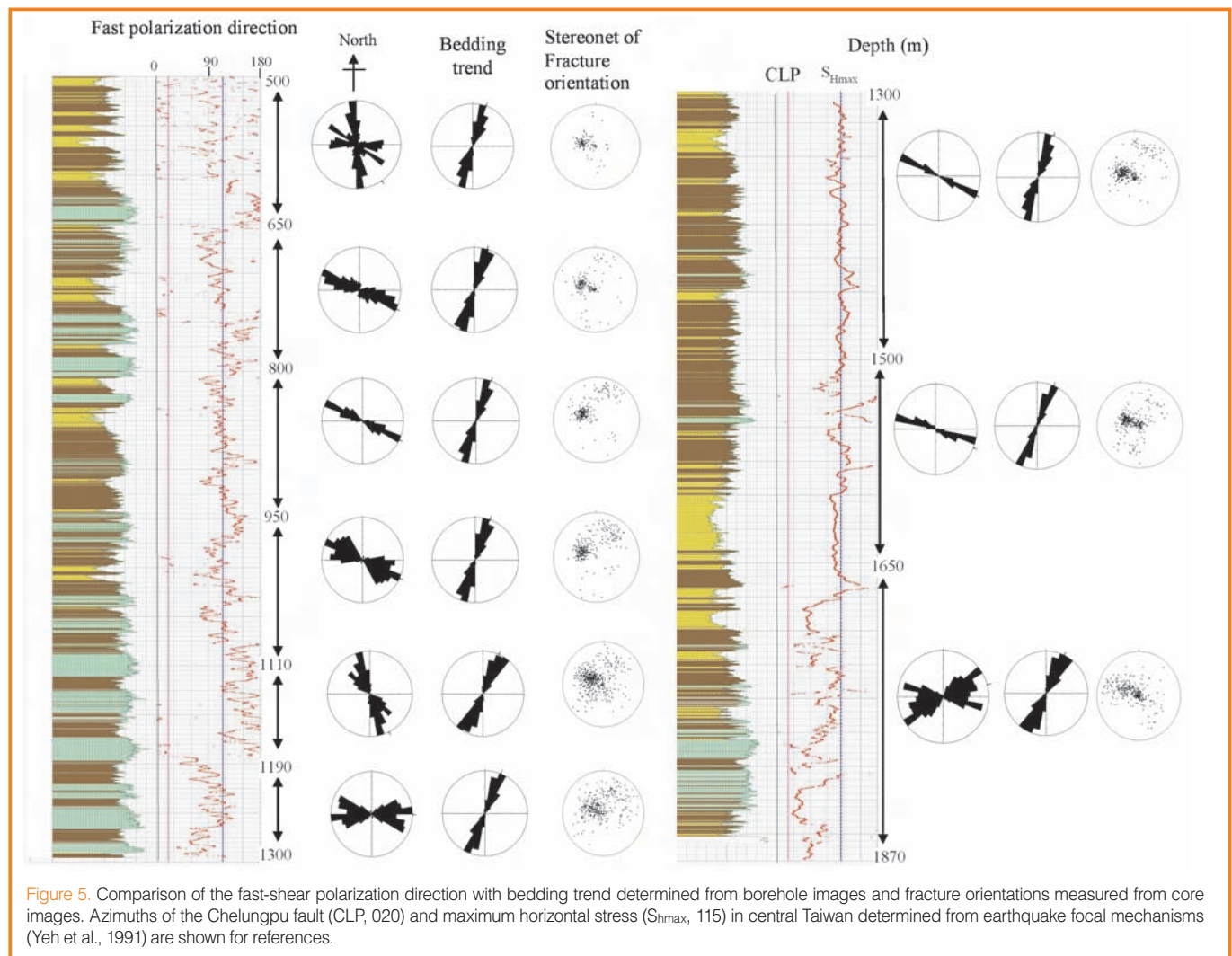


Figure 5. Comparison of the fast-shear polarization direction with bedding trend determined from borehole images and fracture orientations measured from core images. Azimuths of the Chelungpu fault (CLP, 020) and maximum horizontal stress (S_{Hmax} , 115) in central Taiwan determined from earthquake focal mechanisms (Yeh et al., 1991) are shown for references.

Drilling Investigations on the Mechanics and Structure of Faults

by Kentaro Omura

doi:10.2204/iodp.sd.s01.22.2007

Fault zone drilling provides valuable insights into understanding the dynamics, physical properties, and structure of an active fault. We drilled into the four major active faults in central and western Japan to directly access mechanics, physical properties, and fault rock distributions in and around the fault zones—the Nojima fault (which appeared by the 1995 Hyogo-ken Nanbu Earthquake, M7.2, also called the Kobe Earthquake); the Neodani fault, which appeared by the 1891 Nobi earthquake (M8.0); the Atera fault of which some parts seemed to have been dislocated by the 1586 Tensho earthquake (M7.9); and the Gofukuji Fault, which is said to have activated more than a thousand years ago. We measured *in situ* stress magnitude and direction in and around a fault zone by hydraulic fracturing and borehole breakout method. Additionally, integrating *in situ* measurements in a deep borehole and ground surface geophysical survey across a fault zone, we observed physical properties and structures of fault zones. The stress state and structure of different faults may reflect different stages in the earthquake pre-event process in the earthquake recurrence cycle.

By the *in situ* stress measurements, we found the differential stress magnitude decreases in the depth close to fracture zones in the Neodani fault (1300-m-deep well; Ikeda et al., 1996) and the Nojima fault (1800-m-deep well; Ikeda et al., 2001a). We also found the orientations of the maximum horizontal compressive stress were nearly perpendicular to the fault strikes of the Nojima Fault (Ikeda et al., 2001a). As for the Atera Fault, the orientation of the maximum horizontal compressive stress was the reverse of the fault moving direction (Ikeda et al., 2001b). These results support the idea that the differential stress is small at narrow zone adjoining fracture zones and the fault is quite "weak" after the earthquake. Additionally, outside the narrow zone the frictional strength of rock is still high. The level of shear stress adjacent to the fault seems to be controlled principally by the frictional strength of rock in and around the fault.

As for the Nojima fault, the pre-shock stress field adjacent to (about 300 m distance from) the fault was estimated by adding the stress change due to the co-seismic slip from the post-shock stress field measured by the hydraulic fracturing method (Yamashita et al., 2004). The reconstructed stress state just before the earthquake was different from that just after the earthquake and shows that the maximum horizontal principal stress direction is oblique to the fault, which is

consistent with the background tectonic stress direction (East-West) before the earthquake. As for the Gofukuji fault, the orientation of the maximum horizontal principal stress adjacent to (about 300 m distance from) the fault was oblique to the fault trace (Omura et al., 2003a). The Headquarters for Earthquake Research Promotion, Japan determined that the Gofukuji fault has not activated for a time longer than the mean earthquake recurrence interval. The strength of the Gofukuji fault may be recovered enough to sustain shear stress on the fault, which is the same situation as estimated pre-shock stress state of the Nojima. The findings on the stress states of Nojima and Gofukuji fault suggest that the fault recovered as hard as the host rock surrounding the fault from the weak strength just after the earthquake, and that the orientation of the stress near the fault changes during the inter-seismic period of the earthquake recurrence cycle.

Downhole physical logging, and macro- and microscopic observation of recovered cores show complicated fault rock distribution in the fault fracture zones. In a schematic view, narrow strongly fractured sub-zones and broad weakly fractured sub-zones are distributed within a fracture zone. The strongly fractured sub-zones are characterized as having low electrical resistance, low density, low P-wave velocity, high porosity, and enlargement of borehole radius (Omura et al., 2003b). In particular, in the Nojima Fault cores, we observed three distinct fracture zones, each including strongly and weakly fractured sub-zones (Kobayashi et al., 2001). X-ray analyses of the Nojima fault cores show that the three fracture zones have different distribution pattern of chemical elements and alteration minerals which were produced by hydrothermal changes associated with fault activities (Matsuda et al., 2004). The fault seems not to have slipped on a specific plane, but on more than one fault plane during earthquake cycles. The complicated fault zone structure should have formed progressively during repeating earthquake cycles.

The drilling method is of great advantage to study the mechanics and structure of fault zones because we can access the materials and internal structure of the fault zones directly. On the other hand, as the depth and the number of drillings are limited, it is important to include significant integrated studies such as geophysical prospect, geophysical observations, laboratory experiments, and numerical simulation.

References

- Ikeda, R., Iio, Y., and Omura, K., 2001a. *In situ* stress measurements in NIED boreholes in and around the fault zone near the 1995 Hyogoken-Nanbu earthquake, Japan. *The Island Arc*, 10(3/4):261–265.
- Ikeda, R., Omura, K., Iio, Y., and Tsukahara, H., 1996. Scientific drilling and *in situ* stresses in active fault zones at Neodani, central Japan. *Proc. 8th Int'l. Symp. On the Observation of the Continental Crust Through Drilling*, 30–35.
- Ikeda, R., Omura, K., Matsuda, T., Mizuochi, Y., Uehara, D., Chiba, A., Kikuchi, A., and Yamamoto, T., 2001b. Central Japan's Atera active fault's wide-fractured zone: An examination of the structure and in-situ crustal stress. *EOS. Trans. Am. Geophys. Union*, 82(47):Abstract T51A-0848.
- Kobayashi, K., Arai, T., Ikeda, R., Omura, K., Sano, H., Sawaguchi, T., Tanaka, H., Tomita, T., Tomida, N., Hirano, S., Matsuda, T., and Yamazaki, A., 2001. Distribution of fault rocks in the fracture zone of the Nojima Fault at a depth of 1140m: Observations from the Hirabayashi NIED core. *The Island Arc*, 10(3/4):411–421, doi:10.1016/j.1440-1738.2001.00339.x.
- Matsuda, T., Omura, K., Ikeda, R., Arai, T., Kobayashi, K., Shimada, K., Tanaka, H., Tomita, T., and Hirano, S., 2004. Fracture-zone conditions on a recently active fault: Insights from mineralogical and geochemical analyses of the Hirabayashi NIED drill core on the Nojima fault, southwest Japan, which ruptured in the 1995 Kobe earthquake. *Tectonophysics*, 378:143–163, doi:10.1016/j.tecto.2003.09.005.
- Omura, K., Ikeda, R., Iio, Y., Arai, T., Kobayashi, K., Shimada, K., Tanaka, T., Hirano, S., and Matsuda, T., 2003b. Logging in a fault fracture zone –A case study at Hirabayashi NIED Borehole drilled through Nojima fault. *BUTSURI-TANSA*, 56:401–414. (Japanese with English abstract)
- Omura, K., Ikeda, R., Matsuda, T., and Mizoguchi, Y., 2003a. Active fault drilling research on stress, electrical and base rock structure – Fault zone structure of Gofukuji fault, central Japan. 2003 General Assembly of the International Union of Geodesy and Geophysics (IUGG), Poster B468.
- Yamashita, F., Fukuyama, E., and Omura, K., 2004. Estimation of fault strength: Reconstruction of stress before the 1995 Kobe earthquake. *Science*, 306:261–263, doi:10.1126/science.1101771.

Author

Kentaro Omura, National Research Institute for Earth Science and Disaster Prevention, Tennoudai 3-1, Tsukuba, Ibaraki, 305-0006, e-mail: omura@bosai.go.jp.

Clay Mineral Composition and Diagenesis: Effects on the Location and Behavior of Faults in the Frontal Portions of Subduction Zones

by Michael B. Underwood

doi:10.2204/iodp.sd.s01.19.2007

One of the more ambitious goals of the Seismogenic Zone Experiment (SEIZE) is to discriminate between the effects of changing intrinsic frictional strength (i.e., gouge versus wall-rock) and the effects of gradual or transient increases in pore pressure within fault zones. In subduction zones, both variables are likely to change with increasing distance down the plate boundary. In addition to sediment's cohesion and coefficient of internal friction, the shear strength of any given stratigraphic interval depends upon fluid pressure and total normal stress. The release of fluids from mudstones during diagenesis (including volatiles generated from organic matter) is modulated by a combination of mechanical compaction, tectonic consolidation, and mineral reactions. Thus, it is essential to determine how permeability, sediment-derived fluid sources, and fluid flow contribute to overpressure conditions within the subduction inputs, beginning seaward of the subduction front at depths of 2500 m or less.

Primary lithostratigraphic architecture exerts a first-order influence over the material properties and tectonic behavior of subduction zones, at least near the toe of the margin wedge. Generic sedimentary facies models for trenches (Piper et al., 1973) show upward thickening and

coarsening trends (from basalt at the base through pelagic ooze, hemipelagic mud, silty turbidites, and sandy turbidites). As glaring exceptions to that norm, however, there are substantial thicknesses of highly permeable sand (abyssal-plain deposits) that continue to move down the subduction path (i.e., beneath the frontal décollement) in Nankai (Ashizuri transect), Barbados, and Cascadia (Underwood and Moore, 1995; Underwood, 2007). Until those sands are lithified by cementation, their high net permeability will control three-dimensional patterns of fluid circulation. The amount and types of clay-size particles within each stratigraphic interval are also important because they affect any sediment's coefficient of friction and permeability. Empirical and experimental studies demonstrate that clay-rich fault gouges are weaker than surrounding wall rocks, typically because of their constituent particle size and mineralogy. Expandable minerals of the smectite group (e.g., montmorillonite) are notorious in the eyes of geotechnical engineers for affecting strata's coefficient of internal friction, compressibility, and permeability (Lupini et al., 1981; Morrow et al., 1992; Saffer and Marone, 2003).

Common hydrous minerals (e.g., smectite and opal) also

increase fluid production during diagenesis. Fluids produced from dehydration reactions become increasingly important as the burial temperature increases and the pore volume is reduced by compaction. To complicate matters further, the thermal structure of subducting lithosphere varies with crustal age, basement relief, and patterns of hydrothermal circulation. The zones of maximum fluid production, therefore, should shift spatially in response to variations in two independent input parameters: heat flow and abundance of hydrous minerals. Moreover, pathways of focused fluid migration will track the architecture of high-permeability sand bodies inherited from the depositional

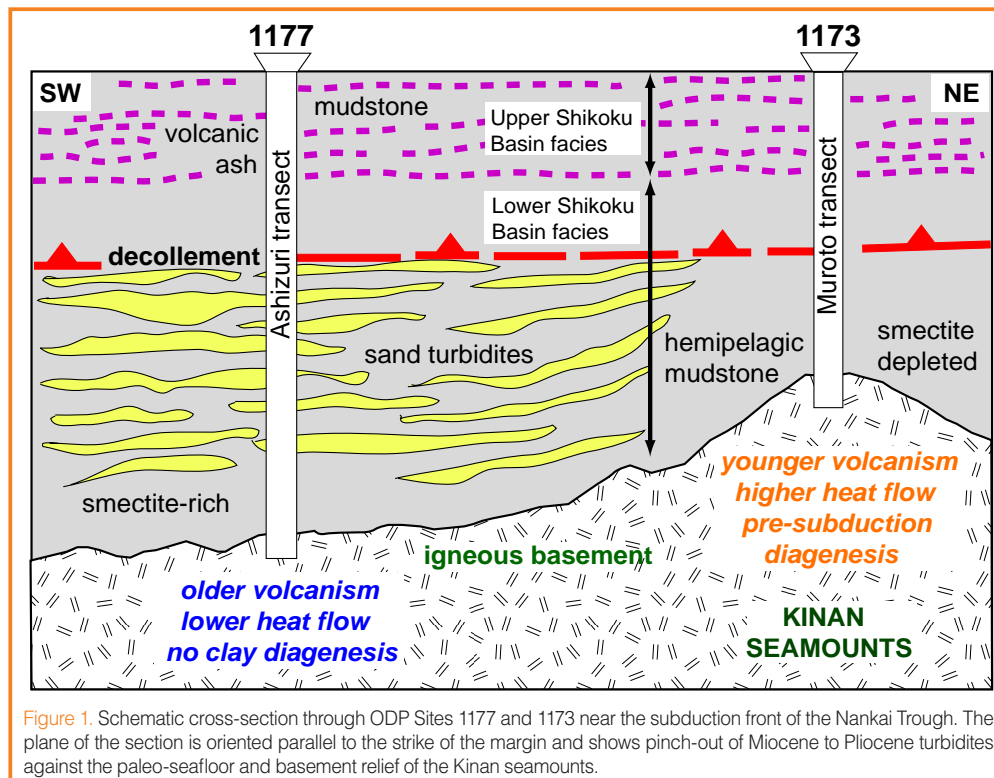
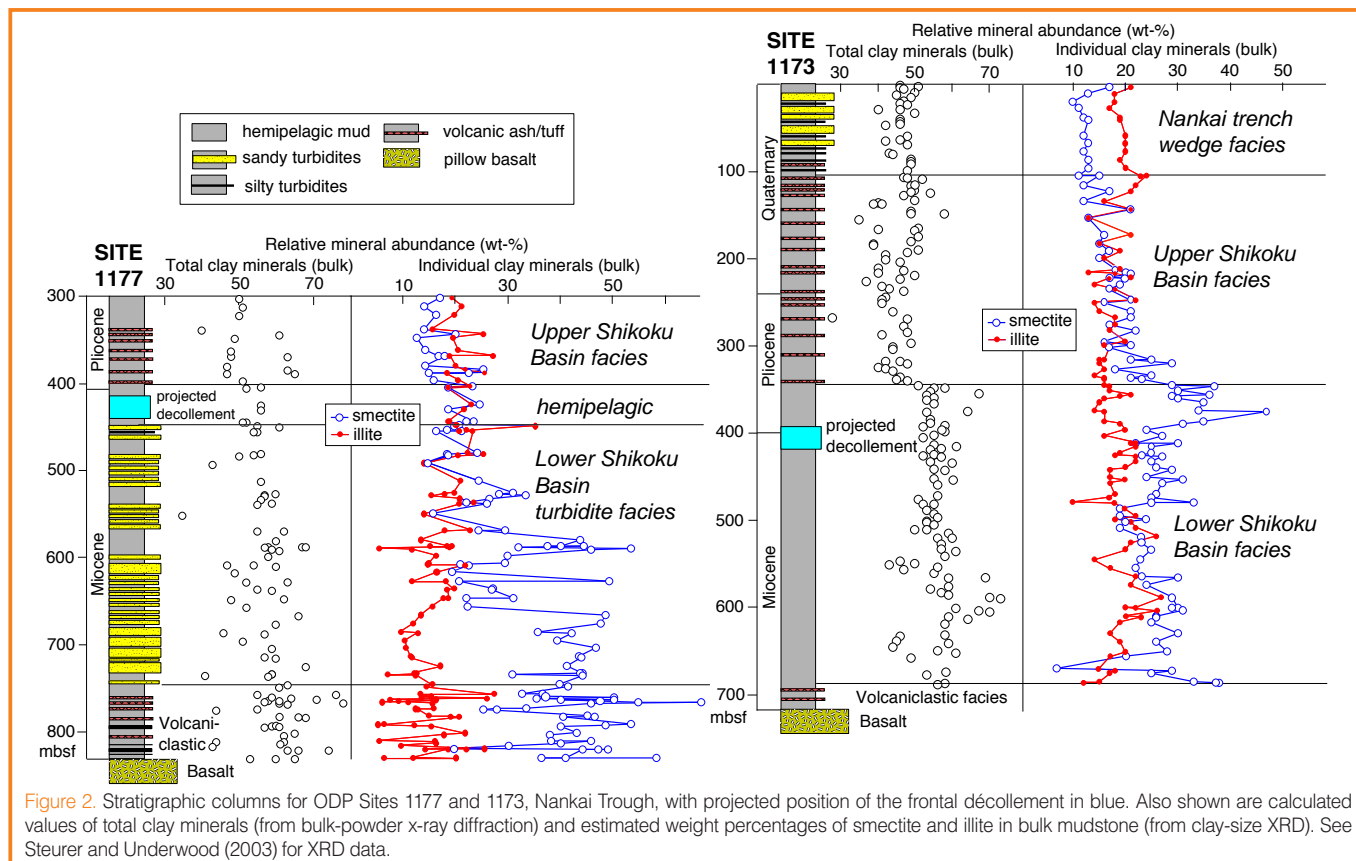


Figure 1. Schematic cross-section through ODP Sites 1177 and 1173 near the subduction front of the Nankai Trough. The plane of the section is oriented parallel to the strike of the margin and shows pinch-out of Miocene to Pliocene turbidites against the paleo-seafloor and basement relief of the Kinan seamounts.



environment (i.e., isolated shoe-string channel sands, stacked channel-levee complexes, unconfined sand sheets, depositional lobes). Compartments of excess pore-fluid pressure are, in many depositional systems, set up initially by those sand-body geometries (Bredehoeft et al., 1988; Flemings et al., 2002). Conversely, if subduction inputs consist of low-permeability mud throughout a system, then diffuse drainage will be retarded, and **focused flow is more likely to follow structural conduits of fracture-enhanced permeability.**

When investigating the change from stable sliding to stick-slip behavior, the “**smectite-to-illite hypothesis**”, in its elementary form, provides scientists with a tractable idea to test (Hyndman et al., 1997; Vrolijk, 1990). But that influential concept is oversimplified because it does not take into account three-dimensional variations in lithostratigraphy, either within or among individual subduction margins. Similarly, the hypothesis fails to account adequately for local and global variability in total clay abundance, the absolute amount of smectite, grain fabric, pore pressure, heat flow, and reaction progress prior to subduction. A more holistic view, stressed by Moore and Saffer (2001), is that several interrelated factors and processes (e.g., precipitation of carbonate and silicate cements, progressive growth of phyllosilicates, clay-mineral dehydration, changes in frictional properties of clay) act collectively to **modulate the strength and mechanical behavior of strata on opposite sides of the updip limit of the seismogenic zone.** The recipe for blending each factor and process almost certainly changes from one subduction margin to another, within each individual margin,

and through time. This natural variability needs to be taken into account when drilling projects target subduction thrusts.

Variability in subduction inputs can lead to substantial differences in how quickly diagenetic reactions progress, both outboard of a subduction front and downdip along the subduction path. This effect is particularly obvious in the Nankai Trough, where heat flow varies with distance from the fossil spreading ridge of the **Shikoku Basin** (Yamano et al., 2003). Inputs of sediment to the **Nankai Trough change in three dimensions** because irregular basement highs deflected turbidity currents during early stages of abyssal-floor sedimentation. Sandy turbidites are the norm, rather than the exception, beneath the frontal décollement where smooth basement enters the subduction zone (Fig. 1). The content of smectite also changes along strike in Nankai because of local perturbations of heat flow and pre-subduction clay diagenesis (Fig. 2). By the time strata pass beneath the toe of the warmer Muroto accretionary prism, the smectite-to-illite reaction advances nearly to completion at the sediment-basalt interface (Fig. 2). In contrast, coeval strata within the nearby (cooler) Ashizuri transect remain virtually unaltered. Accurate predictions of where and how much fluid volume might be released through deeper dehydration reactions demand accurate three-dimensional knowledge of the starting materials and thermal structure.

Each subduction margin around the world displays its own idiosyncrasies. The frontal décollement in the Barbados accretionary prism occupies a stratigraphic interval that is

San Andreas Fault Zone Mineralogy, Geochemistry, and Physical Properties from SAFOD Cuttings and Core

by John G. Solum, Stephen Hickman, David A. Lockner, Sheryl Tembe, Jim P. Evans, Sarah D. Draper, D.C. Barton, David L. Kirschner, Judith S. Chester, Frederick M. Chester, Ben A. van der Pluijm, Anja M. Schleicher, Diane E. Moore, Carolyn Morrow, Kelly Bradbury, Wendy M. Calvin, and Teng-fong Wong

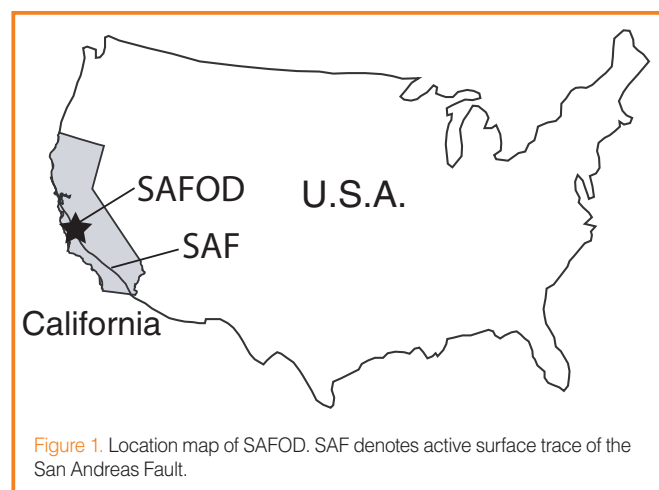
doi:10.2204/iodp.sd.s01.34.2007

Introduction

The San Andreas Fault Observatory at Depth (SAFOD), drilled near the town of Parkfield, California (Fig. 1) (Hickman et al., 2004) as part of the U.S. National Science Foundation's EarthScope Project (see <http://www.earthscope.org>), provides a continuous set of samples through the active San Andreas Fault (SAF) zone. These samples can help address decades-old questions such as apparent weakness of the SAF (Zoback, 2000) providing the unparalleled opportunity to constrain the parameters that control the behavior of plate bounding faults like the San Andreas.

Samples collected from SAFOD also complement studies of exhumed fault zones. While studies of exhumed fault zones have benefit from regionally extensive exposures that allow for detailed mapping and analyses (Chester and Chester, 1998; Evans and Chester, 1995), such studies also have inherent limitations including uncertainty about stress states and styles of deformation (i.e., seismogenic vs. creeping). Moreover, mineral assemblages in exhumed fault zones can be altered during exhumation, obscuring fault-related mineral assemblages and textures (Solum et al., 2003; Solum and van der Pluijm, 2004).

The SAFOD target zone contains two parallel strands that generate repeating M2 earthquakes in addition to having a component of creep (Nadeau et al., 2004). Therefore, SAFOD also offers the opportunity to obtain samples from seismogenic and aseismic faults and to constrain the rheology of the active SAF system.



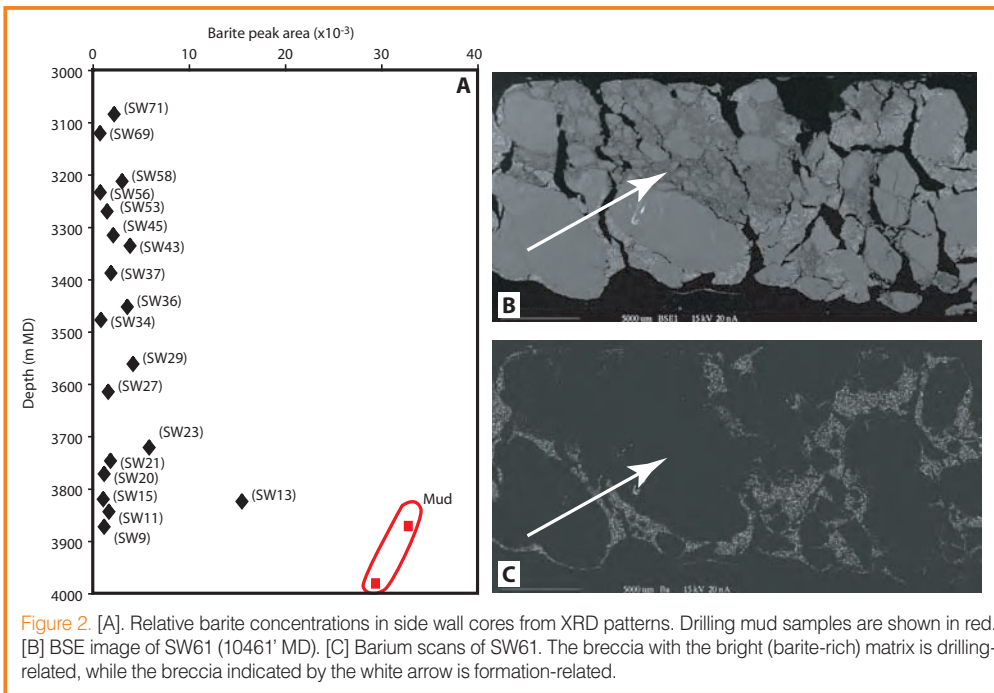
Samples Collected

Three types of samples were collected during drilling of the SAFOD main hole: rotary drill cuttings, spot cores, and percussive sidewall cores. A complete list of samples is available at: <http://safod.icdp-online.org/>.

The vast majority of samples collected to date are cuttings (>99% of the length of the hole). Two groups of rotary cuttings were collected at 3-m intervals over the entire length of the hole. One set was composed of unwashed cuttings (cuttings mixed with drilling mud collected as they come off the shale shaker), while the other was composed of washed cuttings, which are equivalent to unwashed cuttings that were gently rinsed on-site to remove drilling mud.

Three spot cores were collected following casing runs—one in a hornblende-biotite granodiorite at 1462–1470 m measured depth (MD), one in an arkose/siltstone at the bottom of the Phase I hole at 3056–3067 m MD, and one at the bottom of the Phase II hole at 3990–3998 m MD. Fifty-two percussive side wall cores were collected from 3081–3953 m MD preceding casing of the Phase 2 hole in August 2005. Most of these samples were in siltstone/shale; however, two were in arkose.

Each type of sample has potential problems that must be addressed individually. For cuttings, these include loss of formation clays during on-site washing; difficulty resolving thin features like thin beds or faults (since cuttings represent an average over a 3-m-long interval); mixing as cuttings travel from the drill bit to the surface; contamination of cuttings derived at the drill bit by borehole collapses and abrades further up the hole; and contamination from materials from the drill string (e.g., steel shavings, paint) or from drilling additives (e.g., nut plug). Problems associated with side wall cores include disruption of natural textures and inducement of fractures during the collection process; contamination of the core from drilling mud (as the tool shoots through the borehole wall into the formation); and the potential that the core will sample the cuttings bed and not the formation. In addition, side wall cores can only be collected from regions of the hole that are relatively in gauge, which can eliminate the sampling weak areas such as fault zones, that are prone to washouts. Side wall cores also provide only a 2.5-cm snapshot of lithology. Drilling mud



contamination of side wall cores can be constrained using XRD and SEM (Fig. 2). SEM characterizations of the side wall cores allow textures that are drilling-induced to be distinguished from natural textures. Spot cores present fewer analytical difficulties than rotary cuttings or side wall cores; however, spot cores sampled less than 0.5% of the length of the SAFOD main hole. It is therefore vital to place spot and side wall cores into a broader geologic context, and this must be done using analyses of rotary cuttings (Fig. 3).

Sample Mineralogies

The mineral assemblages of samples were characterized using x-ray diffraction (XRD) (Solum et al., submitted), optical microscopy (Almeida et al., 2005; Barton et al., 2005; Draper et al., 2005; Evans et al., 2005), infrared reflectance (IR) (Calvin and Solum, 2005), scanning electron microscopy (SEM) (Hickman et al., 2005) and transmission electron microscopy (TEM) on select spot core samples (Schleicher et al., 2006). A summary of cuttings and core mineralogy is shown in Fig. 2.

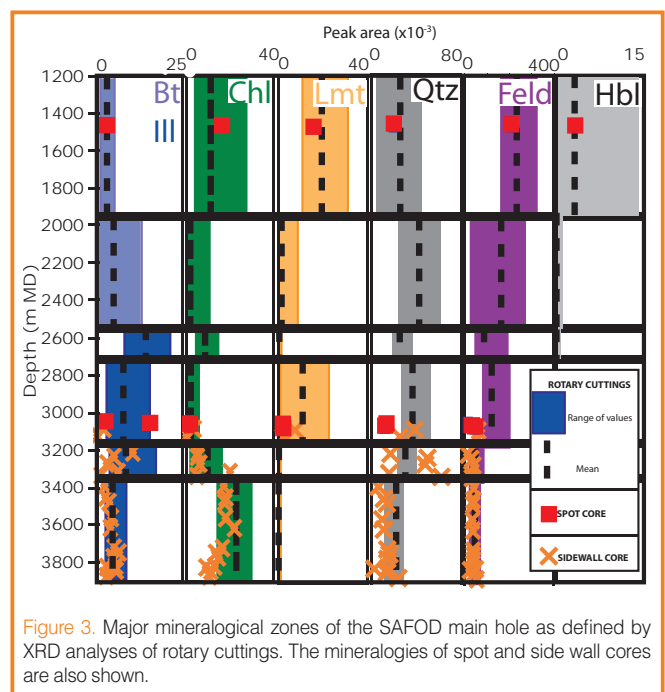
Changes in mineralogy inferred from cuttings strongly correlate with geophysical logs (Solum et al., submitted), indicating that cuttings analyses reveal real lithologic boundaries and faults. These changes define mineralogical zones that are likely fault-bounded.

After penetrating the sedimentary cover, the hole entered Salinian granitic rocks. At 1926 m MD the hole crossed the Buzzard Canyon Fault (Rymer et al., 2003) and entered a series of arkosic sediments composed of an upper and a lower unit separated by a large fault at ~2560 m MD (Solum et al., submitted; Draper et al., in prep.), and containing a potentially active member of the SAF system at 3067 m MD. The

hole entered a series of mudrocks (Great Valley sequence) at 3158 m MD, which are separated from a mineralogically distinct series of Great Valley mudrocks by an actively creeping member of the SAF system that is causing casing deformation (Zoback et al., 2005). This formation extends to the bottom of the hole at 3998 m MD.

At least five major faults were crossed during drilling (Figs. 2 and 4), including an actively creeping member of the SAF system that is causing casing deformation at a depth of 3295–3313 m MD (Zoback et al., 2005). The creep occurs

within a low-velocity zone interpreted as the damage zone of the active SAF (Zoback et al., 2005). Between 3322 m and 3353 m MD, this zone contains up to ~2 wt% serpentine, preliminarily identified as lizardite with minor chrysotile, based on crystal morphologies, (Solum et al., submitted); however, given the limitations inherent in the use of cuttings, the relationship of this serpentine to faulting cannot be definitively established until Phase III drilling in the summer of 2007. Two major faults, one at 2545–2560 m MD and one at 3067 m MD, are clay-rich (>50 wt%) containing a neoformed mixed-layer clay (Solum et al., submitted; Schleicher et al., 2006). The Buzzard Canyon Fault at 1926–1235 m MD is rich in quartz and feldspars (>80 wt%) and contains relatively little clay (<3 wt%). These preliminary results highlight the



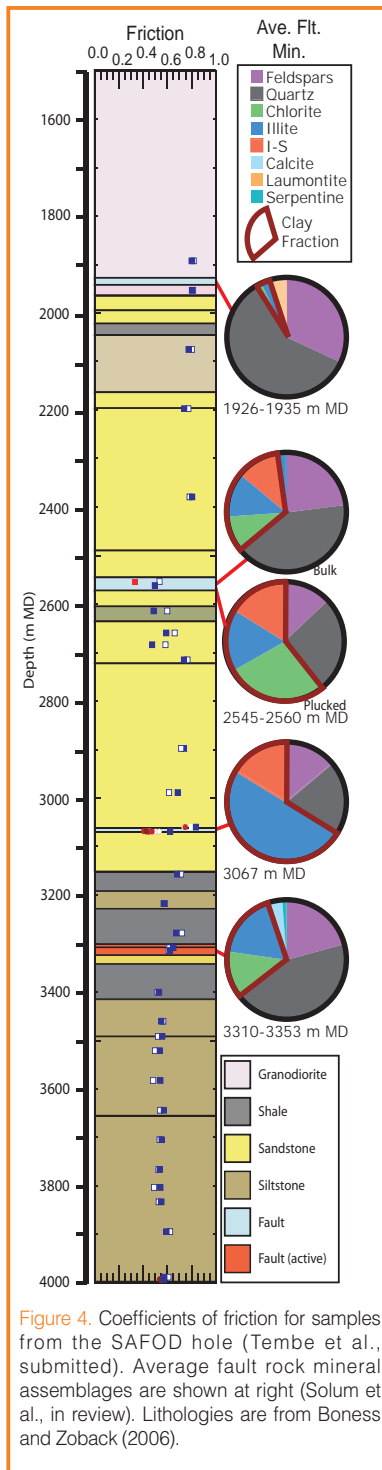


Figure 4. Coefficients of friction for samples from the SAFOD hole (Tembe et al., submitted). Average fault rock mineral assemblages are shown at right (Solum et al., in review). Lithologies are from Boness and Zoback (2006).

($\mu=0.40-0.55$ vs. $\mu=0.55-0.80$). Plucked grains of clay-rich fault rocks from 256 m MD have $\mu=0.33$, while bulk samples from that depth have $\mu \approx 0.45$. This indicates that analyses of bulk samples provide an upper bound on the coefficient of friction, and that the properties of fault rocks can be better constrained by plucking grains of fault rocks from bulk cuttings. Analyses of plucked fault rocks from the section of the hole that contains the actively creeping fault are ongoing.

compositional and rheological heterogeneity of the faults of the SAF system at SAFOD.

Alteration phases such as clays, zeolites, and some feldspars may record alteration by fluids that were confined by sealing faults. In addition, Kirschner et al. (2005) found that the stable isotopic composition of carbonates plucked from cuttings at 3100–3950 m MD fell into two partially overlapping populations. One occurred more frequently in fault zones, while the other occurred more frequently in protolith. This suggests that in the region of SAFOD faults are tapping a fluid reservoir that is not seen in the protolith.

Constraining the frictional properties of the SAF is a key objective of SAFOD. Tembe et al. (2005) showed that cuttings preserve meaningful information about the frictional properties of the rocks penetrated during drilling, with faults generally weaker than adjacent protolith

Conclusions

The ongoing studies briefly discussed here will help to increase the understanding of the behavior of the active SAF. Further, comprehensive studies of all of the faults penetrated during drilling of SAFOD provide the opportunity to constrain the rheological, structural, and geochemical evolution of this section of the SAF. Analyses of cuttings and Phase I and II cores define the broad geologic framework of the SAFOD area and will help guide the selection of targets for Phase III drilling in the summer of 2007.

References

Almeida, R., Chester, J.S., Chester, F.M., Kirschner, D.L., Waller, T.D., and Moore, D.E., 2005. Mesoscale structure and lithology of the SAFOD Phase 1 and II Core Samples. *Eos Trans. AGU*, 86(52), Fall Meet. Suppl., Abstract T21A-0454.

Barton, D., Bradbury, K.K., Solum, J.G., and Evans, J., 2005. Structural and lithologic characterization of the SAFOD pilot hole and phase one main hole. *Eos Trans. AGU*, 86(52), Fall Meet. Suppl., Abstract T21A-0451.

Boness, N.L. and Zoback, M.D., 2006. A multiscale study of the mechanisms controlling shear velocity anisotropy in the San Andreas Fault Observatory at Depth. *Geophysics*, 71:131–146, doi:10.1190/1.2231107.

Calvin, W.M. and Solum, J.G., 2005. Drill hole logging with infrared spectroscopy. *Geothermal Resources Council Trans.*, 29:565–568.

Chester, F.M. and Chester, J.S., 1998. Ultracataclastic structure and friction processes of the Punchbowl fault, San Andreas system, California. *Tectonophysics*, 295:199–221, doi:10.1016/S0040-1951(98)00121-8.

Draper, S.A., Boness, N.L., and Evans, J.P., 2005. Source and significance of the sedimentary rocks in the SAFOD borehole: Preliminary analysis. *Eos Trans. AGU*, 86(52), Fall Meet. Suppl., Abstract T24B-02.

Evans, J., Moore, D., Kirschner, D., and Solum, J.G., 2005. Lithologic characterization of the deep portion of the SAFOD drill hole. *Eos Trans. AGU*, 86(52), Fall Meet. Suppl., Abstract T21A-0450.

Evans, J.P. and Chester, F.M., 1995. Fluid-rock interaction in faults of the San Andreas system; inferences from San Gabriel Fault rock geochemistry and microstructures. *J. Geophys. Res.*, 100:13007–13020, doi:10.1029/94JB02625.

Hickman, S., Solum, J., Moore, D., Chester, J., Guillemette, R., Draper, S., Tembe, S., Boness, N., and Summers, R., 2005. Photographs and scans of SAFOD phase 2 sidewall sores, SAFOD phase 2 sample party, Menlo Park, Calif., U.S.A., http://geoweb.tamu.edu/Faculty/chesterj/safod/products/Phase_2_Sidewall_Cores.ppt

Hickman, S., Zoback, M., and Ellsworth, W., 2004. Introduction to special section: Preparing for the San Andreas Fault Observatory at Depth. *Geophys. Res. Lett.*, 31:L12S01, doi:10.1029/2004GL020688.

Electron Microscopy of Clay Minerals in Mudrocks from the San Andreas Fault Observatory at Depth (SAFOD)

by Anja M. Schleicher, Ben A. van der Pluijm, Laurence N. Warr, and John G. Solum

doi:10.2204/iodp.sd.s01.33.2007

Introduction

The San Andreas Fault Observatory at Depth (SAFOD) drill site situated near Parkfield, California (Hickman et al., 2004) offers the opportunity to assess the interplay between clay formation, faulting, and fluid migration in an active fault zone through direct sampling from depth and comparison with exhumed fault strands (Chester et al., 2004; Evans and Chester, 1995; Solum and van der Pluijm, 2004). Recent electron microscopy and x-ray diffraction (XRD) studies of rock fragments and cuttings from this drill site show abundant clay minerals in the host rock, on fracture surfaces, and within mineralized veins (Schleicher et al., 2006; Solum et al., 2006). It is, therefore, of importance to determine the timing of clay formation in relation to pre-, syn-, or post-faulting activities, and to establish their influence on the seismic behavior of the San Andreas Fault (Wu, 1975). Within this context, the formation of clays at depth is a potential weakening mechanism of crustal-scale faults (Warr and Cox, 2001; Wintsch et al., 1995; Zoback, 2000).

In this study of mineral transformations, the scanning electron microscope (SEM) and transmission electron microscope (TEM) are used to provide new insights into the nano-scale characteristics of clay minerals, and to evaluate the mineralogical characteristics of very fine-grained particles in fault rocks from the SAFOD drill hole. Using high-resolution TEM, the following aspects are being investigated: i) the microstructural characteristics of the clay mineral phases down to the nanometer scale, ii) the clay polytype structures by selected-area diffraction analysis (SAED), iii) the microchemistry of clay particles using analytical electron microscopy (AEM) and elemental geochemistry (ICP), and iv) the hydration state of smectite using wet-cell XRD and TEM. Based on these investigations, different events of clay formation can be assessed in order to characterize diagenetic or hydrothermal fluid-driven growth processes.

Sampling and Methods

Fine-grained, clay-rich rock fragments up to 1 cm in average length were collected from a spot-core of a clay-rich shear zone at 3067 m measured depth (MD, upper star in Fig. 1). This part of the borehole represents a potentially active section of the San Andreas fault zone, although it is

currently not considered to contain the main fault trace (Zoback et al., 2005). The samples show distinct polishing and striations on particle surfaces and on fracture surfaces. Some of these carefully washed rock chips were ultrasonically treated to remove surface particles and to study their nature.

Other rock fragments with similarly polished surfaces were found at 3436 m MD from inside a core catcher after a failed coring attempt (lower star in Fig. 1). In an attempt to preserve the mineralogical structure, natural hydration state, and textural properties, specimens were bottled and embedded in resin directly on site. The travel-time of rock-chips from the bottom of the hole to the surface is about 7.5 hours. The fractured core chips were cleaned of drilling mud using dry paper towels and placed into small sample bottles containing 50% methanol and 50% LR White resin. In the laboratory, the solvent was progressively removed by using increasing concentrations of LR White resin following the procedure of Kim et al. (1995). Polymerization was achieved by transferring to casting molds, and the bubbles were removed in a vacuum desiccator. Finally, the samples were hardened in a vacuum oven at 60°C for 24 h. Backup samples were stored in humidity-controlled vessels to avoid drying and any contact with liquid water.

SEM of thin sections prepared from the impregnated rock fragments allowed pre-selection of locations of interest that were subsequently investigated by TEM. Small Cu-washers were glued on these areas and thinned using an ion mill apparatus. All

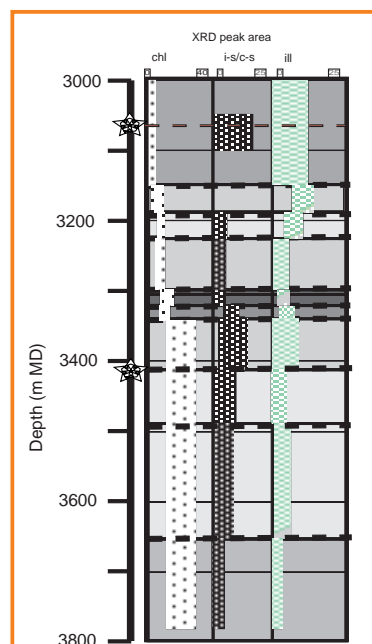


Figure 1. Mineralogic characteristics of the SAFOD main hole obtained from XRD powder patterns. Main minerals are chlorite (chl), illite (ill), mixed-layer illite-smectite and chlorite-smectite (i-s/c-s). Major boundaries are shown by dashed lines and bands correspond to lithologic units (Solum et al., 2006).

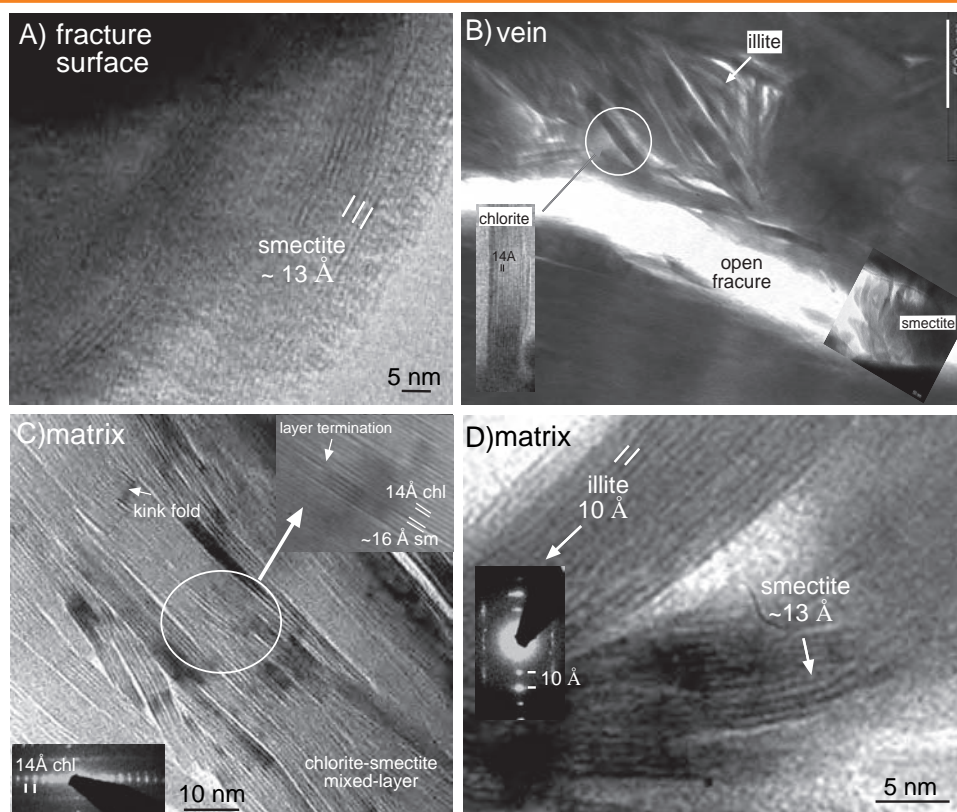


Figure 2. Low and high resolution TEM images of [A] smectite ultrasonically separated from fracture surfaces, [B] smectitic vein fillings that are surrounded by packets of chlorite and illite crystals, [C] rock-matrix samples with interstratifications of chlorite and smectite (note microstructures such as kink folds and layer terminations), and [D] packets of illite growth with illite-smectite mixed-layering and smectite.

electron microscopy work was conducted in the EMAL at the University of Michigan, using the methods described in Warr and Nieto (1998). Microscopy was undertaken using a Philips CM12 scanning transmission electron microscope at an operating voltage of 120 kV and a beam current of 20 μ A. High-resolution imaging was conducted at magnifications between 50,000 \times and 350,000 \times . Chemical analysis was performed in scanning mode by energy-dispersive spectrometry analysis over areas of 100 nm² using a Kevex Quantum solid-state detector.

Results and Ongoing Work

At least three different structural types of smectite-occurrence could be distinguished in the SAFOD mud-rock fragments: **i) fracture surfaces with thin films and slicken-fibers** (Fig. 2A, Schleicher et al., 2006), **ii) vein mineralization in the rock matrix** (Fig. 2B), and **iii) the matrix containing chlorite, smectite, chlorite-smectite, and illite-smectite mixed-layerings** (Figs. 2C and 2D). **The thin films** that cover the fracture surfaces at 3067 m and 3436 m MD reveal smectitic aluminosilicate minerals with a variable cation content of Na, K, Ca, Mg, and Fe. These compositions differ from the smectite minerals of the fresh drilling mud. A smectite phase with a composition similar to the fracture coatings was detected in the mineralized veins at 3436 m MD. Here, chlorite and illite crystals occur as mixed-

layerings together with a discrete smectite phase covering the margins of the veins.

In contrast, the matrix shows small areas with discrete smectite phases; **however, most smectites occur as mixed-layers of illite-smectite and chlorite-smectite.** They usually occur together with large packets of illite and chlorite. SEM investigations of these minerals reveal large irregular detrital grains with curved and damaged particle shapes. They are surrounded by a compacted fabric (presumably bedding parallel), perpendicular to the polished fractures and containing notably higher concentrations of K, Mg, and Fe. Illite, chlorite, and interstratifications of smectite with chlorite and illite have also been recognized by Solum et al. (2006) in the whole-rock XRD patterns. Based on first analysis

of illite diffraction patterns (SAED), ordered and disordered 1M polytypes can be distinguished, whereas a higher-temperature 2M₁ illite polytype has not yet been recognized.

Preliminary observations of samples impregnated on site also indicate the coexistence of authigenic illite-smectite and discrete smectite particles that were not disturbed during embedding and polymerization. However, the characterization of microstructures and comparison with non-impregnated material are not yet fully determined and require more detailed study.

Discussion

Based on the ongoing electron microscopy study of SAFOD drill rocks, illite, chlorite, and smectite in combination with diverse mixed-layered minerals occur in the argillaceous lithologies. However, the TEM analysis in particular shows that the minerals were formed in texturally different microstructural sites, **suggesting different formation processes.**

Among the key observations is a natural smectite phase on the fracture surfaces that occurs as oriented platy and fibrous minerals, forming thin film coatings with slicken-fibers (Fig. 2A). This clay phase is interpreted as an authigenic phase formed by **dissolution-precipitation reactions**

during the movement of aqueous fluids along permeable fractures and veins at temperatures possibly up to ~130°C (Moore and Reynolds, 1997; Schleicher et al., 2006; Williams et al., 2005). The fibrous nature suggests fault creep as the environment for their formation, but the timing of initial fracture formation remains uncertain, so that the clay-films could also represent growth along reactivated faults structures.

The large packets of illite and chlorite in the matrix show curved and damaged particle shapes with kink bands and layer terminations (Fig. 2C) that occur together with smectitic mixed-layering. The ordered and disordered 1M illite polytypes, based on SAED patterns, reflect the likely transformation of illite-smectite to smectite in the diagenetic compaction processes. Such events are well known, for example, in argillite lithologies of the Salton Sea geothermal system (Yau et al., 1987) or the Gulf Coast (Freed and Peacor, 1992).

Further investigations will be necessary to detail specific mineral reactions and swelling behavior of clays at the crystal lattice scale. Particularly important is to determine the formation mechanisms (e.g., layer-by-layer replacement vs. dissolution and neocrystallization) and fabrics of the clays, and to establish the timing of reactions in relation to the deformation history of the fault rocks.

Acknowledgements

Our SAFOD research is supported by the EarthScope Program of the U.S. National Science Foundation (NSF) and by the Deutsche Forschungsgemeinschaft (DFG).

References

- Chester, F.M., Chester, J.S., Kirschner, D.L., Schulz, S.E., and Evans, J.P., 2004. Structure of large-displacement, strike-slip fault zones in the brittle continental crust. In Karner, G.D., Taylor, B., Driscoll N., Kohlstedt D. (Eds.), *Rheology and Deformation in the Lithosphere at Continental Margins*. New York (Columbia University Press), 223–260.
- Evans, J.P. and Chester, F.M., 1995. Fluid-rock interaction in faults of the San Andreas system; inferences from San Gabriel Fault rock geochemistry and microstructures. *J. Geophys. Res.*, 100:13007–13020, doi:10.1029/94JB02625.
- Freed, R.L. and Peacor, D.R., 1992. Diagenesis and formation of authigenic illite-rich I/S crystals in Gulf Coast shales: TEM study of clay separates. *J. Sediment. Petrol.*, 62:220–234.
- Hickman, S., Zoback, M., and Ellsworth, W., 2004. Introduction to special section: Preparing for the San Andreas Fault Observatory at Depth. *Geophys. Res. Lett.*, 31:L12S01, doi: 10.1029/2004GL020688.
- Kim, J.W., Peacor, D.R., Tessier, D., and Elsass, F., 1995. A technique for maintaining texture and permanent expansion of smectite interlayers for TEM observations. *Clays and Clay Minerals*, 43:51–57, doi:10.1346/CCMN.1995.0430106.
- Moore, D.W. and Reynolds, R.C. 1997. *X-ray Diffraction and the Identification and Analysis of Clay Minerals, 2nd Edition*. Oxford, U.K. (Oxford University Press).
- Schleicher, A.M., van der Pluijm, B.A., Solum, J.G., and Warr, L.N., 2006. The origin and significance of clay minerals on surfaces, in fractures and in veins from SAFOD borehole samples (Parkfield, California). *Geophys. Res. Lett.*, 33: L16313, doi:10.1029/2006GL026505.
- Solum, J.G. and van der Pluijm, B.A., 2004. Phyllosilicate mineral assemblages of the SAFOD Pilot Hole and comparison with an exhumed segment of the San Andreas Fault System. *Geophys. Res. Lett.*, 31:L15S19, doi:10.1029/2004GL01990.
- Solum, J.G., Hickman, S.H., Lockner, D.A., Moore, D.E., van der Pluijm, B.A., Schleicher, A.M., and Evans, J.P., 2006. Mineralogical characterization of protolith and fault rocks from the SAFOD main hole. *Geophys. Res. Lett.*, 33:L21314, doi:10.1029/2006GL027285.
- Warr, L.N. and Cox, S., 2001. Clay mineral transformations and weakening mechanisms along the Alpine Fault, New Zealand. *Geol. Soc. Lond. Spec. Publ.*, 186:85–101.
- Warr, L.N. and Nieto, F., 1998. Crystallite thickness and defect density of phyllosilicates in low-temperature metamorphic pelites: a TEM and XRD study of clay-minerals crystallinity-index standards. *Canad. Min.*, 36:1453–1474.
- Williams, C.F., D'Alessio, M.A., Grubb, F.V., and Galanis, S.P., 2005. Heat flow in the SAFOD main hole. *Eos Trans. AGU*, 86 (52), Fall Meet. Suppl., Abstract T23E-07.
- Wintsch, R.P., Christoffersen, R., and Kronenberg, A., 1995. Fluid-rock reaction weakening of fault zones. *J. Geophys. Res.*, 100(B7):13021–13032.
- Wu, F.T., Blatter, L., and Robertson, H., 1975. Clay gouges in the San Andreas Fault system and their possible implications. *Pure Appl. Geophys.*, 113:87–96, doi:10.1007/BF01592901.
- Yau, Y.-C., Peacor, D.R., and McDowell, D., 1987. Smectite-to-illite reactions in Salton Sea shales; a transmission and analytical electron microscopy study. *J. Sediment. Res.*, 57:335–342.
- Zoback, M.D., 2000. Strength of the San Andreas fault. *Nature*, 405:31–32.
- Zoback, M.D., Hickman, S., and Ellsworth, W., 2005. Overview of SAFOD Phases 1 and 2: Drilling, sampling and measurements in the San Andreas Fault zone at seismogenic depth. *Eos Trans. AGU*, 86(52), Fall Meet. Suppl., Abstract T23E-01.

Authors

Anja M. Schleicher, Universität Würzburg, Geologisches Institut, Pleicherwall 1, 97070 Würzburg, Germany, e-mail: aschleic@umich.edu.

Ben A. van der Pluijm, University of Michigan, Department of Geological Sciences, 1100 University Avenue, C.C. Little Building, Ann Arbor, Mich. 48109, U.S.A.

Laurence N. Warr, Centre de Géochimie de la Surface (CNRS-ULP), 1 rue Blessig, 67084 Strasbourg, France.

John G. Solum, U.S. Geological Survey, Earthquake Hazards Team, 345 Middlefield Road, MS 977 Menlo Park, Calif. 94025, U.S.A.

Real-time Mud Gas Monitoring: A Technique to Obtain Information on the Composition and Distribution of Gases at Depth While Drilling

by Thomas Wiersberg and Jörg Erzinger

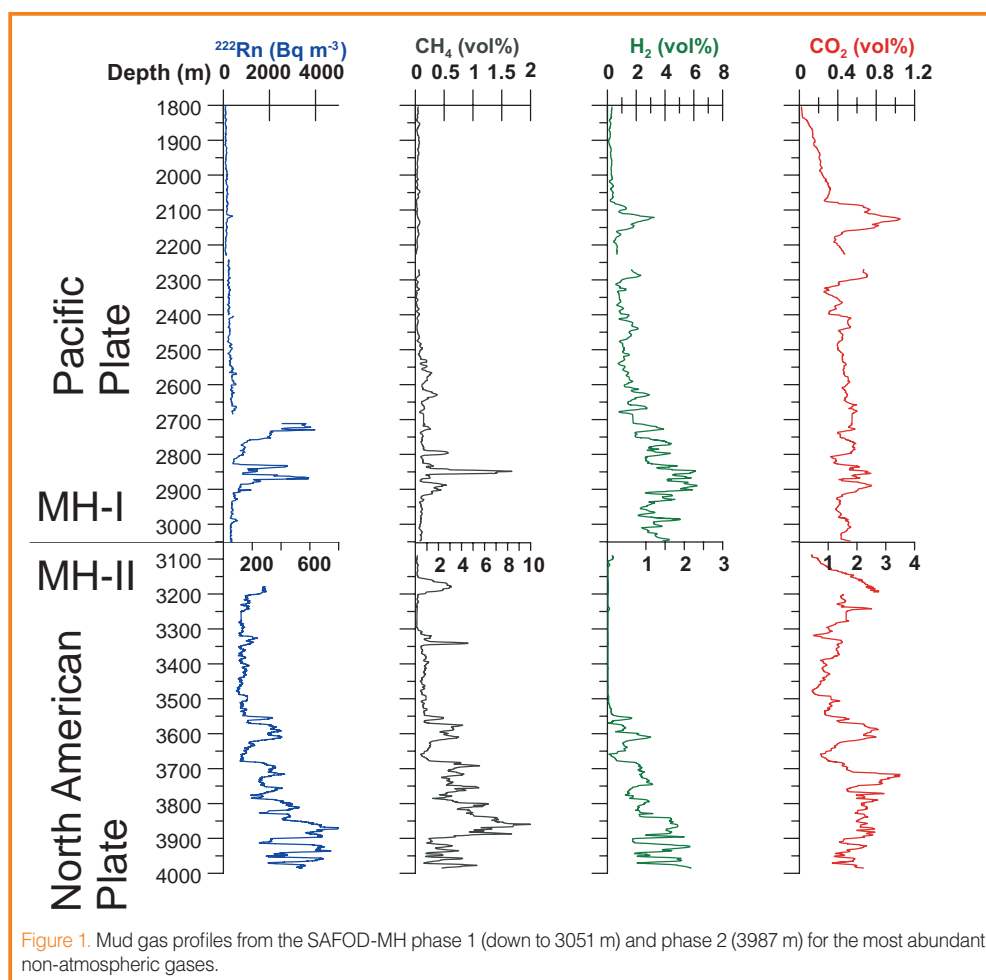
doi:10.2204/iodp.sd.s01.36.2007

Several techniques have been applied to obtain information on the composition of gases and fluids in drill holes, such as downhole fluid sampling, gas and fluid analysis during pumping tests, or *in vacuo* degassing of drill core samples. All these techniques can yield valuable information on the geochemistry of gases, but they are less useful for obtaining a continuous dataset on the distribution and composition of gases at depth. To reveal such data during drilling, we have developed a technique where gas is extracted from circulating drill mud with an agitator and continuously piped into a nearby laboratory trailer for on-line analysis. In addition, we routinely determine electrical conductivity, pH, and temperature continuously during the drilling operation within the mud pit at 10-min intervals.

Hydrocarbons, helium, radon, and carbon dioxide are the most suitable gases for the real-time detection of fluid-bearing horizons such as shear zone, open fractures, sections of enhanced permeability, and occurrences of permafrost methane hydrate. Gas analysis is carried out with a quadrupole mass spectrometer for N₂, O₂, Ar, CO₂, CH₄, He, H₂, and H₂S; a gas chromatograph (GC) equipped with a flame ionization detector (FID) for hydrocarbons (CH₄, C₂H₆, C₃H₈, n-C₄H₁₀, and i-C₄H₁₀), and a custom-built Lucas cell alpha-detector for ²²²Rn activity. When significant amounts of non-atmospheric gases are detected, off-line gas samples are automatically collected from the gas line for further investigations on isotopes (e.g. noble gases, carbon, and hydrogen) to reveal information on the origin and evolution of deep-seated fluids. The technique has been applied successfully on several International Continental Scientific Drilling Program (ICDP) projects, such as SAFOD (San Andreas Fault

Observatory at Depth), Mallik, and German Continental Deep Drilling Program KTB (Erzinger et al., 2004; Wiersberg et al., 2005; Zimmer and Erzinger, 1995).

As an example, we present results from the SAFOD Main Hole, drilled in 2004–2005 within the framework of ICDP. SAFOD wants to achieve a better understanding on the processes at active plate-bounding fault systems at the location of their origin. Knowledge about the role and origin of fluids and gases associated with the San Andreas Fault (SAF) zone is relatively poor. Besides the open question on how fluids are linked with fault zone processes in general, outstanding topics include the spatial distribution of fluids at depth, and, in particular, the contribution of mantle-derived fluids to the total fluid inventory of the SAF.



The pilot hole (PH) and the main hole (MH) were both drilled at a **short distance from each other. In contrast to the vertical PH, which penetrates 768 m of Quarternary and Tertiary sediments into Cretaceous granite down to 2168 m final depth, the MH was deviated towards the SAF and re-enters sedimentary strata below 1930 m, where it remains down to the bottom of the hole (3987 m). Geophysical and geological observations identify the SAF in a depth interval of ~3100–3450 m.**

In the lower, sedimentary part of the SAFOD-MH, drilled in 2004 (1900–3051 m) and 2005 (3051–3980 m), **the most abundant non-atmospheric gases in drill mud were hydrogen (up to 6 vol %), methane (up to 10 vol %), and carbon dioxide (up to 4 vol %). The concentration of helium remained low (>20 ppmv), whereas radon activity reached values of up to 5000 Bq m⁻³. Two major sections could be identified where these gases were enriched in mud gas: from 2700–2900 m and from >3550 m to the bottom of the hole at 3987 m (Fig.1).** A positive correlation between the numbers of beddings and fractures in these sections, identified by geophysical logging, and the radon activity implies that fluids enter the hole through open fissures. Furthermore, the radon activity indicates that the fluids are actively circulating. In both sections, radon also correlates positively with H₂, CO₂, and (in part) CH₄; **however, the relative proportions of these gases are different in both sections. The upper and lower sections are enriched in ²²²Rn and H₂, and in CO₂ and CH₄, respectively.**

Based on their distinct chemical compositions, we conclude that both sections represent individual hydrologic systems. Evidence for mixing is only slight. **The gas concentrations found in the drill mud between 2900 m and 3550 m depths are low, especially for ²²²Rn. Only two sections, at 3150–3200 m and at 3340 m, show some higher gas concentrations. The spike at 3340 m, very close to the active part of SAF (3310 m), is almost exclusively composed of hydrocarbons. We assume that these are trapped in permeable sands embedded in less permeable strata, an interpretation supported by lithological data.**

The air-corrected ³He/⁴He ratios of off-line mud gas samples are lower than the atmospheric ratio, but higher than the mean crustal values of ≤0.1 Ra; therefore, **helium is a mixture of crustal helium with a small portion of mantle-derived helium. Down to a depth of 3051 m, air-corrected ³He/⁴He ratios of >0.45 Ra show that the contribution of mantle-derived helium is small (approx. 5%) on the Pacific plate, which composes the southwestern portion of the SAF. The ³He/⁴He ratios become significantly higher at depths below 3500 m on the North American plate, where ³He/⁴He ratios of 0.9 Ra were found, revealing a mantle contribution of 10%–12% for the total helium budget (Wiersberg and Erzinger, 2007).**

Based on our observations, we conclude that the role of mantle-derived fluids in seismic processes at the SAF is small. The distinct helium isotopic compositions down to 3051 m and below 3500 m depths, with only little evidence for mixing between both hydrologic systems, again demonstrate that the SAF in some way acts as a barrier for fluid migration. **Mantle-derived fluids migrate predominately through permeable country rock and leak to some extent into the SAF.**

References

- Erzinger, J., Wiersberg, T., and Dahms, E., 2004. **Real-time mud gas logging during drilling of the SAFOD pilot hole in Parkfield, CA.** *Geophys. Res. Lett.*, 31:L15S18, doi:10.1029/2003GL019395.
- Wiersberg, T. and Erzinger, J., 2007. A helium isotope cross-section through the San Andreas Fault at seismogenic depth. *Geochem. Geophys. Geosyst.*, 8:Q01002, doi:10.1029/2006GC001388.
- Wiersberg, T., Erzinger, J., Zimmer, M., Schicks, J., and Dahms, E., 2005. **Real-time gas analysis at the Mallik 2002 gas hydrate production research well.** In Dallimore, S.R. and Collett, T.S. (Eds.), *Scientific Results from Mallik 2002 Gas Hydrate Production Research Well Program, Mackenzie Delta, Northwest Territories, Canada.* Geological Survey of Canada, Bulletin 585.
- Zimmer, M., and Erzinger, J., 1995. **On the geochemistry of gases in formation and drilling fluids—results from the KTB.** *Sci. Drill.*, 5:101–110.

Authors

Thomas Wiersberg and Jörg Erzinger, GeoForschungsZentrum Potsdam, Section 4.2, Telegrafenberg B323, 14473, Potsdam, Germany, e-mail: wiers@gfz-potsdam.de.

Low-Velocity Damage Zone on the San Andreas Fault at Depth near SAFOD Site at Parkfield Delineated by Fault-Zone Trapped Waves

by Yong-Gang Li, Peter E. Malin, and John E. Vidal

doi:10.2204/iodp.sd.s01.09.2007

Introduction

We deployed a dense linear array of forty-five seismometers across and along the San Andreas fault (SAF) near the SAFOD site at Parkfield in 2003 to record fault-zone trapped waves generated by near-surface explosions and microearthquakes located within the fault zone. Observations and 3-D finite-difference simulations of the fault-zone trapped waves generated by microearthquakes at different depths show a ~100–200-m-wide low-velocity zone (LVZ) along the SAF reaching to depths of 6–7 km or more, within which shear velocities are reduced by 20%–40% on average from wall-rock velocities, with the maximum velocity reduction of 40%–50% in a 30–40-m-wide fault core zone, indicating the localization of severe damage on the SAF. The damage zone is not symmetric but extends farther on the southwest side of the main fault trace. The width and velocities of this zone delineated by trapped waves are confirmed by the results of the SAFOD drilling and logs that show high porosity and multiple slip planes in a ~200-m-wide LVZ across the SAF with velocity reduction of ~20%–30% at ~3.2 km depth, within which a ~35-m-wide severely damaged zone is seen around the main slip (Hickman et al., 2005). Recently, the downhole seismograph installed in the SAFOD mainhole at ~3 km depth recorded prominent fault-zone guided waves with long-duration dispersive wavetrains after S-arrivals from microearthquakes occurring below (Ellsworth and Malin, 2006). Finite-difference simulations of these waves show a ~30–40-m-wide core zone with velocities as low as 50% of the intact rocks embedded in the wider fault zone with intermediate velocity reduction, indicating that the damage zone on the SAF at Parkfield extends to the depth of at least several kilometers below 3 km.

The Fault Zone Observatory

The spatial extent of fault weakness, and the loss and recouping of strength across the earthquake cycle are critical ingredients in our understanding of fault mechanics. In order to relate present day crustal stresses and fault motions to the geological structures formed in their past earthquake histories, such as the matured San Andreas Fault (SAF), we must understand the evolution of fault systems on many spatial and time scales. Extensive field and laboratory research and numerical simulations indicate that fault zones

undergo high, fluctuating stress and pervasive cracking during an earthquake (Chester et al., 1993). While we know slip is localized on faults because of their lower strength compared to the surrounding bedrock, the magnitude of strength reduction and its spatial extent at seismogenic depth are still not well constrained (Hickman and Evans, 1992).

Near Parkfield, California, many researchers have observed a LVZ surrounding the surface trace the SAF (Roecker et al., 2004; Thurber et al., 2003; Unsworth et al., 1997). This zone is from a few hundred meters to 1 km wide, and has velocity reductions of 10%–30% and V_p/V_s ratios on the order of 2.3. The LVZ is thought to be caused by intense fracturing during earthquakes, brecciation, liquid-saturation, and possibly high pore-fluid pressures near the fault core. Recent results from drilling logs at the Parkfield San Andreas Fault Observatory at Depth (SAFOD) show a LVZ more than one hundred meters wide at ~3 km depth, indicating a severely damage zone associated with the SAF (Hickman et al., 2005). Pore fluids arising from depth appear to hold a complex relationship with this damage zone, with its outer portions appearing to be more permeable than its core (Lockner et al., 2000).

Highly damaged fault rocks along the SAF at Parkfield create a LVZ that can trap seismic waves (Ben-Zion, 1998; Li et al., 1990). Using fault-zone trapped waves generated by explosions and microearthquakes, and recorded at surface seismic arrays at Parkfield, Li et al. (1997, 2004) have delineated a ~150–200-m-wide low-velocity waveguide along the SAF, appearing to extend to seismogenic depths beneath

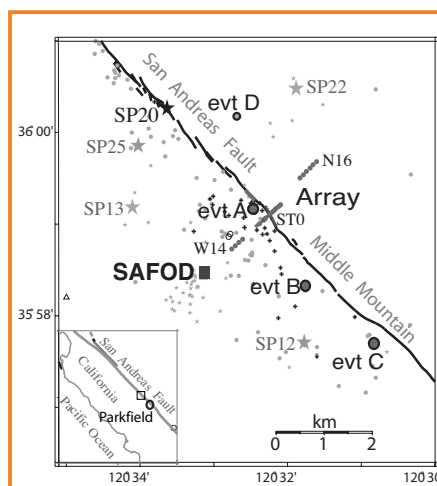


Figure 1. Map shows locations of linear seismic arrays of forty-five PASSCAL RT130s (circles along the line) deployed across and along the San Andreas fault near the SAFOD site (filled square), five explosions (stars) detonated by USGS, small shots (stars), and microearthquakes (dots) recorded at our array in the fall of 2003. Station ST0 in the array was located on the main fault trace. Dots denote thirty-seven earthquakes at different depths showing fault-zone trapped waves used for measurements shown in Fig. 3. Event A is a M2.2 SAFOD target event occurring at ~3 km depth on Julian date R293 in 2003. Events A, C, and D are deeper earthquakes; waveforms from them are shown in Fig. 2.

Middle Mountain, within which the shear-velocities are reduced by 20%–50%. This distinct zone is interpreted as being a damage zone along the SAF that accumulated in the recurrence of ruptures in major earthquakes over geological time.

Recently, prominent fault-zone guided waves have been recorded in the SAFOD mainhole at ~3 km depth, suggesting that a SAF-related low-velocity waveguide extends to deeper levels (Ellsworth and Malin, 2006). In this article, we discuss the fault-zone trapped waves recorded at the linear seismic array deployed across the SAF near the SAFOD site in 2003

and at the seismometers installed in the SAFOD mainhole. The data from local microearthquakes occurring at different depths provide better constraints on the depth extent of the damage structure of the SAF. These results help extend the direct measurements of fault-zone properties in the SAFOD mainhole to a 3-D structural image of the SAF zone.

Data and Results

Coordinated by SAFOD PIs, in the fall of 2003 we deployed a dense linear seismic array of forty-five PASSCAL RT130 seismometers across and along the SAF near the SAFOD

site ~15 km NW of Parkfield to record fault-zone trapped (guided) waves for site characterization before drilling (Fig. 1). We recorded ~100 local earthquakes occurring at depths between 2 km and 12 km and five explosions in the fan-geometry detonated by the USGS researchers. The fault-zone trapped waves (FZTWs) generated by microearthquakes and explosions are used to delineate the rock damage extent and physical properties along the SAF at seismogenic depths.

Figure 2 exhibits seismograms recorded at cross-fault array for three microearthquakes near the SAFOD site, showing prominent FZTWs with large amplitudes and long wavetrains after S-arrivals at stations close to the SAF main trace in a width range of ~150–200 m for events A and C occurring within the fault zone. In contrast, trapped waves are not clear at the same stations for event D occurring ~1 km away from the fault zone, and stations located out of the fault zone register brief body waves for these three events, indicating the existence of a LVZ to form a waveguide along the SAF. It is seen that the LVZ extends farther on the southwest side of the main fault trace on which station ST0 was located. We noted some seismic energy trapped within a branch fault (BF) which may connect to the main fault at depth. The FZTWs partitioned from the main fault to this branch fault have been recorded at the borehole seismograph installed in the SAFOD mainhole (Malin et al., 2006). The FZTWs from event C occurring at ~11 km depth show much longer wavetrains than those from the shallower event A at the 3 km depth,

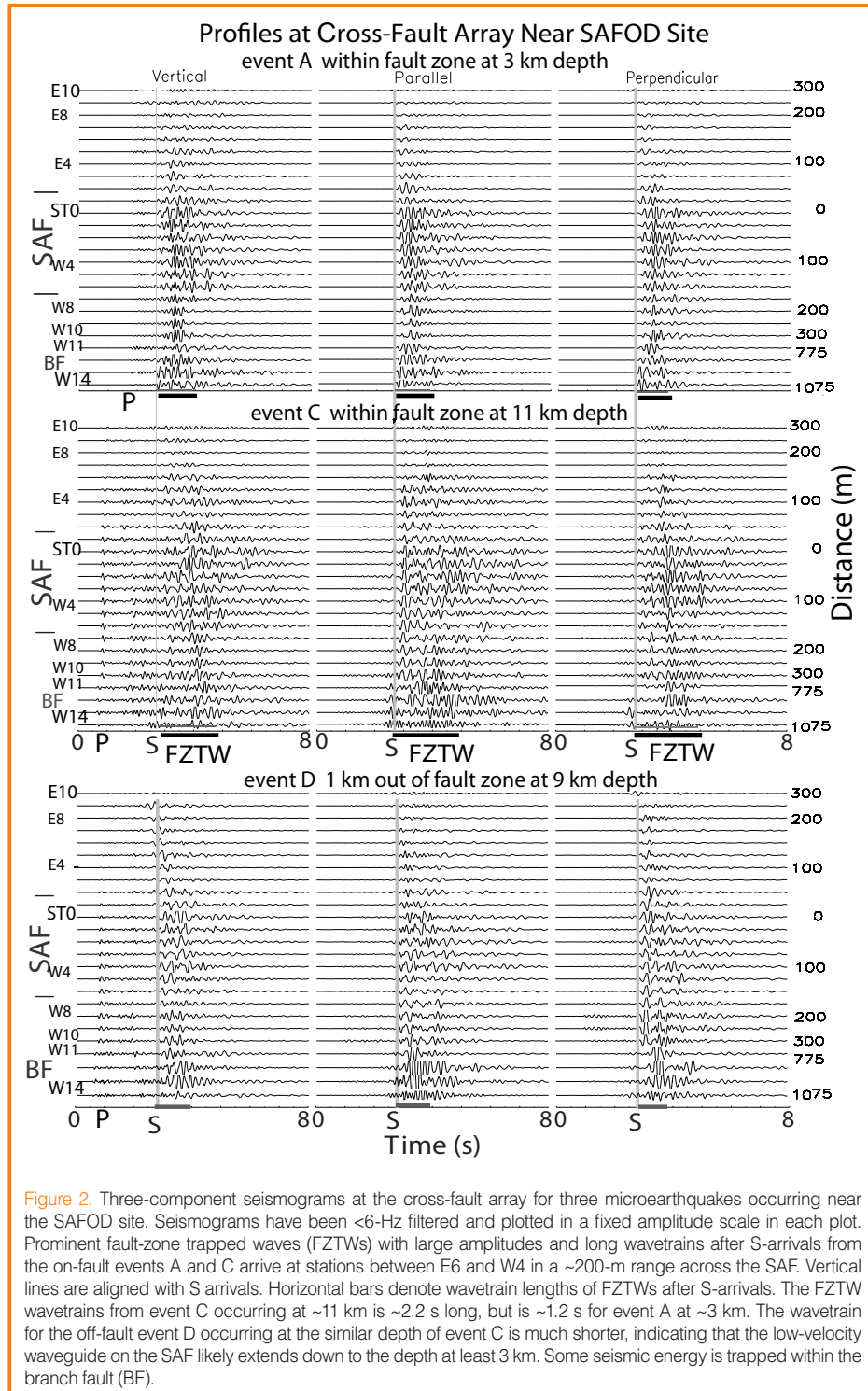


Figure 2. Three-component seismograms at the cross-fault array for three microearthquakes occurring near the SAFOD site. Seismograms have been <6-Hz filtered and plotted in a fixed amplitude scale in each plot. Prominent fault-zone trapped waves (FZTWs) with large amplitudes and long wavetrains after S-arrivals from the on-fault events A and C arrive at stations between E6 and W4 in a ~200-m range across the SAF. Vertical lines are aligned with S arrivals. Horizontal bars denote wavetrain lengths of FZTWs after S-arrivals. The FZTW wavetrains from event C occurring at ~11 km is ~2.2 s long, but is ~1.2 s for event A at ~3 km. The wavetrain for the off-fault event D occurring at the similar depth of event C is much shorter, indicating that the low-velocity waveguide on the SAF likely extends down to the depth at least 3 km. Some seismic energy is trapped within the branch fault (BF).

indicating that the low-velocity waveguide on the SAF likely extends to seismogenic depths deeper than 3 km. In contrast, the same stations registered much shorter wavetrains after S-arrivals for the off-fault event D at ~9 km depth compared to those from the on-fault event C, although these two events occurred at a similar depth and distance from the array. In order to examine the depth extension of the LVZ on the SAF, we used the data from thirty-seven local earthquakes located within the fault zone at different depths with the raypath incidence angles to the array smaller than 30° from vertical (Fig. 3A). Figure 3B shows seismograms and envelopes at station ST0 located on the main fault trace for eleven on-fault events at different depths near the SAFOD site. S-arrivals for these events are aligned at 2 s. The length of fault-zone trapped wavetrains following S-arrivals progressively increases from ~1.2 s to ~2.2 s as the event depths increase from 2.6 km to 11.7 km. In contrast, much shorter wavetrains after S-arrivals with flat changes in length are registered at the same station for eleven other events located away from the fault zone in a similar depth range. Figure 3C shows the measured wavetrain lengths of FZTWs registered at stations within the fault zone for thirty-seven on-fault events and thirteen off-fault events at depths between 2 km and 12 km. The lengths of FZTWs for on-fault events increase from 1.0 s to 2.2 s as the depth increases from ~2 km to ~12 km, but shorter wavetrains with flat depth-dependent changes are measured at the same stations for off-fault events. Stations located out of the fault zone registered much short wavetrains after S-arrivals for all these events. These observations indicate that the low-velocity waveguide formed by the damage zone on the SAF extends across seismogenic depths to at least ~7 km, although the velocity reduction (damage magnitude) within the zone becomes smaller with depth due to the larger confined stress at greater depths.

In the fall of 2005, a borehole seismograph was placed down the SAFOD mainhole at a depth of ~3 km, where the SAFOD drilling and logging records suggest the active SAF is present (Hickman et al., 2005). This downhole seismograph recorded prominent fault-zone guided waves from the deeper events (Ellsworth and Malin, 2006). For example, Figure 4 shows FZTWs with large amplitudes and long dispersive wavetrains generated by an aftershock of the M6 Parkfield earthquake at ~6 km depth within the fault zone, indicating the existence of a continuous low-velocity fault core zone between this event and the borehole seismometer. Thus, the damage zone on the SAF must extend at least several kilometers below the 3 km depth.

Based on our observations of fault-zone trapped waves at the surface array and borehole seismometer in the SAFOD mainhole, we constructed a velocity and *Q* model across the SAF near the SAFOD site (Fig. 5A). The wall-rock velocities are constrained by tomography profiles at Parkfield (Roecker et al., 2004; Thurber et al., 2003). Using a 3-D FD code (Graves, 1996), we simulated FZTWs generated by explosions to determine the shallow 1–2 km fault zone structure,

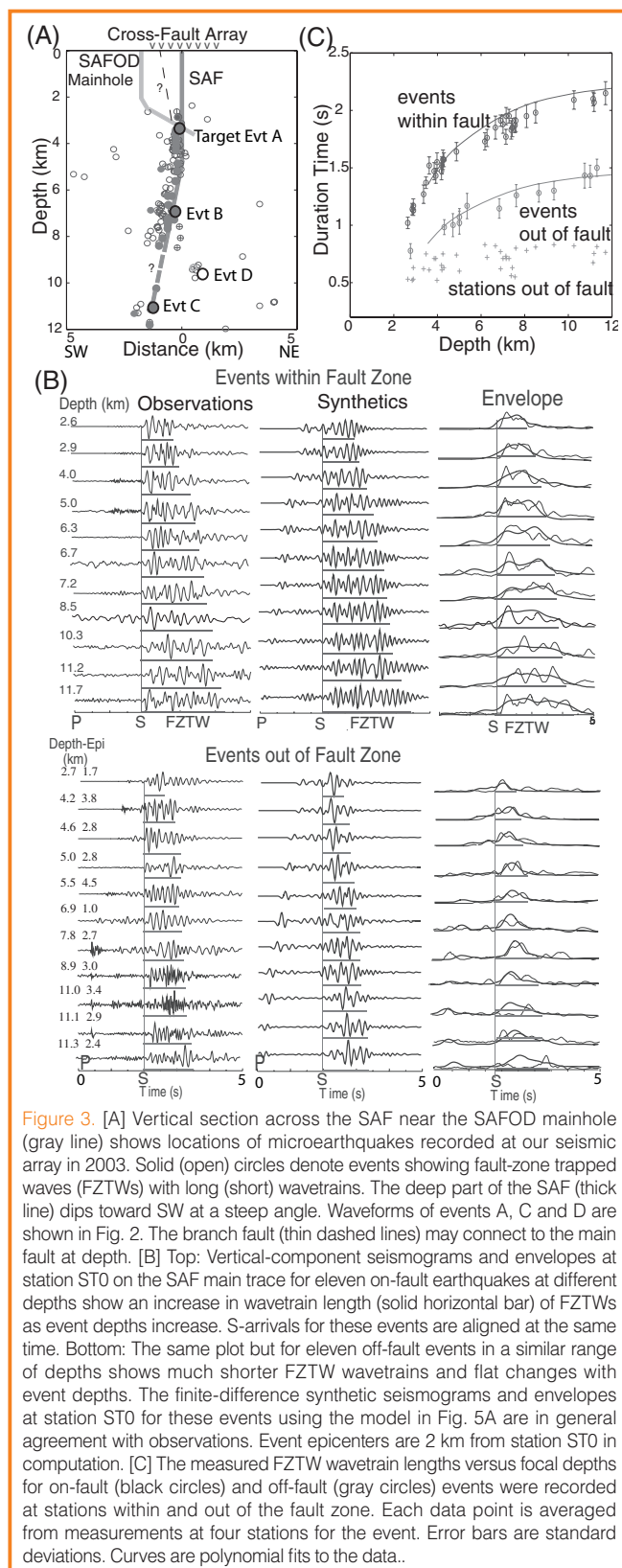


Figure 3. [A] Vertical section across the SAF near the SAFOD mainhole (gray line) shows locations of microearthquakes recorded at our seismic array in 2003. Solid (open) circles denote events showing fault-zone trapped waves (FZTWs) with long (short) wavetrains. The deep part of the SAF (thick line) dips toward SW at a steep angle. Waveforms of events A, C and D are shown in Fig. 2. The branch fault (thin dashed lines) may connect to the main fault at depth. [B] Top: Vertical-component seismograms and envelopes at station ST0 on the SAF main trace for eleven on-fault earthquakes at different depths show an increase in wavetrain length (solid horizontal bar) of FZTWs as event depths increase. S-arrivals for these events are aligned at the same time. Bottom: The same plot but for eleven off-fault events in a similar range of depths shows much shorter FZTW wavetrains and flat changes with event depths. The finite-difference synthetic seismograms and envelopes at station ST0 for these events using the model in Fig. 5A are in general agreement with observations. Event epicenters are 2 km from station ST0 in computation. [C] The measured FZTW wavetrain lengths versus focal depths for on-fault (black circles) and off-fault (gray circles) events were recorded at stations within and out of the fault zone. Each data point is averaged from measurements at four stations for the event. Error bars are standard deviations. Curves are polynomial fits to the data.

seismograms for the SAFOD drilling target event occurring ~3 km near the array site using the model in Fig. 5A. Figure 4C exhibits synthetic seismograms at the SAFOD mainhole seismograph located at 3 km depth within the fault core zone for a deep event at 6 km with the epicenter 3 km SW of the site using the same model. We obtained a good fit of synthetics to observations, suggesting that this model is applicable for

interpretation of the damage structure on the SAF at Parkfield to at least 6 km. Using the fault-zone model in Fig. 5A, we also simulated seismograms at station ST0 on the main fault trace for eleven on-fault earthquakes and eleven off-fault earthquakes at depths between 3.6 km and 11.2 km for comparison with observed seismograms at this station (Fig. 3). The lengths of synthetic FZTW wavetrains increase with the event depth for on-fault events, which generally agrees with observations. On the other hand, the synthetic seismograms for off-fault events showed much shorter wavetrains after S-arrivals and less change in the wavetrain length with depth. These modeling results further indicate that the low-velocity waveguide (damage zone) on the SAF at Parkfield likely extends across the seismogenic depth of at least 6–7 km.

Conclusion

Observations and modeling of fault-zone trapped waves recorded at dense linear seismic arrays across the SAF at the surface and at the downhole seismograph installed in the SAFOD mainhole show the existence of a distinct low-velocity damage zone along the SAF at Parkfield, within which seismic velocities are reduced by 30%–50% from wall-rock velocities. The damage zone likely extends to the depth of at least 6–7 km. This zone is thought to be caused by intense fracturing during earthquakes, brecciation, liquid-saturation, and possibly high pore-fluid pressure nears the fault. The damage zone is asymmetric, broader on the southwest side of the main fault trace. The asymmetry may imply that the fault zone has a significant cumulative damage due to previous large earthquakes on the SAF. When a fault ruptures, it may preferentially damage the already weakened rocks in the zone, even though those rocks are not symmetrically distributed on either side of the main slip plane (Chester et al., 1993). Alternately, greater damage may be inflicted in the extensional quadrant than the compressional quadrant near the propagating crack tip (Andrews, 2005).

Although the structural model for the SAF at Parkfield delineated by FZTWs (Fig. 5A) explains part of the data, it is still a simple one. The true structure in three dimensions may be more complicated. It will be further studied using more data from deep events recorded at surface and downhole seismic arrays to document variations in the extent and magnitude of rock damage along the fault strike and with depth, as well as their relationship with the rupture distribution and stress variations over multiple length and time scales. This study contributes essential information towards further understanding of faulting mechanics and earthquake hazards at matured faults like the San Andreas fault.

Acknowledgments

This study is supported by EarthScope Grant EAR0342277, USGS Grant NEHRP20060160, and the SCEC. Special thanks to S. Hickman, W. Ellsworth, and M. Zoback for their

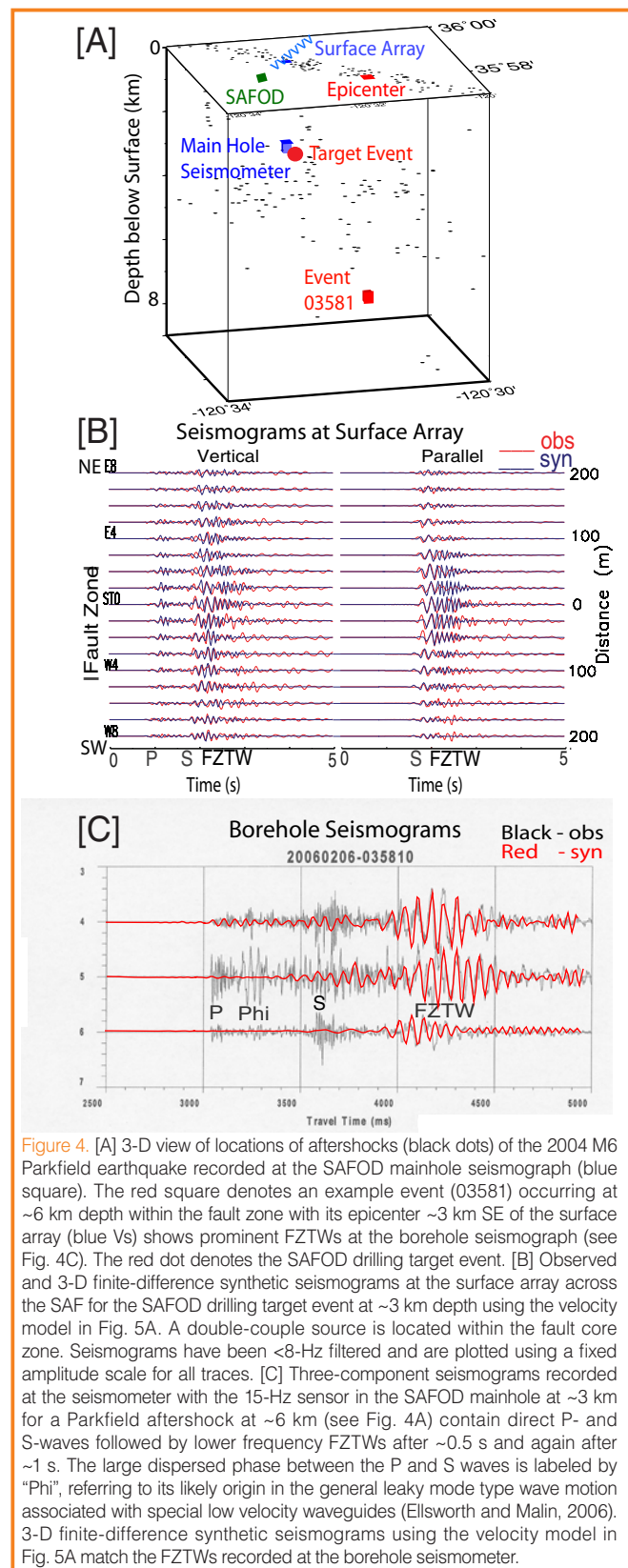


Figure 4. [A] 3-D view of locations of aftershocks (black dots) of the 2004 M6 Parkfield earthquake recorded at the SAFOD mainhole seismograph (blue square). The red square denotes an example event (03581) occurring at ~6 km depth within the fault zone with its epicenter ~3 km SE of the surface array (blue Vs) shows prominent FZTWs at the borehole seismograph (see Fig. 4C). The red dot denotes the SAFOD drilling target event. [B] Observed and 3-D finite-difference synthetic seismograms at the surface array across the SAF for the SAFOD drilling target event at ~3 km depth using the velocity model in Fig. 5A. A double-couple source is located within the fault core zone. Seismograms have been <8-Hz filtered and are plotted using a fixed amplitude scale for all traces. [C] Three-component seismograms recorded at the seismometer with the 15-Hz sensor in the SAFOD mainhole at ~3 km for a Parkfield aftershock at ~6 km (see Fig. 4A) contain direct P- and S-waves followed by lower frequency FZTWs after ~0.5 s and again after ~1 s. The large dispersed phase between the P and S waves is labeled by "Phi", referring to its likely origin in the general leaky mode type wave motion associated with special low velocity waveguides (Ellsworth and Malin, 2006). 3-D finite-difference synthetic seismograms using the velocity model in Fig. 5A match the FZTWs recorded at the borehole seismometer.

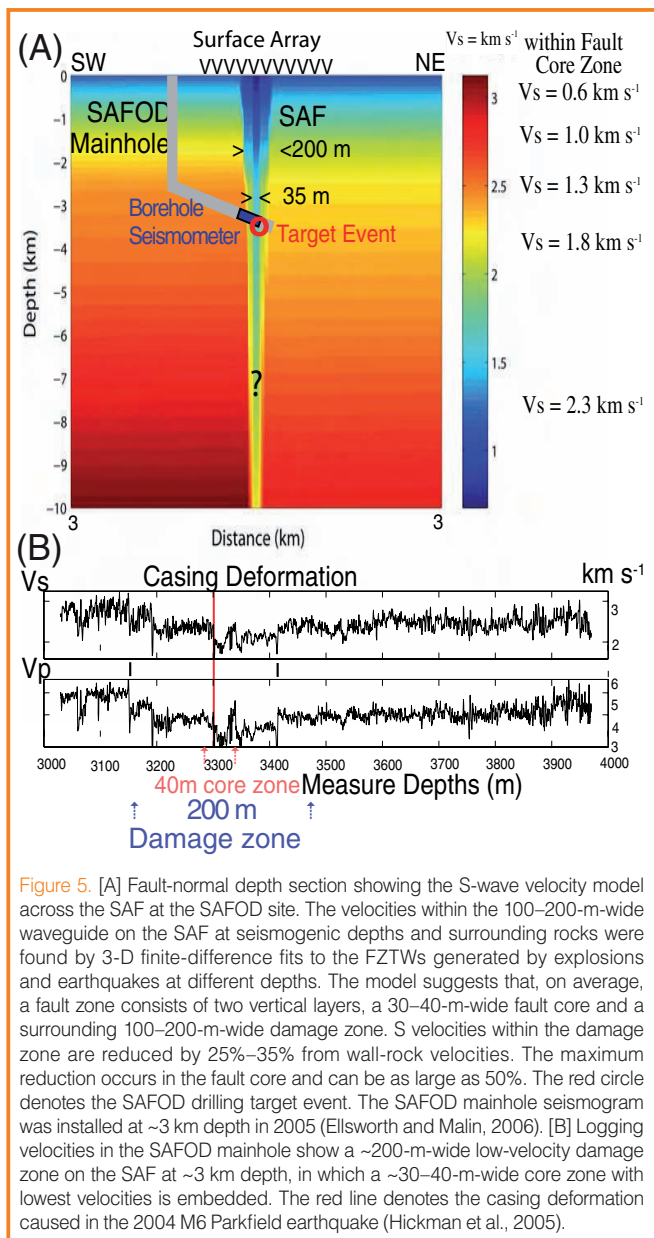


Figure 5. [A] Fault-normal depth section showing the S-wave velocity model across the SAF at the SAFOD site. The velocities within the 100–200-m-wide waveguide on the SAF at seismogenic depths and surrounding rocks were found by 3-D finite-difference fits to the FZTWs generated by explosions and earthquakes at different depths. The model suggests that, on average, a fault zone consists of two vertical layers, a 30–40-m-wide fault core and a surrounding 100–200-m-wide damage zone. S velocities within the damage zone are reduced by 25%–35% from wall-rock velocities. The maximum reduction occurs in the fault core and can be as large as 50%. The red circle denotes the SAFOD drilling target event. The SAFOD mainhole seismogram was installed at ~3 km depth in 2005 (Ellsworth and Malin, 2006). [B] Logging velocities in the SAFOD mainhole show a ~200-m-wide low-velocity damage zone on the SAF at ~3 km depth, in which a ~30–40-m-wide core zone with lowest velocities is embedded. The red line denotes the casing deformation caused in the 2004 M6 Parkfield earthquake (Hickman et al., 2005).

coordination, and E. Cochran, C. Thurber, S. Roecker, M. Rymer, R. Catchings, A. Snyder, L. Powell, B. Nadeau, N. Boness, and D. McPhee for their collaborations in our experiments at Parkfield. The author was supported by the ICDP to attend the ICDP-IODP Fault-Zone Drilling Workshop in Japan in 2006.

References

- Andrews, D.J., 2005. Rupture dynamics with energy loss outside the slip zone. *J. Geophys. Res.*, 110:B01307, doi:0.1029.
- Ben-Zion, Y., 1998. Properties of seismic fault zone waves and their utility for imaging low-velocity structure. *J. Geophys. Res.*, 103:12567–12585.
- Chester, F., Evans, J., and Biegel, R., 1993. Internal structure and weakening mechanisms of the San Andreas fault. *J. Geophys. Res.*, 98:771–786.
- Ellsworth, W.L. and Malin, P.E., 2006. A first observation of fault guided PSV-waves at SAFOD and its implications for fault characteristics. *EOS, Trans. AGU*, 87(52), Abstract T23E-02.

- Hickman, S.H. and Evans, B., 1992. Growth of grain contacts in halite by solution-transfer: Implications for diagenesis, lithification, and strength recovery. In Evans, B., and Wong, T.-F. (Eds.), *Fault Mechanics and Transport Properties of Rocks*, San Diego, Calif., (Academic Press), 253–280.
- Hickman, S.H., Zoback, M.D., and Ellsworth, W.L., 2005. Structure and composition of the San Andreas fault zone at Parkfield: Initial results from SAFOD Phase 1 and 2. *EOS, Trans. AGU*, 83(47):237.
- Li, Y.G., Ellsworth, W., Thurber, C., Malin, P., and Aki, K., 1997. Observations of fault-zone trapped waves excited by explosions at the San Andreas fault California. *Bull. Seism. Soc. Am.* 87:210–221.
- Li, Y.G., Leary, P., Aki, K., and Malin, P., 1990. Seismic trapped modes in Oroville and San Andreas fault zones. *Science*, 249:763–766.
- Li, Y.G., Vidale, J.E., and Cochran, S.E., 2004. Low-velocity damaged structure on the San Andreas fault at Parkfield from fault-zone trapped waves. *Geophys. Res. Lett.* 31:L12S06.
- Lockner, D., Naka, H., Tanaka, H., Ito, H., and Ikeda, R., 2000. Permeability and strength of core samples from the Nojima fault of the 1995 Kobe earthquake. *USGS Open file, Report 00-129*, 147–152.
- Malin, P.M., Shalev, E., Balven, H., and Lewis-Kenedi, C., 2006. Structure of the San Andreas Fault at SAFOD from P-wave tomography and fault-guided wave mapping. *Geophys. Res. Lett.*, 33:L13314, doi: 10.1029/2006GL025973.
- Roecker, S., Thurber, C., and D. McPhee. 2004. Joint inversion of gravity and arrival time data from Parkfield: New constraints on structure and hypocenter locations near the SAFOD drill site. *Geophys. Res. Lett.*, 31:L12S04, doi: 10.1029/2003GL019396.
- Thurber, C., Roecker, S., Roberts, K., Gold, M., Powell, L., and Rittger, K., 2003. Earthquake location and 3-D fault zone structure along the creeping section of the San Andreas fault near Parkfield, CA: Preparing for SAFOD. *Geophys. Res. Lett.* 30:1112–1115.
- Unsworth, M., Malin, P., Egbert, G., and Booker, J., 1997. Internal structure of San Andreas fault at Parkfield, CA. *Geology*, 356–362.

Authors

Yong-Gang Li, Zumberge Hall, Department of Earth Sciences, University of Southern California, 3651 Trousdale Parkway, Los Angeles, Calif. 90089, U.S.A., e-mail: ygli@usc.edu.

Peter E. Malin, Division of Earth and Ocean Sciences, 109A Old Chemistry Box 90227, Duke University, Durham, N.C., 27708, U.S.A.

John E. Vidale, Department of Earth and Space Sciences, University of California, 595 Charles Young Drive East, Box 951567, Los Angeles, Calif., 90095-1567, U.S.A.

High-resolution Imaging of Fault Zone Structures with Seismic Fault Zone Waves

by Yehuda Ben-Zion, Zhigang Peng, Michael Lewis, and Jeff McGuire

doi:10.2204/iodp.sd.s01.23.2007

Large fault zone (FZ) structures with damaged rocks and material discontinuity interfaces can generate several indicative wave propagation signals. High crack density may produce prominent scattering and non-linear effects. A preferred prominent orientation can lead to shear wave splitting. A lithology contrast can produce FZ head waves that propagate along the material interface with the velocity and motion polarity of the faster medium. A coherent low velocity layer may generate FZ trapped waves. These signals can be used to obtain high-resolution imaging of the subsurface structure of fault zones, and to track possible temporal evolution of FZ material properties. Several results have emerged from recent systematic analyses of such signals. The trapped waves are generated typically by ~100-m-wide layers that extend only to ~3–4 km depth and are characterized by 30%–50% velocity reduction and strong attenuation (Ben-Zion et al., 2003; Lewis et al., 2005; Peng et al., 2003). The trapping structures appear to be surrounded by broader anisotropic and scattering zones limited primarily to the shallow crust (Fig. 1). Results associated with

anisotropy and scattering around the North Anatolian fault using repeating earthquake clusters do not show precursory temporal evolution (Peng and Ben-Zion, 2004, 2005, 2006). The anisotropy results show small co-seismic changes, while the scattering results show larger co-seismic changes and post-seismic logarithmic recovery. The temporal changes probably reflect damage evolution in the top few hundred meters of the crust. **Systematic analyses of head waves along** several sections of the San Andreas fault reveal material interfaces that extend to the bottom of the seismogenic zone (Ben-Zion and Malin, 1991; McGuire and Ben-Zion, 2005). Joint arrival time inversions of direct and FZ head waves and waveform modeling imply (Fig. 2) velocity contrasts of 20% or more in the top 3 km and lower contrasts of 5%–15% in the deeper section (Ben-Zion et al., 1992; Lewis et al., 2007). In several places, analyses of trapped and head waves indicate that the shallow damaged layers are asymmetric across the fault (Lewis et al., 2005, 2007). The observed damage asymmetry may reflect preferred propagation direction of earthquake ruptures (Ben-Zion and Shi, 2005).

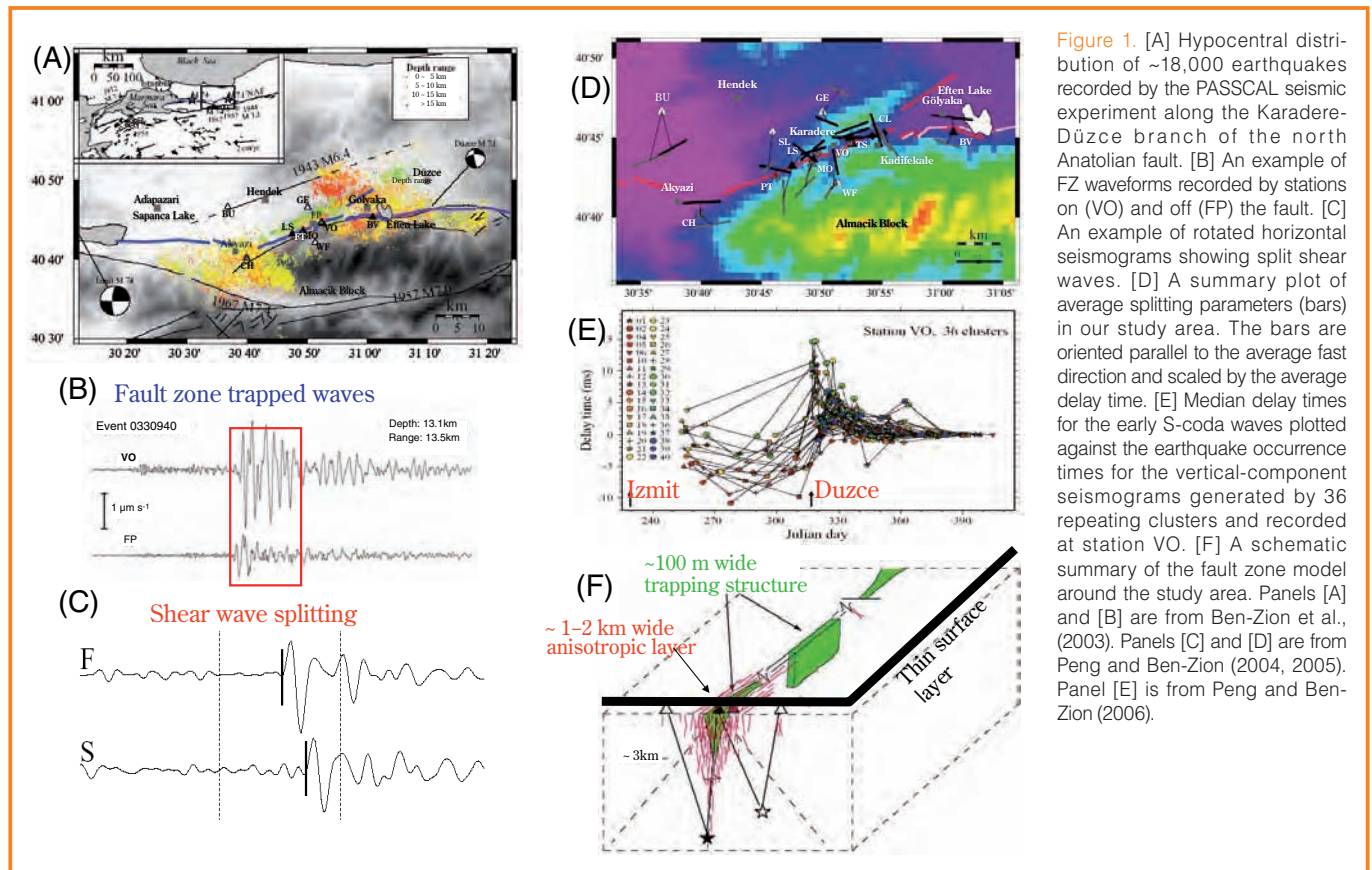


Figure 1. [A] Hypocentral distribution of ~18,000 earthquakes recorded by the PASSCAL seismic experiment along the Karadere-Düzce branch of the north Anatolian fault. [B] An example of FZ waveforms recorded by stations on (VO) and off (FP) the fault. [C] An example of rotated horizontal seismicograms showing split shear waves. [D] A summary plot of average splitting parameters (bars) in our study area. The bars are oriented parallel to the average fast direction and scaled by the average delay time. [E] Median delay times for the early S-coda waves plotted against the earthquake occurrence times for the vertical-component seismicograms generated by 36 repeating clusters and recorded at station VO. [F] A schematic summary of the fault zone model around the study area. Panels [A] and [B] are from Ben-Zion et al., (2003). Panels [C] and [D] are from Peng and Ben-Zion (2004, 2005). Panel [E] is from Peng and Ben-Zion (2006).

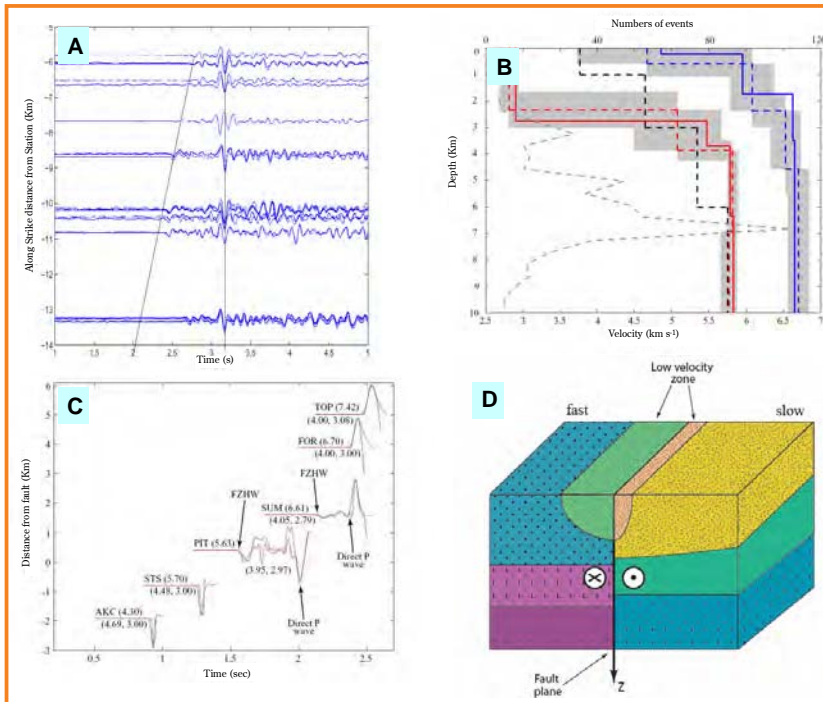


Figure 2. [A] Vertical component P waveforms at Northern California Seismic Network (NCSN) station BHR northeast of the San Andreas Fault (SAF) south of Hollister with direct body wave (vertical line) and first arriving fault zone head wave (diagonal line). [B] Inversion results of P wave velocity contrast across the SAF versus depth from arrival times of head and direct waves. The solid red and blue lines are the best-fitting velocity profiles for the slow and fast sides of the fault, respectively, out of 10 inversion runs. The dashed red and blue lines are the average depth and velocity of each layer, respectively, from the 10 inversions, and the grey shaded areas around the means represent the standard deviation of the depth and velocity of that layer. The dashed black line is the initial velocity and depth model used in the inversion. The dashed gray line (top horizontal axis) gives the number of events as a function of depth. [C] Example of synthetic waveform fits (red) for observed seismograms (blue) for stations on the fast and slow sides of the SAF. Some of the direct P and head wave arrivals are indicated by arrows with corresponding labels. The average P wave velocities in km s^{-1} of the crustal block used to generate the synthetic seismograms are given in parentheses under the waveforms. [D] A schematic diagram of the inferred velocity structure of the SAF south of Hollister, consisting of two layered quarter-spaces, joined along a sharp material interface, and a shallow asymmetric low velocity zone around the fault. Panel [A] is from McGuire and Ben-Zion (2005). Panels [B]-[D] are from Lewis et al., (2007).

Acknowledgments

The discussed studies were supported by the NSF, USGS and SCEC.

References

- Ben-Zion, Y. and Malin, P., 1991. San Andreas fault zone head waves near Parkfield, California. *Science*, 251:1592–1594, doi:10.1126/science.251.5001.1592.
- Ben-Zion, Y. and Shi, Z., 2005. Dynamic rupture on a material interface with spontaneous generation of plastic strain in the bulk. *Earth Planet. Sci. Lett.*, 236:486–496, doi: 10.1016/j.epsl.2005.03.025.
- Ben-Zion, Y., Katz, S., and Leary, P., 1992. Joint inversion of fault zone head waves and direct P arrivals for crustal structure near major faults. *J. Geophys. Res.*, 97:1943–1951.
- Ben-Zion, Y., Peng, Z., Okaya, D., Seeber, L., Armbruster, L.G., Ozer, N., Michael, A.J., Baris, S., and Aktar, M., 2003. A shallow fault zone structure illuminated by trapped waves in the Karadere-Duzce branch of the North Anatolian Fault, western Turkey. *Geophys. J. Int.*, 152:699–717, doi:10.1046/j.1365-246X.2003.01870.x.
- Lewis, M.A., Ben-Zion, Y., and McGuire, J., 2007. Imaging the deep structure of the San Andreas Fault south of Hollister with joint analysis of fault-zone head and direct P arrivals. *Geophys. J. Int.*, 169, 1028–1042, doi:10.1111/j.1365-246X.2006.03319.x.
- Lewis, M.A., Peng, Z., Ben-Zion, Y., and Vernon, F., 2005. Shallow seismic trapping structure in the San Jacinto fault zone. *Geophys. J. Int.*, 162:867–881, doi:10.1111/j.1365-246X.2005.02684.x.
- McGuire, J. and Ben-Zion, Y., 2005. High-resolution imaging of the Bear Valley section of the San Andreas Fault at seismogenic depths with fault-zone head waves and relocated seismicity. *Geophys. J. Int.*, 163:152–164, doi:10.1111/j.1365-246X.2005.02703.x.
- Peng, Z. and Ben-Zion, Y., 2004. Systematic analysis of crustal anisotropy along the Karadere-Düzce branch of the north Anatolian fault. *Geophys. J. Int.*, 159:253–274, doi:10.1111/j.1365-246X.2004.02379.x.
- Peng, Z. and Ben-Zion, Y., 2005. Spatio-temporal variations of crustal anisotropy from similar events in aftershocks of the 1999 M7.4 İzmit and M7.1 Düzce, Turkey, earthquake sequences. *Geophys. J. Int.*, 160(3):1027–1043, doi:10.1111/j.1365-246X.2005.02569.x.
- Peng, Z. and Ben-Zion, Y., 2006. Temporal changes of shallow seismic velocity around the Karadere-Duzce branch of the north Anatolian fault and strong ground motion. *Pure Appl. Geophys.*, 163:567–600, doi:10.1007/s00024-005-0034-6.
- Peng, Z., Ben-Zion, Y., Michael, A.J., and Zhu, L., 2003. Quantitative analysis of seismic trapped waves in the rupture zone of the 1992 Landers, California earthquake: Evidence for a shallow trapping structure. *Geophys. J. Int.*, 155:1021–1041, doi:10.1111/j.1365-246X.2003.02109.x.

Authors

Yehuda Ben-Zion, Department of Earth Science, University of Southern California, Los Angeles, 90089, Calif., U.S.A., e-mail: benzion@usc.edu.

Zhigang Peng, School of Earth and Atmospheric Sciences, Georgia Institute of Technology, Atlanta, Ga., 30332-0340, U.S.A.

Michael Lewis, Department of Earth Science, University of Southern California, Los Angeles, 90089, Calif., U.S.A.

Jeff McGuire, Department of Geology and Geophysics, Woods Hole Oceanographic Institution, Woods Hole, Mass., 02543, U.S.A.

Modern and Ancient Out-of-Sequence Thrust in the Nankai Trough: Insight from Laboratory-Derived Properties and Seismic Data

by Takeshi Tsuji, Hidekazu Tokuyama, Gaku Kimura, and Shinya Okamoto

doi:10.2204/iodp.sd.s01.15.2007

Introduction

At convergent plate margins, characteristics of out-of-sequence thrusts (OOSTs) are important for understanding the nature of earthquake mechanisms and deformation of the accretionary prism. To understand the characteristics of OOSTs, Integrated Ocean Drilling Program (IODP) plans to drill through the seismogenic OOST in the Nankai Trough. In this phase, however, the seismogenic OOST is too deep to penetrate, so its properties have only been estimated from seismic data. Seismic reflection data from the Nankai Trough off the Kii Peninsula in southwest Japan (Figs. 1 and 2) image a strong negative polarity OOST (or splay fault) reflection branching from the major plate boundary fault (Park et al., 2002; Tsuru et al., 2005). This OOST might have ruptured during the 1944 Tonankai earthquake and associated tsunami (Tanioka and Satake, 2001). The negative polarity reflection of the OOST has been interpreted to indicate elevated fluid pressure in the fault zone (Park et al., 2002). From seismic data alone, the reflection polarity is highly useful information for estimating fault zone properties. However, polarity of deep seismic reflections is also affected by acoustic dispersion, and the fracture zone causes wavelet tuning (Costain and Coruh, 2004). Therefore, full characterization of OOST solely using reflection polarity is not possible. To investigate characteristics of a seismogenic OOST, we determined acoustic properties of discrete samples obtained from the fossil OOST outcrop in Nobeoka, and compared them with those of an active Kumano OOST imaged on seismic profile off the Kii peninsula. Because the Nobeoka OOST is interpreted as a fossil OOST, preserves *in situ* structure, and crops out (Kondo et al., 2005), it is ideal for evaluating characteristics of a seismogenic OOST.

Results and Discussions

P-wave and S-wave velocities of discrete (minicore-shaped) samples

were measured in dry conditions because in saturated conditions fluid dispersion masks pressure effects (Tsuji et al., 2006). We observed anisotropy of velocity in the hanging wall of the Nobeoka OOST attributed to foliation of polytic phyllite (Fig. 3). Foliation-normal P-wave velocities in the hanging wall are $\sim 700 \text{ m s}^{-1}$ slower than the foliation-parallel velocities. In contrast, the footwall is composed of brittle, deformed, chaotic shales and fine sandstones, and velocities in the footwall are lower than those in the hanging wall. Furthermore, velocities increase just above the fault core (gray zones in Fig. 3), where velocity anisotropy at atmospheric pressure is weak and velocity increase with pressure is less apparent. These characteristics may be caused by the filling of most cracks with quartz, which is observed just above the fault core in the Nobeoka OOST. The shear-related dewatering and consolidation may also affect elastic moduli just above the fault core.

Comparison of the acoustic properties of the fossil Nobeoka OOST (determined from outcrop samples) and the active Kumano OOST (calculated from seismic reflection

data) is warranted by the two thrusts' similar tectonic settings and lithologies. Weathering has affected properties of the Nobeoka OOST, but overall results from the hanging wall and the footwall should reflect trends of *in situ* properties. Furthermore, for the comparison of the fossil Nobeoka and active Kumano OOSTs, we calculated water-saturated P-wave velocities from velocities determined under dry conditions via Gassmann's relation. If we assume an average bulk density of 2.5 g cm^{-3} , a seafloor depth of 2 km, an OOST depth of 7 km, and hydrostatic conditions, effective pressure in the Kumano OOST is calculated to be $\sim 73 \text{ MPa}$. Assuming that velocities at 55 MPa represent those at *in situ* effective pressures, the contrast between foliation-normal P-wave velocities in hanging wall samples and footwall samples is $>600 \text{ m s}^{-1}$. The change in P-wave velocities across the fault core of the Nobeoka OOST ($<600 \text{ m s}^{-1}$) is larger

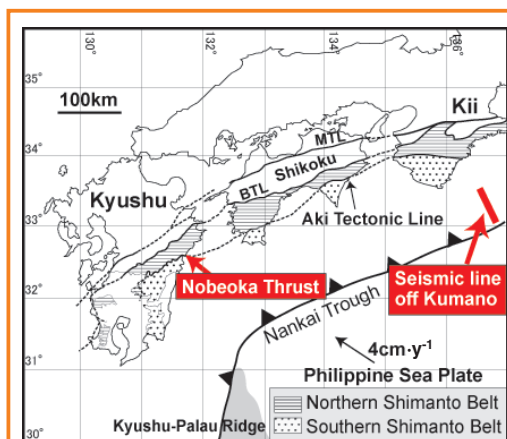


Figure 1. Locations of the Nobeoka OOST and the seismic line off Kumano.

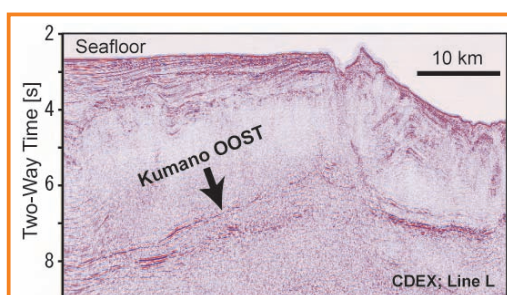


Figure 2. Out-of-sequence thrust on seismic reflection profile off Kumano. This profile crosses the planned IODP site.

than that estimated from the reflection amplitude of the Kumano OOST (Tsuru et al., 2005). Therefore, Kumano OOST reflection amplitudes can be explained only by the difference in matrix elastic moduli of the Nobeoka OOST.

To compare Poisson's ratios of the Nobeoka and the active Kumano OOSTs, we modeled amplitude variation with offset (AVO) using the average P-wave and S-wave velocities of Nobeoka samples at 55 MPa and saturated conditions. The angle-dependent reflection coefficient (thick line in Fig. 4), obtained by the Zoeppritz equation compared to that of the active Kumano OOST obtained by a two-ship, long-offset survey (dots in Fig. 4; Tsuru et al., 2005), shows a far offset reflection coefficient lower than that of the active Kumano OOST. If Poisson's ratios in the footwall are higher ($\sigma \sim 0.25$) than those of the Nobeoka OOST, the AVO response of the Nobeoka OOST coincides well with that of the active Kumano OOST. Because Poisson's ratio becomes higher with increasing pore fluid pressure (Dvorkin et al., 1999), high fluid pressure in the footwall likely explains the AVO response of the active Kumano OOST.

Acknowledgements

When we measured velocities of the outcrop discrete samples, F. Kono, T. Saeki, and H. Mochinaga (JOGMEC) provided devices to measure the velocities. Furthermore, we thank J. Ashi (ORI, Univ. Tokyo), G. Moore (CDEX, JAMSTEC), C. Moore (University of California, Santa Cruz), T. Tsuru (Cosmo Oil), and M. Coffin (ORI, University of Tokyo) for valuable discussions. Seismic reflection data (Fig. 2) are courtesy of CDEX, JAMSTEC.

References

Costain, J.K. and Çoruh, C., 2004. Basic theory of exploration seismology with Mathematica notebooks and examples on CD-ROM. *Handbook of Geophysical Exploration*,

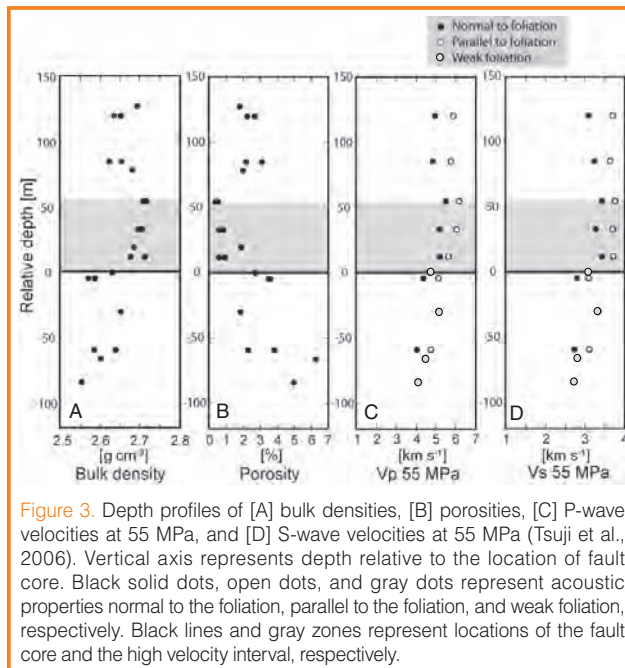


Figure 3. Depth profiles of [A] bulk densities, [B] porosities, [C] P-wave velocities at 55 MPa, and [D] S-wave velocities at 55 MPa (Tsuji et al., 2006). Vertical axis represents depth relative to the location of fault core. Black solid dots, open dots, and gray dots represent acoustic properties normal to the foliation, parallel to the foliation, and weak foliation, respectively. Black lines and gray zones represent locations of the fault core and the high velocity interval, respectively.

the Nankai subduction zone. *Science*, 297:1157–1160, doi:10.1126/science.1074111.

Tanioka, Y. and Satake, K., 2001. Detailed coseismic slip distribution of the 1944 Tonankai earthquake estimated from tsunami waveforms. *Geophys. Res. Lett.*, 28:1075–1078, doi:10.1029/2000GL012284.

Tsuji, T., Kimura, G., Okamoto, S., Kono, F., Mochinaga, H., Saeki, T., and Tokuyama, H., 2006. Modern and ancient seismogenic out-of-sequence thrusts in the Nankai accretionary prism: Comparison of laboratory-derived physical properties and seismic reflection data. *Geophys. Res. Lett.*, 33:L18309, doi:10.1029/2006GL027025.

Tsuru, T., Miura, S., Park, J.-O., Ito, A., Fujie, G., Kaneda, Y., No, T., Katayama, T., and Kasahara, J., 2005. Variation of physical properties beneath a fault observed by a two-ship seismic survey off southwest Japan. *J. Geophys. Res.*, 110:B05405, doi: 10.1029/2004JB003036.

Seismic Exploration, Volume 1, Amsterdam (Elsevier).

Dvorkin, J., Mavko, G., and Nur, A., 1999. Overpressure detection from compressional- and shear-wave data. *Geophys. Res. Lett.*, 26:3417–3420, doi:10.1029/1999GL008382.

Kondo, H., Kimura, G., Masago, H., Ohmori-Ikehara, K., Kitamura, Y., Ikesawa, E., Sakaguchi, A., Yamaguchi, A., and Okamoto, S., 2005. Deformation and fluid flow of a major out-of-sequence thrust located at seismogenic depth in an accretionary complex: Nobeoka Thrust in the Shimanto Belt, Kyusyu, Japan. *Tectonics*, 24:TC6008, doi: 10.1029/2004TC001655.

Park, J.-O., Tsuru, T., Kodaira, S., Cummins, P.R., and Kaneda, Y., 2002. Splay fault branching along

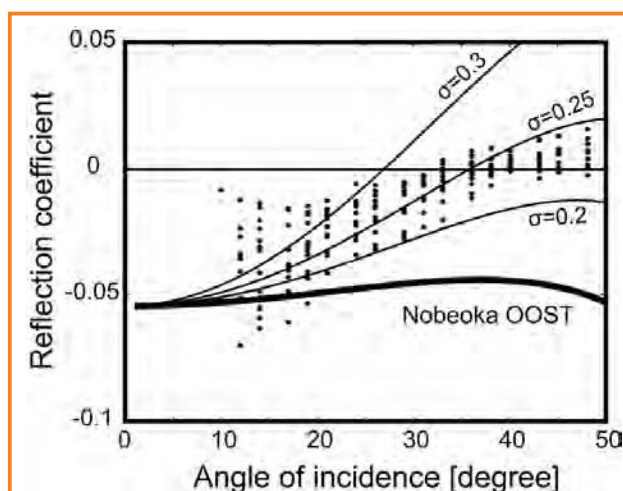


Figure 4. Comparison of angle-dependent reflection coefficients of discrete Nobeoka OOST samples (thick line) (Tsuji et al., 2006); the active Kumano OOST from seismic reflection data (solid dots) (Zone B in Tsuru et al., 2005). Thin lines represent reflection coefficients parameterized by Poisson's ratio. Poisson's ratios in the footwall of the Nobeoka OOST are lower than that of the active Kumano OOST, suggesting high fluid pressures in the footwall of the active Kumano OOST.

Authors

Takeshi Tsuji, Ocean Research Institute, The University of Tokyo, 1-15-1 Minamidai, Nakano-ku, Tokyo 164-8639, Japan, e-mail: tsuji@ori.u-tokyo.ac.jp.

Hidekazu Tokuyama, Ocean Research Institute, The University of Tokyo, 1-15-1 Minamidai, Nakano-ku, Tokyo 164-8639, Japan.

Gaku Kimura, Shinya Okamoto Department of Earth and Planetary Sciences, The University of Tokyo, Hongou 7-3-1, Bunkyo-ku, Tokyo, 113-0033, Japan.

Comparison between Three Out-of-Sequence Thrusts from Japan and Alaska: Implications for Nankai Drilling Targets from the Rock Record

by Christie D. Rowe

doi:10.2204/iodp.sd.s01.31.2007

Increasing recognition has been given to the importance of thrust faults of the “out-of-sequence” geometry as part of the seismogenic plate boundary at subduction zones. The “Good Friday Earthquake” (Prince William Sound, Alaska, 1964) produced a significant tsunami and substantial uplift of a few islands inboard of the trench. Plafker (1972) suggested this could be explained if the rupture propagated up the subduction plate boundary and reached the seafloor by slip on a higher angle splay fault, or out-of-sequence thrust (OOST). Similar tsunami generation mechanisms have been suggested for the December 2004 Sumatra earthquake and tsunami for the area directly offshore Banda Aceh (Simon Day and Steven Ward, personal communications). A large-scale OOST is a primary drilling target of the planned Nankai riser drilling project (Kimura et al., 2003).

The Nobeoka Thrust in the Shimanto Complex (Kyushu Island, Japan), very well described by Kondo et al. (2005) and Okamoto et al. (2006), is an excellent locality to study OOSTs. The Nobeoka Thrust juxtaposes two belts of the Shimanto Complex-accreted rocks with a substantial thermal gap (~70°C), suggesting total throw is 8.6–14.4 km (Kondo et al., 2005). The hanging wall and footwall are comprised of marine sedimentary rocks of Eocene age. Metamorphism of the hanging wall includes ductile deformation of quartz overprinting earlier brittle structures. The footwall contains only evidence of brittle deformation, further emphasizing the thermal gap. The hanging wall damage zone is thin, crowned by a pseudotachylite-bearing fault surface only a few meters above the main contact. The fault core is comprised of about 10–20 cm of dense, subtly foliated cataclasite (A. Yamaguchi, personal communication).

The Uganik Thrust of the Kodiak Accretionary Complex (Afognak Island, Alaska) exhibits remarkable similarity to the Nobeoka Thrust. The thermal gap is approximately 30°C–50°C (C. Rowe, J. Hower, and O. Beyssac; unpublished data). The hanging wall is early- to mid-Cretaceous Uyak Complex, comprised of a greenstone-argillite-chert mélange with rare ductile overprinting of brittle structures (Byrne, 1985). The footwall (Kodiak Formation) is black slate and sandstone with a strong characteristic planar flaggy cleavage which is overprinted by tight folding and cleavage-parallel shear fabrics formed during subduction (Sample, 1986). The hanging wall exhibits a highly deformed, stretched, folded damage zone within 1–2 m of the fault. Mechanisms of deformation include both ductile and granular flow. The fault core

is extremely narrow, about 0.5 m of intensely veined S/C cataclasites. The footwall contains several densely veined subsidiary shear zones 0.5–2 m wide which have experienced many more episodes of brittle deformation than the surrounding footwall rocks. The concentration of quartz veins is elevated to 10–50 percent above background in these zones. These subsidiary shear zones persist for approximately 85 m below the Uganik Thrust, decreasing in size and frequency with distance from the thrust surface.

The Isthmus Bay Fault is a small offset (tens to hundreds of meters) thrust fault within the Ghost Rocks Formation (a mélange complex) of Kodiak Island, Alaska. Although the hanging wall and footwall of the fault are indistinguishable in the conditions of maximum burial—225°C–250°C; 280–320 MPa (Vrolijk et al., 1988)—the fault-filling veins formed at significantly shallower conditions (140°C; C. Rowe, unpublished data), suggesting that fault activation followed a period of exhumation. The hanging wall massive sandstone is cut by steeply dipping quartz and calcite veins, possibly related to rupture of the thrust. The footwall is comprised of stratally disrupted turbidites, which are cut by the thrust at a high angle to the fabric. The footwall damage zone is identifiable by a dense network of quartz and calcite veins, and occasional small volumes of vein-supported hydraulic breccias. This zone was observed about 15 m structurally below the fault. The fault core is a thick (8–13 cm) multiply cemented breccia; sandstone breccia is cemented by calcite, which was re-brecciated and cemented by quartz. This fault core suggests strong coupling between brittle deformation and substantial fluid flow in faults of the shallow portion of the accretionary prism.

All three OOSTs display extreme asymmetry, with the footwall damage zones two orders of magnitude thicker than the hanging wall damage zones. Evidence of substantial hydrofracture and veining are pervasive in the footwall damage zone and nearly absent from the hanging wall damage zone. This is true when the hanging wall is measurably higher metamorphic grade (Nobeoka Thrust and Uganik Thrust) and when the hanging wall and footwall are of the same grade (Isthmus Bay Thrust). In the case of the deeper, greater offset OOSTs (Nobeoka and Uganik), the fault core itself is dense cataclasite and unlikely to act as a conduit to up-dip fluid flow. However, the shallower OOST (Isthmus Bay) contains a fault core dominated by veins and hydrofracture brecciation. Therefore, it is possible that at

shallower structural levels, the fault core itself may be the primary conduit for up-dip fluid advection.

When OOSTs are seismically imaged, a strong negative polarity reflector is usually used to identify the fault. This is most likely caused by the presence of aqueous fluids in or near the fault. In the case of these three ancient OOSTs, the most likely structural reservoir for fluids is the highly fractured and veined footwall damage zone. This imaged area is structurally below the actual fault core and below the measured thermal gap where most offset must necessarily occur. As a drilling target, it is important to search for the core of seismogenic OOST structurally above the imaged fault.

References

- Byrne, T., 1985. The Uyak Complex: A brittle-ductile shear zone. *GSA Abstracts with Programs*, 19(6):440.
- Kimura, G., Tobin, H., and Group, N.W., 2003. *NanTroSEIZE: The Nankai Trough Seismogenic Zone Experiment Complex Drilling Project*. Socorro, NM (New Mexico Tech), 33.
- Kondo, H., Kimura, G., Masago, H., Ohmori-Ikehara, K., Kitamura, Y., Ikesawa, E., Sakaguchi, A., and Okamoto, S., 2005. Deformation and fluid flow of a major out-of-sequence thrust located at seismogenic depth in an accretionary complex: Nobeoka Thrust in the Shimanto Belt, Kyushu, Japan. *Tectonics*, 24(6):TC6008, doi:10.1029/2004TC001655.
- Okamoto, S., Kimura, G., Takizawa, S., and Yamaguchi, H., 2006. Earthquake fault rock indicating a coupled lubrication mechanism. *e-Earth*, 1:23–28.
- Plafker, G., 1972. Alaskan earthquake of 1964 and the Chilean earthquake of 1960: Implications for arc tectonics. *J. Geophys. Res.*, 77:901–925.
- Sample, J.C., 1986. *Structure, Tectonics, and Sedimentology of the Kodiak Formation, Kodiak and Adjacent Islands, Alaska*. University of California - Santa Cruz, Calif. (University of California - Santa Cruz), 156 pp.
- Vrolijk, P., Myers, G., and Moore, J.C., 1988. Warm fluid migration along tectonic melanges in the Kodiak accretionary complex, Alaska. *J. Geophys. Res.*, 93:10313–10324.

Author

Christie D. Rowe, Earth & Planetary Science, University of California, Santa Cruz, 1156 High Street, Santa Cruz, Calif. 95064, U.S.A., e-mail: crowe@pmc.ucsc.edu.

Seismology inside the Fault Zone: Applications to Fault-Zone Properties and Rupture Dynamics

by William L. Ellsworth, Peter E. Malin, Kazutoshi Imanishi, Steven W. Roecker, Robert Nadeau, Volker Oye, Clifford H. Thurber, Felix Waldhauser, Namoi L. Boness, Stephen H. Hickman, and Mark D. Zoback

doi:10.2204/iodp.sd.s01.04.2007

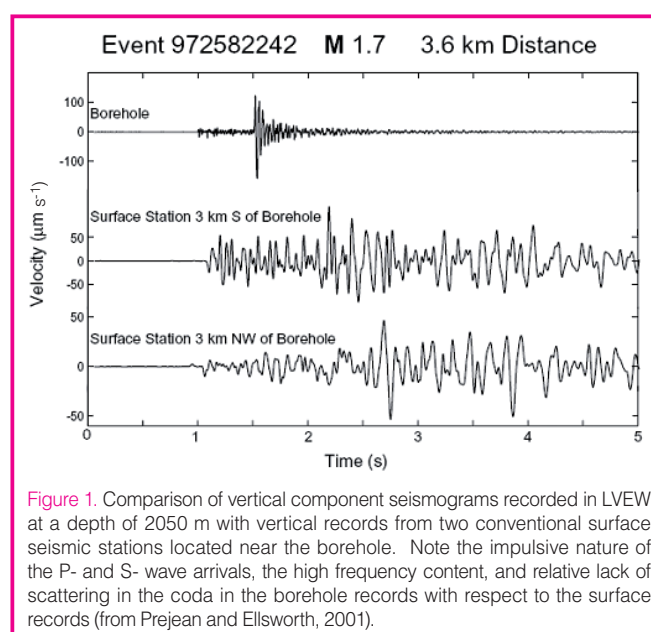
A central goal of seismology is to understand the physics of earthquakes and other sources of seismic waves in the Earth. We would like to understand how dynamic instabilities are nucleated, how they evolve in space and time, and how they come to rest. To achieve this goal, we need observations that are truly broadband with respect to source process time scales. Because the high-frequency limit of a seismogram directly controls the spatial scale at which we can resolve these processes, the requirement for “broadband” means bandwidth that is sufficient to record the shortest pulse produced by the physical system (a delta function being the ultimate broadband signal). Although there is considerable uncertainty at present about the upper frequency limit needed to capture dynamic processes, it is clearly well above the frequency range of standard seismological instrumentation (typically 30–40 Hz for 100 sample-per-second data). Even when instruments are capable of observing frequencies above 1 KHz, they must be sited close enough to the source to overcome the attenuation of the high frequency waves due to scattering and anelastic loss during propagation from the source. The natural solution to this problem is to emplace the instrumentation within the near-field of the source in boreholes and deep mines. This paper presents a review of some recent results from three deep (>2 km) boreholes in California. The three boreholes considered are the Long Valley Exploratory Well, the San Andreas Fault Observatory at Depth (SAFOD) Pilot Hole, and the SAFOD Main Hole.

The Long Valley Exploratory Well (LVEW) is a 3.0-km-deep research drill hole located near the center of Long Valley caldera in eastern California. The well was drilled in a series of stages beginning in 1989, and completed to a total depth of 2996 m in 1998 (Sackett et al., 1999) as part of the International Continental Drilling Program (ICDP) Long Valley Coring Project. Prior to the final stage of drilling, a 3-component 10-Hz seismometer, installed at a depth of 2050 m from September 1997 through May 1998, recorded tens of thousands of local events during the 1997–1998 seismic crisis in Long Valley Caldera (Prejean and Ellsworth, 2001). The value of recording at depth is clearly evident in the comparison of near-source recordings made at the surface and deep underground (Fig. 1).

In the fall of 2002, the well was converted into a deep geophysical observatory which now has a 3-component 4.5-Hz seismometer installed at a depth of 2600 m. Earthquakes as small as M2.5 have been observed at

distances as close as 300 m from the seismometer (Fig. 2). Currently, the data sample rate is limited to 500 sps, which limits the highest resolvable frequency to 200 Hz. All data are available through the Northern California Earthquake Data Center (<http://www.ncedc.org/>). While this sample rate is adequate to detect even such small events, it is not adequate to resolve the event corner frequency. Increasing the sample rate alone, however, will not guarantee that source processes can be measured. The attenuation of seismic waves, even over distances of hundreds of meters, presents a formidable challenge to the modeler. The trade-off between earthquake source parameters and attenuation makes it difficult to separate path effects from source effects. Ide et al. (2003) overcame this problem by employing a spectral ratio method to re-interpret some of the earthquakes analyzed earlier by Prejean and Ellsworth (2001). The reanalysis demonstrated how propagation effects can contaminate source parameters interpreted from individual event recordings, even in the high frequency environment of the deep borehole.

The importance of wave attenuation and scattering even in the high Q environment of a deep borehole was further reinforced by seismic data collected by the 32-level, 1240-m-long array installed in the 2.1-km SAFOD Pilot Hole (Chavarria et al., 2004). This vertical borehole was drilled in 2002 as an ICDP project and part of the pre-Earth Scope site



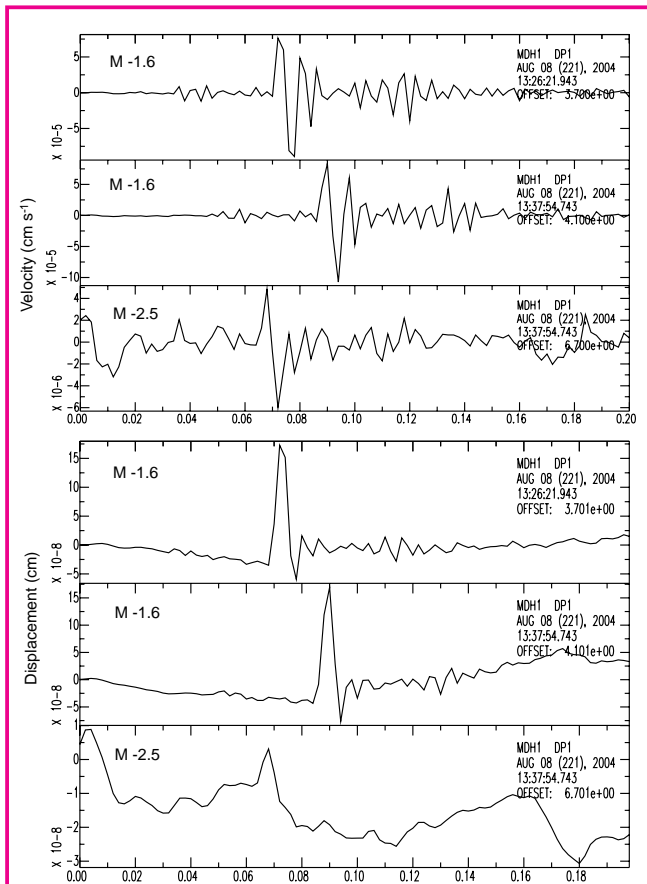


Figure 2. Seismograms of microearthquakes located approximately 300 m from the instruments in the LVEW at a depth of 2600 m. Although the seismogram sampling rate of 500 sps is too low to capture any details of the source process, the seismic moment of the events can still be easily measured from the area under the displacement pulse.

investigation program at SAFOD. Installed in granite between 856 m and 2096 m below ground level, the array recorded at sample rates between 500 sps and 1000 sps from September 2002 to April 2005. All data are available through the Northern California Earthquake Data Center. The effects of propagation on the seismograms are clearly evident in Fig. 3, which shows the seismograms of a microearthquake

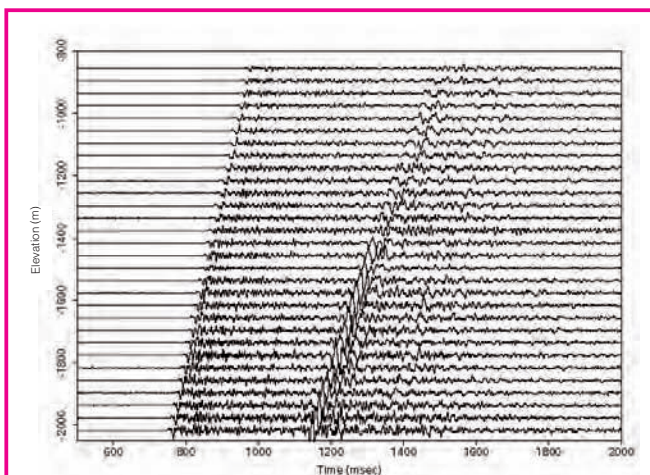


Figure 3. Local earthquake recorded on the SAFOD Pilot Hole Array illustrating the effect of wave propagation on the frequency content of body waves.

located about 2.5 km from the array. Note the loss of high frequency content as the wave propagates up the borehole.

Imanishi and Ellsworth (2006) applied a multi-window spectral ratio (MWSR) to seismograms of earthquake multiplets recorded in the SAFOD Pilot Hole. This procedure extended the method of Ide et al. (2003) by stacking multiple time windows of the direct body wave and its early coda to suppress noise and improve the recovery of the spectral ratio (Fig. 4). Results of their study indicated that there is no scale-dependence to static stress drop or apparent stress for earthquakes on the San Andreas Fault between M0.2 and M2.1.

The SAFOD Main Hole was drilled through the San Andreas Fault to a total vertical depth of 3.1 km in 2005. It provides a portal into the inner workings of a major plate boundary fault that makes it possible to conduct spatially extensive and long-duration observations of active tectonic processes within the actively deforming core of the San Andreas Fault.

To meet the scientific and technical challenges of building the observatory, borehole instrumentation systems developed for use in the petroleum industry and by the academic community in other deep research boreholes have been deployed in the SAFOD pilot hole and main hole over the past three years. These systems included 15-Hz omni-directional and 4.5-Hz gimballed seismometers, micro-electro-mechanical accelerometers, tiltmeters, sigma-delta digitizers, and a fiber optic interferometric strainmeter. A 1200-m-long, 3-component 80-level clamped seismic array was also operated in the main hole for 2 weeks of recording in May of 2005, collecting continuous seismic data at 4000 sps.

Some of the observational highlights included capturing one of the SAFOD target repeating earthquakes in the near-field at a distance of 420 m, with accelerations of up to 200 cm s⁻¹ and a static displacement of a few microns (Fig. 5). Numerous other local events were observed over the summer by the tilt and seismic instruments in the pilot hole, some of which produced

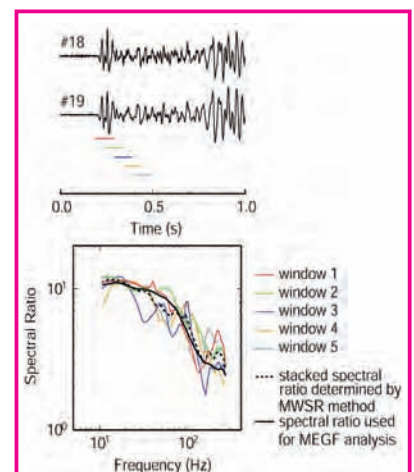


Figure 4. Example of MWSR method for measuring the spectral ratio of two earthquakes (from Imanishi and Ellsworth, 2006). Each colored spectral ratio is derived from the corresponding time window indicated on the seismograms. The averaged spectra in the stack more closely resemble the theoretical spectral ratio for the omega-squared model than the individual spectra. This is because the cancellation of path effects even for earthquakes at nearly the same location is not exact, and multiple windows suppress the uncorrelated noise introduced by multipaths between source and receiver.

strain offsets of several nanostrain on the fiber optic strain-meter.

An exciting discovery made in the SAFOD Main Hole was a new type of seismic wave: a fault zone guided P-wave (Fig. 6). This phase arrives between the P- and S-waves, is normally dispersed, and has a clear Airy phase. It was recorded by 15-Hz seismometers located 2650 m below ground, 3270 m along the inclined borehole, and approximately 40 m from the center of a major fault that the borehole crossed. This fault has caused deformation of the borehole casing, indicating that it is one of the active stands of the San Andreas system. The existence of this phase depends on unique relationships between the P and S velocities of the fault and surrounding rocks, as well as their thicknesses. Its propagation speed, low frequency cut-off, and Airy phase frequency thus give special insights into the structure and multi-stranding of the San Andreas Fault zone.

In summary, observations of earthquakes at very short distances in the three borehole observatories in California demonstrate the many advantages of observing earthquake processes at short distances in deep wells. Near-source recordings are essential for the study of earthquake source processes, particularly the nucleation and early growth of dynamic rupture. SAFOD data will continue to provide a benchmark for theoretical and numerical models of earth-

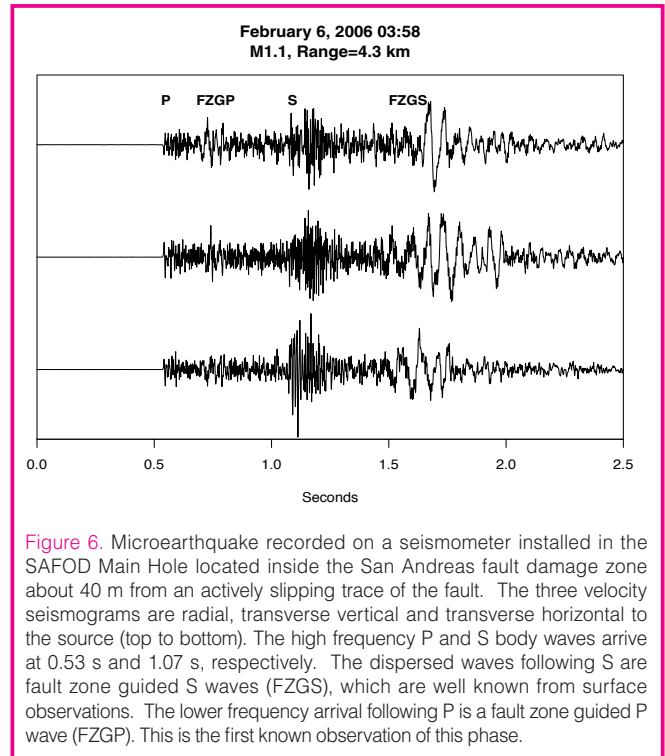


Figure 6. Microearthquake recorded on a seismometer installed in the SAFOD Main Hole located inside the San Andreas fault damage zone about 40 m from an actively slipping trace of the fault. The three velocity seismograms are radial, transverse vertical and transverse horizontal to the source (top to bottom). The high frequency P and S body waves arrive at 0.53 s and 1.07 s, respectively. The dispersed waves following S are fault zone guided S waves (FZGS), which are well known from surface observations. The lower frequency arrival following P is a fault zone guided P wave (FZGP). This is the first known observation of this phase.

quake processes and laboratory rock experiments, and complementary data to near-source observations of large magnitude earthquakes. Numerical simulations of the earthquake on rate-and-state faults have now advanced to the point that they can produce numerically accurate models that span the slow earthquake loading cycle and dynamic rupture on fault patches of comparable dimension to the SAFOD target earthquakes. We should anticipate a productive interchange between observations, theories, models and laboratory experiments, as we begin to gather data in the near field of the target earthquakes.

References

Chavarria, A., Malin, P.E., and Shalev, E., 2004. The SAFOD Pilot Hole seismic array: Wave propagation effects as a function of sensor depth and source location. *Geophys. Res. Lett.*, 31:L12S07, doi:10.1029/2003GL019382.
 Ellsworth, W.L. and Malin, P.E., 2006. A first observation of fault guided PSV-waves at SAFOD with implications for fault character-

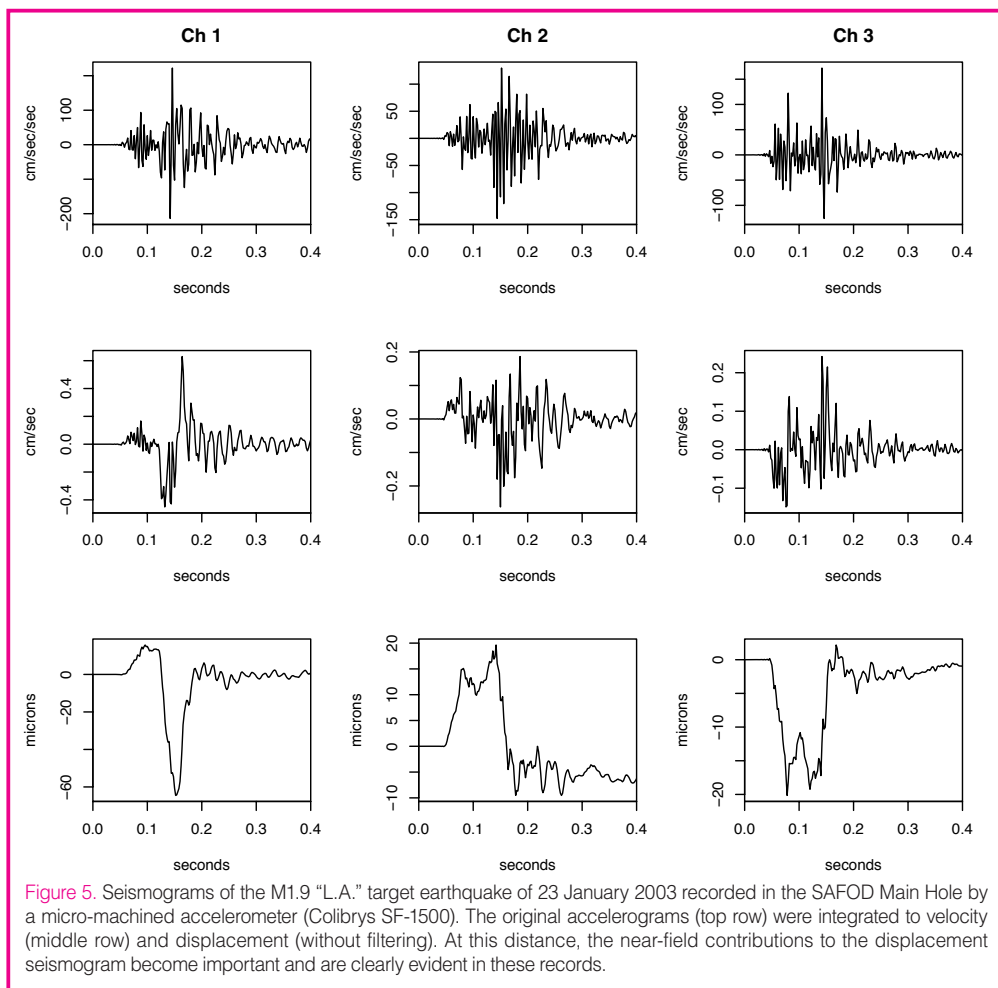


Figure 5. Seismograms of the M1.9 "L.A." target earthquake of 23 January 2003 recorded in the SAFOD Main Hole by a micro-machined accelerometer (Colibrays SF-1500). The original accelerograms (top row) were integrated to velocity (middle row) and displacement (without filtering). At this distance, the near-field contributions to the displacement seismogram become important and are clearly evident in these records.

istics. *EOS Trans. Am. Geophys. U.* 87(52): Abstract T23E-02.

- Ide, S., Beroza, G.C., Prejean, S.G., and Ellsworth, W.L., 2003. Apparent break in earthquake scaling due to path and site effects on deep borehole recordings. *J. Geophys. Res.*, 108(B5), 2271, doi:10.1029/2001JB001617.
- Imanishi, K., and Ellsworth, W.L., 2006. Source scaling relationships of microearthquakes at Parkfield, CA, determined using the SAFOD pilot hole array. In Abercrombie, R.E., McGarr, A., Di Toro, G., and Kanamori, H. (Eds.), *Earthquakes: Radiated Energy and the Physics of Faulting*, *Geophys. Monogr.* 170, Washington D.C. (American Geophysical Union), 81–80.
- Prejean, S.G. and Ellsworth, W.L., 2001. Observations of earthquake source parameters at 2 km depth in Long Valley Caldera, eastern California. *Bull. Seismolog. Soc. Am.*, 91: 165–177, doi:10.1785/0120000079.
- Sackett, P.C., McConnell, V.S., Roach, A.L., Priest, S.S., and Sass, J. H., 1999. Long Valley Coring Project, 1998 – Preliminary Stratigraphy and Images of Recovered Core. *U.S. Geological Survey Open-File Report 99-158*.

Authors

William L. Ellsworth, 3A-109, U.S. Geological Survey (USGS), 345 Middlefield Road Mail Stop 977, Menlo Park, Calif. 94025, U.S.A., e-mail: ellsworth@usgs.gov

Peter E. Malin, 109A Old Chemistry Box 90227, Duke University, Durham, N.C. 27708, U.S.A., e-mail: malin@duke.edu

Kazutoshi Imanishi, Geological Survey of Japan, Institute of Geology and Geoinformation (AIST), Tsukuba Central 7, 1-1-1 Higashi, Tsukuba, 305-8567, Japan.

Steven W. Roecker, Department of Earth and Environmental Sciences, Rensselaer Polytechnic Institute, Science Center 1S06, Troy, N.Y. 12180, U.S.A.

Robert Nadeau, Berkeley Seismological Lab., 207 McCone Hall, University of California Berkeley, Calif. 94720-4760, U.S.A.

Volker Oye, Norwegian Seismic Array (NORSAR), P.O. Box 53, N-2027 Kjeller, Norway.

Clifford H. Thurber, Department of Geology and Geophysics, University of Wisconsin, 1215 West Dayton Street, Madison, Wis. 53706, U.S.A.

Felix Waldhauser, LDEO-Seismology Geology and Tectonophysics, 210 Seismology, 61 Route 9W – P.O. Box 1000, Palisades, N.Y. 10964, U.S.A.

Namoi L. Boness, Chevron, Energy Technology Centers (ETC), San Ramon, Calif. 94583, U.S.A.

Stephen H. Hickman, USGS, 345 Middlefield Road, Menlo Park, Calif. 94025, U.S.A.

Mark D. Zoback, Department of Geophysics, Stanford University, Mitchell Bldg., Stanford, Calif. 94305, U.S.A.

Related Web Link

<http://www.ncedc.org/>

Monitoring of Rock Mass Behavior at the Closest Proximity to Hypocenters in South African Gold Mines

by Hiroshi Ogasawara and the Research Group for Semi-controlled Earthquake-Generation Experiments in South African Deep Gold Mines

doi:10.2204/iodp.sd.s01.11.2007

To bridge the scale gap between a laboratory scale and a large earthquake scale, we need experiences in an intermediate scale at the smallest distance from the hypocenters (Fig. 1). However, the closest monitoring is not always easy, and the San Andreas Fault Observatory at Depth (SAFOD) is an exceptional opportunity to obtain experiences from natural small earthquakes (Hickman et al., 2004). Tremors in deep mines resemble natural small earthquakes, being also good to take a close look at the hypocenters (Spottiswoode and McGarr, 1975). Recently, modern monitoring is carried out with wider dynamic range and frequency band (Mendecki, 1997). The Research Group for the Semi-controlled Earthquake-Generation Experiments in South African Deep Gold Mines (SeeSA) have been co-operating with ISS International Ltd. and South African gold mines to study rock mass behavior (Iio, 1995; Iio and Fukao, 1992; Ishii and the Research Group for Semi-Controlled Earthquake Generation Experiment at South African Gold Mines, 1996; Nicolaysen, 1992; Ogasawara et al., 2001, 2002a, 2005a, 2005b; Sumitomo, 1998). We have deployed eight experimental sites at four gold mines at depths of a few km (Fig. 2; Ogasawara et al., 2002a, 2005a, 2005b), and at one of these we are collaborating with ICDP-DAFSAM/NSF-NELSAM project (PI: Ze'ev Reches).

In 1996, at the Western Deep Levels South Mine (currently Mponeng mine; Fig. 2), we deployed an array of nine triaxial accelerometers within 100 m of potential hypocenters of $M > 2$ earthquakes, successfully delineating the finest details of small earthquakes. The relationship between seismic moment and corner frequency was the same as that for

medium or large natural earthquakes (Ogasawara et al., 2002b). The source processes of some $M < 1$ or smaller earthquakes were as complicated as large, natural earthquakes (Yamada et al., 2005).

During 2000–2003 at the Bambanani mine (Figs. 2 and 3), we successfully recorded the rock-mass behavior in the entire life span of $M_{2.4}$ and $M_{2.5}$ earthquakes ($M_{w2.9}$ and $M_{w2.0}$, respectively, in Fig. 4a; Ishii et al., 2000; Ogasawara et al., 2005a; Takeuchi, 2005). We installed an Ishii strainmeter (Ishii et al., 1997) within 100 m of the seismic sources and recorded the data continuously with resolutions of 25-Hz and 24-bit. The initial significant change was by an $M_{w0.2}$ event in September 2001 within a few tens of meters. The largest event ($M_{w3.0}$) within 250 m of the strainmeter took place in 2002, however, not close enough to cause the largest strain change. The largest strain changes were associated with two M_2 events within 100 m of the strainmeter in 2003 (yellow circles in Fig.3, upper). The strain change was as large as 100 microstrain, corresponding to several MPa. Such a large change is recorded only at the closest distance from the seismic fault. Channel 1 subparallel to the maximum principal stress was contracting until the M_2 sequence and then was released by the sequence.

However no accelerating strain preceded the hundreds of co-seismic steps for the catalogued seismic events, even for those of ~ 100 microstrain (stress drop ~ 7 MPa) (Ogasawara et al., 2005a; Takeuchi, 2005).

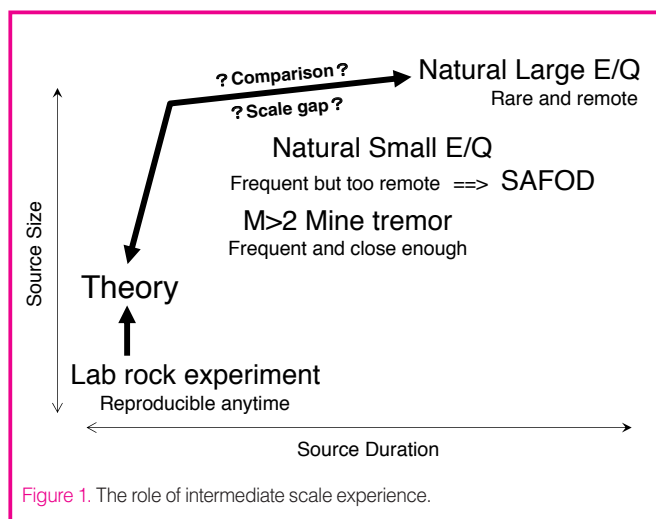


Figure 1. The role of intermediate scale experience.

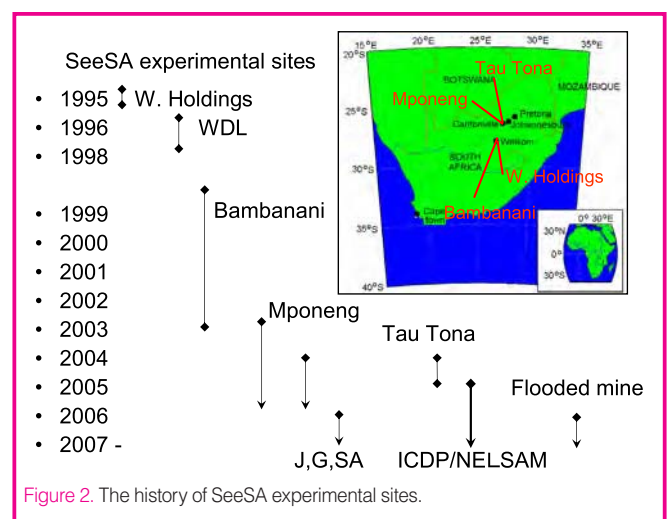


Figure 2. The history of SeeSA experimental sites.

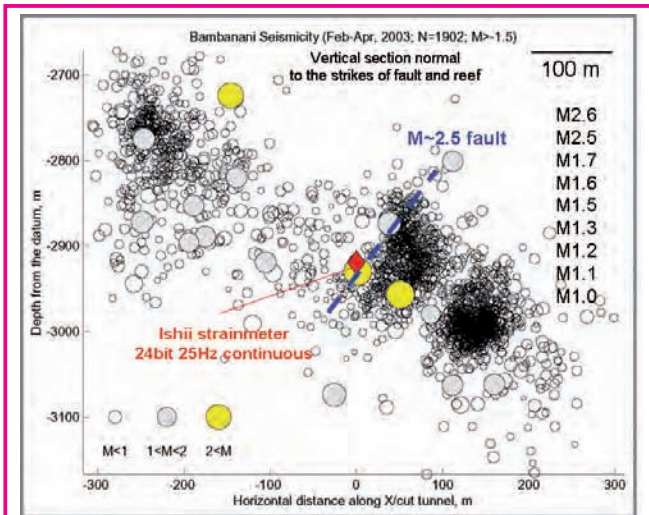


Figure 3. Configuration of an Ishii strainmeter, the M2.5 fault and the seismicity (Feb-Apr 2003) at the site at the Bamabanani mine, Welkom.

Thoroughly going through the strain recordings, Yamamoto et al. (2006) found that the Ishii strainmeter picks up seismic events smaller than $M = -1$ (much more than those catalogued by the mine's seismic network). They also found hundreds of the aftershocks having variable senses of strain steps and postseismic changes. This suggests the strainmeter was located within the aftershock area.

The step response to the catalogued earthquake accompanied overshoot and ringing (Fig. 4b; hereinafter, **dynamic**

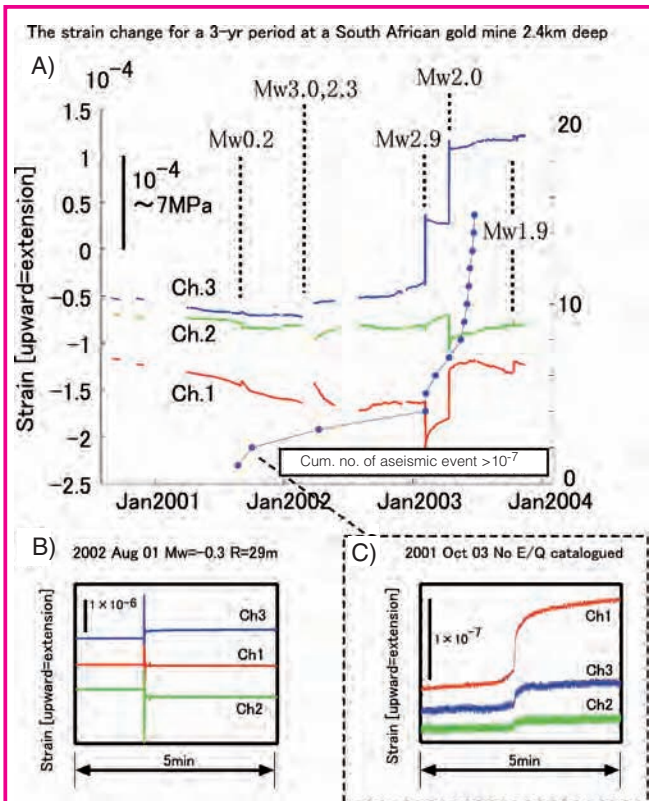


Figure 4. [A] A three-year strain changes (red, green, and blue lines) and cumulative number of aseismic events (LDR events; connected blue dots). [B] A typical response to a catalogued seismic event. Note the dynamic response (overshoot and ringing) associated with the strain step. [C] A typical example of slow step with clear forerunner (after Naoi et al., 2006 b).

Statistics of strain events $> 10^{-7}$

Out of 70 events ($> 10^{-7}$)

{ 38: catalogued E/Q ($M > -0.5$)

{ 32: others

{ 6: Significant Dynamic Response

{ 11: Not easily categorized

{ 15: Little Dynamic Response (LDR)

{ 3: Very slow, some preceded by forerunner

{ 12: Others

Figure 5. The statistics of the strain events (data after Naoi et al., 2006a).

response). However, Naoi et al. (2006a) found that slow strain-steps as small as 0.1 microstrain were also frequently recorded with little dynamic response (LDR). They found that the step durations were variable and significantly longer than normal seismic steps (Fig. 4c; the moments possibly correspond to $M = -1$ or smaller seismic events). Interestingly, most LDR events took place after the large strain change and few very slow events were preceded by the significant accelerating strain (Figs. 4c and 5).

The entire lifespan of a large natural earthquake includes loading, foreshocks, main rupture, aftershocks, and postseismic deformation. Slow events are also associated. The forerunning, accelerating deformation is not often observed, however.

For $-1 < M < 2$ mine tremors, we again observed almost the same set of phenomena. Additionally, we could find the clear forerunners associated only with the small, slow strain event. We were able to see them because we were able to install strainmeters within seismic sources.

Monitoring the smaller subsets of the phenomena (gray area in Fig. 6) could be interesting. To get the time and magnitude range closer to those for AE, we start the strain

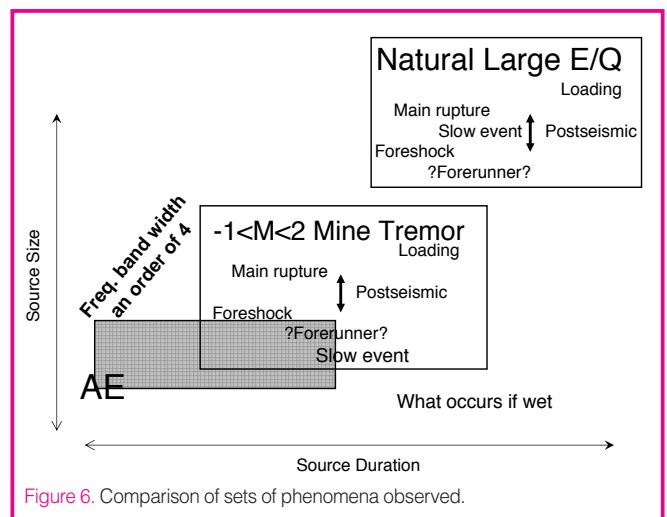


Figure 6. Comparison of sets of phenomena observed.

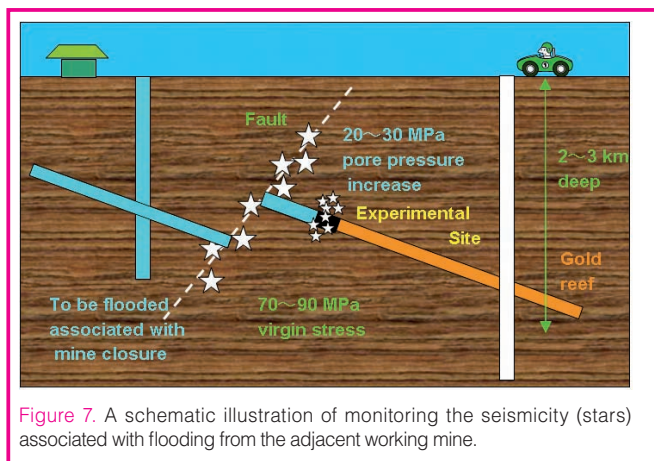


Figure 7. A schematic illustration of monitoring the seismicity (stars) associated with flooding from the adjacent working mine.

monitoring with much higher sampling rate at new sites. One of these is carried out collaterally with Nakatani et al., (2006) who attempted to monitor the wide dynamic/frequency range of fracturing process from AE (up to 200 kHz) to seismic events at a potential seismic fault.

At the previous experimental sites, the rock mass was not saturated with water. We also have to learn what behavior can be seen under wet conditions, and along these lines, the flooded South African gold mines are very unique cases to provide us with good experimental sites. We can investigate 1) the effects of flooding and the corresponding rising water levels on the stability of faults and other geological features, 2) the effects of seismicity on inter-mine water plugs and mine barriers pillars, and 3) seismic damage risks to neighboring mines in areas in which mines are mature.

These investigations are very crucial because the behavior of highly stressed rock mass during flooding is presumably analogous to that during natural earthquake swarms or stable or unstable slip at natural great earthquake hypocenters under water-saturated conditions. We cannot access inside the earthquake swarm in Japan, but we can do it in South Africa.

References

Hickman, S., Zoback, M., and Ellsworth, W., 2004. Introduction to special section: Preparing for the San Andreas Fault Observatory at Depth. *Geophys. Res. Lett.*, 31:L12S01, doi:10.1029/2004GL020688.

Iio, Y., 1995. Earthquake prediction in South African gold mines. *Iwanami Science* 65:279–281 (in Japanese).

Iio, Y. and Fukao, Y., 1992. Call for joining international experiment in South African gold mines. *Newsletter, Seismol. Soc. Jpn.*, 3(6):8–9 (in Japanese).

Ishii, H. and the Research Group for Semi-controlled Earthquake Generation Experiments at South African Gold Mines, 1996. Semi-controlled experiment in a gold mine in South Africa (5) — strain observation by borehole strain meters. *Abstracts. 1996 Japan Earth Planet. Sci. Joint Meeting*: A58 (in Japanese).

Ishii, H., Nakao, S., Ogasawara, H., and the Research Group for Semi-controlled Earthquake Generation Experiment at South

African Gold Mine, 2000. Continuous monitoring of strain by 25 Hz 24 bit sampling using Ishii's borehole strainmeter on a hypocentral fault where an $M > 3$ event is expected - semi-controlled experiment in a gold mine in South Africa (25). *Abstracts. Seism. Soc. Jpn.*, 2:A58 (in Japanese).

Ishii, H., Yamauchi, T., and Kusumoto, F., 1997. Development of high sensitivity bore hole strain meters and application for rock mechanics and earthquake prediction study. *Rock Stress*. Rotterdam (Balkema), 253–258.

Mendecki, A.J. (Ed.), 1997. *Seismic Monitoring in Mines*. London (Chapman and Hall), 262 pages.

Nakatani, M., Carstens, R., Stanchits, S., Philipp, J., van Aswegen, G., Ide, S., Miyake, H., Yabe, Y., Ogasawara, H., Dresen, G., Manthei, G., Ward, T., and Sumitomo Norihiko International Research Group for Semi-controlled Earthquake Generation Experiment at South African Gold Mine, 2006. An ultra-accessible fault of an impending earthquake at a 3.5 km depth in a South African gold mine. *Abstract, the Japan Geoscience Union Meeting 2006*, S109-P004.

Naoi, M., Ogasawara, H., Takeuchi, J., Yamamoto, A., Shimoda, N., Morishita, K., Ishii, H., Nakao, S., van Aswegen, G., Mendecki, A.J., Lenegan, P., Ebrahim-Trollope, R., and Iio, Y., 2006a. Small slow-strain steps and their forerunners observed in gold mine in South Africa. *Geophys. Res. Lett.*, 33:L12304, doi: 10.1029/2006GL026507.

Naoi, M., Ogasawara, H., Takeuchi, J., Shimoda, N., Morishita, K., Ishii, H., Nakao, S., Mendecki, A.J., van Aswegen, G., Ebrahim-Trollope, R. and Iio, Y., 2006b. *Newsletter, Seismol. Soc. Jpn.*, 18(1), cover page (in Japanese).

Nicolaysen, L.O., 1992. International semi-controlled experiment on seismic events: a review of the background and proposal. *Newsletter, Seismol. Soc. Jpn.*, 3(6):9–27.

Ogasawara, H. Miwa, T., and The Research Group for Semi-controlled Experiment in South African Gold Mines, 2002b. Microearthquake scaling relationship using near-source, redundant, wide-dynamic-range accelerograms in a South African deep gold mine. In Ogasawara, H., et al. (Eds.), *Seismogenic Process Monitoring*, Rotterdam (Balkema), 151–164.

Ogasawara, H. and The Research Group for Semi-controlled Experiments in South African Gold Mines, 2002a. Semi-controlled earthquake generation experiment in South African gold mine. A review of the semi-controlled earthquake generation experiment in South African Deep Gold Mines (1992-2001). In Ogasawara, H., et al. (Eds.), *Seismogenic Process Monitoring*, Rotterdam (Balkema), 119–150.

Ogasawara, H., Sato, S., Nishi, S., Sumitomo, N., Ishii, H., Iio, Y., Nakao, S., Ando, M., Takano, M., Nagai, N., Ohkura, T., Kawakata, H., Satoh, T., Kusunose, K., Cho, A., Mendecki, A., Cichowicz, A., Green, R.W.E., and Kataka, M.O., 2001. Semi-controlled seismogenic experiments in South African deep gold mines. *Proc. 5th Internat. Symp. Rockburst and Seismicity Mines*, 293–300.

Ogasawara, H., Takeuchi, J., Shimoda, N., Ishii, H., Nakao, S., van Aswegen, G., Mendecki, A.J., Cichowicz, A., Ebrahim-Trollope, R., Kawakata, H., Iio, Y., Ohkura, T., Ando, M., and the Research Group for Semi-controlled Earthquake-Generation Experiments in South African deep gold mines,

- 2005a. High-resolution strain monitoring during M-2 events in a South African deep gold mine in close proximity to hypocentres. *Proc. 6th Internat. Symp. Rockburst and Seismicity in Mines*, 385–391.
- Ogasawara, H., Takeuchi, J., Shiimoda, N., Nakatani, M., Kato, A., Iio, Y., Kawakata, H., Yamada, T., Yamauchi, T., Ishii, H., Satoh, T., Kusunose, K., Otsuki, K., Kita, S., Nakao, S., Ward, A.K., McGill, R., Murphy, S.K., Mendecki, A.J., van Aswegen, G., and the Research Group for Semi-controlled Earthquake Generation Experiments in South African Deep Gold Mines, 2005b. **Multidisciplinary Monitoring of the Entire Life Span of an Earthquake and its Practical Strategy in South African Gold Mines**, *Proc. 6th Internat. Symp. Rockburst and Seismicity in Mines*, 393–398.
- Spottiswoode, S.M. and McGarr, A., 1975. Source parameters of tremors in a deep-level gold mine. *Bull. Seismol. Soc. Amer.*, 65:93–112.
- Sumitomo, N., 1998. International joint research: semi-controlled earthquake generation experiment. *Chikyu Monthly*, 229:391–394 (in Japanese).
- Takeuchi, J., 2005. A study of strain changes associated with earthquakes observed within 100m in Bambanani mine, South Africa (in Japanese). **M.S. thesis, Ritsumeikan University, Kusatsu.**
- Yamada, T., Mori, J.J., Ide, S., Kawakata, H., Iio, Y., and Ogasawara, H., 2005. Radiation efficiency and apparent stress of small earthquakes in a South African gold mine. *J. Geophys. Res.*, 110, B01305, doi:10.1029/2004JB003221.
- Yamamoto, A., Ogasawara, H., Takeuchi, J., Shimoda, N., Naoi, M., Morishita, K., Ishii, H., Nakao, S., Mendecki, A., van Aswegen, G., Lenegan, P., Ebrahim-Trollope, S., and Sumitomo Norihiko International Research Group for Semi-controlled Earthquake Generation Experiment at South African Gold Mine, 2006. The aftershocks for ultra-micro-earthquakes seen in 25Hz continuous recordings with Ishii strainmeter within M2 source area. *Abstract, the Japan Geoscience Union Meeting 2006*, S109-P004.

Authors

Hiroshi Ogasawara, Faculty of Science and Engineering, Ritsumeikan University, 1-1-1 Noji Higashi, Kusatsu, 525-8577, Japan, e-mail: ogasawar@se.ritsumei.ac.jp.

The Research Group for Semi-controlled Earthquake-Generation Experiments in South African Deep Gold Mines, members from Ritsumeikan University, the University of Tokyo, Kyoto University, Nagoya University, Tohoku University, Tono Research Institute of Earthquake Science (TRIES) Japan, National Institute of Advanced Industrial Science and Technology (AIST) Japan, Kanazawa University, ISS International Ltd., Open House Management Solutions Ltd (OHMS), Seismogen CC., Geohydroseis CC., Gesellschaft für Materialprüfung und Geophysik (GMuG), GeoForschungsZentrum Potsdam (GFZ), Western Deep Levels, South mine, Bambanani mine, Tau Tona mine, Buffelsfontein mine, East Rand Proprietary mine.

Dynamics of Earthquake Faulting in Subduction Zones: Inference from Pseudotachylytes and Ultracataclasites in an Ancient Accretionary Complex

by Kohtaro Ujiie

doi:10.2204/iodp.sd.s01.21.2007

The fault rocks in ancient accretionary complexes exhumed from seismogenic depths may provide an invaluable opportunity to examine the mechanisms and mechanics of seismic slip in subduction thrusts and splay faults. In order to understand the dynamics of earthquake faulting in subduction zones, we analyzed pseudotachylytes and ultracataclasites from the Shimanto accretionary complex in southwest Japan.

Pseudotachylytes

The following conclusions were derived from the analysis of pseudotachylytes (Ujiie et al., 2007a):

1. At seismogenic depths in the subduction zone, a cataclastic thrust zone develops at the top of the mélangé, and the coseismic slip is concentrated into a narrow zone less than a few millimeters thick.
2. The pseudotachylyte displays a fragment-laden, glass-supported texture resulting from rapid cooling of the frictional melt (Fig. 1), which is consistent with a very short cooling time of the melt layer calculated using thermal modeling. The rapid cooling of the melt layer is due to its narrow thickness, resulting in the fast healing of the coseismic slip zone by the solidified melt layer.
3. The pseudotachylyte is derived from the frictional melting of an illite-rich ultracataclasite layer. The

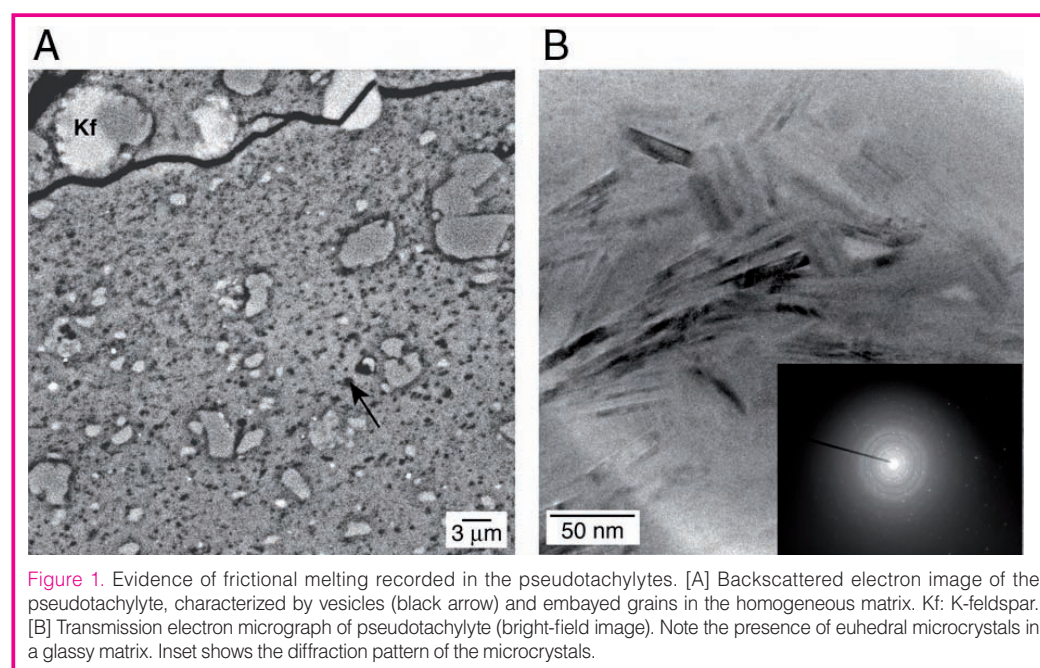
variation in the volume fraction of unmelted grains in the pseudotachylyte matrix primarily represents the difference in the initial volume fraction of illite in the ultracataclasite layer prior to frictional melting. The minimum melting temperature is 1100°C, which is ~850–920°C greater than the maximum temperatures recorded in the host rocks.

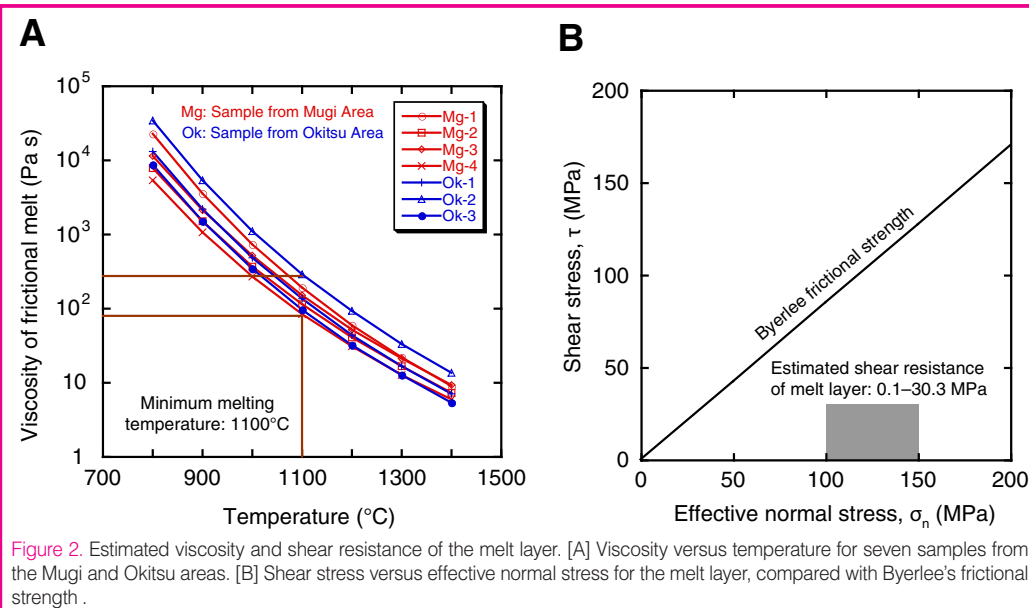
4. The viscosity and shear resistance of the melt layer are very low (Fig. 2); therefore, the dynamic weakness of the fault, acceleration of seismic slip, and propagation of instability can possibly occur during an earthquake. This would contribute, at least locally, to the efficiency with which stored strain energy is released and, hence, to the earthquake magnitude in subduction zones.
5. Such frictional melting of the illite-rich slip zone may be applicable to subduction thrusts and faults in other accretionary complexes. The melting of the illite-rich slip zone is likely to form a hydrous melt layer, possibly leading to a high water content in these pseudotachylytes.

Ultracataclasites

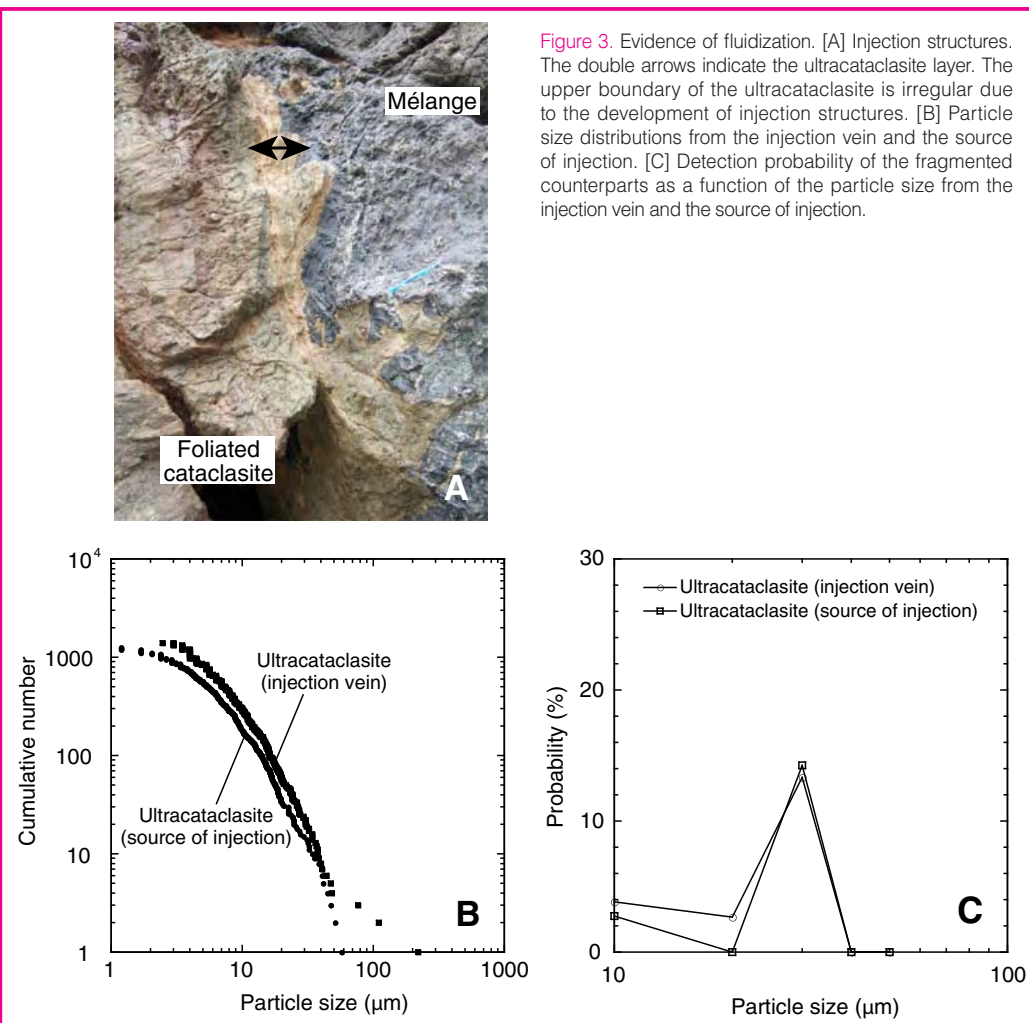
The new observations of ultracataclasites within the subduction thrust and their possible relevance to the dynamic slip processes are summarized below (Ujiie et al., 2007b).

The thrust faults in the Shimanto accretionary complex of southwest Japan imbricate the mélangé derived from sedimentary rocks and basalt, which represent a duplex underplating associated with the downward step of the subduction thrust at seismogenic depths (4–6 km deep, 130–150°C). One well exposed duplex-fault zone consists mainly of foliated cataclasites and ultracataclasites derived from basalt. The fault zone structure suggests slip localization along the 2–20-cm-thick ultracataclasite layer at the





boundary between different lithologies. The ultracataclasite layer is marked by fluid-related processes, as shown by the alteration along the ultracataclasite and the concentration of veins near the ultracataclasite. New observations of the ultracataclasite layer have revealed that fluidization could occur during the localized slip.



Fluidization is suggested by the injections of granular material into the mélange without the sorting of finely-grained particles, and by the quantitative data that few particles in the injected material have fragmented counterparts (Fig. 3). The fluidization during localized slip under fluid-infiltrated conditions is likely due to thermal pressurization, and injection structures may represent hydraulic fracturing normal to the least principal stress.

References

Ujiiie, K., Yamaguchi, H., Sakaguchi, A., and Toh, S., 2007a. Pseudotachylytes in an ancient accretionary complex and implications for melt lubrication during subduction zone earthquakes. *J. Struct. Geol.*, 29:599–613, doi:10.1016/j.jsg.2006.10.012.

Ujiiie, K., Yamaguchi, A., Kimura, G., and Toh, S., 2007b. Fluidization of granular material in a subduction thrust at seismogenic depths. *Earth Planet. Sci. Lett.*, 259:307–318, doi:10.1016/j.epsl.2007.04.049.

Author

Kohtaro Ujiiie, Institute for Research on Earth Evolution (IFREE), Japan Agency for Marine-Earth Science and Technology (JAMSTEC), 3173-25 Showa-machi, Yokohama-city, Kanagawa 236-0001, Japan, e-mail: ujiiiek@jamstec.go.jp.

Precise Temperature Measurements and Earthquake Heat Associated with the 1999 Chi-Chi, Taiwan Earthquake

by Yasuyuki Kano, Jim Mori, Ryo Fujio, Takashi Yanagidani, Setsuro Nakao, Hisao Ito, Osamu Matsubayashi, and Kuo-Fong Ma

doi:10.2204/iodp.sd.s01.40.2007

Introduction

The frictional heat generated during earthquake faulting is thought to be the largest part (80% to 90%) of the total seismic energy budget, and geophysicists have long discussed the level of heat that should be observable (Brune et al., 1969; Lachenbruch and Sass, 1980; Scholz, 2002; Terada, 1930). Precise temperature measurements across the fault immediately after an earthquake can provide the most unambiguous answer; **however, there has never been a significant near-fault temperature change observed for any previous large earthquake that can be attributed to the frictional heating.** This is because there has been no appropriate site for temperature measurements around a fault at depth just after an earthquake. The most promising way to reach the fault zone in order to observe the frictional heat is to drill a borehole to the area where large slip occurs. There have been several drilling projects to reach deep areas of the fault zone, such as the Taiwan Chelungpu fault Drilling Project (TCDP), San Andreas Fault Observatory at Depth (SAFOD), and the planned NanTroSEIZE project. We reported the first successful temperature measurement of deep fault zone boreholes that was drilled by TCDP at the Chelungpu fault, Taiwan (Kano et al., 2006). An observation of a temperature increase, and thus an estimate of the heat generated, provides information about the frictional strength during faulting and the level of driving stress for an earthquake. These are key unknown values of important parameters that are necessary for understanding the physical process of earthquake ruptures.

In this paper we outline the results of the precise temperature measurement in TCDP Hole A as an attempt to directly measure the frictional heat produced by an earthquake.



Figure 1. The precise temperature instrument that was installed in the well head of TCDP Hole A.

Then, we present the importance of measuring the thermal property of rocks around the fault in addition to the precise temperature measurement—the effect of thermal conductivity of the material on the temperature gradient proposed by Matsubayashi et al. (2005) is not negligible on the results of the pre-

cise temperature measurement. The details of our temperature measurement in the Chelungpu fault and its interpretation are presented in Kano et al. (2006).

Precise Measurements at TCDP Hole A

Following the 21 September 1999 Chi-Chi earthquake, the TCDP bored two holes which penetrated the fault at depths of about 1100 m (Ma et al., 2006) near the town of DaKeng in the northern part of the rupture zone. During the earthquake, this area had large surface rupture, and a fault displacement of about 8 m is estimated from seismic data. The boreholes provided the rare opportunity to make temperature measurements in a fault zone with large slip from a recent earthquake. The precise temperature observations were carried out in one of the boreholes (Hole A) during September 2005, six years following the earthquake. The borehole is cased with steel pipe so that there is no water flow between the borehole and surrounding rock, enabling much more stable temperature measurements.

In order to obtain a high-resolution (0.003°C) temperature profile, we developed a borehole instrument containing two quartz oscillator thermometers, separated by 3 m. The instrument was slowly lowered (about 1.0 m min^{-1}) and raised (about 0.4 m min^{-1}) in the borehole between the depths of 900 m and 1250 m, producing four independent temperature profiles across the fault zone, during 20 and 21 September (Fig. 1). The continuous recording of temperature at 10 s intervals produced 5–15 readings per meter.

All the temperature profiles show small temperature signatures, which are a small temperature increase above the geothermal gradient in the region of the fault zone at the depth of 1111 m. Kano et al. (2006) simply modeled this temperature signature as a residual temperature anomaly originating in frictional heat produced by fault slip.

Modeling of Temperature Anomaly

The temperature signature produced by frictional heat is modeled by heat conduction from the fault plane as a heat source. Here we simply modeled the signature assuming one-dimensional heat conduction, in which heat produced on a thin plane is conducted to the direction perpendicular to the plane (Officer, 1974). We assumed that all the heat generated was consumed to increase the temperature of thin

fault surface. The temperature change at the point that x m away from the fault surface after t s is

$$T(x,t) = \frac{S}{2\sqrt{\pi\alpha t}} e^{-x^2/4\alpha t} \quad (1)$$

where α is the heat diffusivity of the media surrounding the fault, and S is the strength of the heat source, which is heat (product of shear stress, τ , and fault slip, u) divided by specific heat, c , and the density, ρ , of the medium with units measured in K m:

$$S = \frac{\tau \cdot u}{c \cdot \rho} \quad (2)$$

Figure 2A shows the spatial variation of temperature signature after five years and ten years from the earthquake (calculated for the parameters $u = 6$ m, $\tau = 1.1$ MPa, $c = 1140$ J kg⁻¹ K⁻¹, $\rho = 2500$ kg m⁻³, and $\alpha = 3.4 \times 10^{-7}$ m² s⁻¹). The amplitude becomes smaller with an increase of t , and the shape of the signature becomes broader. The amplitude of the peak of the temperature anomaly is only 0.06 K after five years. Figure 2B shows the temporal variation of temperature signature on the fault and at the point 1 m and 10 m apart from the fault plane.

Spatial Variation of Thermal Conductivity

The temperature profile is strongly affected by the variations of thermal conductivity of the surrounding material. Kano et al. (2006) interpreted the observed temperature profile assuming the background temperature gradient is constant. They ignored the effect of spatial variation of thermal conductivity on the temperature gradient; however, the spatial variation of thermal conductivity around the Chelungpu fault is large enough to affect the interpretation of the temperature anomaly (Matsubayashi et al., 2005). Using thermal conductivity data in Hole A, Tanaka et al. (2007) reinterpreted the temperature data by Kano et al. (2006) and suggested that the temperature signature detected by Kano et al. (2006) might be a result of thermal conductivity fluctuations, rather than a residual heat from frictional faulting. Tanaka et al. (2007) measured the thermal conductivity with core soaked in epoxy resin to fill the cracks. Doing this introduces error in the measurement of thermal conductivity because of the low value of thermal conductivity of epoxy resin compared to rocks. The effect of epoxy resin is not well evaluated. Their data, in addition, is not sampled around fault zone, which brings error to the prediction of temperature variation. To extract the heat signature produced by fault slip, we had to make

measurements of the spatial variation of material thermal conductivity and examine its effect.

The relationship between temperature gradient (dT/dz) and thermal conductivity, κ , at depth, z , is

$$\frac{dT}{dz} = \frac{q}{\kappa(z)} \quad (3)$$

where q is heat flow. Assuming constant q , we can predict a temperature variation produced only by the spatial variation of κ ,

$$T(z) = q \int \frac{1}{\kappa(z)} dz \quad (4)$$

This means that the temperature gradient produced by constant heat flow is not constant in the medium that has spatial variation of thermal conductivity. Here we predict the background temperature gradient in the temperature profile from the thermal conductivity measured using the core samples of Hole B (Matsubayashi et al., 2005). They measured the thermal conductivity every 0.04–1.5 m for the cores in which water content is carefully preserved before the measurement. We assume that the thermal conductivity, and thus lithology and porosity, in Hole A and Hole B are continuous with 26-m depth difference. Figure 3 shows the predicted temperature profile assuming a constant heat flow of 60 mW m⁻² together with the observed temperature anomaly. The depth of Hole B is shifted by 26 m, which is the difference between the 1111 m fault zone detected in Hole A and the 1137 m fault zone in Hole B. To calibrate the response delay included in the observed temperature anomaly that is caused by thermal inertia of the temperature instrument, observed and predicted temperature anomalies are low-pass

filtered (40 m). We can see peaks in the predicted temperature anomaly (1110 m, 1150 m, and 1190 m) compared to the observed temperature anomaly (1110 m and 1190 m). Those peaks in the corrected temperature observations reflect variations of thermal conductivity that are caused by differences of rock type and porosity around the fault zone.

The peak in the predicted temperature profile is smaller than the observed temperature anomaly around 1111 m, which is modeled as the heat signature of fault slip in Kano et al. (2006), and is considered to be a temperature increase superimposed on background temperature fluctuation. The contribution of residual frictional heat produced by the fault slip is then smaller than the peak modeled in Kano et al. (2006). Thus, their estimation of heat produced gives an upper bound of heat generated by fault slip. The apparent coefficient of friction is estimated to be 0.04–0.08. Laboratory

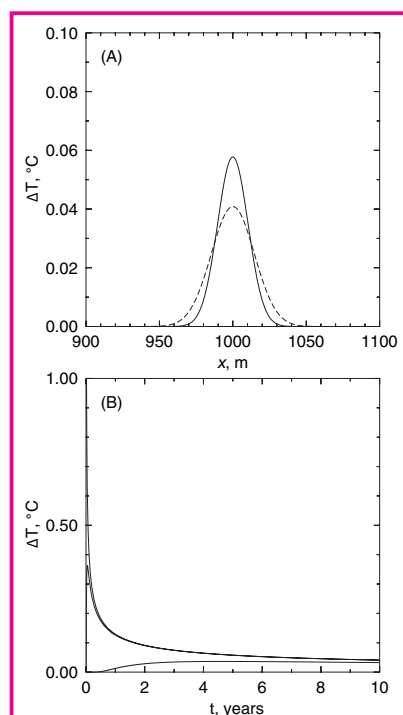


Figure 2. [A] Spatial and [B] temporal variations of temperature signature calculated for $u = 6$ m.

determinations of the static coefficient of friction are generally quite high, 0.6 to 0.7 (Byerlee, 1978) or 0.35 to 0.5 for shales (Morrow et al., 1992), and would produce much higher amounts of heat if these values are used for the dynamic coefficient of friction.

The assumption that the thermal conductivities in Hole A and Hole B are continuous is not necessarily true, since the lithology and thermal property may be three-dimensionally inhomogeneous. The best way to remove the background temperature profile is to use thermal conductivity data from Hole A to predict the temperature fluctuations contained in the temperature measurements from Hole A. There is, however, applicable thermal conductivity data measured only from the core of Hole B. To model the residual frictional heat more precisely, we need an appropriate depth correction between Hole A and Hole B.

Summary

Measuring temperature around the fault zones is a way to obtain knowledge of frictional heat produced during earthquakes and thus the energy budget, which are key unknown parameters that are necessary for understanding the physical process of earthquake ruptures. The spatial variations of material thermal conductivity may be another factor that affects the temperature signature, which is sometimes very similar to the temperature signature produced by the frictional heat of fault slip. To obtain the correct background temperature profile, we need to correct the observed temperature signature using thermal conductivities of the formation. When we make temperature measurement to seek residual frictional heat along the fault, it is important to measure material thermal properties that have enough resolution to remove the background temperature fluctuations. In our particular case, we do not have enough thermal conductivity data from Hole A to completely calibrate the temperature signature. The calculated heat in our present results was an upper bound, and it implies a very low level of dynamic friction during faulting for this region of large slip. The low level of friction we obtained needs to be confirmed for other events, and, if verified, indicates that low friction mechanisms are needed to explain the dynamic rupture process of large earthquakes.

Acknowledgements

This work was partially supported by the Kyoto University 21st Century Center of Excellence (KAGI21) and other Grants in Aid for Scientific Research (16253003) from the Ministry of Education, Culture, Sports, Science, and Technology of Japan and the National Science Council of Taiwan.

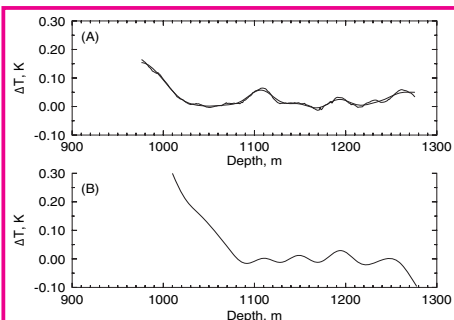


Figure 3. [A] Observed temperature anomaly in Hole A and [B] temperature anomaly predicted from the thermal conductivity measurement of core from Hole B. The depth of Hole B is shifted by 26 m, which is the difference between the 1111 m fault zone detected in Hole A and the 1137 m fault zone in Hole B. Thick lines shows the temperature anomalies that are low pass filtered with cutoff length of 40 m.

References

- Brune, J., Henyey, T., and Roy, R., 1969. Heat flow, stress, and rate of slip along the San Andreas fault, California. *J. Geophys. Res.*, 74:3821–3827.
- Byerlee, J.D., 1978. Friction of rocks. *Pure Appl. Geophys.*, 116:615–626, doi:10.1007/BF00876528.
- Kano, Y., Mori, J., Fujio, R., Ito, H., Yanagidani, T., Nakao, S., and Ma, K.-F., 2006. Heat signature on the Chelungpu Fault associated with the 1999 Chi-Chi, Taiwan earthquake. *Geophys. Res. Lett.*, 33:L14306, doi:10.1029/2006GL026733.
- Lachenbruch, A.H. and Sass, J.H., 1980. Heat flow and energetics of the San Andreas fault zone. *J. Geophys. Res.*, 85:6185–6222.
- Ma, K.-F., Song, S.-R., Tanaka, H., Wang, C.-Y., Hung, J.-H., Tsai, Y.-B., Mori, J., Song, Y.-F., Yeh, E.-C., Sone, H., Kuo, L.-W., and Wu, H.-Y., 2006. Slip zone and energetics of a large earthquake: Results from the Taiwan Chelungpu-fault Drilling Project (TCDP). *Nature*, 444:473–476, doi:10.1038.
- Matsubayashi, O., Lin, W., Hirono, T., Song, S., and Hung, J., 2005. Characterization of unfractured wall rocks of TCDP Hole-B by combination of thermal-property and TDR measurements in laboratory. *Eos Trans. AGU*, 86(52), Fall Meet. Suppl., Abstract T51A-1321.
- Morrow, C., Radney, B., Byerlee, J., 1992. Frictional strength and the effective pressure law of montmorillonite and illite clays. In Evans, B., and Wong, T.F. (Eds.), *Fault Mechanics and Transport Properties of Rocks*. San Diego, Calif. (Academic Press), 69–88.
- Officer, C.B., 1974. *Introduction to Theoretical Geophysics*, New York (Springer-Verlag).
- Scholz, C.H., 2002. *The Mechanisms of Earthquake Faulting, 2nd Edition*, New York (Cambridge University Press), 158–167.
- Tanaka, H., Chen, W.M., Kawabata, K., and Urata, N., 2007. Thermal properties across the Chelungpu fault zone and evaluations of positive thermal anomaly on the slip zones: Are these residuals of heat from faulting? *Geophys. Res. Lett.*, 34: L01309, doi:10.1029/2006GL028153.
- Terada, T., 1930. On the heat generated by the deformation of the Earth crust. *Bull. Earthquake Res. Inst.*, 8:377–383.

Authors

Yasuyuki Kano, Jim Mori, Ryo Fujio, Takashi Yanagidani, and Setsuro Nakao, Disaster Prevention Research Institute, Kyoto University, Gokasyo, Uji, 611-0011, Japan., e-mail: kano@rcep.dpri.kyoto-u.ac.jp.

Hisao Ito, Japan Agency for Marine Earth Science and Technology, 3173-25, Showa-machi, Kanazawa-ku, Yokohama, Kanazawa, 236-0001, Japan.

Osamu Matsubayashi, National Institute of Advanced Industrial Science and Technology, No.7, Higashi 1-1-1, Tsukuba, 305-8567, Japan.

Kuo-Fong Ma, National Central University, No.300, Jhongda Road, Jhongli City, Taoyuan County, 32001, Taiwan (R.O.C.).

The Coseismic Fault Weakening Processes Inferred from Frictional and Transport Properties of Fault Rocks, TCDP

by Hiroki Sone, Hiroyuki Noda, and Toshihiko Shimamoto

doi:10.2204/iodp.sd.s01.06.2007

Faults weaken during coseismic slip, and many factors affect the weakening process. Among these are the frictional properties and permeability of fault-consisting materials. The Taiwan Chelungpu-fault Drilling Project recovered cores from 500 m to 2000 m depth, penetrating several distinct major fault planes that are likely the slip planes from the 1999 Chi-Chi Earthquake (Ma et al., 2006). We measured transport properties of fault rocks and conducted high-velocity friction experiments using drill core samples from two fault zones at 1111 m and 1153 m depths (FZA1111 and FZA1153), and attempted to reconstruct the coseismic fault weakening processes due to the change in frictional coefficient and the effect of thermal pressurization (Sibson, 1973).

Gas permeability of the fault rock samples were measured in a tri-axial apparatus using a steady-flow method with nitrogen gas for several pore pressure gradients (0.1–2.0 MPa) at effective pressures up to 140 MPa. Results show that permeability values range between 10–14 and 10–18 m², and also that permeability is 1–2 orders lower in FZA1111 than in FZA1153. Data under various pore pressure gradients allowed us to subtract the Klinkenberg effect for gas permeability, and thus we estimate the water permeability to be several factors lower. High-velocity frictional experiments were conducted at a normal stress of 0.7 MPa, using a high-velocity ring-shear friction apparatus. Velocity was continuously controlled so that the velocity history reproduces the coseismic slip history derived from a study based on waveform inversions (Ji et al., 2003). The frictional coefficient decreased with acceleration and slip down to 0.1–0.2, and then recovered as the fault slip decelerated to a level below its initial friction. This indicates that a velocity weakening behavior was observed as the fault weakened by slip weakening as well.

The coseismic fault weakening process was modeled using these laboratory-derived physical properties based on equations of thermal pressurization by Lachenbruch (1980). The overall features of the resulting fault strength curve matched well with fault traction curves from inversion studies (see Fig. 1). Also the introduction of thermal pressurization seemed to

enhance the difference between laboratory- and inversion-derived curves, in terms of both stress drop and weakening distance, D_c . However, temporal resolutions of waveform inversions are limited by the frequencies of the waveforms used, and thus the stress drops and weakening distances are not directly comparable. Recent studies show that inversion results preserve information on the seismological fracture energies accurately, but not the stress drop values and weakening distances (Guatteri and Spudich, 2000). We determined the apparent seismological fracture energies from the laboratory derived curve, but the physical interpretation of such manipulation was indefinite. It is important to understand which features are comparable, and which are not, between the laboratory-determined fault strength curves and traction curves derived from seismological studies.

References

- Guatteri, M. and Spudich, P., 2000. What can strong-motion data tell us about slip-weakening fault-friction law? *Bull. Seismol. Soc. Am.*, 90:98–116, doi:10.1785/0119990053.
- Ji, C., Helmberger, D. V., Wald, D. J. and Ma, K. F., 2003 Slip history and dynamic implications of the 1999 Chi-Chi, Taiwan, earthquake. *J. Geophys. Res.* 108(B9): 2412, doi:10.1029/2002JB001764.
- Lachenbruch, A.H., 1980. Frictional heating, fluid pressure, and the resistance to fault motion. *J. Geophys. Res.*, 85:6097–6112.
- Ma, K.F., Tanaka, H., Song, S.R., Wang, C.Y., Hung, J.H., Tsai, Y.B., Mori, J., Song, Y.F., Yeh, E.C., Soh, W., Sone, H., Kuo, L.W., and Wu, H.Y., 2006. Slip zone and energetics of a large earthquake from the Taiwan Chelungpu-fault drilling project. *Nature*, 444:473–476, doi: 10.1038.
- Sibson, R.H., 1973. Interactions between temperature and pore fluid pressure during an earthquake faulting and a mechanism for partial or total stress relief. *Nature*, 243:66–68.

Authors

Hiroki Sone, Hiroyuki Noda, and Toshihiko Shimamoto, Department of Geology and Mineralogy, Division of Earth and Planetary Sciences, Graduate School of Science, Kyoto University, Kitashirakawa Oiwakecho, Sakyo-ku, Kyoto, 606-8502, Japan. e-mail: shima@kueps.kyoto-u.ac.jp

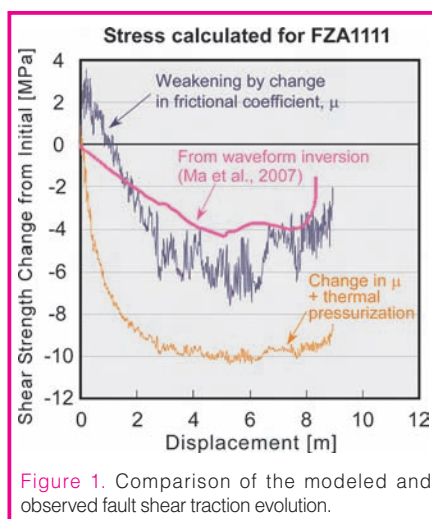


Figure 1. Comparison of the modeled and observed fault shear traction evolution.

Drilling and Completion Challenges in Fault Zones: Lessons Learned from ICDP Projects

by Bernhard Prevedel

doi:10.2204/iodp.sd.s01.25.2007

Introduction

Scientific drilling projects conducted within the framework of the International Continental Scientific Drilling Program (ICDP) and the German Continental Deep Drilling Program (KTB) represent important milestones in fault zone (FZ) drilling. This abstract intends to highlight the technical problems and potential solution pathways in such drilling programs as well as their business implications in today's hydrocarbon hype. Special attention will be paid to the fact that scientific wells today are no longer seen as pure drilling events, but rather as long-term downhole observatory installations, requiring specialized completion technology and advanced planning before drilling.

Lessons from the KTB and ICDP Projects

During the 9.1 km ultra deep KTB drilling program in Germany several fault zones in the drilled amphibolite facies crystalline rock suite were truncated. Severe drilling problems occurred primarily at a depth between 6.9 and 7.3 km depth in a main fault zone characterized by cataclasis, secondary mineralization, fluid inflow and a pronounced seismic reflectivity of the whole steeply dipping fault zone. Main contributors to the difficulties were stress-induced breakouts that increased rapidly with time especially in the central part of the fault to up to ten times the nominal drilled volume, as observed through repeated caliper logs. The other factor creating drilling setbacks were caliper reduction in a zone consisting of chlorite gneisses at 8300 m depth. Both issues finally made additional cementing, sidetrack drilling, or protracted casing setting necessary, and led to a time loss and a cost overrun of approximately 20%.

Similar breakout phenomena were observed in the drilling of main hole of the San Andreas Fault Zone Observatory at Depth (SAFOD), where the 8" hole section developed cave-outs of 20" and more in the lower 60 degree deviated section of the well from approximately 3.0 to 4.0 km, a depth range where the active trace of the San Andreas Fault is suspected.

Another observation during the drilling of fault zones is sudden changes in formation fluid pressure. For example, during the drilling of the 1000-m-deep Corinth borehole, a pressure surge of approximately 10 bars was observed at a depth of 760 m when penetrating the fault.

A selection of the most important lessons learned from previous drilling efforts in fault zones includes; 1) careful planning with multi-disciplinary industry and academia advisory panels is necessary, including extended well-bore stability planning; 2) use of a top drive plus vertical steering system with downhole motors is advised, to ensure operational speed and precision in drilling, and also in logging (including use of downhole MWD/LWD systems); 3) expandable casings or casing-drilling systems for loose and unstable formations or extended casing scheme with additional casings needs to be planned beforehand; 4) enhanced pumping and mud carrying capacity of the drilling mud to balance under- or overpressures is necessary; 5) wireline coring techniques for successful and rapid sample gain are advantageous; 6) synergy between research drilling projects and programs need to be developed; and 7) designs of scientific wells for life are necessary.

The last point represents a significant paradigm change from the way we regarded scientific well drilling in the past. Today such wells are planned and designed for long life, involving permanent monitoring arrays and completion technologies, very similar to the ones employed in the oil and gas industry.

Downhole Observatories

Completion technology is a term from the oil field industry that stands for the equipment installed in a well after the drilling phase, enabling the production of either (i) hydrocarbons in oil and gas or (ii) the acquisition of data from research wells. Although the objectives are different, the equipment designs and investment efforts are almost the same.

Long-term downhole data acquisition today is ensured from completed scientific wells by means of permanent monitoring technology. They can in principle be categorized in two basic embodiments:

Type-1: Outside the casing cemented cables and sensors (outside casing arrays = OCA), which are primarily based on (i) fiber-optic sensors and cables for distributed temperature, pressure, rock strain and acceleration measurements, as well as (ii) analogue sensors on copper cables for electric conductivity, seismic and pressure measurements.

The main characteristics for this entirely analogue sensor technology are the requirement for a pressure-isolating wellhead outlet design, its system ruggedness combined with highest redundancy and no external power requirement.

Type-2: Inside the casing semi-permanently installed tools (inside casing arrays = ICA), which are instruments run primarily on fiber/electrical armoured cable, like digital 3-component seismometer, tiltmeter, accelerometer and other logging equivalent sensors.

Main features of this primarily digital technology are its persistent problems of cable survival in long-term deployments, sensitivity to gas attack on elastomers, poor sensor coupling to the borehole wall, limited overall system redundancy, but good stability of the sensors in a high temperature environment.

Present Drilling Market

One key indicator of today's market development is the utilization of the worldwide rig fleet, both for marine and land drilling units. Their day-rates rose since 1994 by a factor of six to seven, with a rig utilization today consistently hitting 100%. As with rig rates, the service industry increased prices recently for equipment and services and further tightened delivery conditions. On an average, prices rose +18% in the last 6 months and delivery times for critical well equipment increased from half a year to one year and in some instances even to 17 months.

Due to the lack of drilling equipment suitable for scientific drilling and coring, the GFZ (GeoForschungsZentrum) Potsdam has decided to design and invest in its own proprietary scientific drilling rig, named Innova Rig. This totally new and **fully hydraulic rig concept, built by a tunnel bore manufacturing works** in southern Germany will be delivered

by the end of 2007. The rig will be operated by a joint industry cooperation company for the drilling of both commercial as well as research projects. GFZ will be the owner of the rig while the drilling contractor partner will be in charge of staffing and daily operations.

The technical highlights of Innova Rig will be its special hybrid rig design and on-board equipment aiming especially at scientific drilling and integrating well proven drilling techniques around a variable application of rotary drilling and coring with the least possible environmental impact. Based on its container-module design, the hook-load will be directly supported by substructure, and rig moves will be greatly reduced in time due to optimized modular truck loads.

The entire energy management of all rig modules is designed from a holistic viewpoint, with highest safety standards due to full automation, integrated noise attenuation design and reduced footprint of the entire drill site. The hoist and feed system are fully hydraulic (no drilling line), constructed to handle doubles including a pipe manipulator to store the tubulars outside the rig on the pipe rack including a torque unit on the catwalk. (See Table 1.)

With this equipment planned, built, and operated for science, a land equivalent to the Integrated Ocean Drilling Program (IODP) research drilling vessels will be at hand for research projects and increase efficiency and hence reduce the high costs of such endeavors. Due to the dual-use concept in industry and academia however, the Innova Rig can be set aside for commercial industry operations and therefore maximize rig utilization and return of investment.

Concluding Remarks

Fault-zone and seismogenic zone drilling projects are complex and must be considered in their planning as well as operation phase as high-tier drilling operations. Due to the present boom in hydrocarbon and mineral exploration, the existing drilling equipment is very short in supply and quite expensive. The special engineering and equipment needs for scientific fault-zone drilling and monitoring instrumentation are not available off the shelf. Therefore, an extended close communication and interaction with research and industry experts are crucial. The establishment of advisory panels, the enhancement of exchange between IODP and ICDP and the joint development of procedures and engineering processes will be important steps to ensure safe fault-zone drilling and stable long-term monitoring observatories at depth in the future.

Author

Bernhard Prevedel, ICDP/OSG (Operational Support Group), GFZ-Potsdam, Telegrafenberg A34, D-14473, Potsdam, Germany, e-mail: prevedel@gfz-potsdam.de.

Table 1. Technical specifications of Innova Rig:

Drilling depth	3500–5000 m
Regular hook-load	3500 kN
Nominal rotary speed	220 rpm (max.)
Rotary torque	40–75 kNm
Wire-line coring speed	500 rpm (max.)
Wire-line coring torque	12–18 kNm
Tripping speed	500 m/hr
Hoist cylinder stroke	22 m
Drive power upper limit	4000 kw
Rid weight (approx.)	370 tons
Mud pumps	3 x 1000kW
WL coring pump	1 x 350 kW
Mud pressure	350 bar (max.)
Mud tank system	240 m ³
General set	3 x 1540 kVA
Rack capacity	>7000 m
Wire-line coring winch	5500 m
Coring line	d=12.7 mm

Drilling Challenge for the NanTro Fault Zone

Drilling by *Chikyu*

by Kazuhiro Higuchi and Shomei Kobayashi

doi:10.2204/iodp.sd.s01.37.2007

The *Chikyu* is a riser-equipped, dynamically positioned, scientific drill ship owned and operated by the Japan Agency for Marine-Earth Science and Technology (JAMSTEC). *Chikyu* was delivered in 2005 and is preparing for the IODP scientific drilling operation (Curewitz et al., 2006; Taira, 2005). For specifications, see Table 1.

To access scientific targets, deeper than ever before beneath the deep-sea floor, the target was set to 7000 m, in water depths initially up to 2500 m, eventually as deep as 4000 m (Taira, 2005). To drill deeper, weighted mud is required to keep holes **stable within the pressure window** higher than pore pressure and lower than fracture pressure. For the circulation of mud and transportation of gas/cuttings, specially designed risers are prepared for *Chikyu*. The high pressure BOP (Blow Out Preventer) aboard *Chikyu* is designed to control the borehole pressure balanced with mud hydrostatic pressure, even in occasional under-balanced conditions. Also, **high-strength drill pipes are necessary** to access deeper targets to endure high torque and high tensile stress. These drill pipes are designed to have large inside diameters to pass through the wireline retrievable core barrel. Several sizes of cemented casings are required to drill through various pressure/stress zones or fractures.

Although *Chikyu* has various state of the art equipment as described above for the deeper scientific drilling, well planned **engineering is the key to achieving the scientific targets** without encountering drilling hazards. Potential drilling hazards might be posed by sea and weather conditions, **weak formation, shallow gas, low fracture gradients, abnormal pressure, high stress, fractured faults, high temperatures, or human error (Fig. 1).**

The drilling engineer's responsibility is to accomplish the objective of the hole, safely, efficiently and economically. The objective might be the access to the target position, depth or formation, data from wireline logging or LWD, samples of core/cuttings/gas/water, testing, or the deployment of monitoring systems.

Table 1: *Chikyu* Specifications

Overall Length	210 m
Breadth (Mid)	38 m
Depth (Mid)	16.2 m
Draft	9.2 m
Derrick Height	107 m
Drillstring Length	10,000 m
Accommodation	150
Speed	~Symbol 10kt

Keys to the success of any drilling are to have accurate pressure, temperature and geology estimation, a **good understanding of what might happen from offset wells, a choice of field-proven reliable tools and procedures, a simple design, preparation for back-up tools and contingency plans, and good communication with related people.**

NanTroSEIZE (Tobin and Kinoshita, 2006) will commence from 2007 to drill a complex splay fault zone. The challenge lies in the lack of offset well data and difficulties regarding predictions of pressure, temperature, and stress. NanTroSEIZE drilling is the first scientific drilling by *Chikyu* and the first access to a large active splay fault of a plate-boundary thrust.

As scientific success is not achieved without drilling success, cooperation and communication between drilling engineers and scientists are **essential points to consider.**

References

- Curewitz, D., Kuramoto, S., and Kawamura, Y., 2006. Drilling vessel *Chikyu*: Status, capabilities, and current operations. *Sci. Drill.*, 3:52–53.
- Taira, A., 2005. The *Chikyu*: Meeting the challenges of a new scientific drilling era. *Sci. Drill.*, 1:32–33.
- Tobin, H. and Kinoshita, M., 2006. NanTroSEIZE: The IODP Nankai Trough seismogenic zone experiment. *Sci. Drill.*, 2:23–27.

Authors

Kazuhiro Higuchi and Shomei Kobayashi, Center for Deep Earth Exploration (CDEX), Japan Agency for Marine-Earth Science and Technology (JAMSTEC), 3173-25 Showa-machi, Kanazawa-ku, Yokohama, Kanagawa 236-0001, Japan, e-mail: higuchik@jamstec.go.jp.

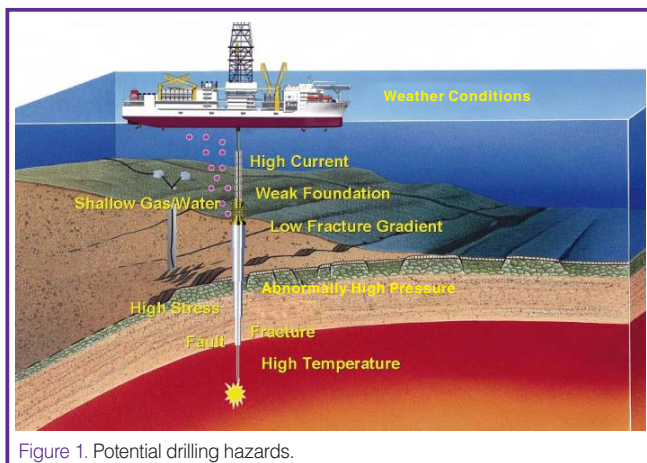


Figure 1. Potential drilling hazards.

Coring Techniques for Scientific Investigation of Faults

by Dennis L. Nielson

doi:10.2204/iodp.sd.s01.24.2007

Introduction

Faulted and fractured rocks are difficult to core because of differential hardness, angular unsupported fragments, under- or over-pressured fluids, and overall fault architecture. Often, the most scientifically interesting parts of the fault are the most difficult to recover. The scientific objectives of the drilling and the techniques required (sampling, logging, monitoring), as well as the depth and geometry of the target, will determine the drilling methods used.

Operational Issues

The character of fault zones often leads to drilling problems. Due to the abrasive nature of faults, the bit may break or more likely wear on the face or inner and outer gauges. Bits may also plug with a piece of core, or their waterways may become blocked by clay or rock fragments. Cores may jam in the bit or core barrel due to small shifts along fractures during the drilling process. Bits can be custom-designed for specific drilling conditions, and bit life and penetration rate may be improved by size and placement of diamonds, hardness of matrix, and location and geometry of waterways.

Hole stability is a critical factor in operational efficiency; it can be controlled by the circulation of mud whose composition and circulation rate can be optimized. Coring in fault zones often encounters different fluid pressure within short distances. Formation overpressure (greater than hydrostatic) leads to the flow of fluids into the hole, and underpressure results in the loss of circulation in permeable rock. Under conditions where circulation is lost, drilling mud flows into the formation rather than returning to the surface. Cuttings can build up in the hole and stick to the drill pipe. This condition tends to be more serious in rotary drilling than coring, where it is common to core ahead without mud returning to the surface. Lightweight injected grout can be used to shut off lost circulation zones and stabilize fractured rock.

A fault can influence directional control, hole inclination, and doglegs (rapid changes in direction). In general, holes tend to curve into a fault, particularly when the core hole and the fault are both at steep angles. Additionally, the drill bit can become "trapped" within a fault and wander down a soft

component, unable to escape. In most cases it is best to plan crossing the fault at as high an angle as possible.

The location of a fault in the subsurface is often uncertain, and intersecting a steeply dipping structure with a vertical borehole is problematic (Are we there yet?). Many coring systems are designed to drill holes at an angle as well as vertically. Directional coring from a borehole is also possible either using a wedge or whip-stock or downhole mud motors. Any of these options allows multiple intersections of a fault to take place from one borehole (multi-laterals).

Core Quality Control

Core is the principal product of most scientific drilling, and core quality is of utmost concern. High-quality core often requires additional effort, time, and cost. Ideally, the core is a continuous and representative sample of the fault; however, faults are generally broken formations (unless cemented by hydrothermal minerals) and can contain materials of dramatically different hardness. This increases the risk that pieces will be lost or that softer parts of the core may be washed away by the drilling fluid. Once the core is cut, mechanical and thermal stress relief are inevitable and result in the formation of secondary fractures.

Improper core handling can also lead to quality control problems, and it is best to have a well formulated protocol before the drilling phase of the project commences. This is especially important when different people are responsible for handling the core. Problems can result during removal of core from the core barrel, and during boxing, labeling, and transportation.

Bore Hole Quality Control

The process of drilling changes the borehole environment from *in situ* conditions. Mechanical disruption results from imposing a hole where there was previously solid rock, and borehole breakouts occur as stress is released. Circulation of drilling mud fills the hole with a fluid that is different from formation fluids in temperature, pressure, and composition. Separate zones that originally had distinct temperature, pressure, and chemistry mix in the borehole. The return to pre-drilling temperatures may require some time (or may never take place). Solids (mud, cement, lost circulation material [LCM]) have probably invaded the rock along faults,

fractures, and intergranular spaces. Fault heterogeneity can mean that the contamination itself may not be uniform. Chemical and physical tracers can be introduced to assess contamination of the core by the drilling fluid.

Drilling Rigs and Coring Techniques

Several different types of drilling rigs are available, and they must be chosen to conform to the objectives of the investigation. Rotary rigs are designed to drill a hole with a high penetration rate, and they are principally used in petroleum and groundwater applications. Rotary drilling uses high weight on bit (WOB) and low rotation rate (rpm) in order to crush the rock. High mud volumes are needed to clear the crushed rock from the borehole. Core can be collected by a rotary rig using a conventional barrel, but the quality is subject to the operating parameters of high WOB and low rpm. In addition, the entire drill string must be tripped to recover core from the conventional barrel. This process can be time-consuming, and conventional coring is normally used for spot coring within a zone of interest.

Diamond coring rigs are designed to collect core samples. They do this by cutting the rock with a diamond bit with relatively low and precise control of the WOB and with high rotation rates. Generally, the penetration rate for coring is less than with rotary methods, and the cost/meter can be relatively high. However, the sample is generally superior to that collected by a rotary rig using a conventional barrel. Core is generally collected by wireline systems where the core barrel is retrieved to the surface using a wire while the drilling rods remain in the hole. Wireline coring was developed for mining applications, and coring equipment comes in standard sizes (PQ = 85 mm, HQ = 63.5 mm; NQ = 47.6 mm), although the labels are not particularly intuitive. Larger sizes may be more beneficial in the sampling of faulted rock. A variation on this technique uses a triple tube where the core is collected into a metal or plastic liner that is placed within the core barrel. The core is slightly smaller (PQ₃ = 83.0 mm, HQ₃ = 61.1 mm), but there is also much less sample disruption.

Slim-hole wireline coring systems are designed to core a telescoped hole where smaller standard sizes are designed to core through larger sizes (PQ>HQ>NQ). Therefore, if penetration is stopped, rods can be left in the hole as casing, and the next smaller size system can be used to continue coring.

Because of the need for the characteristics of both rotary and diamond coring, several hybrid rigs have been constructed. These rigs can drill rotary and set casing and then switch to wireline diamond coring for the collection of core samples. Examples of this type of rig include the DOSECC (Drilling, Observation and Sampling of the Earth's Continental Crust) Hybrid Coring System (DHCS) that has

been used to core the Long Valley, Hawaii, and Chicxulub Scientific Drilling Projects. The DHCS can attach to most large rotary rigs, thereby limiting its shipping costs. ICDP's new Innova Rig is a self-contained rig that performs both coring and rotary functions.

Concluding Statement

Faults often have complex histories and, as a result, they show three-dimensional architecture with intricate cross-cutting features. A borehole (core sample) is small, and by itself is largely one-dimensional. Because of the complexity of faults and the quality control issues discussed above, it is advantageous to incorporate logging to support the interpretation of the core. In particular, imaging logs are of great value for their ability to orient fractures in the core and, in some cases, to document material that was lost during the coring process. Temperature logs are also of great value in determining the location and characteristics of zones where fluids are either entering or exiting the borehole. Multiple completions drilled directionally from the same borehole are useful for documenting fault heterogeneity.

Author

Dennis L. Nielson, DOSECC, Inc., P.O. Box 58857, Salt Lake City, Utah 84158-0857, U.S.A., e-mail: dnielson@dosecc.org.

Core Handling and Real-Time Non-Destructive Characterization at the Kochi Core Center: An Example of Core Analysis from the Chelungpu Fault

by Weiren Lin, Tetsuro Hirono, En-Chao Yeh, Wataru Tanikawa, and Wonn Soh

doi:10.2204/iodp.sd.s01.35.2007

Abstract

As an example of core analysis carried out in active fault drilling programs, we report the procedures of core handling on the drilling site and non-destructive characterization in the laboratory. This analysis was employed on the core samples taken from Hole B of the Taiwan Chelungpu-fault Drilling Project (TCDP), which penetrated through the active fault that slipped during the 1999 Chi-Chi, Taiwan earthquake. We show results of the non-destructive physical property measurements carried out at the Kochi Core Center (KCC), Japan. Distinct anomalies of lower bulk density and higher magnetic susceptibility were recognized in all three fault zones encountered in Hole B. To keep the core samples in good condition before they are used for various analyses is crucial. In addition, careful planning for core handling and core analyses is necessary for successful investigations.

Introduction

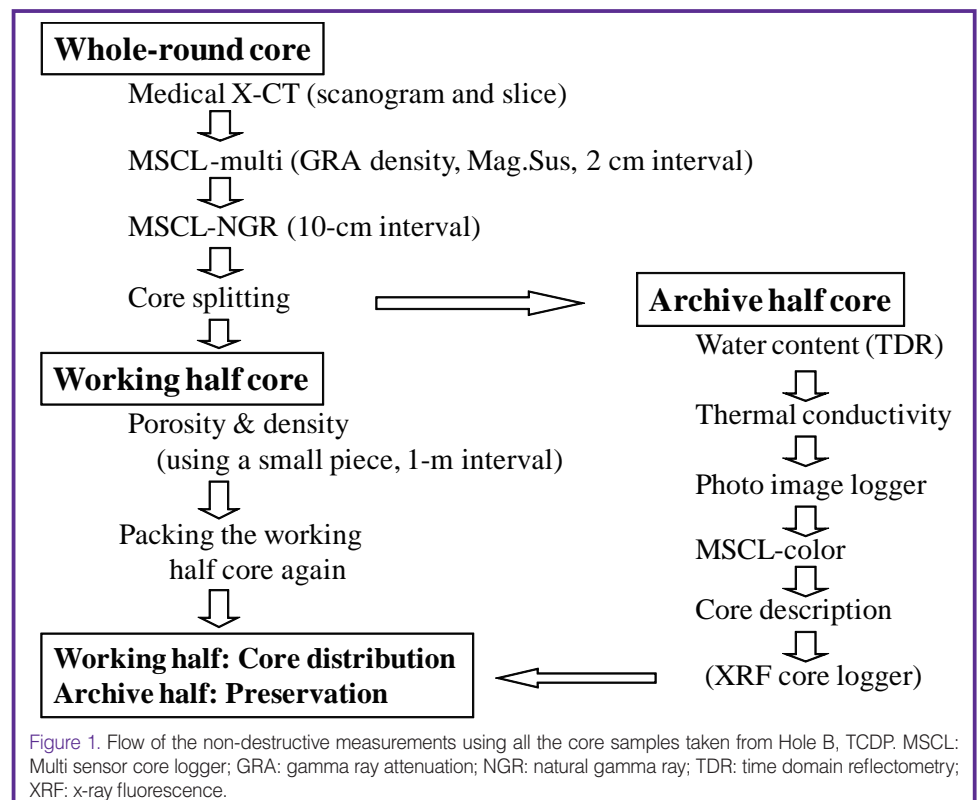
An enormous and damaging earthquake (Mw7.6) occurred in west-central Taiwan on 21 September 1999 due to the convergence between the Philippine Sea and Eurasian plates (Shin and Teng, 2001). Its epicenter was located at the vicinity of the country town of Chi-Chi, and the hypocenter was at about 10 km depth. Abundant teleseismic observation data of the earthquake revealed that the slip displacement and slip velocity increased to as much as 8 m and 300 cm s^{-1} , respectively, but the high-frequency acceleration decreased when the rupture propagated from south to north. For this reason, it was suggested that the fault at the northern segment was lubricated during rupturing (Ma et al., 2003). In order to solve questions about the mechanism of earthquake generation and rupture propagation of the fault, the Taiwan Chelungpu-fault Drilling Project (TCDP) was undertaken (Ma et al., 2006). The drilling site is

located in the northern segment where a large surface coseismic displacement occurred.

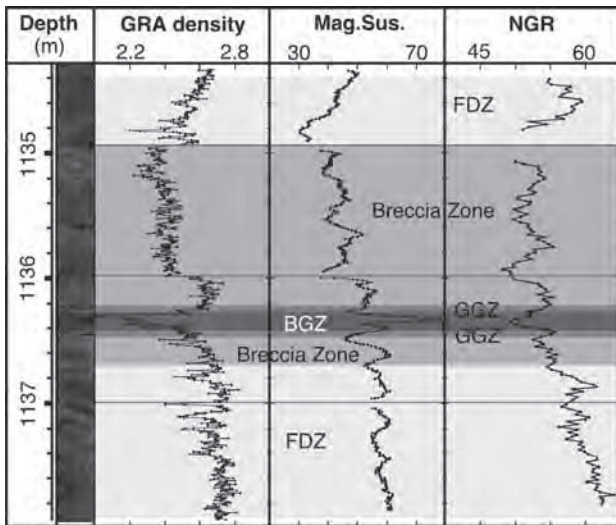
We joined the TCDP and transported all the cores of Hole B taken from the depth range 950–1350 m to the KCC, Japan to conduct continuous non-destructive measurements. From the excellent scientific results, original papers were published (Hirono et al., 2006a, 2006b), while others have been submitted and some are still under preparation. Here, we only report the procedures of core handling and non-destructive characterization and show several valuable examples of the measurement results.

Core Handling on the Drilling Site

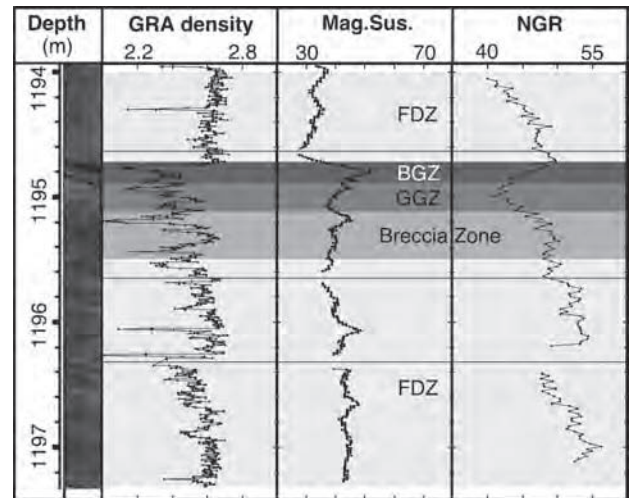
In order to keep the retrieved core samples in good condition, we paid close attention to i) prevent moisture change while the core was undergoing non-destructive measurement, and until the working half cores were split for individual sampling, ii) avoid contact with oxygen, and iii) keep them cool (but not less than 0°C) to minimize possible chemical reactions and/or biological activity. The most



(A) FZB1136



(B) FZB1194



(C) FZB1243

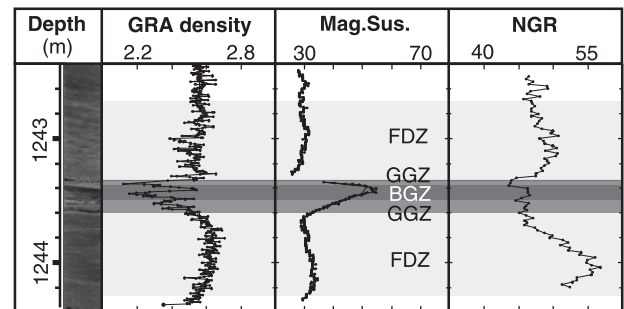


Figure 2 Density, magnetic susceptibility (Mag Sus), and natural gamma ray radiation (NGR) logs from [A] FZB1136, [B] FZB1194, and [C] FZB1243. The units are $g\ cm^{-3}$, 10-5SI, and cps, respectively. FDZ, fracture-damaged zone; BGZ, block gouge zone; GGZ, gray gouge zone (Hirono et al., 2006b).

important thing for on-site core handling is packing the core samples as quickly as possible after core recovery. Needless to say, to prevent mechanical **damaging during the planned shipping or land transporting to the KCC, Japan**, we also filled any gaps between core and the wooden core box with cushioning materials. The flow chart of the routine works of core handling for all the cores of Hole B on the drilling site is as follows:

- Wash cores gently and carefully
- Cut core into an appropriate length to fit the size of core box
- Measure core length
- Take core picture for every 1-m with a scale and a color bar
- Jacket core with a tray half pipe and cover with shrink wrap
- Put core with a wet sponge into an aluminum pack with a very effective sealing ability.
- Replace air in the pack with N2 gas
- Remove extra N2 gas from the pack
- Seal the aluminum pack
- Put core in core box with cushioning materials
- Store the core box in a refrigeration container at 4°C even during shipping and land transporting.

Of course, we paid special attention to fault zone cores in handling them more quickly and carefully.

In order to determine *in situ* stress orientations and to estimate magnitudes, we did anelastic strain recovery (ASR) measurement using a few cores by the same method as Lin et al (2006). Because the anelastic strain recovers **immediately** from the *in situ* stress released by drilling, the measurements have to be conducted as quickly as possible after retrieving the core sample. Therefore, we did it at the on-site laboratory on the drilling site.

Non-Destructive Measurements at the KCC

Figure 1 shows the work flow for non-destructive measurements on the core of Hole B, TCDP conducted at the KCC. First, an x-ray CT image is taken, while the core sample is still in the aluminum wrapping (ideally without any change in moisture and without oxidation). Next the aluminum packaging was opened and subsequent measurements with the MSCL-multi (Multi-Sensor Core Logger), core splitting and the measurement of thermal conductivity were performed in an optimized process in order to minimize waiting time and avoid moisture vaporization. The **physical properties** obtained from the measurements are **GRA (gamma ray attenuation), wet-bulk density, magnetic susceptibility, NGR (natural gamma ray), porosity, dry-bulk density, volumetric**

water content (by Time Domain Reflectometry, TDR indirect measurement), thermal conductivity, and color indexes (L^* , a^* , b^* which correspond to brightness, chromaticity of red-green and blue-yellow, respectively). Moreover, x-ray CT scanograms, slice images on the whole-round core, and optical pictures on split surfaces are available. Unfortunately, the accuracy and reliability of P-wave velocity and electrical resistivity data by the MSCL were low, so that the data need further calibration and discussion before interpretation. In addition, mainly due to a problem with poor smoothness of the split core surface, the analyses to identify chemical elements by using XRF (x-ray fluorescence) core logger are also pending.

Examples of Measurement Results

(1) MSCL measurement results

The Hole B drilling penetrated the Chelungpu fault and recovered core samples ranging from about 950 m to 1350 m in vertical depth. Three fault zones—FZB1136 (fault zone at about 1136 m depth in Hole B), FZB1194, and FZB1243—were recognized in the core samples on-site as series within the Chelungpu fault system. The results of MSCL measurements (see Fig. 2) revealed distinct anomalies, lower wet-bulk densities, and higher magnetic susceptibilities within black gouge zones in all three fault zones (Hirono et al., 2006b). Higher magnetic susceptibilities can indicate that they have experienced intense shearing and/or frictional heating. The non-destructive continuous physical property measurements can provide important preliminary knowledge for understanding the faulting mechanism of the 1999 Chi-Chi earthquake.

(2) An ASR measurement result

We showed an example of the application of the ASR method for stress measurement on the drill core of the TCDP hole penetrated into the active Chelungpu fault. The anelastic strains of a drill core specimen in nine directions, including six independent directions, were measured using wire strain

gauges after having retrieved the core from the borehole to ground level (Lin et al., 2007). The core specimen was sandstone taken from a depth of 592 m in Hole A. Acquired anelastic strains (Fig. 3A) were extensions – they reached several hundred microstrains, which is a level high enough to ensure satisfactory measurement accuracy. These strains were used for a three-dimensional analysis to determine the orientations and estimation of the magnitudes of the principal *in situ* stresses. The orientations determined by the strain data are shown in Fig. 3B. The estimated magnitudes of the maximum, intermediate, and minimum principal stresses are 14.6 MPa, 12.6 MPa, and 12.1 MPa, respectively. The obtained results can be considered as valid; consequently, it can be said that the anelastic strain recovery measurement is well suited to the task of directly determining the orientations of principal *in situ* stresses and of estimating the magnitude of the stresses at great depth. The results of these stress measurements suggest both the orientation and magnitude of current stress at the vicinity of the Chelungpu fault in TCDP holes might be influenced by the fault rupturing.

Summary

As an example of core analysis carried out for the active fault drilling program, we reported the procedures of core handling and non-destructive characterization employed for the core samples taken from Hole B of the Taiwan Chelungpu-fault Drilling Project. Then, we showed two examples of the results; one is the non-destructive physical property measurements carried out at the KCC, Japan. Distinct anomalies of lower bulk density and higher magnetic susceptibilities were recognized in all three fault zones encountered in Hole B. Another example is carried out on the drilling site. Anelastic strain was measured by using a core sample after the *in situ* stress was released. It shows the anelastic strain result was satisfactory and can be used for determining three-dimensional principal stress orientations and estimating their magnitudes. Needless to say, the studies using core samples are important for scientific drilling, specifically for active fault drilling programs. However, it is more important

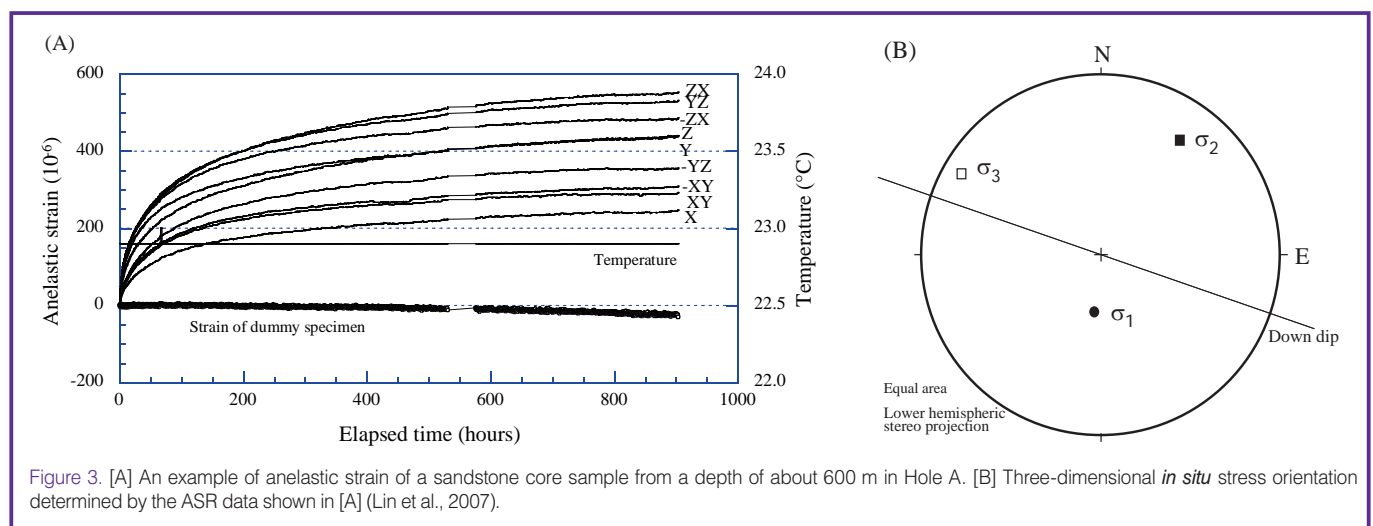


Figure 3. [A] An example of anelastic strain of a sandstone core sample from a depth of about 600 m in Hole A. [B] Three-dimensional *in situ* stress orientation determined by the ASR data shown in [A] (Lin et al., 2007).

to keep cores in the good conditions before they are used for various analyses. Careful planning for core handling and core analysis is necessary for successful investigations.

Acknowledgements

First, we thank the principal investigators, Y.-B. Tsai, C.-Y. Wang, K.-F. Ma, S.-R. Song, and J.-H. Hung of TCDP for giving us the opportunity to use all the cores of Hole-B for the measurements at KCC. We also thank the working group in Japan including Y. Hashimoto, H. Sone, L.-W. Kuo, O. Matsubayashi, K. Aoike, H. Ito, M. Kinoshita, M. Murayama, and other colleagues from CDEX/JAMSTEC and Marine Work Japan, Ltd., and many students from Kochi University. We are very grateful for much kind cooperation of B. Lin and Y. Wei and others of the drilling company, as well as Taiwanese assistants and students from NCU and NTU during the handling of cores on site.

References

- Hirono, T., Ikehara, M., Otsuki, K., Mishima, T., Sakaguchi, M., Soh, W., Omori, M., Lin, W., Yeh, E.-C., Tanikawa, W., and Wang, C.-Y., 2006a. Evidence of frictional melting from disk-shaped black material, discovered within the Taiwan Chelungpu fault system. *Geophys. Res. Lett.*, 33:L19311, doi:10.1029/2006GL027329.
- Hirono, T., Lin, W., Yeh, E.-C., Soh, W., Hashimoto, Y., Sone, H., Matsubayashi, O., Aoike, K., Ito, H., Kinoshita, M., Murayama, M., Song, S.-R., Ma, K.-F., Hung, J.-H., Wang, C.-Y., and Tsai, Y.-B., 2006b. High magnetic susceptibility of fault gouge within Taiwan Chelungpu fault: Nondestructive continuous measurements of physical and chemical properties in fault rocks recovered from Hole B, TCDP. *Geophys. Res. Lett.*, 33:L15303, doi:10.1029/2006GL026133.
- Lin, W., Kwasniewski, M., Imamura, T., and Matsuki, K., 2006. Determination of three-dimensional *in situ* stresses from anelastic strain recovery measurement of cores at great depth. *Tectonophysics*, 426:221–238, doi:10.1016/j.tecto.2006.02.019.
- Lin, W., Yeh, E.-C., Ito, H., Hirono, T., Soh, W., Wang, C.-Y., Ma, K.-F., Hung, J.H., and Song, S.-R., 2007. Preliminary results of stress measurement by using drill cores of TCDP Hole-A: An application of anelastic strain recovery method to three-dimensional *in situ* stress determination, *Terr. Atm. Ocean Sci.*, 18:379–393, doi:10.3319/TAO.2007.18.2.379(TCDP).
- Ma, K.-F., Brodsky, E.E., Mori, J., Ji, C., Song, T.-R.A., and Kanamori, H., 2003. Evidence for fault lubrication during the 1999 Chi-Chi, Taiwan, earthquake (Mw7.6), *Geophys. Res. Lett.*, 30:1244–1247, doi:10.1029/2002GL015380.
- Ma, K-F, Tanaka, H., Song, S.-R., Wang, C.-Y., Hung, J.-H., Tsai, Y.-B., Mori, J., Song, Y.-F., Yeh, E.-C., Soh, W., Sone, H., Kuo, L.-W., and Wu, H.-Y., 2006. Slip zone and energetics of a large earthquake from the Taiwan Chelungpu-fault drilling project. *Nature*, 444:473–476, doi:10.1038/nature05253.
- Shin, T.-C. and Teng, T.-L., 2001. An overview of the 1999 Chi-Chi, Taiwan, Earthquake. *Bull. Seismol. Soc. Am.*, 91:895–913, doi:10.1785/0120000738.

Authors

Weiren Lin, Wataru Tanikawa, and Wonn Soh, Kochi Institute for Core Sample Research, Japan Agency for Marine-Earth Science and Technology, B200 Monobe, Nankoku, Kochi, 783-8502 Japan, e-mail: lin@jamstec.go.jp.

Tetsuro Hirono, Department of Earth and Space Science, Graduate School of Science, Osaka University, Toyonaka 560-0043, Osaka, Japan.

En-Chao Yeh, National Taiwan University, No.1, Sec. 4, Roosevelt Road, Taipei, 106147, Taiwan (R.O.C.).

Third-Party Borehole Seismic Experiments during the Ocean Drilling Program

by Ralph A. Stephen, Stephen A. Swift, S. Thompson Bolmer, and Hartley Hoskins

doi:10.2204/iodp.sd.s01.08.2007

Introduction

The first borehole seismic experiments on DSDP and ODP were two-ship Oblique Seismic Experiments (Stephen, 1979; Stephen, et al., 1979, 1980; Swift, et al., 1988). By recording on the drill ship and shooting explosives out to ranges of 8 km, the upper 1.5 km of the upper crust (Layer 2) adjacent to the borehole could be imaged (Fig. 1; Stephen and Harding, 1983). Azimuthal anisotropy (Stephen, 1981, 1985) and lateral heterogeneity (Stephen, 1988; Swift and Stephen, 1989) could also be studied by shooting circles of shots at a fixed range from the borehole.

Western Atlantic South of Bermuda (DSDP Hole 418, Leg 102)

Third-party borehole seismic experiments on the Ocean Drilling Program began with an Oblique Seismic Experiment at Site 418 in the Western Atlantic south of Bermuda on Leg 102. The experiment confirmed the velocity structure of upper Layer 2 including azimuthal anisotropy and azimuth-dependent scattering. It is interesting to note that travel-

time and amplitude data from two Oblique Seismic Experiments on 110-ma crust in the slow-spreading western North Atlantic and fast-spreading northwestern Pacific show that compressional velocities within layer 2 are, within experimental error, identical (Kong et al., 1985).

Southwest Indian Ridge (Hole 735B, Leg 118)

Normal incidence Vertical Seismic Profiles (VSP) were carried out on ODP Legs 104, 109, and 111 before the VSP at Hole 735B on Leg 118 on the Southwest Indian Ridge. This experiment measured velocities corresponding to Layer 3 which was consistent with the gabbroic petrology of the cores. Anomalously high attenuation was also observed, prompting the hypothesis that the gabbro cored may not actually represent the bulk of Layer 3 material.

Argo Abyssal Plain (Hole 765, Leg 123)

In thick sedimentary sequences VSPs can be very useful in correlating the drilling results with the seismic reflection profiling results. This was demonstrated on ODP Leg 123 which drilled in the Argo Abyssal Plain (Leg 123 Shipboard Scientific Party, 1990a; b). VSPs were also carried out on ODP Legs 127/128, 129, 131, and 146.

Costa Rica Rift (Hole 504B, Legs 111 and 148)

The VSP data acquired at Hole 504B in the eastern equatorial Pacific on Leg 148 helped to constrain the velocity-depth structure at the site (Swift, et al., 1996, 1998a, 1998b) and showed that upper Layer 3 at this site, at a depth of over 2 km into the crust, did not consist of gabbros but rather consisted of the lower portions of the sheeted dykes (Detrick et al., 1993). VSPs were also carried out on Leg 156.

Gas Hydrates on the Blake Ridge (Holes 994, 995, and 997; Leg 164)

Both offset and normal incidence VSPs were run on Leg 164 to study the seismic velocity structure of gas hydrates on the Blake Ridge, offshore South Carolina. Seismic velocities measured in three drill holes through the gas hydrate deposit indicated that substantial free gas exists to at least 250 m beneath the bottom-simulating reflector (BSR; Holbrook

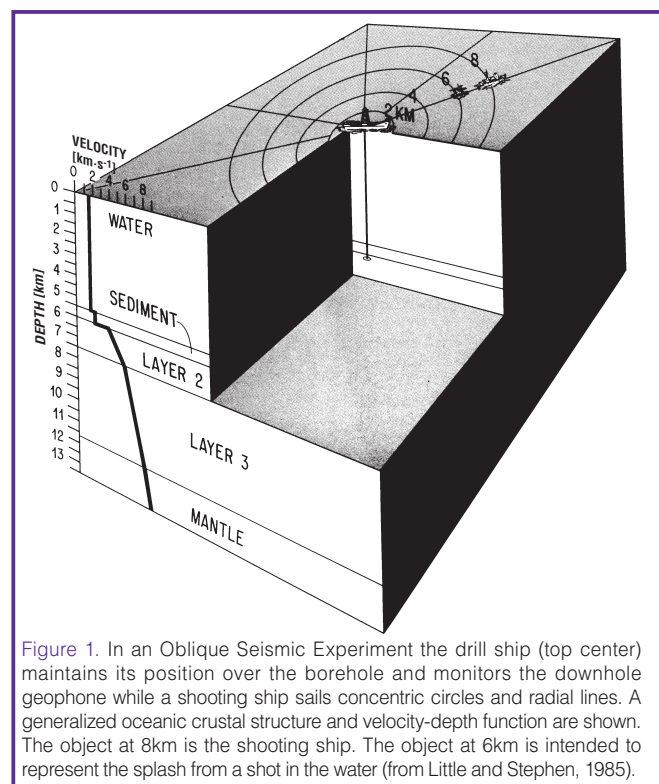


Figure 1. In an Oblique Seismic Experiment the drill ship (top center) maintains its position over the borehole and monitors the downhole geophone while a shooting ship sails concentric circles and radial lines. A generalized oceanic crustal structure and velocity-depth function are shown. The object at 8km is the shooting ship. The object at 6km is intended to represent the splash from a shot in the water (from Little and Stephen, 1985).

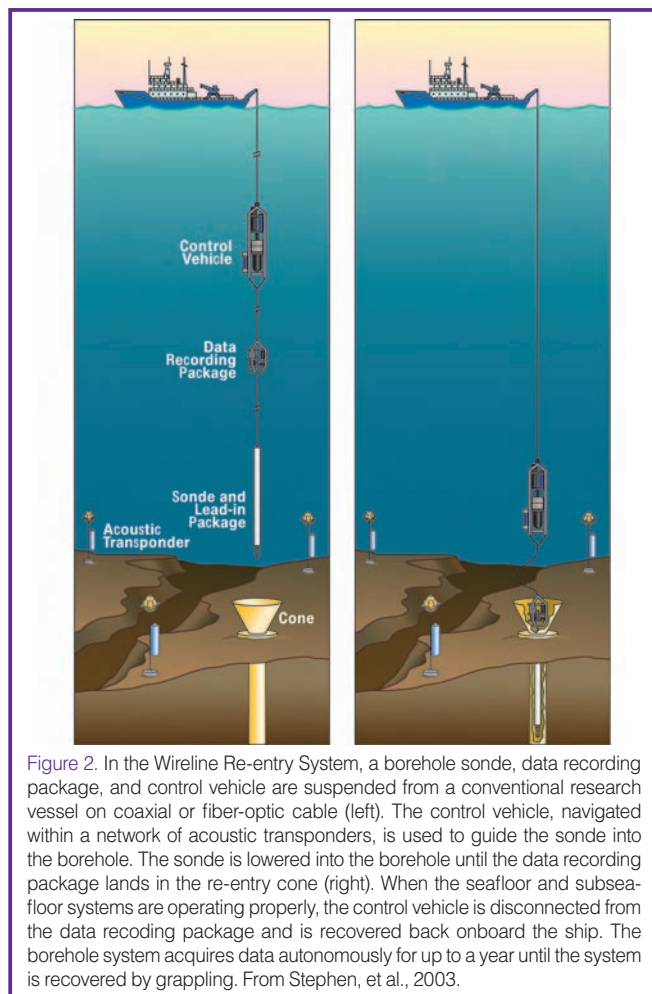


Figure 2. In the Wireline Re-entry System, a borehole sonde, data recording package, and control vehicle are suspended from a conventional research vessel on coaxial or fiber-optic cable (left). The control vehicle, navigated within a network of acoustic transponders, is used to guide the sonde into the borehole. The sonde is lowered into the borehole until the data recording package lands in the re-entry cone (right). When the seafloor and subseafloor systems are operating properly, the control vehicle is disconnected from the data recording package and is recovered back onboard the ship. The borehole system acquires data autonomously for up to a year until the system is recovered by grappling. From Stephen, et al., 2003.

et al., 1996). Both methane hydrate and free gas exist even where a clear BSR is absent. The low reflectance, or blanking, above the BSR is caused by lithologic homogeneity of the sediments rather than by hydrate cementation.

Seismology with the Wireline Re-entry System

The ODP era also saw the development of systems for re-entering boreholes from conventional research vessels and submersibles after the drill ship left the site (Fig. 2; Legrand et al., 1989; Montagner et al., 1994a; Spiess et al., 1992). Borehole seismic experiments and installations that used wireline re-entry technology were carried out in DSDP Holes 534 (Blake-Bahama Basin; Bradley et al., 1997; Stephen et al., 1994) and 396 (Mid-Atlantic Ridge at 23 degrees north; Montagner et al., 1994a) and in ODP Hole 843B (south of Oahu; Stephen et al., 2003). The latter experiment (the Ocean Seismic Network Pilot Experiment) carried out a test of three configurations of broadband seafloor seismic installation in preparation for extending the Global Seismic Network to the deep ocean.

Broadband Borehole Seismology

A new innovation on ODP was the deployment of broadband seismometers in boreholes (Suyehiro et al., 2006). Whereas

the conventional VSPs and offset VSPs mentioned above operate in the frequency range of 1–100 Hz (similar to the band used for reflection and refraction seismology), broadband seismometers are used in earthquake seismology and operate in the frequency range of 0.001–10 Hz. The first broadband borehole seismometer test was carried out from the drill ship on Leg 128 in the Japan Sea in 1989 (Kanazawa et al., 1992; Suyehiro et al., 1992). The first submersible-assisted broadband borehole seismometer test was carried out on the Mid-Atlantic Ridge (Montagner et al., 1994a, 1994b). On the Ocean Seismic Network Pilot Experiment a broadband borehole sensor in ODP Hole 843B was compared with a shallow buried and a seafloor seismometer for a period of over three months (Stephen et al., 2003). Subsequently, four permanent broadband borehole seismic observatories were installed in the western Pacific and Japan Trench on Legs 186, 191 and 195 (Araki 1999; Araki et al. 2004; Suyehiro et al., 2002). Three other boreholes have been drilled specifically for borehole seismic installations: at the Ninety-east Ridge, near the Hawaii-2 Observatory, and in the equatorial Pacific.

Acknowledgements

RAS would like to thank the Earthquake Research Institute at the University of Tokyo for a six-month Visiting Professorship during which this synthesis was carried out.

References

- Araki, E., 1999. *Geophysical nature of broadband seismic signals in deep oceans. PhD thesis, University of Tokyo, Tokyo.*
- Araki, E., Shinohara, M., Sacks, S., Linde, A., Kanazawa, T., Shiobara, H., Mikada, H., and Suyehiro, S., 2004. Improvement of seismic observation in the ocean by use of seafloor boreholes. *Bull. Seism. Soc. Am.*, 94:678–690.
- Bradley, C.R., Stephen, R.A., Dorman, L.M., and Orcutt, J.A., 1997. Very low frequency (0.2–10.0Hz) seismoacoustic noise below the seafloor. *J. Geophys. Res.*, 102(11):703–711,718, doi:10.1029/96JB3183.
- Detrick, R.S., Collins, J.A., Stephen, R.A., and Swift, S.A., 1994. *In situ* evidence for the nature of the seismic layer 2/3 boundary in oceanic crust, *Nature*, 370:288–290, doi:10.1038/370288a0.
- Holbrook, W.S., Hoskins, H., Wood, W.T., Stephen, R.A., Lizarralde, D., and Leg 164 Science Party, 1996. Methane hydrate and free gas on the Blake Ridge from vertical seismic profiling. *Science*, 273:1840–1843, doi: 10.1126/science.273.5283.1840.
- Kanazawa, T., Suyehiro, K., Hirata, N., and Shinohara, M., 1992. Performance of the ocean broadband downhole seismometer at site 794. In K. Tamaki, Suyehiro, K., Allan, J., McWilliams, M., et al. (Eds.), *Proceedings of the Ocean Drilling Program, Scientific Results 127/128 Part 2*, College Station, Texas (Ocean Drilling Project), 1157–1171.
- Kong, L., Brocher, T.M., and Stephen, R.A., 1985. Spreading rate independence of oceanic seismic layer 2. *Geophys. Res. Lett.*, 12:219–222.

- Leg 123 Shipboard Scientific Party, 1990a. **Explanatory Notes**. In Ludden, J.N., Gradstein, F.M., et al. (Eds.), *Proceedings of the Ocean Drilling Program, Initial Report*. College Station, Texas (Ocean Drilling Program), 27–59.
- Leg 123 Shipboard Scientific Party, 1990b. **Site 765**. In Ludden, J.N., Gradstein, F.M., et al. (Eds.), *Proceedings of the Ocean Drilling Program, Initial Report*. College Station, Texas (Ocean Drilling Program), 63–267.
- Legrand, J., Echardour, A., Floc'h, H., Floury, L., Gieskes, J., Harmegnies, F., Loaec, G., Pozzi, J.-P., Raer, Y., and Stephen, R., 1989. **Campagne FARE: Wireline reentry of DSDP Hole 396B using the NADIA system**. *EOS Trans. Am. Geophys. Union*, 70:729–730, 741.
- Little, S.A. and Stephen, R.A., 1985. **Costa Rica Rift borehole seismic experiment**, Deep Sea Drilling Project Hole 504B, Leg 92. *Init. Repts. DSDP*, 83:517–528.
- Montagner, J.P., Karczewski, J.-F., Romanowicz, B., Bouaricha, S., Lognonne, P., Roult, G., Stutzmann, E., Thiriot, J.-L., Brion, J., Dole, B., Fouassier, D., Koenig, J.-C., Savary, J., Floury, L., Dupond, J., Echardour, A., and Floc'h, H., 1994a. **The French Pilot Experiment OFM-SISMOBS: first scientific results on noise level and event detection**. *Physics of the Earth and Planetary Interiors*, 84:321–336, doi: 10.1016/0031/9201(94)90050-7.
- Montagner, J.P., Romanowicz, B., and Karczewski, J.-F., 1994b. **A first step toward an oceanic geophysical observatory**. *EOS Trans. Am. Geophys. Union*, 75:150–151, 154.
- Spiess, F.N., Boegeman, D.E., and Lowenstein, C., 1992. **First ocean-research-ship-supported fly-in re-entry to a deep ocean drill hole**. *Mar. Tech. Soc. J.*, 26:3–10.
- Stephen, R.A., 1979. **The oblique seismic experiment in oceanic crust - equipment and technique**. *Mar. Geophys. Res.*, 4:213–226, doi: 10.1007/BF00286406.
- Stephen, R.A., 1981. **Seismic anisotropy observed in upper oceanic crust**. *Geophys. Res. Lett.*, 8:865–868.
- Stephen, R.A., 1985. **Seismic anisotropy in the upper oceanic crust**. *J. Geophys. Res.*, 90(11):383–311, 396.
- Stephen, R.A., 1988. **Lateral heterogeneity in the upper oceanic crust at DSDP Site 504**. *J. Geophys. Res.*, 93:6571–6584.
- Stephen, R.A., and Harding, A.J., 1983. **Travel time analysis of borehole seismic data**. *J. Geophys. Res.*, 88:8289–8298.
- Stephen, R.A., Koelsch, D., Berteaux, H., Bocconcelli, A., Bolmer, S., Cretin, J., Etourmy, N., Fabre, A., Goldsborough, R., Gould, M., Kery, S., Laurent, J., Omnes, G., Peal, K., Swift, S., Turpening, R., and Zani, C., 1994. **The Seafloor Borehole Array Seismic System (SEABASS) and VLF Ambient Noise**. *Mar. Geophys. Res.*, 16:243–286, doi: 10.1007/BF01224745.
- Stephen, R.A., Loudon, K.E., and Matthews, D.H., 1979. **The oblique seismic experiment on Deep Sea Drilling Project leg 52**, In Donnelly, T., Francheteau, J., Bryan, W., Robinson, P., Flower, M., and Salisbury, M. (Eds.), *Initial Reports of the Deep Sea Drilling Project, 51-53*, Washington, DC (U.S. Government Printing Office), 675–704.
- Stephen, R.A., Loudon, K., and Matthews, D.H., 1980. **The oblique seismic experiment on DSDP Leg 52**. *Geophys. J. R. Astron. Soc.*, 60:289–300.
- Stephen, R.A., Spiess, F.N., Collins, J.A., Hildebrand, J.A., Orcutt, J. A., Peal, K.R., Vernon, F.L., and Wooding, F.B., 2003. **Ocean seismic network pilot experiment**. *Geochem. Geophys. Geosyst.*, 4:1092, doi: 10.1029/2002GC000485.
- Suyehiro, K., Araki, E., Shinohara, M., and Kanazawa, T., 2002. **Deep sea borehole observatories ready and capturing seismic waves in the Western Pacific**. *EOS Transactions (Supplement)*, 83:621, 624–625, doi: 10.1029/2002EO000420.
- Suyehiro, K., Kanazawa, T., Hirata, N., Shinohara, M. and Kinoshita, H., 1992. **Broadband downhole digital seismometer experiment at Site 794: A technical paper**. In Tamaki, K., Suyehiro, K., Allan, J., McWilliams, M., et al. (Eds.), *Proceedings of the Ocean Drilling Program, Scientific Results*, College Station, Texas (Ocean Drilling Program), 1061–1073.
- Suyehiro, K., Montagner, J.-P., Stephen, R.A., Araki, E., Kanazawa, T., Orcutt, J., Romanowicz, B., Sacks, S., and Shinohara, M., 2006. **Ocean seismic observatories**. *Oceanography*, 19:144–149.
- Swift, S.A., and Stephen, R.A., 1989. **Lateral heterogeneity in the seismic structure of upper oceanic crust, Western North Atlantic**. *J. Geophys. Res.*, 94:9303–9322.
- Swift, S.A., Hoskins, H., and Stephen, R.A., 1996. **Vertical seismic profile into upper oceanic crust at Hole 504B**, In Alt, J.C., Kinoshita, H., Stokking, L.B., Michael, P.J., et al. (Eds.), *Proceedings of the Ocean Drilling Program, Scientific Results*, Washington, DC (U.S. Government Printing Office), 339–347.
- Swift, S.A., Kent, G.M., Detrick, R.S., Collins, J.A., and Stephen, R.A., 1998a. **Oceanic basement structure, sediment thickness, and heat flow near Hole 504B**. *J. Geophys. Res.*, 103:15377–15391.
- Swift, S.A., Lizarralde, D., Hoskins, H., and Stephen, R.A., 1998b. **Seismic attenuation in upper oceanic crust at Hole 504B**. *J. Geophys. Res.*, 103:27193–27206.
- Swift, S.A., Stephen, R.A., and Hoskins, H., 1988. **Structure of upper oceanic crust from an Oblique Seismic Experiment at site 418A, Western North Atlantic**, In Salisbury, M.H., Scott, J.H., et al. (Eds.), *Proceedings of the Ocean Drilling Program, Scientific Results*, Washington, DC (U.S. Government Printing Office), 97–113.

Authors

Ralph A. Stephen, Department of Geology and Geophysics, Woods Hole Oceanographic Institution, Clark South 282, MS#24, Woods Hole, Mass. 02543, U.S.A., e-mail: rstephen@whoi.edu

Stephen A. Swift, Department of Geology and Geophysics, Woods Hole Oceanographic Institution, Clark South 286A, MS#24, Woods Hole, Mass. 02543, U.S.A.

S. Thompson Bolmer, Department of Geology and Geophysics, Woods Hole Oceanographic Institution, Clark South 286B, MS#24, Woods Hole, Mass. 02543, U.S.A.

Hartley Hoskins, Computer and Information Services, Department of Geology and Geophysics, Woods Hole Oceanographic Institution, Woods Hole, Mass. 02543, U.S.A.

Borehole Seismic and Strain Observatories in Seafloor Settings—Experiences after ODP Legs 186, 191, 195 and Future Plans

by Eiichiro Araki and Kiyoshi Suyehiro

doi:10.2204/iodp.sd.s01.13.2007

Borehole Seismo-Geodetic Observatories

In the period of Ocean Drilling Program Legs 186, 191, and 195, we successfully deployed a set of seismo-geodetic sensors in deep seafloor boreholes in four locations (JT1, JT2, WP1, and WP2). The JT1 and JT2 borehole observatories are located in the landward slope of the Japan Trench, where we expect seismic activity beneath the observatories. These borehole observatories gave us good platforms to look at the dynamic process on the plate boundary in the seafloor.

The WP1 and WP2 are considered a part of a global seismic network of observatories currently distributed mostly on land and ocean islands. For permanent seismic observation in the seafloor setting, installation of broadband seismic sensors in the seafloor borehole was recommended, and candidate locations were chosen (Suyehiro et al., 2006). The WP1 and WP2 sites are one of the first borehole observatories to implement such a permanent seafloor observatory.

We called these seafloor borehole observatories "NEREID" ('Neath Seafloor Equipment for Recording Earth's Internal Deformation). The NEREID observatories are characterized by several key features that are thought to acquire optimum performance from the borehole sensors.

Firstly, sensors are cemented at the bottom of the borehole. This is very important because long-period seismic and tilt/strain sensors are sensitive to fluid flow around them, so it is necessary to **couple them to the ground very well**. Cementing sensors at the bottom of the borehole was able to fix sensors rigidly **in place, and eliminated fluid around the sensors**. Cementing is necessary especially for strainmeters, because the strain of the ground should be transmitted to the sensing cylinder of the strainmeter by some means. **On land, it has been widely practiced for that purpose.**

Secondly, separate cables connect borehole sensors uphole for power feeding and seafloor data recording. This is to deal with possible failure of the sensors, cables, and connectors in the borehole during and after the installation in the borehole. It worked very well, **and we were able to replace failed sensors after the installation without affecting operation of other sensors.**

Sensors deployed in these observatories were configured to target specifications needs in each location of the observatories. For JT1 and JT2 observatories, a tiltmeter (AG510), a strainmeter (dilatometer and three component types), and broadband seismometers (CMG1T, PMD) are chosen to mainly target the earthquakes and slow deformation processes below the observatory. The WP1 and WP2 observatories are important for **monitoring global seismic activity**, so two identical broadband seismometers (Guralp CMG1T) were installed for redundancy.

Data from borehole sensors are recorded in the seafloor. Electric power necessary for these sensors is **provided by a stack of seawater batteries or lithium batteries stored in a titanium sphere**. Data are recovered by ROV by retrieving the data recorder because the amount of the recorded seismic data was as large as 10GB per year.

We conducted visits to each observatory for data recovery and maintenance once a year or more. From most of the observatories,

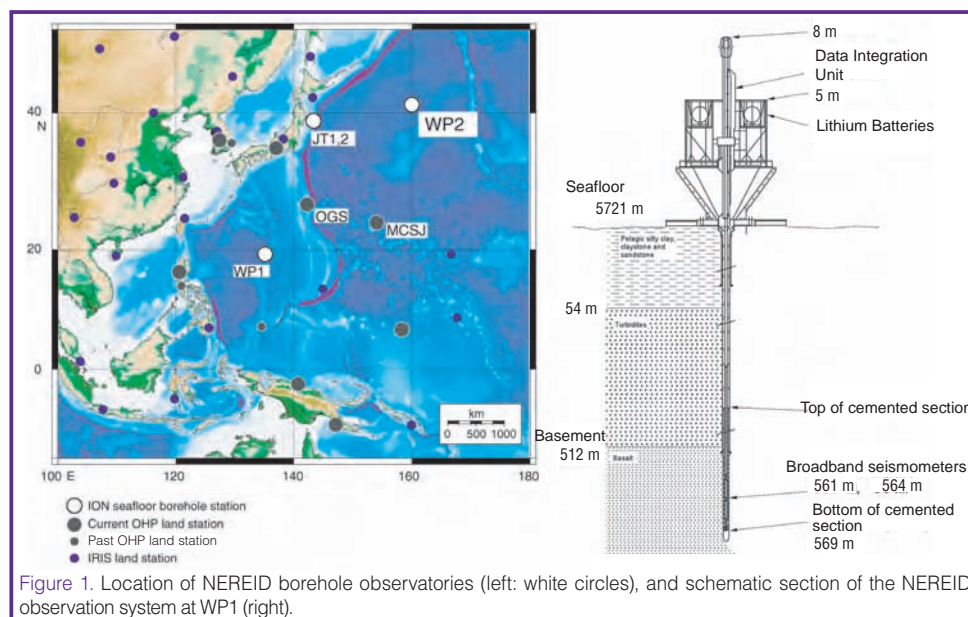


Figure 1. Location of NEREID borehole observatories (left: white circles), and schematic section of the NEREID observation system at WP1 (right).

Table 1. Period of data obtained from the NEREID observatories since 1999 (JT1, JT2, WP1, WP2)

	1	2	2	2	2	2	2	2
	9 9 9	0 0 0	0 0 1	0 0 2	0 0 3	0 0 4	0 0 5	0 0 6
Event	NT99-12		KY0111	KY020 KY0207 KR0208	NT03C NT0311	NT04C NT0411 CMG+PMD KR0409 airgun NS/EW	NT0508 GBOX installation JT1 PG recovery	NT0609 JT1 Airgun (NS/EW) PG+DPG+Seis installation
JT1 TILT JT1 CMG1T JT1 PMD JT1 strain JT1 PG JT1 DPG	○			7/22	1/14	6/15 10/14		5/21
JT2 CMG1T JT2 TILT JT2 PMD JT2 strain JT2 PG	○		9/15 12/19	6/27 9/18	6/17			
WP1 CMG1T(1) WP1 CMG1T(2)								
WP2 CMG1T(1) WP2 CMG1T(2)								

data for more than a year were recovered so far (Table 1). The observatories are still functional more than 5 years post-installation.

Improvement of Seismic and Tilt Measurement

The seismic data from the NEREID borehole observatories exhibited excellent performance with low background noise. The JT1 borehole seismometer showed less horizontal noise than a seismometer in the seafloor by 80 dB (Araki et al., 2004) in a 1000-second period. As a result, we were able to see effects of long period ocean gravity waves tilting the ground (at JT1 borehole 1.2 km below seafloor). This environment in the borehole enabled us to detect smaller teleseismic events (Shinohara et al., 2006), resulting in better understanding of seismic structure in the deep solid earth, such as structure of the transition zone of the Earth's mantle (Suetsugu et al., 2005).

Effects of earth tide were also seen in the seismic records from JT1, JT2, and WP2 boreholes. The observed tidal effect can be explained by deformation of ground due to tidal force on the solid earth. Broadband seismometers in the seafloor also show tidal effects, but this is usually the effect from tidal motion of water on the seafloor.

Furthermore, up to a year period, we investigated the stability of boreholes from tilt records. JT2 borehole tilt drifted at approximately 7 microradians per year. JT1 borehole showed a similar drift rate. JT1 and JT2 boreholes are located at a seismogenic plate boundary with different background seismicity. We sought slow events in the tilt record, as well as local earthquakes, to evaluate the activity of subducting plate boundary. No slow event was identified during the initial observation period in these boreholes.

Borehole seismometers are also very useful for observing local seismic activity. Figure 2 compares a small local earthquake's records from JT1 NEREID borehole observatory and nearby seafloor OBSs (Ocean Bottom Seismographs). The OBS records exhibit monotonic response around 10 Hz

especially in the horizontal component. This prevents precise analysis of the hypocenter and mechanism of earthquakes. Borehole records do not show such a response for all components; therefore, installing seismometers in boreholes will be very important for the study of dynamic processes of earthquakes beneath the seafloor.

Future Plans

We continue observations in existing long-term observatories. Activities in these borehole observatories include not only data recovery but also renovation of seafloor equipment to allow very long-term (more than several years) continuous observations by tiltmeter.

On the basis of present experiences of seismo-geodetic observation in the existing ODP seafloor boreholes, we plan on future long-term borehole observation in the IODP era. We proposed to implement scientific long-term borehole observatories in the Nankai Trough south of Japan as a part of NanTroSEIZE project. The area where Nankai Trough drilling is conducted covers a whole subduction process of oceanic plate, before the subduction to seismo-genesis of mega-thrust earthquake of magnitude greater than 8.

The plan of Nankai Trough borehole observatory includes CORKs (see Becker and Davis, 2005) and a long-term obser-

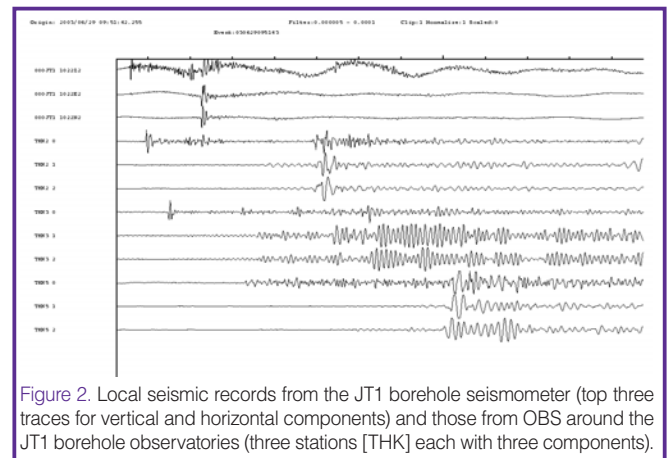


Figure 2. Local seismic records from the JT1 borehole seismometer (top three traces for vertical and horizontal components) and those from OBS around the JT1 borehole observatories (three stations [THK] each with three components).

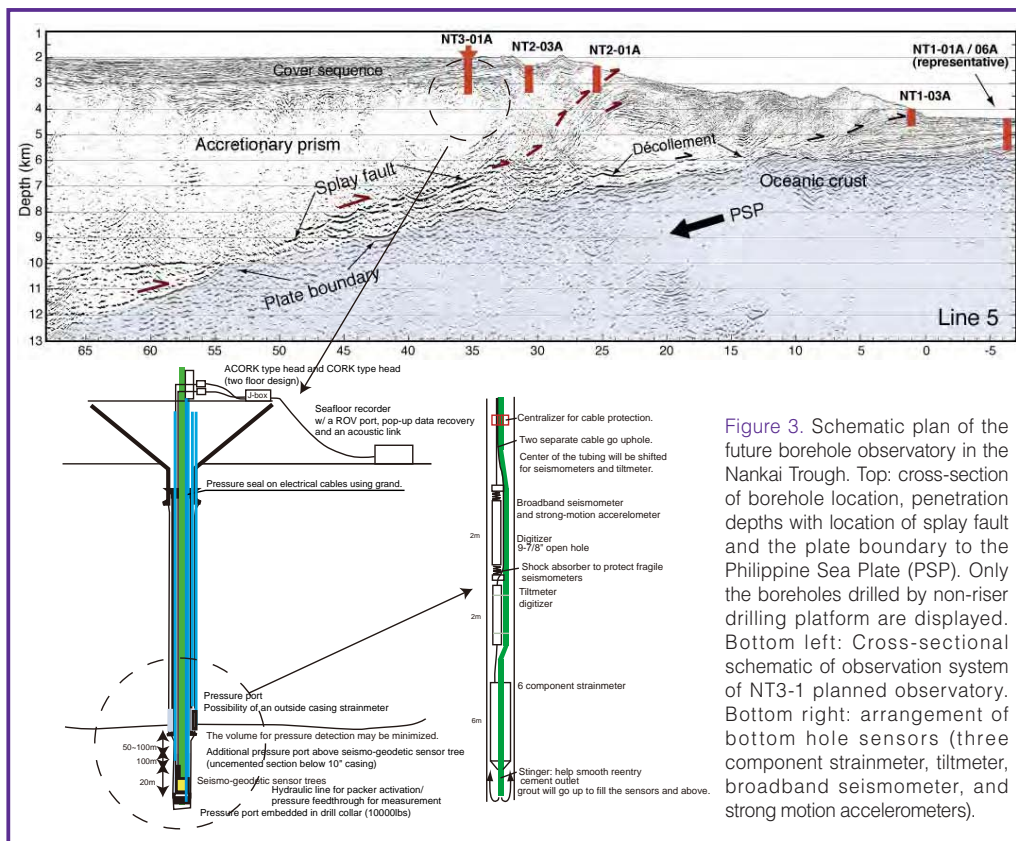


Figure 3. Schematic plan of the future borehole observatory in the Nankai Trough. Top: cross-section of borehole location, penetration depths with location of splay fault and the plate boundary to the Philippine Sea Plate (PSP). Only the boreholes drilled by non-riser drilling platform are displayed. Bottom left: Cross-sectional schematic of observation system of NT3-1 planned observatory. Bottom right: arrangement of bottom hole sensors (three component strainmeter, tiltmeter, broadband seismometer, and strong motion accelerometers).

vatory in a deep borehole of 3.5 km below the seafloor that requires a riser drilling platform. In addition to these observatories, we also plan to establish a seismo-geodetic-hydrological observatory that integrates the present A-CORK system for hydrological measurement and NEREID system for seismo-geodetic measurement. Figure 3 shows a schematic diagram of the observation system. At the bottom of the borehole drilled by a non-riser platform, we plan to install a three-component strainmeter, a tiltmeter, a strong motion accelerometer, and a broadband seismometer. We will also install a hydraulic tube below the seismic sensors to measure pore-pressure. By integrating various observation parameters obtained from the borehole observatory, we expect to obtain a better understanding of dynamics in the plate boundary of the Nankai Trough.

Understanding the seismogenesis of mega-thrust earthquakes, which is one of the major targets of the Nankai Trough drilling project (NanTroSEIZE), cannot be achieved solely by activities during drilling. Continuous long-term observations in these borehole observatories should play a key role in documenting and understanding ongoing subduction processes. Sufficient infrastructures and science-technology commitment are required to realize continuous long-term observations to achieve scientific goals. JAMSTEC will establish a scientific seismic network (DONET) around the area of the Nankai Trough drilling by 2010. The network utilizes submarine fiber optic cable to feed power and transmit data from instruments installed in the seafloor. We also plan to connect the borehole observatories to the DONET submarine cable network to assure long-term

realtime observations using the IODP boreholes.

References

- Araki, E., Shinohara, M., Sacks, S., Linde, A., Kanazawa, T., Shiobara, H., Mikada, H., and Suyehiro, K., 2004. Improvement of seismic observation in the ocean by use of seafloor boreholes. *Bull. Seismol. Soc. Am.*, 94:(2)678–690, doi: 10.1785/0120020088.
- Becker, K. and Davis, E.E., 2005. A review of CORK designs and operations during the Ocean Drilling Program. In Fisher, A.T., Urabe, T., Klaus, A., and the Expedition 301 Scientists (Eds.) *Proceedings of the Integrated Ocean Drilling Program, Volume 301*, College Station, Texas (Integrated Ocean Drilling Program Management International, Inc.), 104, doi: 10.2204/iodp.proc.301.104.2005.
- Shinohara, M., Araki, E., Kanazawa, T., Suyehiro, K., Mochizuki, M., Yamada, T., Nakahigashi, K., Kaiho, Y., and Fukao, Y., 2006. Deep-sea borehole seismological observatories in the Western Pacific: temporal variation of seismic noise level and event detection. *Ann. Geophys.*, 49(2/3):625–641.
- Suetsugu, D., Shinohara, M., Araki, E., Kanazawa, T., Suyehiro, K., Yamada, T., Nakahigashi, K., Shiobara, H., Sugioka, H., Kawai, K., and Fukao, Y., 2005. Mantle discontinuity depths beneath the West Philippine Basin from receiver function analysis of deep-sea borehole and seafloor broadband waveforms. *Bull. Seismol. Soc. Am.*, 95(5):1947–1956.
- Suyehiro, K., Montagner, J.-P., Stephen, R.A., Araki, E., Kanazawa, T., Orcutt, J., Romanowicz, B., Sacks, S., and Shinohara, M., 2006. Ocean seismic observatories. *Oceanogr.*, 19(4):144–149.

Authors

- Eiichiro Araki**, Japan Agency for Marine-Earth Science and Technology (JAMSTEC), 2-15 Natsushima-cho, Yokosuka, 237-0061, Japan, e-mail: araki@jamstec.go.jp.
- Kiyoshi Suyehiro**, Japan Agency for Marine-Earth Science and Technology (JAMSTEC), 2-15 Natsushima-cho, Yokosuka, 237-0061, Japan.

BABHY—A New Strategy of Hydrofracturing for Deep Stress Measurements

by Takatoshi Ito, Kentaro Omura, and Hisao Ito

doi:10.2204/iodp.sd.s01.38.2007

Paradox

Hydraulic fracturing in a vertical borehole induces fractures that will be vertical and normal to the minimum horizontal stress S_h (parallel to the maximum horizontal stress S_H), if there is no influence of natural fractures. The induced fractures close with venting and open with re-pressurization. At those times, there appear two kinds of critical borehole pressure, the reopening pressure P_r and the shut-in pressure P_s , which characterize the variation of borehole pressure during the test. The conventional theory tells us that those two pressures are related to the two stress components of S_H and S_h as follows (Haimson and Cornet, 2003):

$$P_r = 3S_h - S_H - P_p \quad (1)$$

$$P_s = S_h \quad (2)$$

Note that P_p is pore pressure in the fracture before opening. Those two equations give the principle for the two values of S_H and S_h to be determined from the two measured pressures of P_r and P_s .

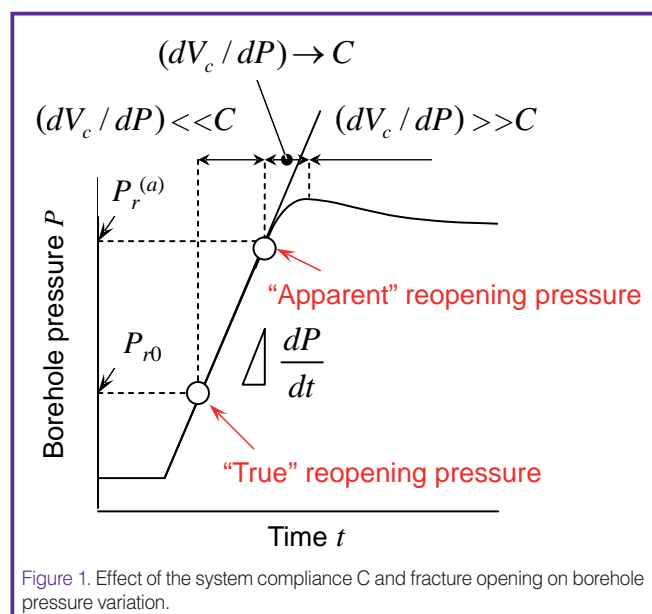
The interpretation of Eq. (2) for P_s is supported by considerable experimental and theoretical works. On the other hand, if the interpretation of Eq. (1) for P_r is also correct, the measured values of P_r and P_s should change independently in response to the combination of S_H and S_h which will vary site by site. However, the data of field tests so far indicate that incidences where the measured reopening pressure lies close to the shut-in pressure (i.e., $P_r = P_s$) are far more numerous than can reasonably be expected (Lee and Haimson, 1989). This strange phenomenon could happen if the crust is in a stress condition of $(S_H - P_p)/(S_h - P_p) = 2$. Nevertheless, it is hard to consider that such a condition has been held everywhere in the crust. It may be more reasonable to consider that, contrary to the conventional theory, the measured reopening pressure does not coincide with the "true" reopening pressure (the borehole pressure at which the fracture truly begins to open from its mouth at the borehole wall) and that pressure takes the same value with the shut-in pressure (i.e., with S_h). If this is true, we could estimate with hydraulic fracturing only the minimum component of stress S_h but not the maximum component of stress S_H , which is the most desired concern in the stress measurement. Furthermore, a serious problem may occur

should such a large error be included in the estimates of maximum stress S_H based on the reopening pressure so far.

True and Apparent Reopening Pressures

In order to explain the paradox described above, we have to take into account two factors which have been ignored in all conventional theory. Those factors are (i) residual aperture of fracture, and (ii) hydraulic compliance of test systems C . The C corresponds to an amount of fluid required to elevate fluid pressure in a test system by a unit magnitude, and it can be represented equivalently as $C = \beta V_{eff}$, where β is the fluid compressibility, and V_{eff} is the effective system volume. While the details of explanation have been described by Ito et al. (1999, 2005, 2006), they can be outlined briefly as follows.

The residual fracture aperture causes pressure penetration into the fracture prior to opening. Evidence of this has already been shown by laboratory studies (Cornet, 1982; Durham and Bonner, 1994; Zoback et al., 1977). The pressure penetration will be almost wholly transmitted to the fracture surface since the net area of contact of the two surfaces is usually a small fraction of their nominal area. Thus, the third component in Eq. (1) should be borehole pressure rather than P_p . The borehole pressure at fracture opening is defined as P_r , and so substituting P_p with P_r in Eq. (1) yields



$$P_r \equiv P_{r0} = \frac{1}{2}(3S_h - S_H) \quad (3)$$

Thus, the effect of including pressure penetration into the fracture prior to opening is to reduce the reopening pressure by a factor of almost two from the value expected using conventional theory (the reduction is precisely two when pore pressure is negligible). We will refer the borehole pressure given by Eq. (3) to the true reopening pressure P_{r0} .

On the other hand, the influence of the compliance C on fracture opening is more problematic; it is concerned with the correct identification of the true reopening pressure from the borehole pressure P minus time t curves. Note that the reopening pressure is usually detected as the borehole pressure P at which the $P - t$ curve is seen to deviate from linearity (Fig. 1). The effect of fracture opening on the borehole pressure variation can be expressed as follows (Ito et al., 1999):

$$\frac{dP}{dt} = \frac{Q}{(dV_c/dP) + C} \quad (4)$$

where dV_c is the change in pressurized fluid volume due to fracture opening. Since the flow rate Q and the system compliance C are constant, Eq. (4) indicates that deviations of the $P - t$ curve from linearity are governed by changes in the value of dV_c/dP and its relative value with respect to C . That is, prior to fracture opening, dV_c/dP is zero and the borehole pressure P increases linearly with t . After fracture opening, dV_c/dP becomes greater than zero, and the $P - t$ curve will deviate from linearity to some degree or other. However, even if a flexible hydraulic tube with small ID (less than 10 mm) is used to convey fracturing fluid from a pump to a test section in a borehole, C is considerably large. As a result, at the early stage of fracture opening, dV_c/dP should be very small compared with C so that no detectable change occurs on the $P - t$ curve, as shown schematically in Fig 1. When P reaches a level of S_h , the stress acting normally to the fracture surface becomes almost equal to or less than the value of S_h anywhere. Such a balanced stress condition leads to the criticality that the fracture aperture increases abruptly with a small increment in borehole pressure. As a result, dV_c/dP becomes a larger value compared with C , and finally the $P - t$ curve begins to deviate from the initial linear trend. The same process occurs regardless of the S_H value. Thus, we provide an explanation as to why incidences where the apparent (or measured) reopening pressure coincides with P_s (i.e., the minimum stress S_h are so common as described above). We will denote hereafter the apparent reopening pressure as $P_r^{(a)}$.

A Strategy for the Maximum Stress Measurements

Thus the strange observation of $P_r^{(a)} = P_s$ in field tests arises because the compliance of typical hydraulic fracturing systems is far larger than that of fracture until P reaches a

level of minimum stress S_h . However, it should be recalled here that the compliance in concern is that of the volume between the flow meter and the fracture mouth. Taking this into account, if the flow meter is placed as close as possible to the test interval, as illustrated in Fig. 2, the system compliance C can be reduced drastically, and a more objective measure of flow entering the fracture can be obtained. In this case, it is not a matter of course what kind of tubing (drill pipe)—flexible tube or stainless pipe with small ID—is used to convey fracturing fluid from a pump to a test interval. To demonstrate this idea, we developed a test system with a downhole flow meter (Ito et al., 2002). The system is basically the same as the conventional one except that the transducer to measure flow rate of injection is installed at the top of a straddle packer tool. Due to this modification, we succeeded in reducing the system compliance C drastically. The straddle packer tool is conveyed in boreholes on 6-conductor wireline. A single high-pressure hose is used to supply pressure from a hydraulic pump at the ground surface to the packer elements and the straddle interval so that a switch valve controllable from the surface is attached to the straddle packer. The system is designed to use in a borehole with 101 mm (HQ size) diameter at depths up to 1 km.

However, such a modification as above is still not sufficient to achieve the stress measurement at depths more than 1 km because of the following reasons.

(a) The stress measurement at deep depths cannot be done, of course, without deep boreholes, which generally have a large diameter, and accordingly the straddle packer tool needs to be large. The large size of the straddle packer tool leads to an increase in the system compliance C .

(b) For monitoring and recording flow rate and pressure during tests of the transducer installed on top of the straddle packer tool, the transducers should be connected with a data acquisition system placed at the ground surface by wires. To do this, it is appropriate to convey the straddle packer tool in

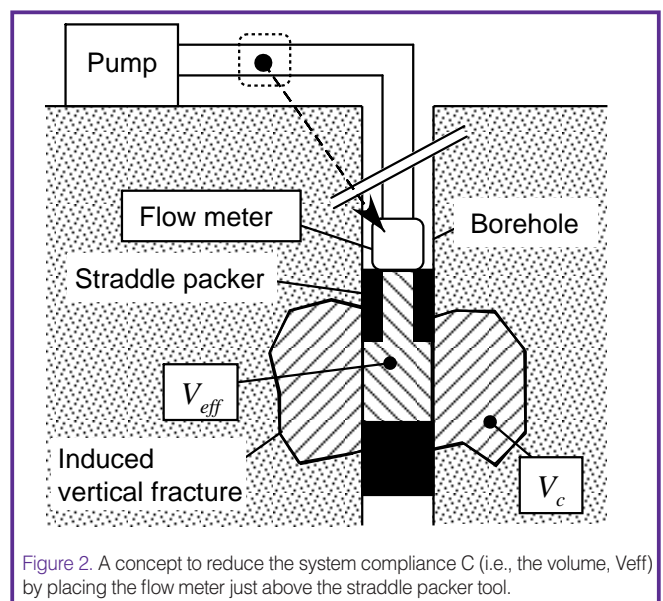


Figure 2. A concept to reduce the system compliance C (i.e., the volume, V_{eff}) by placing the flow meter just above the straddle packer tool.

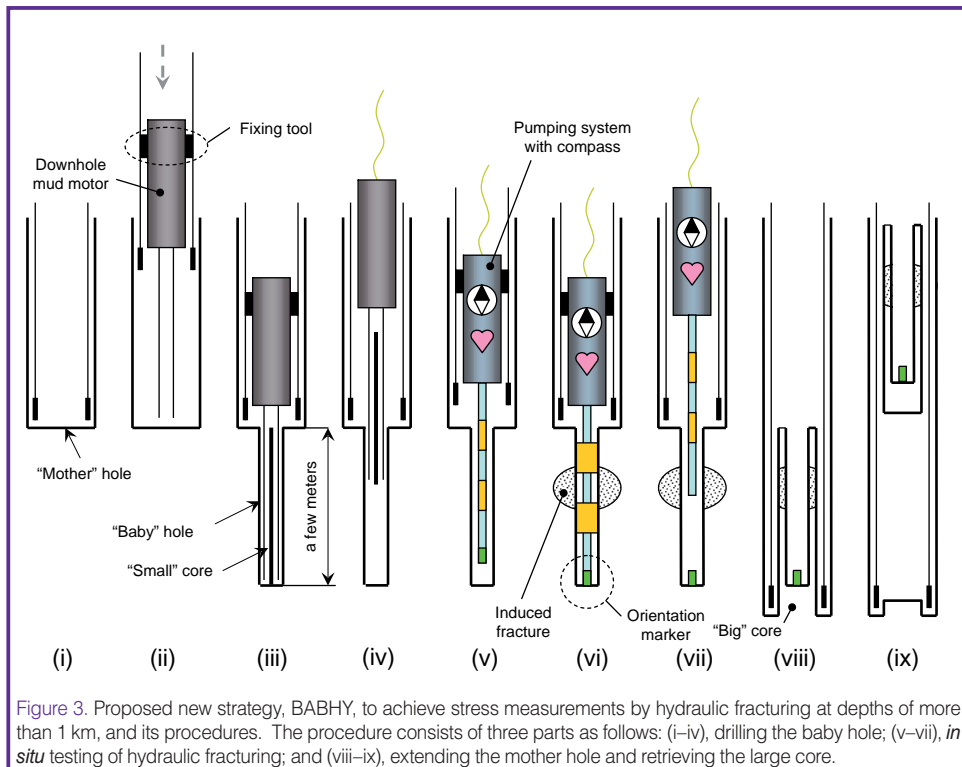


Figure 3. Proposed new strategy, BABHY, to achieve stress measurements by hydraulic fracturing at depths of more than 1 km, and its procedures. The procedure consists of three parts as follows: (i–iv), drilling the baby hole; (v–vii), *in situ* testing of hydraulic fracturing; and (viii–ix), extending the mother hole and retrieving the large core.

iii) Pump drilling mud through the drill pipe to drive the mud motor in the compact drilling tool, and drill the baby hole at the bottom of the mother hole.

iv) Retrieve the compact drilling tool and the small core, inspect pre-existing fractures in the core, and determine the depth of test section(s) in the baby hole.

v) Lower the straddle packer tool in the drill pipe on wireline, and fix it onto the drill pipe.

vi) Lower the drill pipe slightly to squeeze the packer element for isolating the test interval, and pressurize the test interval to induce axial fractures by using the pump installed in the tool. During the test, the pressure and flow rate of injected fluid and the

boreholes on wireline. The use of wireline is also effective to save the time for the tool running in boreholes. However, as the depth of measurement becomes greater, so does the risk for the tool to become stuck in the borehole. The financial risk in losing the advantages of wireline logging is very severe. For this reason, the straddle packer tool has generally been conveyed so far on drill pipe in the case of deep measurement, but the use of drill pipe makes it hard to arrange the wires connecting the downhole transducers and the surface data acquisition system.

Realistic Proposal: BABHY

Such a dilemma could be solved by a new strategy appropriate for the stress measurement at deep depths, as shown in Fig. 3. There are two components used in the strategy: (i) the compact drilling tool with a built-in mud motor, and (ii) the straddle packer tool with a pump and a digital compass. Each is conveyed in drill pipe on wireline. The compact drilling tool is used to drill an additional hole, several tens of millimeters in diameter and a few meters in length, at the bottom of an original borehole, and the hydraulic fracturing is carried out in the drilled hole by using the small packer tool. The additional hole and the original borehole are referred to the “baby” hole and the “mother” hole, respectively. The procedure can be outlined as follows.

- i) Set drill pipe with coring bit in the mother hole.
- ii) Lower the compact drilling tool in drill pipe on wireline and fix it onto the drill pipe.

tool orientation are monitored by the transducers installed in the tool and transmitted through wireline to the data acquisition system at the surface.

vii) Retrieve the straddle packer tool while leaving the orientation marker at the bottom of the baby hole.

viii) Lower and set a core barrel, and drill out the test section for getting the big core.

ix) Retrieve the big core, and inspect the fractures induced by pressurization in step (vi). The fracture orientation can be determined from the orientation marker in the core and the tool orientation recorded in step (vi).

Subsequently, the reopening pressure $P_r^{(a)}$ and the shut-in pressure P_s will be detected from the records of pressure and flow rate during the test. Finally, the stress magnitudes S_H and S_h will be estimated from those detected pressures based on Eqs. (2) and (3), assuming $P_r^{(a)} = P_{r0}$, since the system compliance is to be sufficiently small, and the stress orientation will be estimated from the fracture orientation

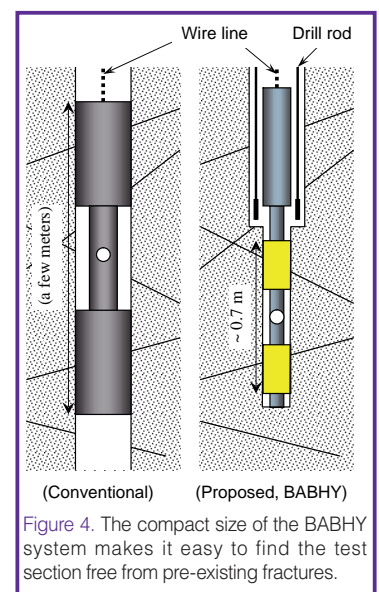


Figure 4. The compact size of the BABHY system makes it easy to find the test section free from pre-existing fractures.

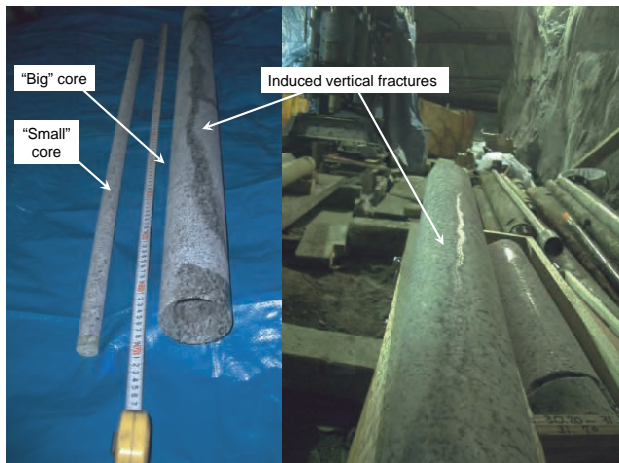


Figure 5. "Small" core (AQ size) retrieved by the baby hole drilling and "big" core (PQ size) retrieved by the over-coring. Hydraulically-induced fractures appeared in the big core.

detected in step (ix). We call this strategy Baby Borehole Hydrofracturing, BABHY for short.

This strategy will allow us to improve many defects in the conventional method as follows. It is easy to reduce the system compliance sufficiently because of a very compact size of the straddle packer tool (Fig. 4). The test section being free from pre-existing fractures can be chosen with certainty by the inspection of the small core, and then the straddle packer tool can be adjusted as the pressurized interval to be located at the chosen test section rightly. Note that the axial length between the top of the upper packer element and the bottom of the lower packer element is very short (less than 1 m) compared with that of a few meters for the conventional tool. The shorter length will make it much easier to choose the test section. We have already completed development of the compact drilling tool, and we are now developing the straddle packer tool. They are designed to be used in the mother holes with diameters larger than 101 mm (HQ size). As a part of the development process, we carried out a field test to confirm the procedure of step (vi) in particular (installing the straddle packer in the baby hole and carrying out hydraulic fracturing) at the Kamioka mine in Japan. For this test, we used a vertical borehole with 123 mm (PQ size) diameter and about 30 m deep drilled from the floor of a chamber at a depth of about 500 m from the ground surface. The baby hole with 47 mm (AQ size) diameter and 1 m length was drilled at the bottom of the borehole. The test succeeded quite well so that a pair of typical fractures in axial direction was induced, and the shape and orientation of the induced fractures were clearly detected from the large retrieved core (Fig. 5).

References

Cornet, F.H., 1982. Analysis of injection tests for *in situ* stress determination. In Zoback, M.D., Haimson, B.C., and Jacobson, M.L. (Eds.), *Proceedings of Workshop XVII, Workshop on Hydraulic Fracturing Stress Measurement*. Menlo Park, Calif. (The Survey), 414–443.

- Durham, W.B. and Bonner, B.P., 1994. Self-propping and fluid flow in slightly offset joints at high effective pressures. *J. Geophys. Res.*, 99:9391–9399.
- Haimson, B.C. and Cornet, F.H., 2003. ISRM suggested methods for rock stress estimation – Part 3: hydraulic fracturing (HF) and / or hydraulic testing of pre-existing fractures (HTPF). *Int. J. Rock Mech. Min. Sci.*, 40:1011–1020.
- Ito, T., Evans, K., Kawai, K., and Hayashi, K., 1999. Hydraulic fracture reopening pressure and the estimation of maximum horizontal stress. *Int. J. Rock Mech. Min. Sci. & Geomech. Abstr.* 36:811–826.
- Ito, T., Igarashi, A., Ito, H., and Sano, O., 2006. Crucial effect of system compliance on the maximum stress estimation in the hydrofracturing method: Theoretical considerations and field-test verification. *Earth Planets Space*, 58:963–971.
- Ito, T., Kato, H., Karino, H., and Hayashi, K., 2002. Hydrofrac stress measurements on true reopening pressure and development a system for the measurements at depths up to 1000 m. In Choi, S.-Y., et al (Eds.), *Proceedings of 2002 ISRM Regional Symposium on Rock Engineering Problems And Approaches in Underground Construction*, 93–100.
- Ito, T., Igarashi, A., Ito, H., and Sano, O., 2005. Problem for the maximum stress estimation by hydraulic fracturing method and its potential solution. *Proceedings of 40th U.S. Rock Mechanics Symposium*, Anchorage, Alaska: ARMA/USRMS 05-862 (CD-ROM).
- Lee, M.Y. and Haimson, B.C., 1989. Statistical evaluation of hydraulic fracturing stress measurement parameters. *Int. J. Rock Mech. Min. Sci. & Geomech. Abstr.*, 26:447–456, doi:10.1016/0148-9062(89)91420-4.
- Zoback, M.D., Rummel, F., Jung, R., and Raleigh, C.B., 1977. Laboratory hydraulic fracturing experiments in intact and pre-fractured rock. *Int. J. Rock Mech. Min. Sci. & Geomech. Abstr.*, 14:49–58, doi:10.1016/0148-9062(77)90196-6.

Authors

Takatoshi Ito, Institute of Fluid Science, Tohoku University, 2-1-1 Katahira Aoba-ku Sendai, 980-8577, Japan, e-mail: ito@ifs.tohoku.ac.jp.

Kentaro Omura, National Research Institute for Earth Science and Disaster Prevention, Tennodai 3-1, Tsukuba, Ibaraki 305-0006, Japan.

Hisao Ito, Japan Agency for Marine-Earth Science Technology (JAMSTEC), 3173-25 Showa-machi, Kanazawa-ku Yokohama, Kanazawa, 236-0001, Japan.

Long-term Monitoring in Deep Boreholes in the Nankai Subduction Zone

by Hisao Ito

doi:10.2204/iodp.sd.s01.43.2007

Introduction

IODP NanTroSEIZE is planning to construct observatories in deep boreholes in the Nankai subduction zone to monitor interseismic behavior at and above the updip limit of seismogenic zone. The deep observatories will be at NT2-03 and NT3-01; NT2-03 will be 3.5-km deep below sea floor to penetrate several splay faults, and NT3-01 will be 6-km deep to penetrate the splay faults and plate boundary fault. Scientific needs for long term *in situ* monitoring at and near splay faults and plate boundary fault include detailed analysis of low frequency/slow events, strain partitioning during interseismic period, and near-source hydrological/seismic/geodetic observations.

Scientific Needs

A deep borehole observatory has advantages in surface noise reduction (Araki et al., 2004), high frequency recording with little attenuation, observation in the close vicinity of

active processes, and installing a vertical sensor array along the borehole to improve the depth resolution (Chavarria et al., 2003).

Drilling through the updip limit of the fault and establishing borehole observatories is important to understand the following issues:

- Crustal deformation throughout the hanging wall to the fault zone
- How the strain caused by the backstop and subducting plate affect the fault plane strain
- Existence of any slip across the fault
- Is the fault locked? Is the fault weak?
- Correlation with asperity inferred from 3-D seismics
- Importance of mesoscopic structure for dynamic rupture
- Slow deformation in fault zone before dynamic rupture
- Structure of plate boundary/splay fault
- Occurrence of dynamic rupture in thin slip zones (main slip) and slow ductile deformation in thick fault zones.

Answers to the following questions may also be provided from a borehole observatory:

- Can both (thin slip zone and thick fault zone) occur within “asperity”?
- How thin or thick are the zones?
- How do they rupture coseismically?
- How do they deform in an interseismic period?
- How are they deforming now?
- How different are they in plate boundary / splay fault?

NanTroSEIZE scientists proposed an observatory plan (Harold and Kinoshita, 2006; Shinohara et al., 2003). One of the most essential parts of the basic idea is a distributed, multi-level multi-sensor system (Fig. 1), with seismometer, tiltmeter, strainmeter, and pressure sensors.

Possible Plan

Based on this basic concept, we have been working on a possible plan for sensors, a downhole telemetry system, a sensor/downhole telemetry system interface, and system installation. We understand that distributed sensors are essential. Currently, strain and pressure sensors need to be

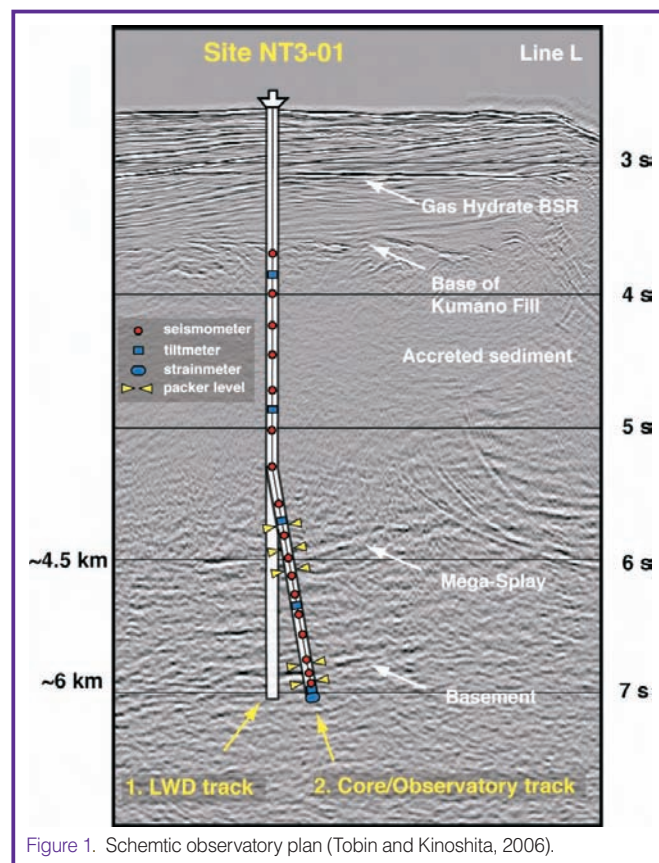


Figure 1. Schematic observatory plan (Tobin and Kinoshita, 2006).

set at the bottom of the hole, and tilt/seismic/temperature monitors may be set at bottom- and mid-hole sections (Fig. 2).

Major Technical Challenges

The following major technical issues for developing a deep borehole observatory in IODP are recognized:

1. Great depths telemetry, sensor, etc.
2. High temperatures (80°C–100°C for 3.5 km, 170°C–180°C for 6 km)
3. Long-term reliability and stability
4. Coupling of the sensors to the formation/casing
5. Geodetic/seismic and pore pressure measurements at multiple intervals (multi-packer vs. multi-hole?)
6. Vertical drilling and core sampling at the fault interval
7. Broadband high dynamic range and high resolution recording
8. Deployment
9. Telemetry system through Christmas tree/wellhead system of riser drill holes
10. Real time monitoring through seafloor cables

Borehole Telemetry System

The system should be reliable and work for many years at high temperatures. At the same time, the system should be able to deliver data that scientists need. The system should be able to be deployed practically and maintained with reasonable efforts. The fundamental requirements may be summarized as follows: **reliability, long mean-time-before-failure (MTBF), redundancy, protection from failure, high dynamic range, continuous recording, low power consumption, and limited number of connections through pressure controlled well head/Christmas tree.**

The system consists of three sections: 1) a downhole module array that digitizes seismic signals continuously and transmits the data to a recorder on sea floor, 2) a subsea recorder that receives data from downhole and stores data, and 3) a communications unit that sends commands from sea surface to the subsea recorder to check the status of the downhole systems and receives QC data (Fig. 3).

The downhole module can also send data from other sensors (e.g., pressure, temperature, and strain monitors) interfaced to auxiliary channels at a lower sampling rate.

Sensor Development

Sensors/sensor housing/connectors should be developed to work under high temperatures and great depth/hostile installation conditions.

We must carefully consider sensor installation in deep boreholes and at multi-levels. **Strainmeters have to be cemented in open hole sections of the borehole. Tiltmeters**

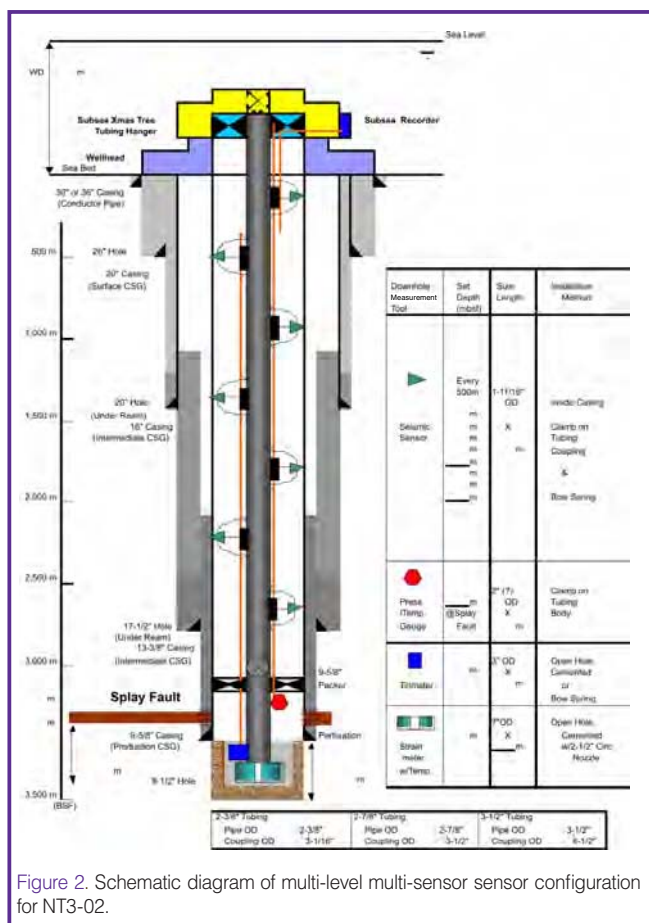


Figure 2. Schematic diagram of multi-level multi-sensor configuration for NT3-02.

and seismometers **might be cemented, however for multi-level installations we need to consider installing them by other methods (e.g., by locking arm or bow spring).**

Pore pressure monitoring is useful as a proxy of strain and pore pressure variation along the fault (Davis et al., 2006; Kano and Yanagidani, 2006). To be useful as a proxy for strain, the compliance of the pressure measurement system needs to be extremely small. For monitoring pore pressure of the fault, the gault must be isolated from other sections of the borehole either by packer or cementing.

Links to Shallow Boreholes/ Land Stations

The NanTroSEIZE deep borehole observatories, which will deploy vertical array sensor systems, **will be linked to a sea floor cable network and NanTroSEIZE shallow borehole observatories to be integrated to three dimensional ocean observatories.** The IODP NanTroSEIZE observatories will be situated at/around the updip limit. Ideally, the IODP NanTroSEIZE observatories would also be integrated with on-land observatories, which would be above the asperities.

Possible Application to Other Projects

The telemetry system and sensors that have been developed for NanTroSEIZE will be applied in other deep boreholes, such as Costa Rica Seismogenesis Project CRISP (Ranero et al., this issue), and also The Kanto Asperity

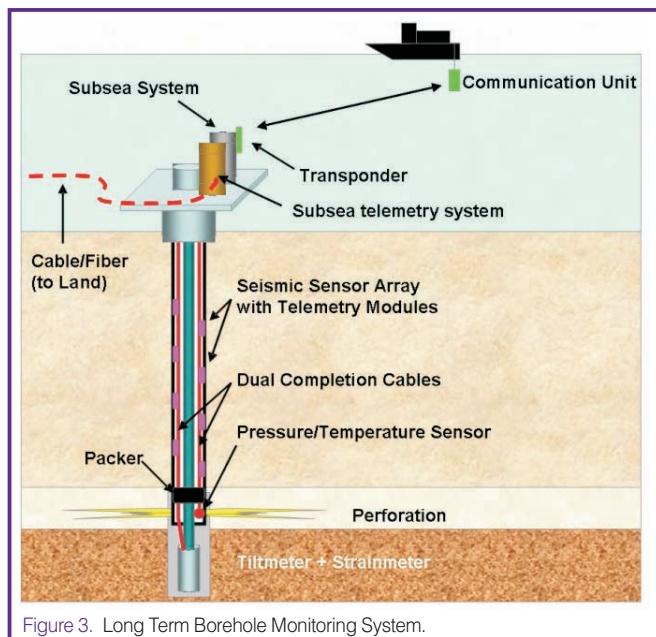


Figure 3. Long Term Borehole Monitoring System.

Project (KAP): KAP is a linked offshore/onshore regional geodetic and seismic network covering the asperity and non-asperity areas of the Kanto Region (Kobayashi et al., 2007). In the KAP, it is proposed to monitor strain, tilt, uplift and seismicity in the area underlain by asperities. This will show the relationship between plate motion, strain accumulation, and earthquake mode.

References

- Araki, E., Shinohara, M., Sacks, S., Linde, A., Kanazawa, T., Shiobara, H., Mikada, H., and Suyehiro, K., 2004. Improvement of seismic observation in the ocean by use of seafloor boreholes. *Bull. Seismol. Soc. Amer.*, 94:678–690, doi:10.1785/0120020088.
- Chavarría, J.A., Malin, P.E., and Shalev, E. 2004. The SAFOD Pilot Hole seismic array: Wave propagation effects as a function of sensor depth and source location. *Geophys. Res. Lett.*, 31: L12S07, doi:10.1029/2003GL019382.
- Davis, E., Becker, K., Wang, K., Obara, K., Ito, Y., and Kinoshita, M., 2006. A discrete episode of seismic and aseismic deformation of the Nankai trough subduction zone accretionary prism and incoming Philippine Sea plate. *Earth Planet. Sci. Lett.*, 242:73–84, doi:10.1016/j.epsl.2005.11.054.
- Kano, Y. and Yanagidani, T. 2006. Broadband hydroseismograms observed by closed borehole wells in the Kamioka mine, central Japan: Response of pore pressure to seismic waves from 0.05 to 2 Hz. *J. Geophys. Res.*, 111:B03410, doi:10.1029/2005JB003656.
- Kobayashi, R., Nakao, S., Nishimura, T., Curewitz, D., Matsu'ura, M., Sagiya, T., Satake, K., Ito, T., Stein, R., Malin, P., Shalev, E., Stephen, R., Sato, T., Mochizuki, K., Hori, T., Kamiya, S. and Naka, S., 2007. Kanto Asperity Project network: a wide geodetic and seismic network covering Kanto asperity and non-asperity regions, IODP CDP proposal #723, http://www.iodp.org/index.php?option=com_docman&task=doc_download&gid=1550.

Shinohara, M., Araki, E., Kamata, M., Kinoshita, M., Kyo, N., Kuroki, K., Kosuge, Y., Kobayashi, S., Konno, S., Goto, T., Saito, S., Suzuki, M., Takahashi, T., Tadokoro, K., Tsunogai, U., Tezuka, K., Nanba, K., Nishi, M., Hino, R., Mikada, H., Morita, N., Yoshida, C., and Ito, H., 2003. Long-term monitoring using deep seafloor boreholes penetrating the seismogenic zone. *Bull. Earthquake Res. Inst. Univ. Tokyo*, 78:205–218.

Tobin, H.J., and Kinoshita, M., 2006. NanTroSEIZE: The IODP Nankai Trough Seismogenic Zone Experiment. *Sci. Drill.*, 2:23–27.

Tobin, H. and Kinoshita, M., 2007. Report on NanTroSEIZE Long-Term Observatories Workshop, July 17-19, 2006, San Jose and Parkfield, California.

Author

Hisao Ito, Center for Deep Earth Exploration (CDEX), Japan Agency for Marine-Earth Science and Technology (JAMSTEC), 3173-25 Showa-machi, Kanazawa-ku, Yokohama, Kanagawa 236-0001, Japan, e-mail: hisaoito@jamstec.go.jp.

Workshop Participants

Last Name	First Name	Country
Ando	Ryosuke	U.S.A.
Araki	Eiichiro	Japan
Ashi	Juichiro	Japan
Babaie	Hassan	U.S.A.
Behrmann	Jan	Germany
Ben-Zion	Yehuda	U.S.A.
Boullier	Anne-Marie	France
Brodsky	Emily	U.S.A.
Byrne	Tim	U.S.A.
Chester	Frederick M.	U.S.A.
Cornet	Francois H.	France
Davis	Earl	Canada
Doan	Mai-Lin	U.S.A.
Dresen	Georg	Germany
Ellsowrth	William L.	U.S.A.
Geraud	Yves	France
Guerin	Gilles	U.S.A.
Hashimoto	Yoshitaka	Japan
Hickman	Steve	U.S.A.
Higuchi	Kazuhiro	Japan
Hori	Takane	Japan
Hung	Jih-Hao	Taiwan
Hyndman	Roy D.	Canada
Ide	Satoshi	Japan
Ito	Hisao	Japan
Ito	Takatoshi	Japan
Johnson	Malcolm	U.S.A.
Kanagawa	Kyuichi	Japan
Kano	Yasuyuki	Japan
Kiang	Tan Hoon	Singapore
Kimura	Gaku	Japan
Kinoshita	Masataka	Japan
Kirschner	David L.	U.S.A.
Kopf	Achim	Germany
Kryc	Kelly	U.S.A.
Kusaba	Yoko	Japan
Li	Yong-Gang	U.S.A.
Lin	Weiren	Japan
Lockner	David	U.S.A.
Ma	Kuo-Fong	Taiwan
Malin	Peter	U.S.A.
Marone	Chris	U.S.A.

Last Name	First Name	Country
Moore	Gregory	Japan
Moore	J. Casey	U.S.A.
Mori	Jim	Japan
Nadeau	Robert M.	U.S.A.
Nielsen	Dennis	U.S.A.
Nikaizo	Akira	Japan
Nishigami	Kin'ya	Japan
Ogasawara	Hiroshi	Japan
Okamoto	Shin'ya	Japan
Omura	Kentaro	Japan
Park	Jin-oh	Japan
Prevedel	Bernhard	U.S.A.
Rack	Frank R.	U.S.A.
Ranero	César R.	Spain
Rechtes	Ze'ev	U.S.A.
Roecker	Steven	U.S.A.
Rowe	Christen D.	U.S.A.
Saffer	Demian	U.S.A.
Saito	Saneatsu	Japan
Sakaguchi	Arito	Japan
Shibata	Ihiro	Japan
Shimamoto	Toshihiko	Japan
Solum	John	U.S.A.
Sone	Hiroki	Japan
Stephen	Ralph	U.S.A.
Suyehiro	Kiyoshi	Japan
Tsuji	Takeshi	Japan
Talwani	Manik	U.S.A.
Tanikawa	Wataru	Japan
Tezuka	Kazuhiko	Japan
Thu	Moe Kyaw	Japan
Tobin	Harold	U.S.A.
Townend	John	New Zealand
Ujii	Kohtaro	Japan
Underwood	Michael	U.S.A.
van der Pluijm	Ben	U.S.A.
Vanucchi	Paola	Italy
von Huene	Ronald	U.S.A.
Wiersberg	Thomas	Germany
Yamaguchi	Asuka	Japan
Zoback	Mark	U.S.A.



Field excursion to the Nobeoka thrust.